PRODUCTION OF HYDROGEN AND UTILIZATION IN FUEL CELL

**A Thesis Submitted
In Partial Fulfillment of the Requirements
For the Degree of**

DOCTOR OF PHILOSOPHY

by

NEERAJ BUDHRAJA
(Roll No. 2K19/PhD/ME/09)

Under the Supervision of

Dr. Amit Pal,	**Dr. R. S. Mishra**,
Professor, Department of	Professor, Department of
Mechanical Engineering,	Mechanical Engineering,
Delhi Technological University	Delhi Technological University

Department of Mechanical Engineering

DELHI TECHNOLOGICAL UNIVERSITY
(Formerly Delhi College of Engineering)
Shahbad Daulatpur, Main Bawana Road, Delhi-110042. India

December, 2024

DELHI TECHNOLOGICAL UNIVERSITY
(Formerly Delhi College of Engineering)
Shahbad Daulatpur, Main Bawana Road, Delhi-110042. India

<u>CANDIDATE'S DECLARATION</u>

I, *Neeraj Budhraja*, hereby certify that the work which is being presented in the thesis entitled **Production of Hydrogen and Utilization in Fuel Cell** in partial fulfillment of the requirements for the award of the Degree of **Doctor of Philosophy**, submitted in the Department of Mechanical Engineering, Delhi Technological University is an authentic record of my work carried out during the period from 1st August 2019 to 28th March 2024 under the supervision of *Prof. Amit Pal* and *Prof. R. S. Mishra*.

The matter presented in the thesis has not been submitted by me for the award of any other degree of this or any other Institute.

Neeraj Budhraja
(2K19/PhD/ME/09)

This is to certify that the student has incorporated all the corrections suggested by the examiners in the thesis and the statement made by the candidate is correct to the best of our knowledge.

(Prof. Amit Pal)   **(Prof. R. S. Mishra)**

Signature of Supervisor(s)   Signature of External Examiner

DELHI TECHNOLOGICAL UNIVERSITY
(Formerly Delhi College of Engineering)
Shahbad Daulatpur, Main Bawana Road, Delhi-110042. India

CERTIFICATE BY THE SUPERVISOR(s)

Certified that *Mr. Neeraj Budhraja* (**Roll No. 2K19/PhD/ME/09**) has carried out his research work presented in the thesis entitled "**Production of Hydrogen and Utilization in Fuel Cell**" for the award of Doctor of Philosophy from Department of Mechanical Engineering, Delhi Technological University, Delhi, under our supervision. The thesis embodies results of original work, and studies are carried out by the student himself and the contents of the thesis do not form the basis for the award of any other degree to the candidate or to anybody else from this or any other University/Institution.

Dr. Amit Pal

Professor,
Department of Mechanical
Engineering,
Delhi Technological University

Dr. R. S. Mishra

Professor,
Department of Mechanical
Engineering,
Delhi Technological University

Date:

ABSTRACT

Hydrogen is an energy carrier with a very high energy density (>119 MJ/kg) while the heating value on volume basis (~8 MJ/L, which is rather low). Pure hydrogen is barely available; thus, it requires extraction from its compounds. Steam reforming and water electrolysis are commercially viable technologies for hydrogen production from water, alcohols, methane, and other hydrocarbons; however, both processes are energy intensive. Current study aims at understanding the methane and ethanol-water mixture pathway to generate hydrogen molecules. The various intermediate species (like CH_X, CH_2O, CH_3CHO) are generated before decomposing methane/ethanol into hydrogen radicals, which later combine to form hydrogen molecules. About 97-98% of production is through steam reforming natural gas. The plasma reforming process was used to produce hydrogen, and the performance of various parameters on the hydrogen production rate was analyzed using three different ultrasonic transducers. Results showed the higher frequency (2.4 MHz) transducer had about 8-10% higher rate of hydrogen production against 1.7 MHz and 0.3 MHz transducers. The input voltage showed a 14-25% increase in hydrogen production rate from 4 kV to 7.5 kV, and beyond 7.5 kV, it declined. Similarly, the higher methanol concentration of 35% and feed flow rate of 3.5 LPM showed the highest hydrogen production rate. A H_2 purification unit was also installed that generated H_2 at about 99% purity level.

The study uses methanol as the feedstock for hydrogen production via a low-temperature methanol-reforming process. A simulation model was developed, where an equilibrium reactor is used for the reforming process. Effects of parameters like temperature, pressure, and Methanol-to-Water (M-to-W) molar ratio were examined. H_2 mole fraction and selectivity rise from 0.54 to 0.64 and from 60.91% to 67.28% when the reaction temperature increases from 100°C to 400°C. At the same time, the methanol conversion rate reached 95% at 400°C. Reactor pressure showed inverse effects where higher pressure reduced both hydrogen mole fraction and selectivity, and a similar reduction was noticed in the methanol conversion rate. M-to-

W molar ratio played a crucial role in the reaction pathway, and the M-to-W ratio is between 0.5 and 1.5 at 400°C and 1 atm. reactor pressure showed the highest H_2 mole fraction (>0.57) and a maximum methanol conversion rate (>90%). Therefore, the present simulating model effectively determined the impacts of various parameters.

Developed simulation model of a methanol-water, and the effects of reaction temperature (RT), reactor pressure (RP), and methanol-to-water (M-to-W) ratio are investigated. In contrast, the optimal conditions for hydrogen selectivity (HS) and feed conversion percentage (FCP) were determined using response surface methodology. Results showed a significant effects on the M-to-W molar ratio ranging between 0.9 and 1.35, whereas higher RT showed a good affinity for higher HS and FCP. The regression analysis showed R^2 values of 0.9877 and 0.9803 for HS and FCP, which is close to unity. Hence, both experimental (and simulated) and predicted values showed better correspondence with each other. In contrast, the optimal HS and FCP of 84.81% and 95.71% were observed at 328°C RT, 2.6 atm. RP and 1.34 M-to-W molar ratio.

A fuel cell generates electricity using hydrogen and oxygen. In the present work, a 1 kW proton exchange membrane fuel cell was evaluated for its performance at variable operating parameters. The operating parameters are important in examining the outputs from the fuel cell. Hydrogen flow rate (HFR) and gas pressure were two operating parameters considered for the cell performance. The hydrogen was generated from a hydrogen production and purification unit, whereas the oxygen was captured from the air. About 61% reduction in the HFR from 13 LPM to 5 LPM resulted in only 29% reduction in output current. In contrast, the addition and subtraction of 10% gas pressure from the rated value resulted in an 8% and 14% decline in output power. Similarly, the fuel cell stack efficiency declined by 10% and 15% with a 10% addition and reduction in the rated gas pressure.

Therefore, the present simulation and optimization provide results that may help to enhance the hydrogen production percentage. Also, the lower HFR reduced the cell output but the H_2 requirement was also reduced significantly, which showed the percentage decline in output was lower than the H_2 percentage saved.

<u>ACKNOWLEDGEMENTS</u>

<u>DEDICATION</u>

To my extraordinary parents, ***Mr. Om Parkash Budhraja*** and ***Mrs. Suresh***, words seem inadequate to express the ocean of gratitude that fills my heart. The path to this research work wasn't always smooth, but their guiding hands were always there to steady me.

The qualities of hardworking, politeness, calmness, helpfulness, focus and determination towards work has come from my parents. My father was an extraordinary person and always inspired me through his patience, hard work, focus towards goal and punctuality. While my mother always teach me calmness, helpfulness and truthfulness. Their consistent efforts made me good person and extremely supportive nature helped me to succeed in my research work.

I would also thank the inspiration and dedication I received from my lovely wife, and my caring family. Their emotional support was always there whenever I required.

TABLE OF CONTENTS

Chapter 5: **Simulation & optimization of hydrogen production**

Chapter 6: **Performance of PEM fuel cell**

Chapter 7: **Conclusions & Future scope**

LIST OF TABLES

LIST OF FIGURES

List of Symbols, Abbreviations and Nomenclature

H_2	Hydrogen	IGCC	Integrated Gasification Combined Cycle
M-to-W	Methanol-to-Water	SCWG	Supercritical Water Gasification
LPM	liter per minute		
kV	kilovolt	MEA	Membrane Electrode Assembly
MHz	Mega-Hertz		
RT	Reaction Temperature	PFSA	perfluorosulfonic acid
RP	Reactor Pressure	AEM	Anion Exchange Membrane
HS	Hydrogen Selectivity		
FCP	Feed Conversion Percentage	MFC-BES	microbial fuel cell-bioelectrochemical system
PEM	Proton Exchange Membrane	KHCF	potassium hexacyanoferrate
HPR	Hydrogen Production Rate	PV	Photovoltaic
RSM	Response Surface Methodology	HPM	Hydrogen-Producing Microbes
MeOH	Methanol Concentration	HCM	Hydrogen-Consuming Microbes
R	Coefficient of correlation	ER	Equivalence Ratio
R^2	Coefficient of regression	S/B	Steam/Biomass
WGSR	Water Gas Shift Reaction	SEI	Specific Energy Input
		IC	Internal Combustion
MSR	Methane Steam Reforming	BA	Butyric Acid
OMW	Olive Mill Wastewater	CMR	Composite Membrane Reactor
S/G	Steam/Glycerol	DME-SR	Dimethyl Ether-Steam Reforming
HTM	Heat Transfer Medium	ATR	Autothermal Reforming
PSA	Pressure Swing Adsorption	TR	Traditional Reactor

V_m	Molar volume	PMR	Plasma Membrane Reactor
HER	Hydrogen Evolution Reaction	MW	Microwave
DI	Deionized	SCCM	standard cubic centimeters per minute
CoP	Conference of the Parties	GDL	Gas Diffusion Layer
MPPT	Maximum Power Point Tracking	TSC	Transpired Solar Collector
TPV	thermophotovoltaic	GHSV	Gas Hourly Space Velocity
DoD	Depth of Discharge	R_{H_2}	Hydrogen production rate
ME	Methanol Electrolysis	W_{H_2}	Amount of hydrogen produced
WE	Water Electrolysis		
HSE	Hybrid Sulfur Electrolysis	T	Total time
SU	Steam Utilization	CCD	Central Composite Design
MCEC	Molten Carbonate Electrolysis Cell	DoE	Design of Experiments
SOE	Solid Oxide Electrolysis	GC	Gas Chromatography
AFC	Ash-Free Coal	TCD	Thermal Conductivity Detector
UCG	Underground Coal Gasification	FFR	Feed Flow Rate
CCS	Carbon Capture Sequestration	ANOVA	Analysis of Variance
GHG	greenhouse gas	df	degree of freedom
LCA	Life Cycle Assessment	ANN-GA	Artificial Neural Network-Genetic Algorithm
FB	Fluidized Bed		
EF	entrained flow	x_{H_2}	Mole fraction of hydrogen
EFB	Empty Fruit Bunches		
AC	Alternating Current	x_{MeOH}	Mole fraction of methanol
DBD	Dielectric Barrier Discharge	W_{total}	Total feed flow rate

η_{system}	System efficiency	ΔH	Change of enthalpy
CL	Catalyst Layer	H_P	Enthalpies of the products
ΔG	Gibbs free energy		
E_O	Reversible voltage	H_R	Enthalpies of the reactants
η	Fuel cell stack efficiency		

CHAPTER 1

INTRODUCTION

1.1. Overview

Global warming and ozone depletion played a significant role in shrinking polar ice caps, mainly releasing the enormous methane underneath. The release of methane has further fastened the effects of global warming [1]. The carbon dioxide discharged from overusing conventional fuels for humans' daily necessities is considered the leading greenhouse gas emitter. Since ancient times, the need for sustainable energy has been considered, but humans' selfish nature drastically over-exploited the fossil fuel reservoirs, creating an imbalance in nature [2]. Further, political influence in the extraction and supply of fossil fuels triggered the world to consider alternative fuels. Hydrogen is one such alternative that has the potential to fulfil the present as well as future needs of energy in various sectors.

Hydrogen has about 119.9 MJ/kg (lower heating value) energy density by weight, which attracted many researchers worldwide. Hydrogen molecules are mainly attached to other elements, and much energy is needed to split/detach hydrogen molecules from their compounds. This high energy consumption operation for hydrogen production has led to expensive, bulky equipment. Researchers and scientists focus on developing quick and economically viable methods to generate hydrogen at larger and application-oriented scales. So far, many methods for hydrogen generation have been developed, varying with the energy availability, raw materials, and the quality and quantity of hydrogen yield (Figure 1.1) [3].
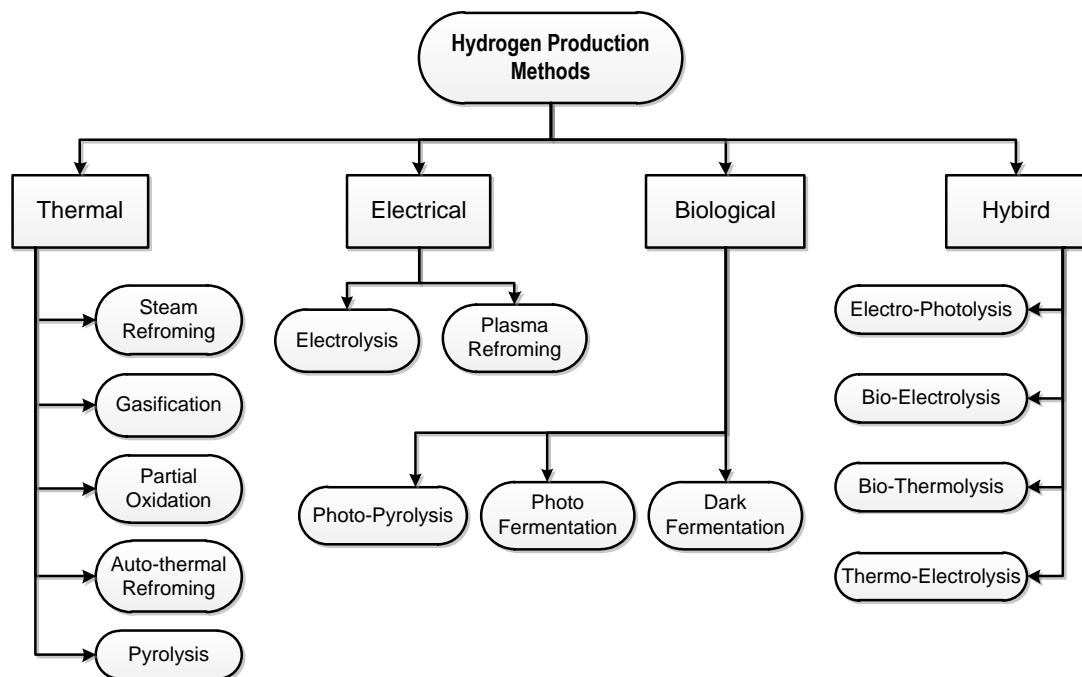
Figure 1.1. Various methods of hydrogen generation

Hydrogen generation through thermal processes demands more energy than any other process because very high temperatures are required in these processes. Among different thermal processes, steam reforming and gasification are primarily employed for industrial hydrogen generation. Methane reforming is done in a steam reformer where high temperatures prompt various reactions required for hydrogen extraction from its compound. At the same time, the use of a catalyst considerably reduces the requirement of high temperatures [4]. In contrast, gasification is performed at a comparatively lower temperature using raw materials like coal and biomass. Using renewable sources like biomass in hydrogen generation makes the process more environment-friendly; however, the high energy requirement from conventional energy sources categorizes it into grey hydrogen [5].

Electrical processes are carried out at comparatively lower temperatures than thermal processes. Nowadays, the electrolysis of water has gained the interest of researchers and scientists due to pure hydrogen gas as an output, which can be used in fuel cells and other industrial processes. Hydrogen from electrolysis can be considered green hydrogen when the energy sources for splitting water are renewable and non-polluting. In contrast, electrolytic cell costs are comparatively higher, counterbalanced

by producing about 99.99% pure hydrogen gas. Plasma reforming is another electrical method currently in the development stage for hydrogen generation. It has comparatively lower energy and temperature requirements than thermal processes but consumes more electricity than other processes [6,7]. Plasma reforming is compatible with different raw materials, while a lower hydrogen production rate and low purity grade of hydrogen yield than electrolysis is a research matter.

Similarly, biological processes require the physical activities of microbes. Biological wastes may be fed into the digester (or reactor), where microbes consume it and generate hydrogen that can later be taken out for various applications. In contrast, hybrid processes are the combination of two or more processes. In hybrid processes, benefits from different hydrogen-producing methods are combined, and a simultaneous process is performed to generate a higher hydrogen gas purity.

1.2. Hydrogen Characteristics

Hydrogen is an energy carrier which has the potential to fulfil present and future demands of the transportation, industrial, and medical sectors. But it is mainly found in the compounded form with other elements. Hydrogen has a 141-119.9 MJ/kg heating value at 25°C and 1 atmospheric pressure. The octane number >130 and the flammable limit of 4 to 75 vol.% in air add-on to the properties as fuel. In contrast, hydrogen has a low energy density by volume, making it challenging for large-volume storage. The expensive carbon fibre cylinders cost approximately 75% of the total cost. The hydrogen symbol, standard state, atomic number, and atomic mass are stated in Figure 1.2.
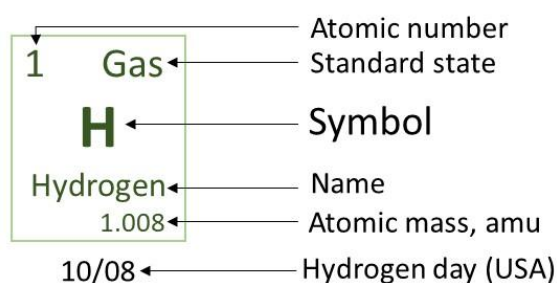
Figure 1.2. Hydrogen symbol, state, and atomic number, and atomic mass

Conversely, hydrogen is a colourless and odourless gas. It has high flammability and an auto-ignition temperature of 535℃. The smaller-sized molecules of hydrogen tend to escape through certain materials, leading to hydrogen embrittlement. Hence, hydrogen leakage is a significant problem for a hydrogen storage system. Various hydrogen characteristics are represented in Table 1.1.

Table 1.1. Characteristics of hydrogen [8–10]

Characteristics	Conditions	SI Unit	Values
Chemical formula	---	---	H_2
Discovery	in the year	---	1776
	by	---	Henry Cavendish
Isotopes	---	---	^1H - ^2H (stable), ^3H - ^7H (unstable)
Molecular weight	---	---	2.016
Density	gas at 0 ℃ and 1 atm	kg/ m^3	0.08987
	solid at -259 ℃	kg/ m^3	857
	liquid at -253 ℃	kg/ m^3	708
Viscosity	at 25 ℃	kg/ m s	0.892×10^{-5}
Specific volume	at 21.1 ℃ and 1 atm	m^3/ kg	11.99
Specific gravity	gas at 0 ℃ and 1 atm	---	0.0696
	liquid at -253 ℃ and 1 atm	---	0.0710
Vapour pressure	at -252.8 ℃	Pa	101.283
Solubility in water	at 15.6 ℃	vol/ vol	0.019
Critical temperature	---	℃	-240
Critical pressure	absolute	kPa	1296.212
Higher heating value	at 25 ℃ and 1 atm	MJ/ kg	141.86
Lower heating value	at 25 ℃ and 1 atm	MJ/ kg	119.93
Heat of fusion	at -259 ℃	kJ/ kg	58
Heat of vaporization	at -253 ℃	kJ/ kg	447
Thermal conductivity	at 25 ℃	kJ/ m s ℃	0.019
Heat capacity (C_P)	gas at 25 ℃	kJ/ kg ℃	14.3
	liquid at -256 ℃	kJ/ kg ℃	8.1
	solid at -259.8 ℃	kJ/ kg ℃	2.63
Specific heat (C_V)	at 21.1 ℃ and 1 atm	kJ/ kg ℃	10.12
Ratio of C_P/C_V	at 21.1 ℃ and 1 atm	---	1.42
Flashpoint	1 atm	℃	-253
Triple point temperature	at 7.042 kPa (abs)	℃	-259.3
Auto-ignition temperature	---	℃	400
Maximum flame temperature	---	℃	1527
Flammable limit	in air	vol.%	4 to 75
Octane number		---	>130

1.3. Hydrogen Pathways

The reaction pathway gives an insight into the various intermediate chemical reactions involved and how the reaction proceeds. Here, two pathways (via methane and alcohol-water) for hydrogen production are discussed in detail.

1.3.1. Methane
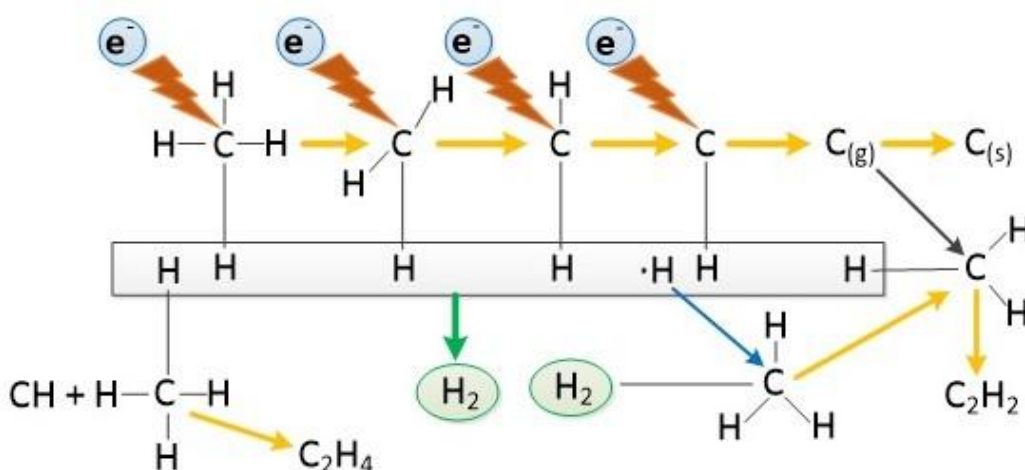
Figure 1.3. Methane decomposition pathway for H_2 production [11]

The proposed reaction pathway of methane (CH_4) decomposition into CH_X (CH_3, CH_2, CH) molecules [12,13] and then into hydrogen and carbon inside a plasma reactor is depicted in Figure 1.3. In a plasma reactor, the electrons get excited when they contact the plasma zone. The high-energy electrons collide with methane molecules, breaking the methane bonds and creating active species for the standard thermodynamic reactions. The CH_4 decomposition results in CH_3, CH_2, and CH molecules at the various threshold energies [14,15] (as described in Table 1.2) and generates •H radicals. The minimum amount of energy that transforms the reactant by activating the hydrogen atoms is called activation energy. It enables the reactants to overcome repulsive forces and break bonds to generate •H radicals. These •H radicals combine to form hydrogen (H_2) molecules, while the standard thermodynamic reactions produce hydrocarbons (C_2). The methane dissociation results in carbon particle deposition inside the reactor, which requires regular removal. Few researchers have used rotating electrodes to remove carbon particle deposits, thus, restricting any

decline in the reactor's efficiency [12,15]. The process does not require a very high temperature (except in the plasma-arc zone) as in methane steam reforming [16]. Thus, the CHx molecules resulting in dehydrogenation inside the plasma reactor are possible under near-ambient conditions.

Table 1.2. Dissociation reactions involved in methane decomposition [11]

Reactions	Threshold energy (eV)	Activation energy (eV)
$e^- + CH_4 \rightarrow CH_3 + H + e^-$	8.8	4.4
$e^- + CH_4 \rightarrow CH_2 + H_2 + e^-$	9.4	4.7
$e^- + CH_4 \rightarrow CH + H_2 + H + e^-$	12.5	4.5
$e^- + CH_4 \rightarrow C + 2H_2 + e^-$	14.0	6.0
$e^- + CH_3 \rightarrow CH_2 + H + e^-$	9.5	4.7
$e^- + CH_3 \rightarrow CH + H_2 + e^-$	10.0	5.5
$e^- + CH_3 \rightarrow C + H_2 + H + e^-$	15.0	7.0
$e^- + CH_2 \rightarrow CH + H + e^-$	8.5	4.25
$e^- + CH_2 \rightarrow C + H_2 + e^-$	8.2	4.9
$e^- + CH_2 \rightarrow C + 2H + e^-$	14.0	6.2
$e^- + CH \rightarrow C + H + e^-$	7.0	3.5

1.3.2. Alcohol-Water Mixture
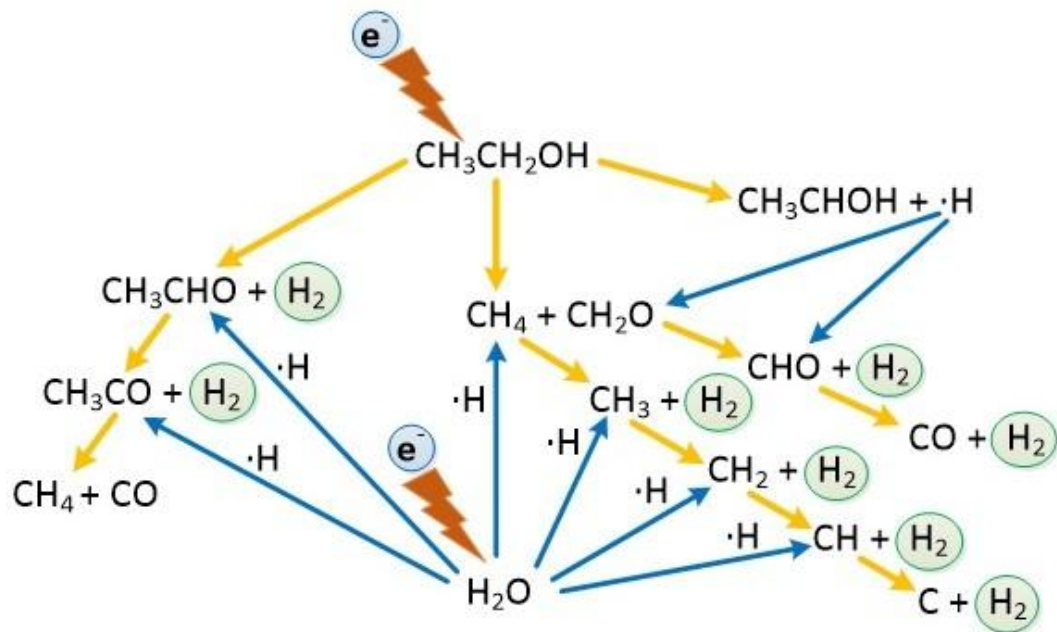
Figure 1.4. Ethanol-Water decomposition pathway for H_2 production [11]

Alcohol-water mixture also has the potential for hydrogen production via plasma reforming. The proposed pathway for ethanol-water decomposition depicting the alcohol-water dissociation into hydrogen molecules via different intermediate species is described in Figure 1.4. Initially, the plasma region excites electrons to higher energy levels of 3-20 eV [17], allowing these excited electrons to collide with the ethanol-water mixture. When the high-energy electrons strike ethanol-water molecules, the water molecules break down into •H, •O, and •OH radicals [18], while the ethanol molecules decompose into H_2, CO, CO_2, and C, following the intermediate species CH_4, CH_2O, CH_3CHO [19]. The electron collision produces ethanol molecules through dehydrogenation, generating •H radicals that later combine to form H_2 molecules [20,21]. The various dissociation reactions involved in the electron-ethanol collusion are presented in Table 1.3 [22]. The electrode's carbon deposition significantly reduces reactor efficiency [18,19]. Researchers have used rotating electrodes to minimize carbon particle deposition to avoid reactor efficiency decline [12].

Table 1.3. Dissociation reactions involved in ethanol decomposition [11]

Reactions	Activation energy (eV)
$e^- + CH_3CH_2OH \rightarrow CH_4 + CH_2O + e^-$	0.75
$e^- + CH_3CH_2OH \rightarrow CH_3CHO + H_2 + e^-$	1.03
$e^- + CH_3CH_2OH \rightarrow CH_3 + CH_2OH + e^-$	4.2
$e^- + CH_3CH_2OH \rightarrow CH_3CHOH + H + e^-$	4.3
$e^- + CH_3CH_2OH \rightarrow CH_3CH_2 + OH + e^-$	4.4
$e^- + CH_3CH_2OH \rightarrow CH_3CH_2O + H + e^-$	4.7
$e^- + CH_3CHOH \rightarrow CH_3CHO + H + e^-$	2.11
$e^- + CH_3CHO \rightarrow CH_3CO + H + e^-$	3.97
$e^- + CH_3CO \rightarrow CH_2CO + H + e^-$	3.14
$e^- + CH_2CO \rightarrow CH_2 + CO + e^-$	3.35
$e^- + CH_2 \rightarrow CH + H + e^-$	4.25
$e^- + CH \rightarrow C + H + e^-$	3.5

1.4. Hydrogen Production Methods

The main challenge related to hydrogen is its availability. Free hydrogen is scarcely available, while hydrogen compounds are plentiful in the universe [23]. The compounded form of hydrogen has low heating values and higher emissions than pure hydrogen. Therefore, hydrogen is extracted from compounds like biomass and natural gas and used for burning and electricity generation. The energies involved in the hydrogen generation processes include thermal, electrical, biochemical, and photonic, respectively [24]. Among various methods, the commonly used methods are steam reforming, gasification, electrolysis, plasma reforming, and anaerobic fermentation (also called BioHydrogen).

1.4.1. Steam Reforming

Steam-reforming is a well-established method broadly used as a thermal process for large-scale hydrogen generation, with over 45% of the total hydrogen generation. The process did not require oxygen, while the greenhouse gases could be used as the reactants, but using catalysts is recommended to lower the temperature requirement. Reactions in the reactor during steam reforming are expressed in Equation (1.1) to Equation (1.4), where ΔH^o is the standard enthalpy of the reaction. Reaction Equation (1.1) is the general reaction of the steam reforming process,

$$C_nH_m + nH_2O \rightarrow nCO + (n + \tfrac{1}{2} m) H_2 \qquad (1.1)$$
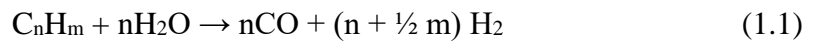
Equation (1.2) describes a methanation reaction where one mole of CO reacts with three moles of hydrogen to form one mole each of methane and water, and it releases energy,

$$CO + 3H_2 \rightarrow CH_4 + H_2O \qquad (1.2)$$
$$\Delta H^o = 206.17 \text{ kJ/mol (exothermic)}$$
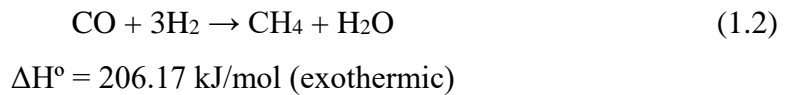
A reversible methane steam reforming reaction is described in Equation (1.3). Here, the opposite of the methanation reaction occurs,

$$CH_4 + H_2O \rightarrow CO + 3H_2 \qquad (1.3)$$
$$\Delta H^o = 206.17 \text{ kJ/mol (endothermic)}$$
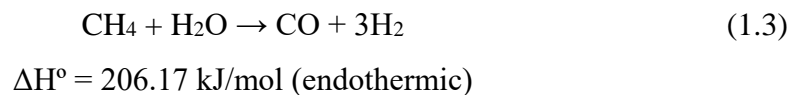
CO gas left out after steam reforming is reacted with superheated steam, and the reaction is called water gas shift reaction as described by Equation (1.4),

$$CO + H_2O \leftrightarrow CO_2 + H_2 \tag{1.4}$$

$\Delta H^o = 41.27$ kJ/mol (forward reaction is exothermic)
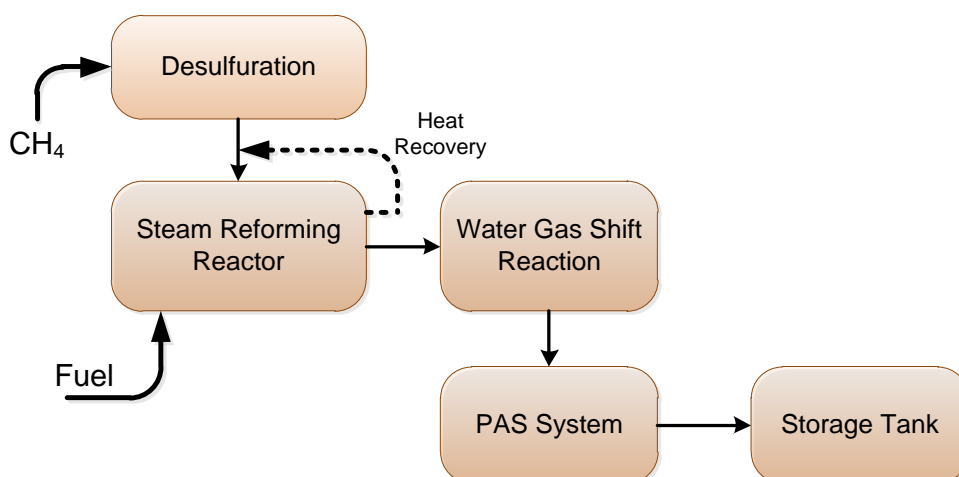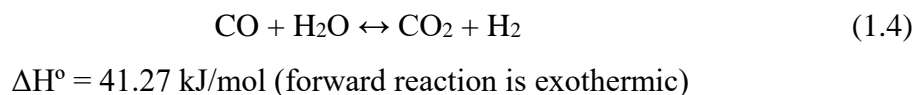
Figure 1.5. Flow chart of methane steam-reforming process

Figure 1.5 displays the flow chart of the methane steam-reforming process, and the schematic diagram of the process, gas cleaning, and water gas shift reaction (WGSR) are shown in Figure 1.6. Methane and superheated steam (water) are passed through a steam reformer, where the overall reaction Equation (1.1) occurs, and syngas containing hydrogen and CO gases are produced. This syngas is filtered, and WGSR is carried out to remove CO and further enhance hydrogen concentration in the final gas.
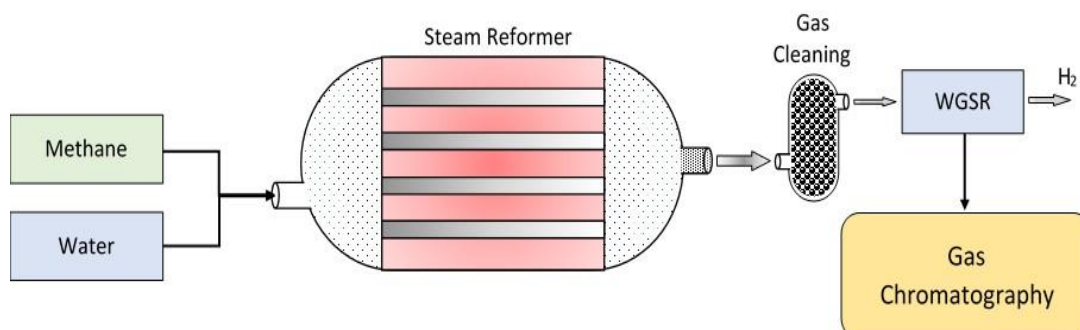
Figure 1.6. Methane Steam Reforming

The overall principle is the same in the steam reforming process; however, many upgrades are carried out to enhance hydrogen yield. The fundamentals of hydrogen generation using catalysts and supporting material for steam reforming are essential for describing the activity and stability of active metal and its support in the catalytic reforming process. The use of novel catalyst and technique structure's growth considerably reduced steam reforming high-temperature requirements to 500°C and 800°C, respectively. *Yoo et al.* used butyric acid (BA)/Ni to support Ni/Al_2O_3 catalyst in the natural gas steam reforming process [25]. Ni dispersion enhanced natural gas conversion to raise H_2 yield, and the best catalytic performance is achieved by 0.25 $BA-Ni/Al_2O_3$ catalyst. Thus, adding butyric acid improved the catalytic performance of the natural gas steam reforming. *Han et al.* discussed the consequences of the Ca/Al molar ratio in ethanol steam-reforming using a $Co/CaO-Al_2O_3$ xerogel catalyst [26]. Co enlarged surface area for reaction, thus improving H_2 yield. $Co/0.5\ CaO-Al_2O_3$ achieves the best catalytic performance. Therefore, low acidity and high surface area are considered key catalysts for higher hydrogen yield in ethanol steam-reforming.

Lu et al. determined the impacts of Lanthanum (La) additive in Ni-based catalysts and Ni's loading in MSR. Ni/Al_2O_3 added La showed higher methanol conversion and H_2 selectivity at reduced CO selectivity below 350°C than Ni/Al_2O_3 alone [27]. However, Ni loading above 10 wt.% lowered methanol and H_2 selectivity conversions, respectively. Therefore, adding La to the Ni-based catalyst produced H_2 at comparatively lower temperatures. In contrast, *Zhang et al.* worked on the effects of TiO_2 and CeO_2 support over the Au-based catalyst in MSR [28]. All catalysts except Au/TiO_2 produced more than 95% H_2 selectivity at 250-350°C. In comparison, higher temperatures beyond 530°C exhibited a decline in H_2 selectivity. The best results are accomplished by the Au-Ti-Ce/Na-ABen catalyst. In contrast, *Casanovas et al.* determined the impacts of noble metals or Ni over La-stabilized CeO_2 catalysts in the steam-reforming using olive mill wastewater (OMW) [29]. The trend of noble metals and Ni over CeLa H_2 selectivity and stability is Pt > Rh > Ru >> Ni > Pd. Catalyst Pt/CeLa with 1 wt.% w/w delivered approx. 40 mL-H_2/ mL OMW at 973 K and for 16000 h^{-1} space velocity, respectively. Therefore, Pt and Rh-based catalyst systems are the most acceptable catalysts for H_2 generation for 24 h of stability.

Rabbani and *Dincer* investigated the impact of a combined power plant for optimal hydrogen generation. An upsurge in hydrogen generation is observed with the rise in steam/glycerol (S/G) ratio and combustion temperature while raising reformer pressure dropped hydrogen generation [30]. Optimal parameters are simulated for hydrogen generation at an S/G ratio of 3, a reforming pressure of 100 kPa, a compressor pressure ratio of 9, and a combustion temperature of 980 K, respectively. Heat recovery for steam reforming will considerably reduce dependence on conventional sources, and many researchers have worked on it. The performance of the indirect heating method in steam methane reforming (SMR) using deionized water as a heat transfer medium (HTM) describes that methanol conversion from an HTM-based indirect heating method is 81.4-89.4% higher than the conventional direct heating method. However, the H_2 mol% is reduced with increasing reaction temperature. At the same time, the heat integration technology in lowering the energy consumption of steam methane reforming (SMR) and pressure swing adsorption (PSA) shows higher temperature boosted the H_2 yield. In contrast, the pressure reduction cut down the H_2 yield. Hence, the heat integration system saved about 60.5% of the energy needed for the SMR-PSA process.

1.4.2. Gasification

Gasification is another thermal process that is economical and carbon dioxide neutral for hydrogen production on a large scale. However, the reactor cost, feedstock purification, and low system efficiency are drawbacks of gasification. Various reactions involved in the gasification process are methanation reaction, where carbon reacts with hydrogen to form methane Equation (1.5) to Equation (1.7):

$$C + 2H_2 \rightarrow CH_4 \tag{1.5}$$
$$\Delta H^o = 75 \text{ kJ/mol (exothermic)}$$

$$CO + 3H_2 \rightarrow CH_4 + H_2O \tag{1.6}$$
$$\Delta H^o = 206.17 \text{ kJ/mol (exothermic)}$$

$$CO_2 + 4H_2 \rightarrow CH_4 + H_2O \tag{1.7}$$
$$\Delta H^o = 165.01 \text{ kJ/mol (exothermic)}$$
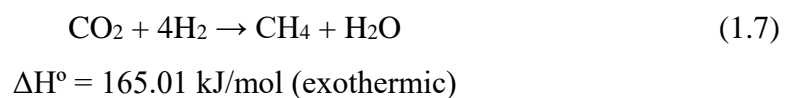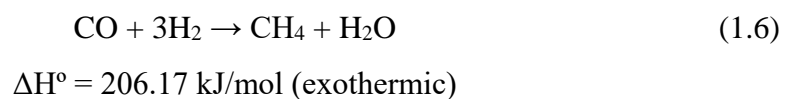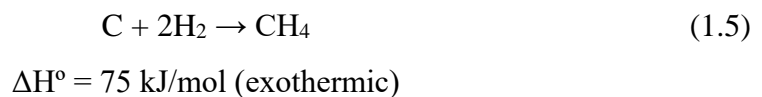
Followed by pyrolysis of methane Equation (1.8):

$$CH_4 + H_2O \rightarrow CO + 3H_2 \tag{1.8}$$

$$\Delta H^\circ = 206.17 \text{ kJ/mol (endothermic)}$$
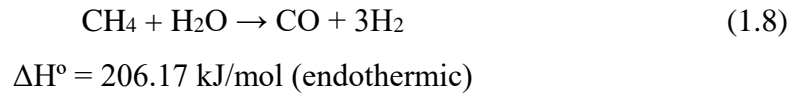
In a water gas reaction, steam enters the reactor to convert free carbon into CO and H_2 Equation (1.9),

$$C + H_2O \leftrightarrow CO + H_2 \tag{1.9}$$

$$\Delta H^\circ = 131 \text{ kJ/mol (forward reaction is endothermic)}$$
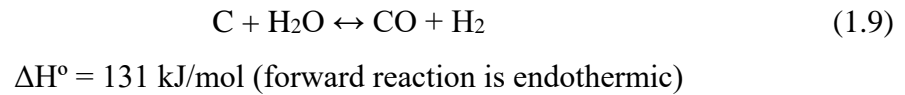
However, water-gas shift reaction Equation (1.10) was carried out to reduce highly reactive CO gas present in syngas, and Boudouard reaction Equation (1.11) again forms CO gas simultaneously,

$$CO + H_2O \leftrightarrow CO_2 + H_2 \tag{1.10}$$

$$\Delta H^\circ = 41.27 \text{ kJ/mol (forward reaction is exothermic)}$$

$$C + CO_2 \rightarrow 2CO \tag{1.11}$$

$$\Delta H^\circ = 172 \text{ kJ/mol (exothermic)}$$
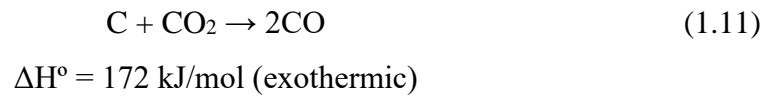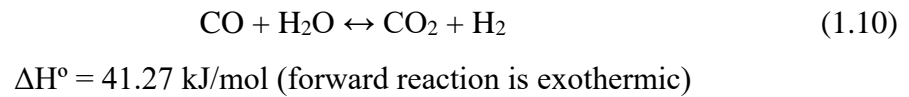
where ΔH° is the standard enthalpy of the reaction.
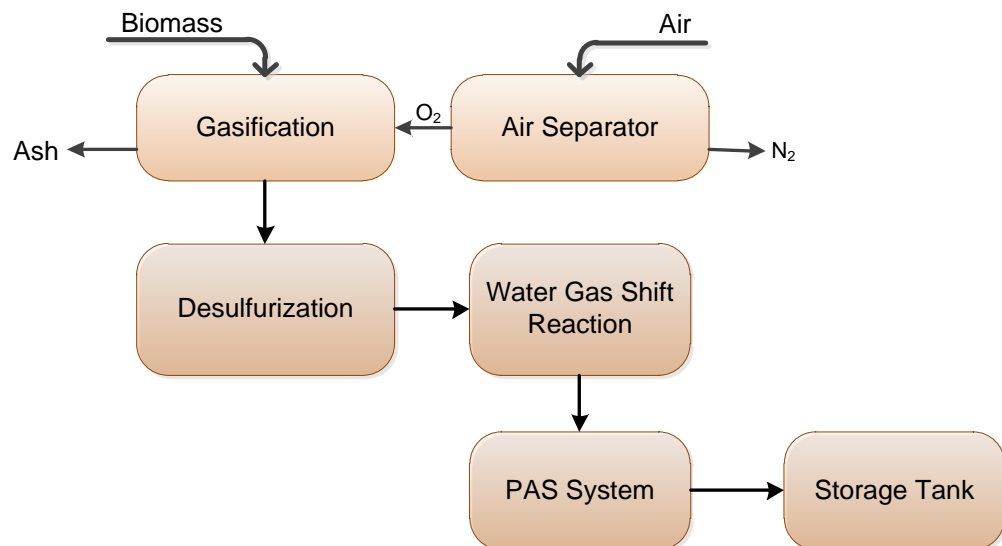
Figure 1.7. Flow chart of a biomass gasification process

The flow chart of the biomass gasification process using biomass as feed is shown in Figure 1.7, and the supercritical water gasification reactor is described with various components in Figure 1.8. Methane enters the reactor, where high-temperature gasification is performed, and the gas coming out of the reactor is hydrogen-rich syngas, which are later purified to get pure hydrogen gas.
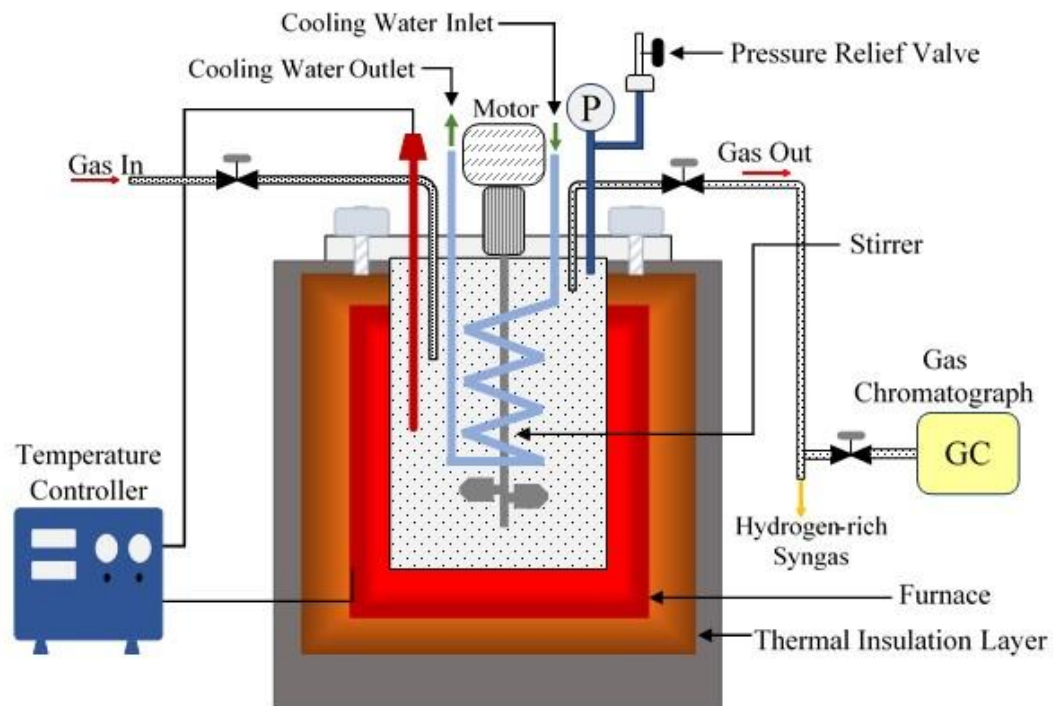
Figure 1.8. Schematic diagram of Supercritical water gasification

Various modifications in gasification reactors have been observed in recent years. *Yilmaz et al.* presented an integrated system's energetic and exergetic analysis with coal gasifiers for electricity, heating, and hydrogen generation [31]. Overall energy and exergy efficiencies achieved are 58.47% and 55.72%; however, the H_2 generation reached 0.085 kg/s from 0.06 kg/s by raising the ambient temperature to 40°C. *Seyitoglu et al.* used the combined coal-based gasification system to analyze hydrogen and power generation's energy and exergy efficiencies [32]. Peak overall energy and exergy efficiencies were 41% and 36.5%, respectively. *Yuksel et al.* analyzed hydrogen generation and liquefaction from the waste material-based combined system. Overall system's energy efficiency observed is 61.57%, and the exergy efficiency achieved is 58.15%; however, the rise in waste material gasification temperature enhanced the plant's overall exergy efficiency to 60%, along with the

increase in the hydrogen production rate of 0.077 kg/s [33]. In comparison, *Hasan* and *Dincer* assessed an integrated gasification combined cycle (IGCC) system for hydrogen generation from used tires. The IGCC produced 11.1 kW of net power with waste tires as the feed for the gasifier [34]. However, the system confirmed 55.01% and 52.31% of energy and exergy efficiencies with a 0.158 hydrogen generation to feedstock ratio.

Kang et al. optimized the supercritical water gasification performance parameters of lignin, cellulose, and waste biomass using catalyst K_2CO_3 and 20 Ni-0.36 Ce/Al_2O_3. Optimized H_2 gas is produced with 100% catalyst loading at 650°C [35]. The effects of CaO on the steam gasification process using various biomass waste materials to generate hydrogen are studied. H_2 concentration and yield are boosted with the CaO addition, while the CO and CO_2 concentrations decline in the syngas gas. The CaO behaviour on the gasification of the rice husk shows improvement in H_2 yield, and a reduction in CO_2 emissions is observed by using CaO (CO_2 sorbent) in the steam gasification [36]. In contrast, the effects of ER and S/B ratio on syngas production using CaO additive in a two-stage fluidized-bed gasifier shows that CaO generates about 37% H_2 in syngas concentration with ER 0.3 and S/B ratio 0.2 in a two-stage additive [37]. Hence, about 6.1-12.8% more H_2 was produced using the second-stage gasifier instead of the first stage. Similarly, another two-staged fluidized-bed gasifier assessing the significance of both the stage temperatures, the ER, and the S/B ratio gives the best results in the hydrogen generation for both stages for an operating temperature of 900°C [38].

The assessment of tomato and pepper residues, wood and paper, and sugarcane bagasse for H_2 generation using air-steam gasification was studied by many researchers. The consequences of temperature and chemical composition of cellulose, hemicellulose, and lignin-based biomass generate higher concentrations of CO and CH_4 in syngas from cellulose and hemicellulose, while the lignin-based biomass generated more H_2 and CO_2 at higher temperatures. *Yan et al.* determined the effects of reaction temperature, residence time, and feed concentration in food waste's supercritical water gasification (SCWG). The optimal condition for the best H_2 yield

without a catalyst is about 2 wt.% of the feed content at 500°C for 60 min [39]. However, H_2 yield and H_2 selectivity are enhanced to 20.37 mol/kg and 113.19% by adding 5 wt.% KOH. *Deniz et al.* performed the hydrothermal gasification of the marine biomass at the temperature range of 300-600°C and the biomass loading between 0.04-0.12 g/ml for one hour. With the biomass loading of 0.08 g/ml, hydrogen yield and the molar fraction calculated are 10.37 mol/kg and 62.51% at 600°C [40]. Hence, hydrogen generation is enhanced with increasing temperature and reducing biomass loading. The performance of the SCWG installed with the solar thermochemical receiver to generate solar heat for biomass gives an H_2 yield of 10-26 mol/kg; hence, the solar receiver fulfilled the heating requirement of the SCWG of the biomass for hydrogen generation.

1.4.3. Electrolysis

In electrolysis, the water molecules split or break down into more minor constituents, i.e., hydrogen and oxygen, when electricity passes through them. It is a well-established and broadly used process after the steam reforming process. The electrolysis of water achieves instant hydrogen generation at a smaller scale. Hydrogen purity is the best advantage in electrolysis because water is the raw material, and no carbon compound generates CO_2 gas.
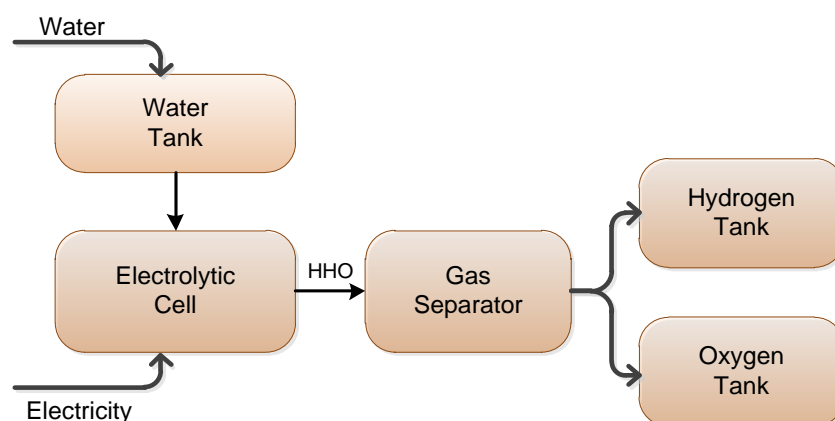
Figure 1.9. Flow chart of the water electrolysis process

The flow chart for the water electrolysis process is demonstrated in Figure 1.9, while the schematic diagram of various electrolytic cells is shown in Figure 1.10. Reactions involved in the electrolysis of water are as follows: -

A reaction that took place at the anode, Equation (1.12),

$$H_2O \rightarrow \frac{1}{2} O_2 + 2e^- + 2H^+ \tag{1.12}$$

$$\Delta E^o = +1.23 \text{ V}$$
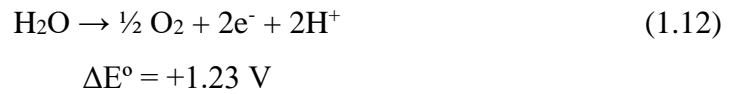
And the reaction that takes place at the cathode, Equation (1.13),

$$2H^+ + 2e^- \rightarrow H_2 \tag{1.13}$$

$$\Delta E^o = 0 \text{ V}$$
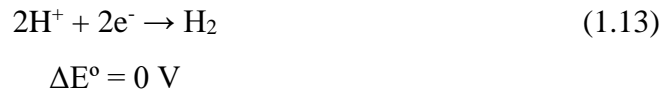
Thus, the overall reaction for electrolysis is given by Equation (1.14),

$$H_2O \rightarrow \frac{1}{2} O_2 + H_2 \tag{1.14}$$

$$\Delta E^o = -1.23 \text{ V}$$

where ΔE^o is the standard potential of the water electrolysis cell at 25°C.
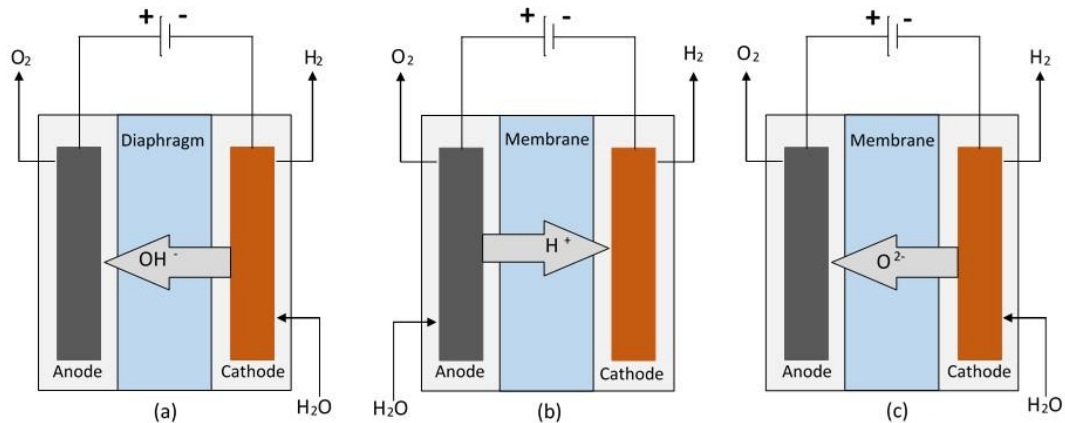
Figure 1.10. The various types of electrolysis cells are (a) alkaline electrolysis cell, (b) proton exchange membrane electrolysis cell, and (c) solid oxide electrolysis cell

Different electrolytic cells using various energy sources affected the hydrogen production rate. However, the influence of operating parameters on hydrogen generation from alkaline water electrolysis shows a rise in amperage, voltage, and electrolyte concentration, which improved the hydrogen generation irrespective of the cathode material used. Overall, higher hydrogen generation is obtained by Zn95%Cr5% and Zn90%Cr10% electrodes over the range of operating parameters [41]. The performance of a PbO_2 anode catalyst mixed with three additives, A, Z, and V, is compared with the commercially available membrane electrode

assembly (MEA) electrolytic cell. The ozone/O_2 and H_2 were generated by feeding pure water, and additives A and Z measured better performance. However, membrane electrode assembly with additive V overcomes the performance decline during power stoppage and restoration [42]. Electrical current fluctuation during water-splitting in alkaline water electrolysis influenced the efficiency loss in non-steady DC applications. For instance, a sort of waveform showed no effect on efficiency loss.

Villagra and *Millet* analyzed proton exchange membrane (PEM) water electrolysis at different operating current densities. I-V performance of the perfluorosulfonic acid (PFSA) polymer membrane with 50-200 µm thickness is measured at 10 A/cm^2 current density and found satisfactory [43]. In comparison, the different material substrates for the electrochemical decomposition of various structured alloys and the newly developed current collectors in alkaline anion exchange membrane (AEM) and MEA were studied. A cathode is electro-deposited with porous current collectors to acquire new cross-linked AEM for high ionic conductivity. The sol-gel method coats anode, which proved unsuitable for covering stainless steel non-woven fabrics.

Bidin et al. demonstrated the effects of sunlight intensity on water splitting. A stronger electric field leads to higher surface tension and, thus, breaks the hydrogen bond [44]. Collimated sunlight triggered hydrogen generation by 53% higher than 31% by conventional light and 16% by dark field. *Belleville et al.* produced hydrogen with a microbial fuel cell-bioelectrochemical system (MFC-BES) decoupled with a redox flow potassium hexacyanoferrate (KHCF) mediator. A current density close to 50 A/m^2 is achieved with an electric potential of 1 V with a 4-hour operation [45]. This desynchronized microbial rate from wastewater treatment reduces the water electrolysis cost for hydrogen generation. A coupled system of water electrolysis and solar photovoltaic (PVH_2 system) was also designed, where a PVH_2 system coupled with a 60 W electrolyzer and 100 W PV system is 77.06% efficient without CO_2 emissions [46]. Controlled cooling of electrolytes at the inlet enhanced the system's efficiency, making it a simple, cheaper, reliable, and more effective method for hydrogen generation without CO_2 emissions.

The performance parameters on methanol electrolysis using a photovoltaic (PV) system show that the PV array must be angled suitably to reduce the solar irradiation mismatch with the demand profile. Moreover, the reduction in system efficiency is estimated to reduce the battery's DoD for lifetime enhancement. The hybrid thermophotovoltaic uses water electrolysis to implement optimal power splitting of concentrated solar radiation. Studies show that proton exchange membrane measured higher efficiency than alkaline electrolysis, but it required desalinized and demineralized feed water for electrolysis [47]. In contrast, solid oxide electrolysis cells operating at a high temperature (700-900°C) generated hydrogen at 80% efficiency without any noble metal catalyst. A life cycle evaluation of proton exchange membrane (PEM) water electrolysis to generate hydrogen at reduced greenhouse gas emissions reduces 75% of CO_2 emissions in the hydrogen generation from the PEM water electrolysis system when run on electricity generated by renewable energy sources [48]. However, the flexibility in operating the volatile electricity production hours defined PEM water electrolysis with a very high share of the renewable energy hydrogen generation by 2050.

1.4.4. Anaerobic Fermentation (BioHydrogen)

When biomass or organic waste is fermented without oxygen in a digester or air-tight environment, methane, CO_2, and H_2 are produced. The process is termed anaerobic fermentation. In contrast, the hydrogen produced in the process is termed BioHydrogen. Though the quantity of BioHydrogen in the gas is deficient, some pre-treatment methods may raise the hydrogen quantity considerably. The process is similar to the biogas production process. The digester used has identical dimensions and properties; the difference lies in the gas extraction. In BioHydrogen production, hydrogen is taken out of the digester before it gets consumed by the methanogenesis bacteria. Two types of microbes are available for fermentation: Hydrogen-Producing Microbes (HPM) and Hydrogen-Consuming Microbes (HCM). Hydrogen-producing microbes are thermophiles, e.g., Clostridium thermocellum and Caldanaerobacter subterraneous [49]. They mainly consume lower hydrocarbon compounds and produce hydrogen and carbon dioxide gas. Simultaneously, the hydrogen-consuming microbes

consume acetic acid and hydrogen to generate methane gas and carbon dioxide. Various pre-treatment methods control the action of HPM and HCM.
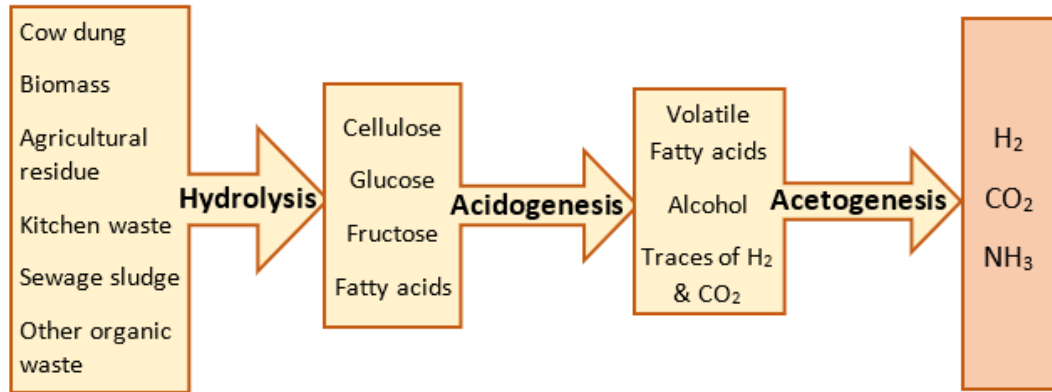
Figure 1.11. Flow chart for BioHydrogen production.

The population of HPM and HCM microbes decides whether the product will be hydrogen or methane [50]. Because if the hydrogen will not be extracted at the correct time, it will be fed by HCM, and the final product will be methane gas. Thus, time is another essential component for BioHydrogen production. To extend the time for hydrogen availability, many pre-treatment methods were performed, which decreased the HCM population and slowed down their activity of consuming hydrogen gas. Biomass and organic wastes are familiar and limitless sources for biogas production, which is also true for BioHydrogen production. However, the cow dung is initially fed to the digester because it is rich in HPM and HCM micro-organisms. Figure 1.11 shows the stage-wise processes involved in the fermentation of biomass/ organic waste during an anaerobic fermentation [51].

In the first stage, hydrolysis occurs, where the heavy carbon compounds (carbohydrates, fats, and proteins) are broken down into more minor chain carbon compounds like cellulose, sucrose, and fatty acids. The process starts when biomass/ organic waste is mixed with water. Generally, a 1:1 ratio of water to feed is considered for feeding into the digester. The overall reaction of hydrolysis is depicted in Equation (1.15),

$$nC_6H_{10}O_5 \ + \ nH_2O \ \rightarrow \ nC_6H_{12}O_6 \qquad\qquad (1.15)$$
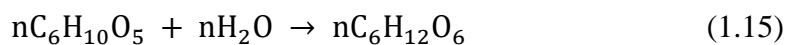
The next stage is acidogenesis. The acidogenic bacteria consume more minor chain carbon compounds (cellulose, sucrose, and fatty acids) to produce simpler compounds: volatile fatty acids, alcohols, carbon dioxide, and hydrogen. The various equations involved in the process are Equation (1.16) to Equation (1.18). Hydrogen production starts from the acidogenesis stage.

$$C_6H_{12}O_6 \rightarrow CH_3CH_2CH_2COOH + 2CO_2 + 2H_2 \qquad (1.16)$$

$$C_6H_{12}O_6 + 2H_2O \rightarrow 2CH_3COOH + 2CO_2 + 4H_2 \qquad (1.17)$$

$$C_{12}H_{22}O_{11} + 5H_2O \rightarrow 4CH_3COOH + 4CO_2 + 8H_2 \qquad (1.18)$$
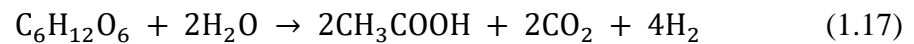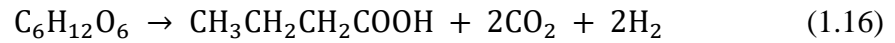
The third stage is a fundamental stage of hydrogen production. Other products like carbon dioxide, acetic acid, and ammonia are also produced, but the main focus is hydrogen production. This stage is called acetogenesis, and the bacteria involved in this stage are called acetogenic bacteria. Acetogenic bacteria consume volatile fatty acids and alcohol to produce hydrogen and carbon dioxide, as shown in Equation (1.19),

$$CH_3COOH + 2H_2O \rightarrow 4H_2 + CO_2 \qquad (1.19)$$
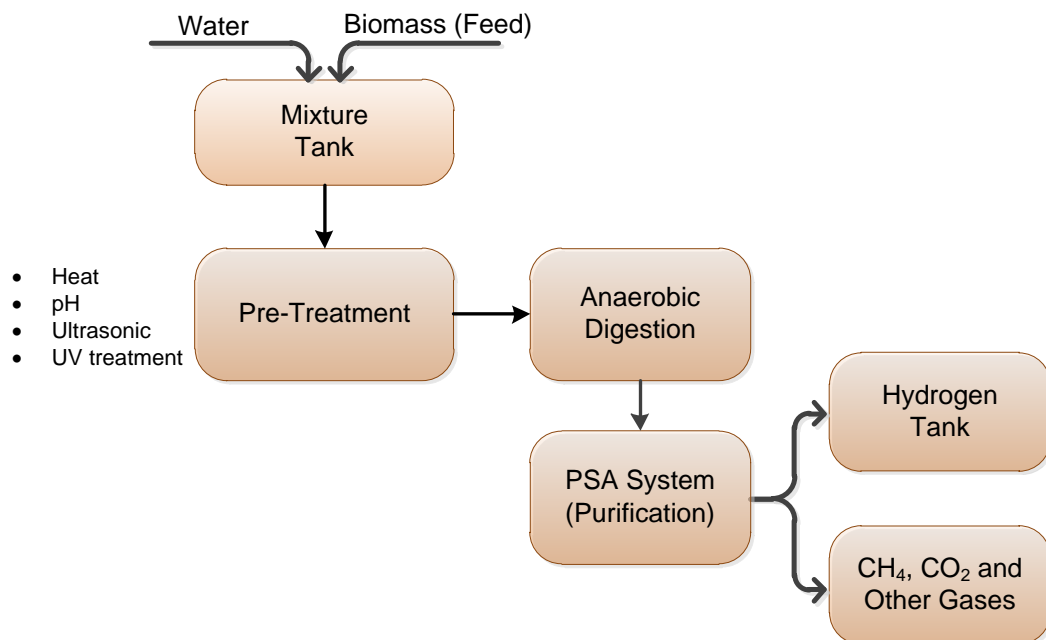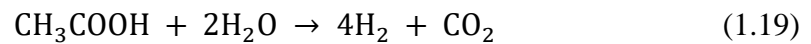
Figure 1.12. Flow chart of the anaerobic fermentation process

In the last stage, hydrogen consumption begins, and methanogenic bacteria trigger methane generation. This stage is called methanogenesis. Since the aim is to separate hydrogen as the desired product, various pre-treatment methods are performed to slow down the methanogenesis process and provide more time for hydrogen withdrawal from the digester. The flow chart of anaerobic fermentation for BioHydrogen production is depicted in Figure 1.12.

1.4.5. Plasma Reforming

The plasma reforming process is performed at low temperatures, and less expensive and bulky equipment is used. Various raw materials, like methane, methanol, ethanol, dimethyl ether, etc., are used in the plasma reforming process to produce hydrogen or H_2-rich syngas. The reactions involved in the ethanol plasma reforming are given by the dry ethanol reforming reaction Equation (1.20),

$$C_2H_5OH + CO_2 \rightarrow 3H_2 + 3CO \qquad (1.20)$$
$$\Delta H^\circ = 313.45 \text{ kJ/mol (endothermic)}$$
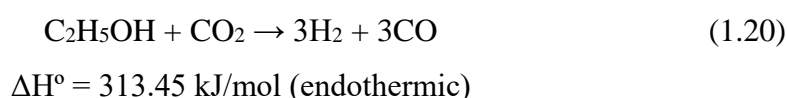
The two other reactions, Equation (1.21) and Equation (1.22), involved in the steam ethanol reforming process are,

$$C_2H_5OH + 3H_2O \rightarrow 6H_2 + 2CO_2 \qquad (1.21)$$
$$\Delta H^\circ = 174 \text{ kJ/mol (endothermic)}$$

$$C_2H_5OH + H_2O \rightarrow 4H_2 + 2CO \qquad (1.22)$$
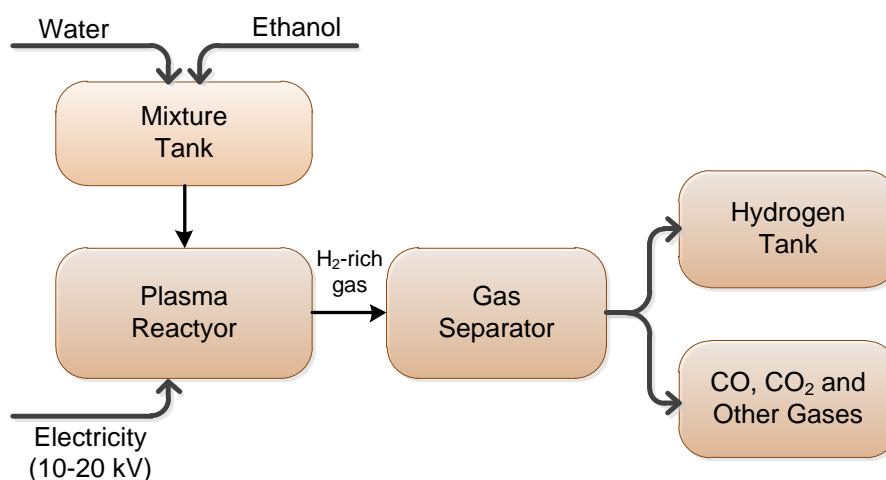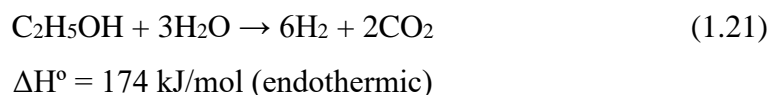
Figure 1.13. Flow chart of ethanol plasma-reforming process

The flow chart of the ethanol plasma-reforming process is shown in Figure 1.13, and a schematic diagram of a gliding plasma arc reactor with various components is shown in Figure 1.14. A high 10-20 kV voltage generates a plasma between two electrodes. This plasma contains very high temperatures, which break hydrogen from its compounds.
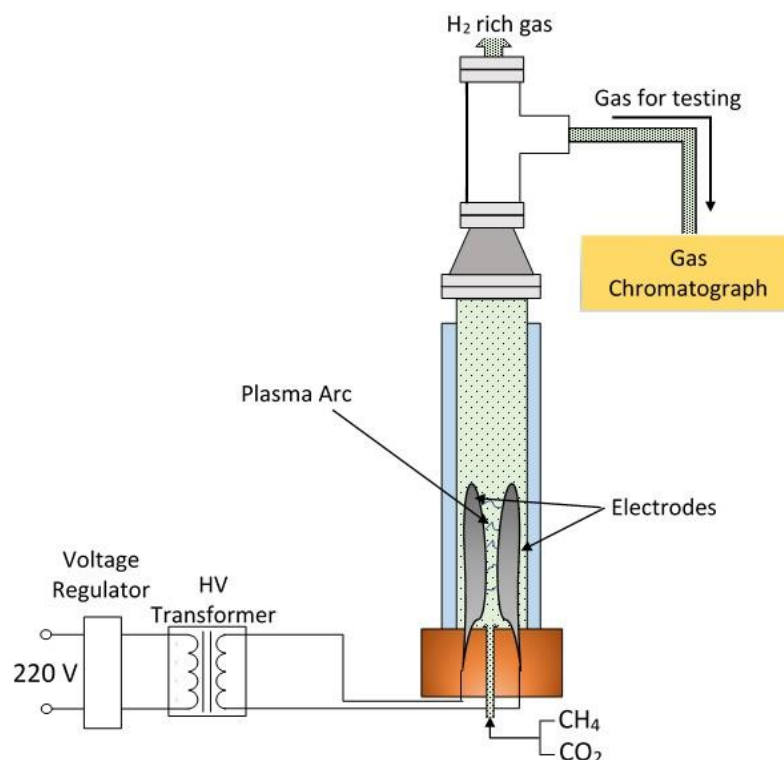
Figure 1.14. Gliding plasma arc reactor

A detailed study is performed to understand the working of various plasma reactors, raw materials, and hydrogen yield/rate. The impacts of the operating constraints on plasma gasification were discussed. Better biomass oxidation has resulted from a lower equivalence ratio (ER), which favoured hydrogen generation. Similarly, hydrogen generation is more at lesser temperatures while lower at higher steam/biomass (S/B) ratios. *Pang et al.* evaluated the functioning of the allo-thermal steam gasification and the non-thermal steam gasification of the wood particles on the hydrogen generation rate using the electrically heated drop tube reactor. Syngas composition produced using plasma-assisted gasification contains H_2 (38.5%), CO (38.4%), CO_2 (12.7%), and CH_4 (10.3%) at 760°C, respectively [52]. A 20% increase is noticed in syngas production by non-thermal plasma systems than allo-thermal

gasification. *Bulychev et al.* analyzed the acoustic plasma method in liquid decomposition at low temperatures [53]. The H_2 production rate attained is 2 L/min with a 100 mL capacity reaction chamber, and the feed rate of about 60-70% of the energy efficiency factor is achieved depending upon the feed mixture composition.

The methane plasma reforming for hydrogen generation shows that a rise in reactant temperature accelerates methane conversion, whereas the specific energy density lowers the H_2 selectivity. The influence of discharge frequency, input power, and liquid feed rate on the plasma-steam reforming of methanol along with synergistic plasma-catalyst systems describes a rise in the frequency, accelerating the methanol conversion initially and then reducing it. In contrast, 17.89% and 21.86% more methanol conversion and H_2 yield was obtained with activated catalyst than without catalyst. *Huang et al.* modified the plasma reforming system by adding a heater and varying the amplification ratio for hydrogen generation from the methanol-water mixture. Effects of increasing operating voltage and temperature showed approximately 50% upsurge in hydrogen generation [54]. In contrast, the influence of discharge power, type of carrier gas, and the moisture content of the raw material in the non-thermal arc plasma reactor show that the Gas yield is enhanced with the rise in discharge power and higher moisture content; however, air as carrier gas showed the best gas yield and H_2/CO ratio against N_2 and Ar.

Shiraishi et al. studied the performance of the Ni electrode and Ni plate on the in-liquid plasma breakdown of methanol for hydrogen generation [55]. The in-liquid plasma method achieves a hydrogen yield of 67% for methanol conversion, and the hydrogen generation rate increases by 2.3-3.5 times with the Ni porous plate placed above the electrode. *Lian et al.* examined the performance of O_2 to C ratios, steam/carbon (S/C) ratios, and specific energy input (SEI) on the oxidative methanol-reforming for onboard hydrogen generation using a gliding arc plasma reactor [56]. Methanol conversion is accelerated with the O_2 to C ratio rise, though the lesser energy efficiency is recorded with the upsurge in either the S/C ratio or SEI. In contrast, the methanol conversion of 88% and energy efficiency of 74% is achieved by an O_2/C ratio of 0.30, an S/C ratio of 0.5, and an SEI of 24 kJ/mol, respectively.

1.4.6. Advantages and Disadvantages

These days, technical advancement has led to the development of hydrogen production techniques, and they are characterized by their advantages and disadvantages for using feedstock and hydrogen generation. Before going to the various methods available for hydrogen generation, it is always better to understand the different properties of hydrogen. It will help develop better techniques for generating, storing, and utilizing hydrogen from a particular feedstock and the available conditions. A few advantages and disadvantages of various hydrogen-producing processes are illustrated: -

➢ Steam Methane Reforming (SMR) and biomass gasification are both energy-consuming thermal processes, where SMR requires 700-1200℃ and gasification requires 500-650℃ temperature for H_2 production.

➢ Although the H_2 yield from SMR and gasification techniques without a catalyst is low, ranging between 45-72%, which could be raised to above 90% using a catalyst like Ni-based Al_2O_3.

➢ Similarly, electrolysis and plasma reforming are electrical processes that generate about 95% (plasma reforming) to 99% (electrolysis) high-purity grade hydrogen at less than 100 ℃.

➢ Electrical processes are cleaner; however, the H_2 production rate is about 2 L/min, which is comparatively lower than thermal processes.

➢ High CO_2 emissions are other drawbacks of SMR and gasification.

➢ Electrolysis also has problems like membrane corrosion, shorter life, and expensive catalyst requirements.

➢ Anaerobic fermentation (Biohydrogen) is a bacterium-based process; therefore, bacterium sensitivity must be examined regularly.

All the processes required technical advancement to reduce the cost of hydrogen with enhanced hydrogen yield at a higher purity grade. Therefore, novel technologies must be established for cost-effectively producing hydrogen with advances in the IC engines for the best possible utilization and, thus, minimizing the environmental impacts by eliminating harmful emissions.

1.5. Application in Fuel Cell

A fuel cell converts chemical energy into electricity in a chemical reaction with oxygen (or any oxidizing substance). A fuel cell comprises an anode (negative), a cathode (positive), and an electrolyte. Fuel (hydrogen) is supplied to the anode and air to the cathode. Consider fuel cells like batteries drain over time; fuel cells don't, and neither requires recharging as batteries do. As long as fuel is consumed, it will keep producing electricity and heat. The different types of fuel cells are:

➢ Proton exchange membrane fuel cell (PEMFC)

➢ Alkaline fuel cell (AFC)

➢ Phosphoric acid fuel cell (PAFC)

➢ Molten carbonate fuel cell (MCFC)

➢ Solid oxide fuel cell (SOFC)

Among all these fuel cells, PEMFC is widely used for power generation

1.5.1. Working of Fuel Cell
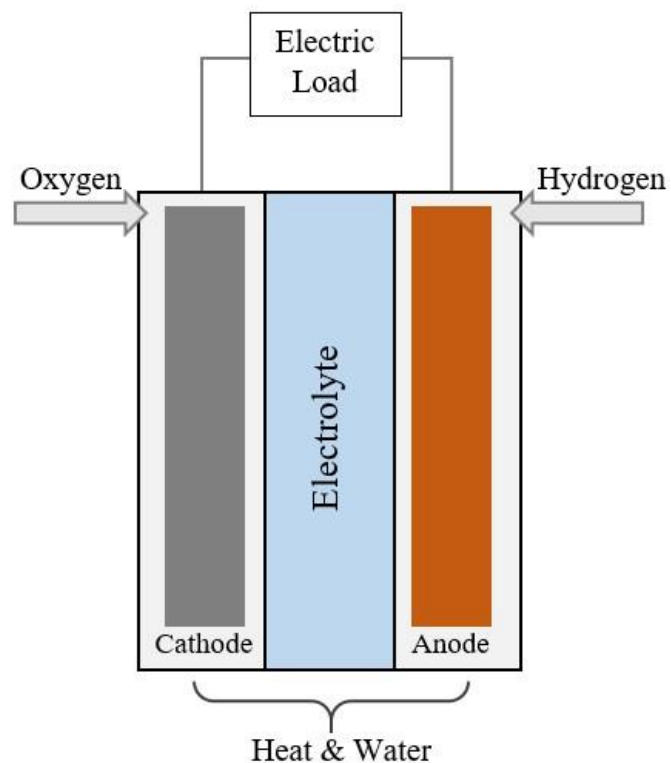
Figure 1.15. Fuel Cell

A fuel cell consists of an anode and cathode enclosed in a container filled with an electrolyte (see Figure 1.15). An external circuit is connected to both anode and cathode for electron transportation. Hydrogen (purity of 99.99%) is supplied to the anode, which oxidizes to generate H+ ions and e- (electrons). Whereas oxygen is provided to the cathode, where H+ ions react with oxygen to produce water and a small amount of heat is also generated. The electromotive force developed at the electrodes is the cell voltage. Thus, an electric current will be available at the external circuit when hydrogen and oxygen are supplied to the fuel cell, depending on the flow rate and chemical activities. The current will be available as long as the fuels are provided for the chemical activity at the electrodes and electrolytes of a fuel cell.

1.5.2. Advantages of Fuel Cells

There are many advantages associated with the utilization of hydrogen in fuel cells. A few benefits of hydrogen fuel cells are as follows:

- ❖ **Energy efficient**: Fuel cells can operate on an efficiency level of more than 80% [57] compared to internal combustion engines, with an efficiency level of around 25%. Power plants also don't have such high efficiency. Their efficiency levels are approximately 35%.

- ❖ Fuel cell units have a **faster charging rate** than internal combustion engine vehicles, making them convenient and flexible.

- ❖ **Easy to store**: Unlike batteries, hydrogen fuel cells don't drain out over time, which means they can be stored for years and years but still work fine.

- ❖ **Zero emissions**: The by-products produced are water and heat; this technology will considerably reduce greenhouse emissions from fossil fuel-based vehicles.

- ❖ **Minimum noise pollution**: Hydrogen-powered vehicles are noiseless compared to internal combustion engines due to the absence of moving parts.

- ❖ **Easy accessibility to fuel cells**: Renewable power sources depend on the right weather, conditions, or geography.

- ❖ High reliability

- ❖ Easy installation and operation

- ❖ Improved quality of the environment

1.5.3. Disadvantages of Fuel Cells

Similarly, there are many disadvantages for hydrogen fuel cells that restrict their usage in the large-scale production of electricity. These are as follows:

❖ **Expense process**: Compared to other forms of energy, hydrogen extraction is expensive, making fuel cells expensive.

❖ **Dependent on renewables**: to power the electrolysis process, one needs energy, and for a truly green solution, this energy has to come from renewable sources like solar and wind.

❖ **Metal embrittlement**: Hydrogen embrittlement leads to corrosion of metals, which is a challenge for its storage and transportation.

❖ **Infrastructure development is still a work in progress**: Limited infrastructure is available currently globally, further adding cost to its transportation. A more viable solution is creating a production plant on site in case large quantities are required.

❖ **Fuel storage**: At room temperature, hydrogen storage is complex due to its gaseous nature.

❖ **Durability**: Fuel cells and electric motors are comparatively less durable than petrol and diesel engines.

❖ **Cost**: Currently, fuel cell technology is high-priced.

❖ Most hydrogen-producing methods release carbon dioxide and other pollutants into the atmosphere.

1.6. Simulation-Modelling of Reactors

Simulation of a chemical plant requires developing models for different processes during plant operation. Only a few works are available for methanol reforming; however, other sources for hydrogen production, like glycerol, biomass, etc., have similar working and influencing parameters. *Unlu* and *Hilmioglu* investigated glycerol steam reforming in an Aspen Plus simulator for hydrogen production [58]. The simulation showed that the reaction temperature directly impacts the hydrogen concentration, while the reactor pressure has adverse effects. The study defined a 9:1 glycerol ratio and 1 atm. pressure at 500°C as the optimum condition for

hydrogen production. *Mohammadidoust* and *Qmidvar* simulated the model developed for wheat straw biomass gasification at supercritical conditions [59]. The model attained a 32.7 kg/h hydrogen production rate at 700°C with 2000 kg/h and 1500 kg/h of water and biomass flow rate. *Tavares et al.* determined the influence of gasification temperature and steam-to-biomass ratio in hydrogen production using Aspen Plus [60]. The simulation showed a high hydrogen content in syngas at higher temperature ranges. *Ye et al.* also developed a model for simulating the influencing parameters in the hydrogen production process. Hydrogen yield increases with the rise in operating temperature and steam-to-carbon ratio [61]. Therefore, the operating temperature and feed ratio are the two most influencing parameters in hydrogen production.

Modelling and simulating various chemical plant components also help determine the impacts of the different process parameters and cost considerations. *Ishaq* and *Dincer* designed a biomass and solar energy-based model for hydrogen production, where the overall system efficiency achieved is 29.9%, while the exergy efficiency is 31.5%, respectively [62]. *Bassyouni et al.* simulated a downdraft gasifier. The authors used date palm waste to produce syngas that contain a hydrogen content of 56.27%, while the other gases are carbon monoxide, carbon dioxide, and methane [63]. *Sanchez et al.* developed a model for an alkaline electrolysis system. The system simulation shows a maximum overall efficiency of 58% at 5 bar and 80 °C of optimum conditions [64]. In contrast, *Chehade et al.* simulated and optimized natural gas steam-reforming plants for hydrogen production. The results show 77.5% less energy consumption while optimizing the process parameters [65].

1.7. Optimization Method

Parameter optimization helps determine the main influencing parameters and achieve optimal results. *Shuang et al.* used a mixed design to optimize hydrogen yield. The authors used a mixture of agricultural waste and obtained an optimized hydrogen yield of 21.0mL/g [66]. In contrast, *Liu et al.* optimized process parameters in biohydrogen plants and achieved a 30.0 mL/g higher hydrogen yield at optimal conditions [67]. *Bi et al.* performed the parameter optimization analysis of a hydrogen liquefaction process. The authors observed a 22.06% drop in specific energy

consumption and a 33.58% rise in the coefficient of performance [68]. Similarly, *Cao et al.* optimized reaction parameters in response surface methodology (RSM) and observed the interactive effects of parameters on ethanol reforming [69]. The results show that the ethanol-to-water molar ratio is the most influencing parameter, while the discharge power and total flow rate are comparatively lesser influencing parameters. Methanol has very close properties to ethanol in the alcohol group; therefore, similar parameters may be considered for the methanol–water-reforming process. Meanwhile, studying the various research articles on alcohol–water-reforming observed that reaction temperature, feed molar ratio, reactor pressure, and reactor type affect the hydrogen production rate.

CHAPTER 2

LITERATURE REVIEW

2.1. Overview

Hydrogen is an energy carrier with a very high energy density (>119 MJ/kg). Pure hydrogen is barely available; thus, it requires extraction from its compounds. Steam reforming and water electrolysis are commercially viable technologies for hydrogen production from water, alcohols, methane, and other hydrocarbons; however, both processes are energy-intensive. The study aims to understand the methane and ethanol-water mixture pathway to generate hydrogen molecules. The various intermediate species (CH_X, CH_2O, CH_3CHO) are generated before decomposing methane/ethanol into hydrogen radicals, which later combine to form hydrogen molecules. The study further discusses the various operating parameters involved in plasma reforming reactors. The dielectric barrier discharge reactor can be operated with or without a catalyst; feed flow rate and discharge power are the most influencing parameters. In a pulsed plasma reactor, feed flow rate, electrode velocity, and gap are the main factors that can raise methane conversion (40-60%). While the gliding arc plasma reactor can generate up to 50% hydrogen yield at optimized values of oxygen/carbon ratio and residence time, the hydrogen yield in the microwave plasma reactor is affected by flow rate and feed concentration.

2.2. Steam Reforming

Steam reforming is a well-established and broadly used thermal process for large-scale hydrogen generation, with over 45% of the total hydrogen generation globally. The steam reforming process did not require oxygen, and while the greenhouse gases could be used as the reactants, catalysts are recommended to lower the temperature requirement. The findings of various studies are depicted in Table 2.1.

Table 2.1. Studies on the steam reforming process for H_2 production

S. No.	Author's Name	Relevant Findings
1.	*Gao et al.* (2015) [70]	• At 700°C, H_2 yield 105.28 g-H_2/kg-tar was achieved. • H_2 content was enhanced from 41.75% to 63.13% with 0-4 steam/carbon. • H_2 yield dropped to 7.97 g-H_2/kg-tar from 105.28 g-H_2/kg-tar for equivalence ratio from 0 to 4.
2.	*Xie et al.* (2015) [71]	• With the rise in the temperature from 550-750°C, the CO_2 adsorption efficiency was enhanced. • Beyond 750°C, the efficiency reduced considerably. • The optimal H_2 yield of 83.8% and H_2 (CO + CH_4) yield of 94.1% was achieved with the steam/carbon ratio 9, space velocity 0.23 h^{-1} at 700°C.
3.	*Pu et al.* (2019) [72]	• A catalyst with 0.05 molar ratio (Sc/Zn) generated 140 µmol/ g-s H_2 at 300°C. • H_2 yield exhibited a minute reduction with the rise in temperature for different Sc/Zn molar ratios. • Catalyst activity and stability over the 220-600°C temperature were achieved with the optimized Sc/Zn molar ratio.
4.	*Ji et al.* (2018) [73]	• CH_4 conversion from an HTM-based indirect heating method was 81.4-89.4% higher than conventional direct heating. • H_2 mol% was reduced with increasing reaction temperature. • SMR reactor with HTM for the indirect heat utilization was less effective under the design consideration.
5.	*Zheng et al.* (2019) [74]	• Enlargement in the height of the fin upgraded the recovery efficiency from 96.3 % for 34 mm to 98.4 % for 46 mm. • Enhancement in the recovery efficiency was noticed with the expansion of fin root width from 3 mm, giving 97.1% efficiency, to 6 mm, giving 98.1% efficiency.
6.	*Kim et al.* (2018) [75]	• The membrane reactor attained 82% of the methane conversion with a 912 kPa pressure difference at 600°C. • With the pressure difference of 1013 kPa and space velocity of 2000 h^{-1}, the hydrogen generation rate and H_2 purity obtained was 0.18 Nm^3/h and 97%.
7.	*Yoo et al.* (2017) [25]	• Augmented Ni dispersion and high methane adsorption capacity exhibited high natural gas conversion and H_2 yield. • The best catalyst performance with the maximum Ni dispersion and CH_4 adsorption was obtained from the 0.25 BA-Ni/Al_2O_3 catalyst.
8.	*Yang et al.* (2016) [76]	• The obligatory reformer diameter and length to charge 167.8 g of catalyst necessary for 1 Nm^3/h hydrogen generation rate were 1 inch and 613 mm. • Methane conversion and H_2 generation rates were 98.0% and 1.97 Nm^3/h at 745°C with 20 wt.% Ni/γ-Al_2O_3 and 10000 h^{-1} space velocity.
9.	*Hou et al.* (2015) [77]	• The vital role of the active metal and support was observed in the activity and stability of the catalyst. • Results revealed that the reforming reaction was mainly operated at high temperatures between 500°C and 800°C.
10.	*Song et al.* (2015) [78]	• An upsurge in the H_2 yield was observed at higher temperatures while the pressure reduction resulted in a lower H_2 yield. • Energy consumption was reduced from 102.12 kJ/mol-H_2 for conventional technology to 40.33 kJ/ mol-H_2 for heat-integrated technology.

Hou et al. discussed the fundamentals of hydrogen generation using catalysts and supporting material in ethanol's steam reforming [77]. The study described the active metal's vital role and support in the catalytic reforming process's activity and stability. The results revealed that the reforming reaction was mainly operated at high temperatures between 500°C and 800°C. Thus, the growth of the novel catalyst and technique structure considerably reduced the steam reforming's high-temperature requirements.

Yoo et al. evaluated the optimal molar ratio of butyric acid (BA)/Ni to support Ni/Al_2O_3 catalyst in natural gas steam reforming. The augmented Ni dispersion and high methane adsorption capacity exhibited enhanced natural gas conversion and high H_2 yield [25]. However, the best catalyst performance with the maximum Ni dispersion and CH_4 adsorption was obtained from the 0.25 $BA-Ni/Al_2O_3$ catalyst. Thus, adding butyric acid improved the catalytic performance of the natural gas steam reforming.

Kim et al. tested the performance of the Pd-based composite membrane reactor (CMR) with Ru/Al_2O_3 catalyst at different transmembrane pressure differences and space velocity for hydrogen generation. The membrane reactor attained about 82% of the methane conversion with a 912 kPa pressure difference at 550°C [75]. With the pressure difference of 1013 kPa and space velocity of 2000 h^{-1}, the hydrogen generation and H_2 purity rate obtained was 0.18 Nm^3/h and about 97%, respectively. Therefore, the Pd-based CMR resulted in resourceful hydrogen generation from steam methane reforming.

Yang et al. designed a compact stand-alone and self-sustaining type reformer with catalysts 15 wt.% and 20 wt.% $Ni/\gamma-Al_2O_3$ for hydrogen generation. The obligatory reformer diameter and length to charge 167.8 g of catalyst necessary for 1 Nm^3/h hydrogen generation rate were 1 inch and 613 mm [76]. The methane conversion and hydrogen generation rates were 98% and 1.97 Nm^3/h at 745 °C with 20 wt.% $Ni/\gamma-Al_2O_3$ and 10000 h^{-1} space velocity of reactants, respectively. Therefore, the steam methane reforming was efficiently executed with high reactant space velocity in the reformer for a high H_2 yield.

Zheng et al. determined the effects of the fin dimensions in the waste heat transfer on methane steam reforming for hydrogen generation. The enlargement in the fin's height upgraded the recovery efficiency from 96.3% for 34 mm to 98.4% for 46 mm [74]. Similarly, the enhancement in the recovery efficiency was noticed with the expansion of fin root width from 3 mm (97.1% efficiency) to 6 mm (98.1% efficiency). Therefore, the improvement in the recovery efficiency from the waste heat resulted in higher steam production, thus boosting the system's hydrogen generation capacity, thus boosting the system's hydrogen generation capacity.

Song et al. analyzed the heat integration technology in lowering the energy consumption of the steam methane reforming (SMR) and pressure swing adsorption (PSA) for the generation of hydrogen [78]. The upsurge in the H_2 yield was observed with the temperature rise, while the pressure reduction resulted in a lowered H_2 yield. Meanwhile, the energy consumption was reduced from 102.12 kJ/mol H_2 for conventional technology to 40.33 kJ/mol H_2 for heat-integrated technology, respectively. Therefore, using the heat integration system in the SMR-PSA process revived about 60.5% of the total energy compared to the conventional method.

Wang and *Wang* inspected the impact of the inlet temperature and space velocity of catalyst $Cu/ZnO/Al_2O_3$ sealed in a micro-reactor for hydrogen generation. The growing space velocity condensed the methanol conversion, while the hydrogen generation rate initially augmented and declined [79]. Thus, the reactor touched the maximum hydrogen production rate of 193.79 ml/ min with 1.61 h^{-1} space velocity. The raised reactor inlet temperature accelerated the H_2 generation in the methanol SR.

Pu et al. inspected the effects of Cu/Sc_2O_3-ZnO catalysts at different temperatures in the methanol-reforming for hydrogen generation. Even for incomplete methanol conversion, the catalyst with Sc/Zn molar ratio of 0.05 generated the best H_2 yield of 140 µmol/g-s at 300°C [72]. Consequently, the H_2 yield exhibited a minute reduction with a further rise in temperature for different Sc/Zn molar ratios after attaining the peak value. Thus, the catalyst activity and stability over the 220-600°C temperature range were accomplished with the optimized Sc/Zn molar ratio for hydrogen generation.

Lu et al. explored the impacts of the Lanthanum (La) additive in Ni-based catalysts and Ni's loading in methanol steam reforming [27]. The Ni/Al_2O_3 with added La showed higher methanol conversion and H_2 selectivity with the reduced CO selectivity below 350℃ compared to Ni/Al_2O_3. However, the Ni loading above 10 wt.% lowered both the conversion of methanol and the H_2 selectivity. Therefore, adding La to the Ni-based catalyst produced H_2 at lower temperatures.

Zhang et al. research the effects of TiO_2 and CeO_2 support over the Au-based catalyst in the steam-reforming alcohol (methanol). All the catalysts except Au/TiO_2 attained higher H_2 selectivity of more than 95% at 250-350℃. Beyond 530℃, a decline in H_2 selectivity because of the WGSR [80]. The best H_2 selectivity was accomplished with the Au-Ti-Ce/Na-ABen catalyst among all the catalysts.

Gonzalez-Gil et al. analyzed the effects of the $V-Ni/Al_2O_3$ catalysts on dimethyl ether steam reforming (DME-SR) in comparison with methanol steam reforming (MeOH-SR). The MeOH-SR and DME-SR reactions showed the direct role of the V-Ni catalysts [81]. The stoichiometric H_2/CO_2 ratio was reached by the MeOH-SR using 3V-Ni at 400℃. However, the DME-SR happened in two steps, imparting H_2 selectivity of 60-70% with 3V-Ni at 500℃ maintained for 4.5 h.

Ji et al. investigated the performance of the indirect heating method in the steam methane reforming (SMR) and deionized water being the heat transfer medium (HTM). Methanol conversion from an HTM-based indirect heating method was 81.4-89.4% higher than the conventional direct heating [73]. However, the H_2 mol% was reduced with increasing reaction temperature. However, the SMR reactor with HTM for the indirect heat utilization was less effective under the design consideration than the direct heating method to produce H_2-rich syngas.

Han et al. discussed the consequences of the Ca/Al molar ratio in the ethanol steam-reforming with $Co/CaO-Al_2O_3$ xerogel catalyst. The enlarged surface area due to Co improved the H_2 yield significantly [26]. In contrast, the best catalytic performance was confirmed with $Co/0.5 Cao-Al_2O_3$. The low acidity and high surface area were considered the critical catalyst factors for ethanol steam-reforming. Thus, the optimal Ca/Al molar ratio with Co addition governed the effective ethanol SR.

Chen et al. analyzed the operating parameters in the two-stage reaction process in ethanol steam-reforming with Ni/Al_2O_3 catalyst and water-gas shift reaction using Fe/Cr_2O_3 catalyst. The two-stage process for the maximum H_2 yield of 4.26 mol/mol-ethanol was approximately 73% higher than the single-stage process with the unique or noble metal catalysts [82]. In contrast, the concentrations of CO_2 and CO in the syngas computed were 21.77% and 0.81%, respectively. Thus, the optimized two-stage process resulted in a higher H_2 yield with reduced CO formation, though the CO_2 concentration was enhanced.

Sepehri et al. evaluated the impacts of Ni loading in Ni/CeO_2 catalysts on the catalytic performance in the autothermal reactor for hydrogen generation [83]. The highest CH_4 conversion and H_2 selectivity were measured with 20 Ni/CeO_2 and 25 Ni/CeO_2 catalysts. Further, the Ni/CeO_2 catalyst qualified the thermal stability test at 700°C for 20 h. Thus, the higher Ni loading for the Ni/CeO_2 catalyst leads to better hydrogen selectivity for autothermal methane reforming.

Zhang et al. examined the implementation of desulfurized Jet-A fuel with $Rh/NiO/K$-La-Ce-Al-O_X catalyst in the autothermal reforming (ATR) hydrogen generation. The influence of parameters like temperature, H_2O to C, and O_2 to C molar ratios was analyzed on the reaction equilibrium in the ATR [84]. The highest H_2 yield of 143.84% and the energy efficiency of 64.74% were attained with 2.5 and 0.5 molar ratios of H_2O to C and O_2 to C at 696.2°C feeding temperature. However, the product gas composition was computed as 29.2% H_2, 0.3% O_2, 43.9% N_2, 0.5% CH_4, 9.1% CO and 14.2% CO_2, respectively.

Chang and *Lee* compared the $Ni/porous$-CeO_2 coated cordierite honeycomb reactor for hydrogen generation with the packed bed reactor. The biogas reforming and methane steam reforming at 900°C and 5 h^{-1} space velocity measured the upsurge in the H_2 yield to 72.52% and 41.29%, whereas the methane conversion enhanced to 22.24% and 43.12%, respectively [24]. The temperature above 700°C and a space velocity of 3 h^{-1} yielded an 80% higher conversion. Hence, higher temperatures resulted in more hydrogen generation.

Chen et al. studied the different methods to activate the biochar from rice husk pyrolysis and then studied Ni-based catalysts' performance for steam-reforming of acetic acid. Notable catalyst performance was obtained from the Ni-supported KOH-HNO$_3$ activated char [85]. However, the carbon conversion and H$_2$ yield of 91.2% and 71.2% were achieved with a steam/carbon ratio 2.5 for a space velocity of 10 h^{-1} at 700°C. Thus, the KOH-HNO$_3$-activated biochar-based catalyst was efficient in the steam-reforming of bio-oil.

Xie et al. optimized the reaction parameters of bio-oil steam reforming in continuous CO$_2$ capture using the Ce-Ni/Co catalyst for hydrogen generation. With the rise in the temperature from 550-750°C, the CO$_2$ adsorption efficiency was enhanced, while beyond 750°C, the efficiency reduced considerably [71]. Although the optimal H$_2$ yield of 83.8% and H$_2$ (+ CO + CH$_4$) yield of 94.1% was reached with the steam/carbon ratio 9, space velocity 0.23 h^{-1} at 700°C. Thus, the temperature at 700°C and the steam-to-carbon ratio of 9 represented the optimal parameters for generating hydrogen.

Gao et al. determined the impacts of the performance parameters in the steam-reforming of tar using NiO/ceramic foam catalysts. At the temperature of 700°C, the peak H$_2$ yield of 105.28 g-H$_2$/kg-tar was achieved [70]. However, the H$_2$ content was enhanced from 41.75% to 63.13% with the steam/carbon ratio of 0-4. The H$_2$ yield dropped sharply from 105.28 g-H$_2$/kg-tar to 7.97 g-H$_2$/kg-tar for equivalence ratio from 0 to 4. Thus, the maximum H$_2$ yield was obtained by optimizing the process parameters.

Macedo et al. compared the traditional reactor (TR) and membrane reactor (MR) for the performance parameters of glycerol steam reforming to generate hydrogen. The highest H$_2$ yield was obtained with elevated temperatures, feed ratios, and pressures in the MR, while the lower pressure favoured TR's H$_2$ yield [86]. With the feed ratio of 12 and 200 kPa pressure, the TR generated 5.09 mol-H$_2$/mol-glycerol at 700°C, whereas the MR generated 5.87 mol-H$_2$/mol-glycerol at 500°C with 15 μm membrane thickness. Hence, the hydrogen generation's temperature in the MR was 200 K less than the TR.

Rabbani and *Dincer* investigated the combined power plant's operating constraints' impact on optimal hydrogen generation. The upsurge in the hydrogen generation was observed with the rise in steam/glycerol (S/G) ratio and combustion temperature, while the rising reformer pressure dropped the hydrogen generation [30]. The simulation showed that the optimal parameters for hydrogen generation were the S/G ratio of 3, reforming pressure of 100 kPa, the compressor pressure ratio of 9, and combustion temperature at 707°C, respectively. Thus, the operating parameters were optimized in the glycerol steam reforming.

Xie et al. analyzed the blast furnace slag's heat recovery in bio-oil steam-reforming. The analysis showed that the H_2 yield initially accelerated and then smoothed with the rise in the temperature and steam/carbon (S/C) ratio [87]. Consequently, the H_2 yield and the H_2 concentration delivered were 1.725 Nm^3/kg (88.8%) and 68.7%, respectively, for the S/C ratio 8 at 700°C. As a result, the sensible heat recovery utilized in the blast furnace manufactured 5-million-ton pig iron and managed 2.55×10^8 Nm^3 of H_2 and 4.35×10^4 tons of bio-oil annually.

Casanovas et al. determined the temperature and fed on the noble metals or Ni over La-stabilized CeO_2 catalysts in the steam-reforming using olive mill wastewater (OMW). The trend of the noble metals and Ni over CeLa hydrogen generation selectivity of product gas and stability were Pt > Rh > Ru >> Ni > Pd. The catalyst Pt/CeLa with 1 wt.% w/w delivered about 40 mL-H_2/mL-OMW at 700°C and for 16000 h^{-1} space velocity, respectively [29]. Thus, the Pt and Rh-based catalyst systems are the finest catalysts for hydrogen generation and product gas selectivity for 24 h of stability.

2.3. Electrolysis

Splitting or breaking down water molecules into hydrogen and oxygen molecules through electricity is termed electrolysis. Electrolysis is a well-established and broadly used process after the steam reforming process. Instant hydrogen generation is achieved by electrolysis of water at a smaller scale. A few studies based on the electrolysis process for hydrogen production are illustrated in Table 2.2.

Table 2.2. Studies based on electrolysis for H_2 production

S. No.	Author's Name	Relevant Findings
1.	*Villagra* and *Millet* (2019) [43]	• PEM electrolysis cells showed optimum current density of 2.5 A/cm^2. • I-V performance of PFSA polymer membrane with 50-200 µm thickness was measured at 10 A/cm^2. • A 2.5-3.0 V cell voltage with low cell efficiencies of the PFSA materials was measured for less than 100 µm thickness.
2.	*Guban et al.* (2019) [47]	• Alkaline electrolysis (AE) was an advanced fuel cell with a relatively simple setup and easy scale-up. • Proton exchange membrane (PEM) measured higher efficiency. • PEM required desalinized and demineralized feed water. • Solid oxide electrolysis cell operates at 700-900°C and generates H_2 at 80% efficiency without any noble catalyst.
3.	*Pushkareva et al.* (2019) [88]	• High performance for H_2 generation was computed for AEMs with up to 3 A/ cm current density at 60°C and 0.5-1.0M KOH concentration. • DI water was not appropriate for H_2 generation due to the sharp rise in the membrane resistance.
4.	*Dobo et al.* (2017) [89]	• About 4620 individual experiments were executed with computerized measurement and data procurement for efficiency loss. • Frequency, offset, and ripple factors influenced the efficiency loss in the non-steady DC applications. • Sort of the waveform showed no effect on the efficiency loss.
5.	*Chakik et al.* (2017) [41]	• Amperage, voltage, and electrolyte concentration showed similar impacts on hydrogen generation. • Rise in amperage, voltage, and electrolyte concentration augmented the H_2 yield irrespective of cathode material. • The iron composition in ZnFe alloy improved the H_2 yield, while the copper composition reduced the H_2 yield.
6.	*Manolova et al.*(2015) [90]	• The cathode was electrodeposited with porous current collectors to acquire new cross-linked AEM for high ionic conductivity. • The sol-gel method to coat the anode proved unsuitable for covering the stainless steel non-woven fabrics. • Improved chemical stability with the original membrane was attained in the highly alkaline environment.
7.	*Kim et al.* (2015) [91]	• A current of 100 A was generated at 80°C by the electrodes of 200 cm^2 surface area electrolyzer. • The stack delivered a uniform total current of 80 A for a non-stop operation of 400 hours. • Electrolyzer with the stack generated H_2 and O_2 at 99% and 98% purity.
8.	*Lamy* (2016) [92]	• Lower-temperature PEMEC exhibited up to 75% energy efficiency at 80°C and 1 A/cm^2. • High-temperature SOEC oscillated between 50-70% energy efficiency at 80°C and 1 A/cm^2.
9.	*AlZahrani* and *Dincer* (2018) [93]	• SOE system accomplished 85.15% energy & 83.14% exergy efficiency. • With 1 MWe power input and 248 kg/h of the water consumption rate, the SOE system generated H_2 and O_2 at 27.75 kg/h and 220.2 kg/h.
10.	*Ehteshami et al.* (2016) [94]	• Current density increases with operating potential while decreasing along the PEM cell length. • The highest operating potential of the PEM cell improved the production ratio and enhanced the H_2 generation rate. • Optimal cell potential (0.94 V) from the cell with membrane Nafion 117 achieved a 1.5 cm^3/min-cm^2 H_2 generation rate.

Dobo and *Palotas* analyzed the effects of the electrical current fluctuation on the water-splitting efficiency of the alkaline water electrolysis. About 4620 individual experiments were carried out, and a computerized measurement and data procurement system was constructed for the efficiency loss [89]. The frequency, offset, and ripple factors were the parameters that influenced the efficiency loss in the non-steady DC applications. At the same time, the sort of waveform showed no effect on the efficiency loss.

Manolova et al. demonstrated the different material substrates for the electrochemical decomposition of the various structured alloys, the alkaline anion exchange membrane (AEM) production, and the newly developed current collectors in the membrane electrode assembly [90]. The cathode was electrodeposited with porous current collectors to acquire new cross-linked AEM for high ionic conductivity. The sol-gel method was used to coat the anode and was proved unsuitable for covering the stainless steel non-woven fabrics. The improved chemical stability with the original membrane was attained in the highly alkaline environment.

Cardoso et al. evaluated the performance of Nickel-rare earth (Ni-RE) metal electrodes on the hydrogen evolution reaction (HER) in 8M potassium hydroxide solution at temperatures ranging from 25°C to 85°C [95]. Ni-dysprosium (Ni-Dy) and Ni-samarium (Ni-Sm) alloys were prepared with 5 wt.% and 10 wt.%. The activation energy of the Ni-RE alloy electrodes was calculated between 47-71 kJ/mol for HER. Consequently, the performance of the Ni-Sm alloys was better at room temperature, while the Ni-Dy alloys performed well at high temperatures.

Pushkareva et al. experimentally compared the various anion exchange membranes (AEMs) for the hydrogen generation with deionized (DI) water at temperatures 40°C, 50°C, and 60°C, and KOH concentrations of 0.1M, 0.5M, and 1.0M, respectively [88]. The high performance for hydrogen generation was computed for all AEMs with up to 3 A/cm^2 current density at 60°C and 0.5-1.0M KOH concentration. However, DI water was not appropriate for hydrogen generation due to the sharp rise in membrane resistance. Thus, the AEM electrolysis technology obtained the H$_2$ concentration in oxygen outflow with the high safety hydrogen flux.

Chakik et al. investigated the influences of the operating parameters on hydrogen generation volume by alkaline water electrolysis. The amperage, voltage, and electrolyte concentration showed similar impacts on hydrogen generation [41]. The rise in amperage, voltage, and electrolyte concentration augmented the hydrogen generation irrespective of the cathode material used. Consequently, the iron composition in the ZnFe alloy improved the hydrogen generation, whereas the copper composition in the ZnFe alloy reduced the hydrogen generation. Thus, the overall higher hydrogen generation was obtained by Zn95%Cr5% and Zn90%Cr10% electrodes over the range of operating parameters.

Kim et al. developed a 26-cell nickel (Ni) stack merged with 52 Ni electrodes, polymer separators, and a lightweight gasket frame for alkaline water electrolysis. The current of 100 A was generated at 80°C by 200 cm^2 surface area electrolyzer electrodes [91]. The stack delivered the uniform total current of 80 A for a non-stop operation of 400 hours. Subsequently, the electrolyzer with the stack generated hydrogen and oxygen with a purity level of 99% and 98%, respectively.

Huang et al. designed a hybrid system of 30 kW for water electrolysis during day and night. The system consisted of a 100 m^2 photovoltaic system of 18 kW and a wind system of 12 kW to produce 25 kg of hydrogen [96]. The system simulation showed that the current density of 100 mA/cm^2 produced 25 kg of hydrogen in the shortest period of 49.2 hours at 60°C. Thus, the decentralized hybrid renewable energy system generated the required power output for water electrolysis to generate H_2 for the fuel cell.

Palhares et al. fabricated a cylindrical acrylic electrolytic cell with 304 stainless steel electrodes to generate hydrogen using a photovoltaic system of 20 W. The experiments were performed for three consecutive days. The results revealed that the hydrogen generation for day 1, day 2, and day 3 was 1.82 L, 1.65 L, and 2.00 L at an average solar irradiance of 755, 659, and 800 W/m^2, respectively [97]. In contrast, the overall efficiency ranged from 1.13-1.15%. Also, the electrical current of the system was affected by solar irradiance; thus, a slight variation in irradiance influenced the hydrogen generation rate drastically.

Bidin et al. demonstrated the effects of sunlight intensity on water splitting for hydrogen generation. The stronger electric field increases surface tension, breaking the hydrogen bond or water splitting [44]. The results showed that the collimated sunlight triggered the hydrogen generation by 53% higher than 31% by conventional light and 16% by dark field. Thus, the collimated daylight exhibited extraordinary potential for optimum hydrogen generation compared to the conventional and dark fields.

Dukic designed a coupled system of water electrolysis and solar photovoltaic (PV) system for hydrogen generation and named it the PVH_2 system. The efficiency of the PVH_2 system coupled with a 60 W electrolyzer and a 100 W PV system was 77.06% without CO_2 emissions [46]. The controlled cooling of the electrolyte at the inlet of the electrolyzer noticeably enhanced the system's efficiency. Thus, the optimal PVH_2 system was a simple, cheaper, reliable, and more effective method for hydrogen generation without CO_2 emissions.

Rabady and *Kenaan* used the hybrid thermophotovoltaic (TPV) water electrolysis for hydrogen generation by the optimal power splitting of concentrated solar radiation [98]. The results showed an 18% effectiveness of the optimal power spectral shaping scheme compared to the wavelength selectivity spectral splitting scheme. In comparison, the employing efficiencies of the concentrating optics, thermal convertor, and electrolysis cell were measured as 0.7, 0.8, and 0.7, respectively. The outcomes described the hybrid TPV electrolysis technology, a pure energy source for high solar-to-hydrogen conversion.

Rahim et al. presented the simulation and optimization of the parameters dominating the coupling of the solar photovoltaic (PV) system and the advanced alkaline electrolyzer (AE). The simulation for the advanced AE was performed at operating temperatures of 40°C, 60°C, and 80°C, respectively, while the result showed the lowest operating voltage at 80°C [99]. The Faraday's efficiency was computed as 98% at 90 mA/cm^2 current density. The MPPT efficiency was proportional to the hydrogen generation rate; thus, better hydrogen generation was accomplished with better MPPT efficiency.

Kovac et al. used a 960 W_p solar power plant to produce zero carbon dioxide emission hydrogen from alkaline water electrolysis. The solar power plant generated a total power of 1.234 MWh in a specified period against the theoretical output power of 1.31 MWh [100]. A triple-cell bipolar alkaline electrolyzer was constructed instead of a single-cell alkaline electrolyzer. The result from the system showed the average hydrogen generation at a rate of 1.138 g/h, respectively.

Tebibel et al. investigated methanol electrolysis for hydrogen generation using solar photovoltaic (PV) panels at horizontal and 36º (altitude of the location) tilt [101]. The result showed 8.18 kg/m^2 and 22.36 g/m^2-d total annual and average daily H_2 production by horizontal PV array design, whereas 8.92 kg/m^2 and 24.38 g/m^2-d total annual and average daily H_2 production by tilted PV array design, respectively. In contrast, the battery captured the energy beyond the electrolyzer power input during low or high irradiation. Thus, the methanol electrolysis process supported a low-cost hydrogen generation process compared to water electrolysis.

Tebibel also examined the effects of the performance parameters on the methanol electrolysis using a solar photovoltaic (PV) system [102]. The consequence of the battery Depth of Discharge (DoD) was inspected on the system's overall performance using parametric sensitivity analysis. The results showed that the PV array must be angled suitably to reduce the solar irradiation mismatch with the demand profile. Also, the reduction in system efficiency was evaluated with a decrease in the battery DoD for lifetime enhancement.

Tebibel and *Medjebour* compared the proton exchange membrane on water, methanol, and hybrid sulphur electrolysis using a photovoltaic (PV) system. The volume of the hydrogen generation was 65% and 95% additional by methanol electrolysis (ME) and hybrid sulphur electrolysis (HSE) in comparison with the water electrolysis (WE) [103]. The average daily hydrogen generation was about 25 g/m^2-d and 29 g/m^2-d for ME and HSE, contrasting with 15 g/m^2-d for WE. The analysis revealed that the solar PV system was tested as a clean energy source and a low-cost system for hydrogen generation through ME and HSE processes.

Toklu et al. investigated the industrial waste heat utilization for hydrogen generation. The calculations showed a 2.65 A/m^2 current density and 18 kg/h hydrogen generation at a steam utilization (SU) ratio of 0.9, inlet steam flow rate of 0.4977 kg/s, and flue gas temperature of 100°C [104]. The higher hydrogen yield was governed by the higher SU, which increased current density and electrolysis voltage. Therefore, an economical waste heat solution was introduced to generate hydrogen by the electrolysis unit.

Belleville et al. produced hydrogen with a microbial fuel cell-bioelectrochemical system (MFC-BES) decoupled with a redox flow potassium hexacyanoferrate (KHCF) mediator. A current density close to 50 A/m^2 was achieved with an electric potential of 1 V with a 4-hour operation [45]. The BES lessened sludge production in wastewater treatment to produce a higher energy vector from a low microbial rate. Thus, the MFC-BES desynchronized microbial rate from wastewater treatment reduces the water electrolysis cost for hydrogen generation.

Hu et al. studied the polarization losses in a molten carbonate electrolysis cell (MCEC) containing a porous Ni electrode. The four gases with varying hydrogen concentrations were used between temperatures 600-650°C [105]. The hydrogen-lean gases showed higher polarization losses. The activation energy calculated was low for the gases containing a lower CO_2 concentration of 24.5% and increased for those with a higher CO_2 concentration of 49.5%. From the measured activation energy, it was concluded that the Ni electrode of the MCEC was under mixed or kinetic control.

Vincent et al. developed an effective membrane electrode assembly (MEA) for anion exchange membrane (AEM) electrolysis to generate hydrogen gas. They explored the effects of the various constraints on the functioning and stability of the AEM electrolyzer [106]. About 1% of K_2CO_3 electrolyte resulted in the best-performing electrolyte with a current density of 500 mA/cm^2 for 1.95 V at 60°C. Thus, on-site hydrogen production was accomplished with the AEM electrolysis technology, making it a clean energy and low-cost system.

Guban et al. compared commonly used fuel cells for hydrogen generation. The alkaline electrolysis (AE) was a technologically advanced fuel cell with a relatively simple setup and easy to scale up [47]. The proton exchange membrane (PEM) measured higher efficiency than AE, but PEM required desalinized and demineralized feed water for electrolysis. The solid oxide electrolysis (SOE) cell operated at a high temperature around 700-900°C generated hydrogen at 80% efficiency without any noble metal catalyst.

AlZahrani and *Dincer* designed a stand-alone solid oxide electrolysis (SOE) system of 1 MWe, which consumed water and electricity for hydrogen and oxygen production. With the proposed design, the SOE system accomplished 85.15% and 83.14% energy and exergy efficiency [93]. With 1 MWe power input and 248 kg/h of the water consumption rate, the SOE system generated hydrogen and oxygen at 27.75 kg/h and 220.2 kg/h, respectively. The optimization of the operation leads to more energetic and exergetic efficient hydrogen generation smoothly with the conventional heating source of electric heaters.

Lamy presented the working principle of low-temperature proton exchange membrane electrolysis cell (PEMEC) and high-temperature solid oxide electrolysis cell (SOEC) [92]. The energy efficiency of both the electrolysis cells was discussed at a given current density. The lower-temperature PEMEC exhibited up to 75% energy efficiency, whereas the high-temperature SOEC oscillated between 50-70% at 80 °C and 1 A/ cm^2 of current density. Several experiments were conducted to validate the results obtained from recent publications theoretically.

Yu et al. examined the performance of PbO_2 anode catalyst mixed with three additives, A, Z, and V, and compared these with the commercially available membrane electrode assembly (MEA) [42]. The ozone/oxygen and hydrogen were generated by feeding pure water. The better performance for higher conductivity was evaluated with the additives A and Z. However, the MEA with additive V performed outstandingly to overcome the performance decline during the power stoppage and restoration.

Abusoglu et al. performed energy and economic analysis of five models: alkaline, proton exchange membrane (PEM), high-temperature water electrolysis, and hydrogen sulfur alkaline electrolysis and dark fermentation, wastewater treatment plant to generate hydrogen using data provided by the plant management [107]. The daily H_2 generation for alkaline, PEM, and high-temperature water electrolysis was 594 kg, 625.4 kg, and 868.6 kg, with thermal efficiencies of 78%, 82%, and 94%. While the electricity cost evaluated was 3.60, 3.43, and 2.47 \$/kg-H_2.

Ehteshami et al. performed the first computational fluid dynamic study, formulating an isothermal, two-dimensional, and single-phase model of ethanol electrolysis on the PEM cell. Current density increased with operating potential while decreasing along the PEM cell length [94]. The highest operating potential of the PEM cell improved the production ratio and enhanced the specific hydrogen generation rate. The optimum cell potential of 0.94 V from the cell with membrane Nafion 117 gave a reasonable productivity rate and 1.5 cm^3/ min-cm^2 of specific H_2 generation rate.

Villagra and *Millet* analyzed the PEM water electrolysis cell for hydrogen generation at different operating current densities. The cost analysis of the PEM water electrolysis cell distinguished the optimum current density, which was determined by about 2.5 A/cm^2 at the current electricity cost scenario [43]. Still, the range could attain up to 10 A/cm^2 of current density. I-V performance of the perfluorosulfonic acid (PFSA) polymer membrane with 50-200 µm thickness was measured at 10 A/cm^2 current density. However, the 2.5-3.0 V cell voltage with low cell efficiencies of the PFSA materials was measured for less than 100 µm thickness.

Bareils et al. conducted the life cycle evaluation of PEM water electrolysis to generate hydrogen at reduced greenhouse gas emissions. A positive reduction of 75% CO_2 emissions in the hydrogen generation from the PEM water electrolysis system was achieved when running on electricity generated by renewable energy sources [48]. The results examined the impact of the electricity mix on global warming potential. However, the flexibility in operating the volatile electricity production hours defined PEM water electrolysis with a very high share of renewable energy hydrogen generation by 2050.

2.4. Gasification

Gasification is another thermal process that is economical and carbon dioxide neutral for hydrogen production on a large scale. Gas like methane enters the reaction, where high-temperature gasification is performed, and the gas coming out of the reactor is hydrogen-rich syngas, which are later purified to get pure hydrogen gas. Some findings of previously published work on hydrogen production via gasification are presented in Table 2.3.

Yilmaz et al. presented the integrated systems energetic and exergetic analysis with coal gasifiers for electricity, heating, and hydrogen generation. The calculated overall energy and exergy efficiencies were 58.47% and 55.72%, respectively [31]. Successively, the hydrogen generation rate grew from 0.06 kg/s to 0.085 kg/s with the climb in the ambient temperature from 0°C to 40°C. Therefore, the integrated coal gasifier-based system was considered more environmentally friendly than the conventional production system.

Mostafavi et al. proposed the innovative M-HyPr-RING process to determine the influence of catalyst loading and sorbent on hydrogen production through catalytic steam-gasification ash-free coal (AFC) coupled with CO_2 capture. The sorbent's significance was to boost hydrogen generation while the catalyst quickened the gasification rate [108]. The carbon conversion and the hydrogen molar fraction of 97% and 85% were attained with 20% catalyst loading and a 2:1 CaO/C ratio at 675°C. Thus, the BL-AFC caused a faster steam gasification rate than the raw BL coal.

Hasan and *Dincer* assessed the integrated gasification combined cycle (IGCC) system for hydrogen generation from used tires with reduced CO_2 emissions. The IGCC produced 11.1 kW of net power with waste tires as the feed for the gasifier [34]. In contrast, the system confirmed 55.01% and 52.31% of energy and exergy efficiencies with a 0.158 hydrogen generation to feedstock ratio. Thus, the waste tires reduced environmental impact and offered better sustainability for the feedstock for hydrogen generation in the IGCC system.

Table 2.3. Published work on H_2 production via the gasification process

S. No.	Author's Name	Relevant Findings
1.	*Kang et al.* (2016) [35]	• Temperature rated highest contribution, followed by catalyst loading, catalyst, and biomass. • Optimized H_2 gas was produced with about 100% catalyst loading at 650°C. • Canola meal delivered the highest average H_2 yield, followed by wheat straw and timothy grass.
2.	*Tian et al.* (2017) [109]	• Lignin-based biomass generated more H_2 and CO_2 at higher temperatures. • The highest H_2 yield of 1.09 Nm^3/kg was measured at 1020°C by lignin. • Cellulose and hemicellulose generated 0.33 and 0.36 Nm^3/kg at 1220°C.
3.	*Yilmaz et al.* (2019) [31]	• The calculated overall energy and exergy efficiencies were 58.47% and 55.72%, respectively. • The hydrogen generation rate grew from 0.06 kg/s to 0.085 kg/s with the climb in the ambient temperature from 0°C to 40°C.
4.	*Hasan* and *Dincer* (2019) [34]	• IGCC produced 11.1 kW of net power with waste tires for the gasifier. • System confirmed 55.01% and 52.31% of energy and exergy efficiencies with 0.158 of H_2 generation to feed ratio. • Waste tires reduced environmental impact and offered better sustainability for the feedstock for H_2 generation.
5.	*Chen et al.* (2019) [110]	• Gasification temperature and coal concentration exhibited direct proportionality with H_2 generation. • Energy and exergy efficiency achieved were 46.6% and 42.6% for the coal concentration of 15 wt.% at 700°C. • The CO_2 and NO_X emissions of the ISCWGC were lower than IGCC system.
6.	*Ibrahimoglu* and *Yilmazoglu* (2020) [111]	• The study focused on the impact of the equivalence ratio (ER) on the plasma reactions for H_2 production. • ER between 0.20 and 0.45 enhanced the H_2 yield in the product gas because of the activated water-gas shift reaction.
7.	*Pang et al.* (2019) [52]	• Syngas composition for plasma-assisted gasification includes 38.5% H_2, 38.4% CO, 10.3% CH_4 & 12.7% CO_2 at 760°C. • A 20% increase was measured in syngas production. • An upsurge of 33% was observed in the reaction rate with the non-thermal plasma gasification system.
8.	*Favas et al.* (2017) [112]	• Lesser temperatures increase the H_2 yield, while higher steam/biomass (S/B) ratio reduces the H_2 yield. • Higher ER and S/B ratios produced low LHV syngas with reduced H_2 content. • A rise in temperature leads to high LHV syngas with higher CO content.
9.	*Mostafavi et al.* (2016) [108]	• Sorbent significantly boosts the H_2 generation while the catalyst quickens the gasification rate. • Carbon conversion and the H_2 molar fraction of 97% and 85% were obtained with 20% catalyst loading and a 2:1 CaO/C ratio at 675°C. • BL-AFC caused a faster steam gasification rate than the raw BL coal.
10.	*Verma* and *Kumar* (2015) [113]	• UCG measures the GHG emissions as 0.91 kg-$CO_{2\text{-eq}}$/ kg-H_2 with CCS and 18.00 kg-$CO_{2\text{-eq}}$/ kg-H_2 without CCS. • Reduction in GHG emissions was measured with the CCS system. • Increased H_2O/O_2 injecting ratio and steam/C ratio enhanced the net life cycle GHG emissions in the UCG-CCS.

Chen et al. accomplished the energy and exergy analysis and the life-cycle environmental assessment of the integrated supercritical water gasification of coal (ISCWGC) to generate hydrogen at low CO_2 emissions [110]. The gasification temperature and coal concentration exhibited direct proportionality with hydrogen generation. The energy and exergy efficiency achieved was 46.6% and 42.6% for the coal concentration of 15 wt.% at 700°C. Consequently, the CO_2 and NO_X emissions of the ISCWGC were reasonably lower than the IGCC system.

Verma and *Kumar* analyzed the life cycle assessment of the underground coal gasification (UCG) greenhouse gas (GHG) for hydrogen generation with and without carbon capture sequestration (CCS) [113]. The UCG measuring the GHG emissions were 0.91 kg of $CO_{2\text{-eq}}$/kg-H_2 with CCS and 18.00 kg of $CO_{2\text{-eq}}$/kg-H_2 without CCS. Hence, the significant reduction in GHG emissions was measured with the CCS system. However, the increased H_2O/O_2 injecting ratio and the steam/carbon ratio marginally enhanced the net life cycle GHG emissions in the UCG with CCS.

Tian et al. experimentally studied the consequences of the temperature and the chemical composition on the gasification of cellulose, hemicellulose, and lignin-based biomass for syngas production [109]. A higher concentration of CO and CH_4 was detected in the syngas generation from cellulose and hemicellulose, while the lignin-based biomass generated more H_2 and CO_2 at higher temperatures. The highest yield of H_2 was measured at 1.09 Nm^3/kg at 1020°C from lignin, followed by 0.33 and 0.36 Nm^3/kg at 1220°C from cellulose and hemicellulose separately. Thus, hydrogen generation from higher lignin-content-based biomass was considered appropriate for gasification.

Seyitoglu et al. used the combined coal-based gasification system to analyze hydrogen and power generation's energy and exergy efficiencies. The pressure swing adsorption (PSA) unit and the high-temperature electrolysis produced H_2 with no electricity input [32]. The CO_2 capture and removal ended with a unique and environmentally friendly system. However, the peak overall energy and exergy efficiencies were 41% and 36.5%, respectively.

Kang et al. optimized the performance parameters of the supercritical water gasification of lignin, cellulose, and waste biomass using catalyst K_2CO_3 and 20 Ni-0.36 Ce/Al_2O_3 [35]. The optimization was based on Taguchi's approach, and the temperature rated the highest contribution, followed by catalyst loading, catalyst type, and biomass type, respectively. The optimized H_2 gas was produced with about 100% catalyst loading at about 650℃. Meanwhile, the canola meal delivered the highest average hydrogen yield, followed by wheat straw and timothy grass.

Pallozzi et al. simulated the dual fluidized-bed steam gasifier installed with catalytic filter candles, ZnO guard bed, LT-WGS reactor, and PSA [114]. The optimum values of the S/B ratio, WGS reaction time, and operating parameters were computed. The higher chemical efficiency was calculated at a higher WGS reactor operating temperature with a maximum of 300℃. Thus, the simulation demonstrated the highest H_2 yield of 75.2 g/kg-biomass, giving the chemical efficiency of 55.1% for 0.8 s of residence time.

Wu et al. performed the two-staged fluidized-bed gasifier experiments to assess the significance of the stage temperatures, the ER, and the S/B ratio for hydrogen production [38]. The higher operating temperatures produced a substantial upsurge in H_2, CO, and CH_4 content, while the CO_2 content dropped with the temperature rise. The operating temperature of 900℃ obtained the best results in the hydrogen generation for both stages. However, the ER ratio 0.2 produced the best H_2 proportion between 0.2 and 0.4, respectively.

Salkuyeh et al. performed the techno-economic analysis along with the life cycle assessment (LCA) of fluidized bed (FB) and entrained flow (EF) gasification to generate H_2-rich syngas from biomass [115]. The EF-based gasification was 11% thermally efficient compared to the FB-based gasification. Also, the life cycle energy consumption was 20% lower for the EF-based option than the FB-based one. Therefore, the LCA of the system was verified as an environmentally friendly system with harmful life cycle greenhouse gas emissions.

Li et al. discussed the CaO effects on the steam gasification process using various biomass waste materials to generate hydrogen. The concentration and yield of H_2 were boosted by adding CaO, while the CO and CO_2 concentrations declined in the syngas gas [116]. However, the surge in the CaO/C ratio from 0 to 2 prompted hydrogen generation. Also, biomass's volatile and carbon content directly influenced the H_2 yield through agricultural waste.

Doranehgard et al. described the CaO behaviour on the gasification of the rice husk by considering the effects of the performance parameters. The improvement in H_2 yield and the reduction in CO_2 emissions were measured in the steam gasification using CaO (CO_2 sorbent) [36]. The result showed a rise in the H_2 yield from 37 to 41 g/kg with the equivalence ratio (ER) elevated from 0.15 to 0.25, while the ER from 0.25 to 0.3, a reduction in H_2 yield was detected. Thus, the gasification temperature was a significant hydrogen production factor.

Deniz et al. performed the hydrothermal gasification of the marine biomass at a temperature of 300-600°C and the biomass loading between 0.04-0.12 g/ml for 1 h without using a catalyst to produce H_2. Further, the impact on the gasification performance was examined with the difference in the reaction temperature and the biomass loading [40]. With the biomass loading of 0.08 g/ml, the hydrogen yield and the molar fraction calculated were 10.37 mol/kg and 62.51% at 600°C. Hence, hydrogen generation was enhanced by increasing temperature and reducing biomass loading.

Shayan et al. assessed the gasification of wood and paper for hydrogen generation using air, O_2-enriched air, O_2, and steam. The highest volume of H_2 was generated from steam, whereas the highest hydrogen content in the product gas was accomplished with O_2 and O_2-enriched air, respectively [117]. However, the gasification temperature adversely affected the hydrogen generation; thus, the product gas's calorific value was dropped. The hydrogen generation and the energy and exergy efficiencies were also reduced with an augmented biomass feeding rate in the gasification process.

Kocer et al. evaluated the tomato and pepper residues' performance in hydrogen generation using air-steam gasification [118]. The O_2 content in the biomass residues was calculated high enough; thus, the air and steam to fuel rates were chosen as 0.05. The O_2 content in the tomato residue was increased, so gasification efficiency improved from 83.45% to 84.03%, respectively. Hence, the H_2 and CH_4 production was influenced by the higher O_2 content of the tomato residue.

Kuo et al. discussed the effects of ER and S/B ratio on the syngas production with CaO additive using a two-stage fluidized-bed gasifier [37]. The two-stage gasifier system without additives exhibited a 2-3% rise in H_2 yield compared to the single gasifier environment. CaO generated about 37% of H_2 in the syngas concentration with ER 0.3 and S/B ratio 0.2 with a two-stage additive. About 6.1-12.8% more H_2 was produced using the second-stage gasifier instead of the first-stage.

Chutichai et al. fabricated the biomass-feed circulating fluidized-bed gasifier to determine the operating parameters for hydrogen generation. The H_2 yield augmented with the higher gasifier temperature, giving the highest H_2 yield at about 700°C [119]. However, the S/B ratio ranged within 0.8-1.2 for the optimal gasification process. The higher H_2 yield by the steam gasification or air-steam gasification resulted from the presence of N_2 in the air.

Cao et al. experimentally investigated sugarcane bagasse gasification for hydrogen generation with supercritical water [120]. The H_2 yield was highest with higher reaction temperature, lower bagasse concentration, and lower residence time. However, the complete bagasse gasification was achieved at 750°C with a catalyst and carbon gasification efficiency of 96.28%. In contrast, the maximum yield of H_2 was touched at 35.3 mol/kg for 650°C and 20 wt.% Na_2CO_3 catalyst loading.

Jin et al. developed the supercritical water gasification (SCWG) kinetic model focused on hydrogen, CO, methane, and CO_2 production. The operating parameters of the SCWG were temperature 560°C, pressure 25 MPa, and residence time 4.66-12.41 s, respectively [121]. The modelling resulted in the growth of H_2 and CO_2 concentrations to 65.62% and 34.29%, remaining constant. It was concluded that the longer residence time supported hydrogen generation.

Yan et al. determined the effects of the reaction temperature, residence time, and feed concentration in food waste's supercritical water gasification (SCWG). The optimal condition for the best H_2 yield without catalyst was about 2 wt.% of the feed content at 500°C for 60 min [39]. However, the H_2 yield and H_2 selectivity in the SCWG were enhanced to 20.37 mol/kg and 113.19% by adding 5 wt.% KOH. Thus, the H_2 yield and H_2 selectivity improvement were observed with high temperature, long residence time, and suitable catalyst concentration.

Sivasangar et al. examined the supercritical water gasification (SCWG) of the empty fruit bunches (EFB) at 380°C temperature and about 240 bar pressure for H_2-rich syngas production [122]. The water-gas shift reaction produced hydrogen; however, the moisture generation further raised the overall H_2 yield. However, the H_2 yield was enhanced to exceed the 45 mmol/ml value for 0.3 g EFB loading and remained in the 45-55 mmol/ml range up to 0.5 g EFB. Thus, the SCWG system was effectively fed by the EFB, having a high moisture content.

Yuksel et al. analyzed the hydrogen generation and liquefaction from the waste material-based combined system for energy and exergy performance. The system showed good performance of the waste material gasification to produce H_2 with the inspected indicators [33]. The overall system energy and exergy efficiencies achieved were 61.57% and 58.15%, respectively. The rise in the waste material gasification temperature enhanced the plant's overall exergy efficiency to 60%, and the hydrogen production rate rose to 0.077 kg/s.

Liao and *Guo* evaluated the performance of the SCWG installed with the solar thermochemical receiver to generate solar heat for producing hydrogen from biomass. The temperature of the SCWG was fed by the high-temperature fluid from the solar receiver [123]. Therefore, the H_2 yield produced by the SCWG was within 10-26 mol/kg. Hence, the solar receiver fulfilled the heating requirement of the SCWG of biomass for hydrogen generation.

2.5. Plasma Reforming

In the plasma zone, the electrons exist at very high temperatures, up to 15,000-20,000°C, and these electrons support the decomposing of the organic matter in the feed. In contrast, inorganic matter deteriorates partially [112,124]. High temperatures completely decompose waste plastics and other hydrocarbons into syngas containing H_2, CO, and a few higher hydrocarbons; however, the system temperature remains near room temperature, and in some reactors, it may reach 300-400°C [125]. *Putra et al.* studied a banana's pseudo-stems H_2 production potential using an in-liquid plasma reactor [126]. The pseudo-stem with long fibres showed 70.7% H_2 yield and 98.8% H_2 selectivity, making it an excellent raw material for H_2 production. Various plasma reactors used for generating H_2 are discussed in Table 2.4.

Table 2.4. Various plasma reforming methods

S. No.	Author's Name	Relevant Findings
		Dielectric Barrier Discharge Plasma Reactor
1.	*Lee* and *Kim* (2013) [18]	• Methanol conversion enhances from 5.7% to 39.1% when electric discharge is raised to 4.0 kV voltage and 50 kHz. • The highest methanol conversion of 39.1% is achieved by 4.0 kV discharge voltage and 50 kHz frequency at 180°C.
2.	*Ulejczyk et al.*(2019) [127]	• At 20 W, the highest H_2 yield obtained is 137.76 L/h with a 3 water/ethanol ratio and 1.4 mol/h feed rate. • Maximum ethanol conversion (71%) is achieved with a 5 water/ethanol ratio at a 0.6 mol/h feed rate.
3.	*Hayakawa et al.* (2019) [128]	• Generates hydrogen gas (99.99% pure) at a 20 mL/min rate at 400 W. • Maximum H_2 production rate is achieved at 150 L/h of NH_3 flow rate at 110 V, and the overall system obtains 28.5%.
4.	*Hayakawa et al.* (2020) [129]	• Maximum H_2 production rate is obtained by 4.5 gap length and 400 W power with the H_2 purity of 100%. • The ammonia conversion rate achieved is 24.4%.
5.	*Song et al.* (2017) [130]	• H_2 yield is enhanced from 23.1% to 28.4% at a 30 mL/min feed rate, CH_4/O_2 ratio of 1, and discharge power of 100 W. • Methane conversion increases from 60.1% to 83.6%.
6.	*El-Shafie et al.* (2019) [131]	• Maximum H_2 flow rate is achieved with a 0.2 L/h steam flow rate at 18 kV and 130°C PMCR heating temperature. • The water conversion rate obtained is 42.51%.
7.	*Zhang et al.* (2022) [132]	• The background temperature played a significant role in n-C_5H_{12} conversion. • Conversion increases up to 225°C and then declines at 250°C.
8.	*Shareei et al.* (2019) [133]	• The influence of applied voltage and Argon flow rate on CH_4 conversion was studied. • About 99.9% methane conversion was observed at 1.84 synthesis gas modules and 10 kV applied voltage.

S. No.	Author's Name	Relevant Findings
— **Gliding Arc Plasma Reactor**		
1.	*Kim* and *Chun* (2014) [134]	• The highest conversion rate is obtained by 69.5 m/s injection gas velocity, 300 L/h CO_2 flow rate at 1 CH_4/CO_2 ratio. • CO_2 destruction rates ranged between 35.7% and 42.6%.
2.	*Lian et al.* (2017) [56]	• The highest CH_4 conversion is obtained at 0.3 O$_2$/C ratio, 0.5 S/C ratio, and 24 kJ/mol SEI. • 74% and 0.45 kWh/Nm^3 are the energy efficiency and cost.
3.	*Wang et al.* (2019) [135]	• The highest H_2 yield is achieved at 30 W input power, 0.71 O/C ratios, 6.5 mm discharge gap, and 24.7 s residence time. • The best H_2 energy yield of 94.5 L/kWh is achieved.
4.	*Baowei et al.* (2020) [136]	• Ideal H_2 yield is achieved with a 0.68 O/C ratio, 18.4 s of residence time with Ar addition of 10 vol% at 32 W. • With 10 vol.% Ar addition, the reactor achieved 48.6% hydrogen yield.
5.	*Lian et al.* (2020) [137]	• CH_4 conversion and H_2 selectivity increase from 24.0% to 87.7% to peak value and H_2O conc. from 0 to 95 mol%. • Water behaved as a homogeneous catalyst, CO oxidant, and side-product. • Both the catalyst and oxidant behaviour of water enhanced hydrogen production.
6.	*Song et al.* (2019) [138]	• Optimal conversion is obtained by a 3 mm discharge gap and 20 kHz discharge frequency at 60 V. • A higher CH_4/CO_2 ratio results in H_2 production, but CH_4 will remain unreacted. • The ideal CH_4/CO_2 ratio is 1-2.
7.	*Wang et al.* (2021) [139]	• H_2 yield and H_2 energy yield of 50.1% and 94.5 L/kWh are achieved at 30 W input power, 0.71 O/C ratio, 6.5 mm discharge gap, and 24.7 s residence time. • Any fluctuation in the above parameters showed a significant decrease in H_2 yield, while CO and CH_4 yield enhanced.
8.	*Liu et al.* (2022) [140]	• Ethanol reforming for hydrogen production in a gliding arc plasma reactor was performed. • The authors achieved 38.6% of the highest H_2 yield during the experimentation.
— **Microwave Plasma Reactor**		
1.	*Czylkowski et al.* (2018) [141]	• Study determined the effect of spraying ethanol microdroplets into an N_2 MW plasma flame at atmospheric pressure. • The highest H_2 production rate with 28% H_2 content is achieved by ethanol and N_2 gas flow rate of 3.7 L/h and 2700 L/h at 5 kW power.
2.	*Czylkowski et al. (2017)* [142]	• The highest H_2 production rate with 27.6% H_2 content is achieved by raising microwave power to 5 kW. • Increased ethanol mass flow rate resulted in higher H_2 production efficiency.
3.	*Sun et al.* (2017) [143]	• The highest H_2 flow rate with 58.1% H_2 content is achieved at 1500 W and 70 vol% ethanol concentrations. • Syngas consisting mainly of H_2 and CO are produced in the reactor, while CH_4, C_2H_2, and CO_2 were present in the traces.
4.	*Chehade et al.* (2020) [65]	• Ceriated tungsten showed higher H_2 production than pure tungsten. • The overall system attained 53% energy efficiency and 44% exergy efficiency.

5.	*Hrycak et al.* (2019) [144]	• The highest H_2 production rate is achieved with a 6000 L/h flow rate at 7.5 kW • A peak energy yield of 21 g/kWh is obtained at 4.5 kW, and a maximum CH_4 conversion of 86.5% is achieved with a 3000 L/h flow rate at 6.5 kW power.
6.	*Zhu et al.* (2021) [145]	• Ethanol decomposes into CH_3CHO and H_2 by high-energy electrons and produces CH_4 and CH_2O. • The H_2O decomposes into •OH and •H radicals.
7.	*Zhu et al.* (2022) [146]	• 80 PPI Cu foamed metal suspended electrode shows a 31.5% increase in total gas flow rate than no suspended electrode. • A 29.5 NL/min peak flow rate of total gas and 0.70 Nm^3/kWh peak energy yield of H_2 production was obtained.
8.	*Akande* and *Lee* (2022) [147]	• A 74.6%-97.7% rise in methane conversion was observed with an increase in the S/C ratio. • The hydrogen production rate rises from 1532 g (H_2)/h to 2247 g (H_2)/h when the absorbed microwave power is raised from 27 to 32 kW.
	Pulsed Plasma Reactor	
1.	*Moshrefi* and *Rashidi* (2018) [12]	• The highest H_2 selectivity is achieved by 9 L/h CH_4 flow rate at 21 W and 2000 rpm electrode speed. • An energy efficiency of 1.46 mol/kJ was obtained without a catalyst.
2.	*Kheirollahivash et al.* (2019) [13]	• The highest H_2 rate (7.96 L/h) is achieved with a 9 L/h CH_4 flow rate at 20W and 200 rpm. • A 36.8 g/kWh of energy yield is obtained.
3.	*Morgan* and *ElSabbagh* (2017) [15]	• At 17.2 kV and 100 SCCM CH_4 flow rates, 85.6% and 40% CH_4 conversion and H_2 selectivity are obtained. • Higher CH_4 conversion (92%) reduces H_2 selectivity to 30.6% and H_2 concentration percentage to 56%.
4.	*Xin et al.* (2020) [22]	• Highest H_2 flow rate and energy yield are achieved at 30 kV and 50% ethanol concentration in water. • Higher voltage helps jumping electrode balls enhance the randomness and strength of discharge.
5.	*Lee* and *Park* (2020) [148]	• 1.41 L H_2 yield obtained by 1:4 ethanol/bio-oil ratio in 20 min. • At 1:1 ethanol/bio-oil and 5 min, the H_2 production reaches a maximum containing 65.51% H_2 content.
6.	*Xin et al.* (2021) [149]	• H_2 and CO consist of about 99% of syngas. • Both high peak voltage and appropriate electrode distance increase the H_2 yield to the maximum value.
7.	*Ghanbari et al.* (2020) [150]	• Effects of Argon flow rate applied voltage catalyst loading and were determined. • A CH_4 conversion of 88.4% and 76.4% were achieved with and without $Ni-K_2O/Al_2O_3$ catalyst.
8.	*Chung et al.* (2018) [151]	• TiO_2 photocatalyst addition showed an improved rate of H_2 evolution. • The H_2 evolution rate also increases with metal loading on the TiO_2 surface. • Alcohol agent also increases the H_2 evolution considerably.

4.3.1. Dielectric Barrier Discharge Plasma Reactor

In a DBD reactor, an alternating current (AC) potential difference is applied between the electrodes. Here, the dielectric barrier that limits charge transport between electrodes covers at least one of the two electrodes; this counteracts the conversion of discharge into a thermal regime transition. The gas transition requires electrodes in concentric cylindrical configurations. The electric discharge initiates alcohol-water dissociation at a comparatively lower temperature.

In the optimization process, *Lee* and *Kim* examined the effects of various parameters in methanol-water decomposition using a hybrid plasma-catalytic (Cu/ZnO supported Al_2O_3 catalyst) reactor, where Copper (Cu) provides active sites and Zinc oxide (ZnO) is a surface stabilizer [18]. It enhances methanol conversion from 5.7% to 39.1% when raising the electric discharge to 4.0 kV and 50 kHz. The result shows the significance of electric discharge in alcohol decomposition.

Ulbejczyk et al. performed ethanol conversion in a DBD reactor and studied the effects of operating parameters on hydrogen production. Results showed that the discharge power, water/ethanol ratio, and feed flow rate influenced the ethanol conversion [127]. At 20W discharge power, 5 water/ethanol ratio, and 0.6 mol/h feed flow rate, the maximum ethanol conversion (71%) is obtained. *Zhang et al.* used simulated gasoline (n-C_5H_{12}) to produce hydrogen-enriched syngas [132]. The background temperature played a significant role in n-C_5H_{12} conversion, where the conversion increases to 498°C and then declines to 523°C.

Hayakawa et al. designed a low-temperature plasma membrane reactor (PMR) that continuously decomposes ammonia (NH_3) into high-purity hydrogen gas [128,129]. The PMR works stage-wise; firstly, plasma decomposes NH_3 into •H radicals, then •H radical adsorption and penetration into the membrane surface takes place, and finally, the •H radicals recombine to form hydrogen molecules. The process generates hydrogen gas (99.99% pure, which feeds directly to the fuel cell) at a 1.2 L/h rate at 400 W input power. PMR gap length and gas differential pressure showed a 120 L/h hydrogen flow rate against a 150 L/h ammonia flow rate at 110 V, giving 28% energy efficiency.

Song et al. investigated the hydrogen production potential of a DBD plasma reactor with & without a NiO/g-Al$_2$O$_3$ catalyst. The DBD plasma and NiO/g-Al$_2$O$_3$ catalyst synergized, resulting in better CH$_4$ conversion and H$_2$ yield [130]. The results showed improved CH$_4$ conversion from 60.1% to 83.6% and H$_2$ yield from 21.3% to 28.4% using a honeycomb catalyst. The observation also showed that the high temperature reduces Nickel oxide (NiO) to Nickel (Ni), affecting the catalyst life; thus, a low temperature is favourable for longer catalyst life. *King et al.* determined the hydrogen production rate from landfill gas/coal mine gas in a DBD reactor [152]. The catalytic DBD reactor generates about 1456 kL/h-H$_2$ at 500°C and near atmospheric pressure.

Shareei et al. studied the influence of applied voltage and Argon flow rate on methane conversion. About 99.9% methane conversion was observed at 1.84 synthesis gas modules and 10 kV applied voltage [133]. Table 2.4 discusses other modified DBD reactors, operating parameters, H$_2$ yield, and production rate. The observation shows that the hydrogen yield is mainly affected by discharge voltage (or power) and feed flow rate. At the same time, temperature, electrode gap length, and O/C ratio have a significantly less or negligible impact on hydrogen yield.

4.3.2. Gliding Arc Plasma Reactor

The gliding arc discharge is another plasma technique that produces warm plasma at about 1000-3000 K gas temperature and, thus, possesses properties between thermal and non-thermal plasmas. It is a transient arc discharge formed between two flat diverging electrodes. The shortest inter-electrode space initiates the arc that glides along the electrodes due to the gas blast and reaches the larger inter-electrode space before it vanishes; then, a new arc is generated, and the process continues.

Lian et al. examined the behaviour of water (at several concentrations) in a gliding arc plasma reactor for methane reforming [137]. During the process, water plays a homogeneous catalyst and CO oxidant between 33 and 95 mol% content and a side-product below 33 mol% concentration. Both a catalyst and an oxidant behaviour of water enhanced hydrogen production, while the side-product behaviour resulted in hydrocarbon formation, drastically reducing hydrogen production.

Wang et al. examined the influence of various other operating parameters in continuous n-heptane decomposition at room temperature and achieved 50.1% H_2 yield and 94.5 L/kWh H_2 energy yield at 30 W input power, 0.71 O/C ratios, 6.5 mm discharge gap, and 24.7 s residence time, respectively [135]. Any fluctuation in the above parameters decreases H_2 yield, while CO and CH_4 yield increases drastically.

Kim and *Chun* designed a similar gliding arc plasma for CO_2 decomposition and CH_4 steam inflow and measured the effects of varying orifice baffles in hydrogen-rich syngas production [134]. The orifice baffles with the smallest inner diameter showed the highest CO_2 destruction rate (42.5%) due to higher retention time while achieving 48% methane conversion at a 300 L/h CO_2 flow rate. In contrast, *Lian et al.* investigated the methanol-reforming in a gliding arc plasma reactor and observed an 88% methanol conversion by 0.3 oxygen/methanol ratio, 0.5 steam/methanol ration, and 24 kJ/mol specific energy input, respectively [56]. It gives high energy efficiency with low energy costs.

Piavis and *Turn* also fabricated a reverse vortex flow plasma reactor and tested the reactor performance for methane reforming. The reactor achieved 66.5% H_2 yield and 79.8% methane conversion at 43.5% efficiency and 144 kJ/mol specific energy requirement [153]. In contrast, Song et al. examined the CH_4-CO_2 decomposition in a rotating gliding arc reactor and observed a 1-2 CH_4/CO_2 ratio ideal for hydrogen production, while a higher ratio resulted in incomplete CH_4 reforming. At the same time, the higher voltage and frequency enhance gas energy yield, whereas overall energy consumption is improved.

Baowei et al. performed the toluene reforming in a gliding arc plasma reactor while adding a smaller amount of Argon (Ar) gas[154]. With 10 vol.% Ar addition, the reactor achieved a 48.6% H_2 yield and 60.2 L/ kWh H_2 energy yield, respectively. *Ma et al.* studied the potential of n-dodecane for hydrogen production in a gliding arc plasma reactor [155]. The highest n-dodecane conversion of 68.1% gives 76.7% H_2 selectivity, while the other products generated are acetylene and ethylene. Both acetylene and ethylene help in the selectivity enhancement of light olefins.

Liu et al. investigated ethanol reforming for hydrogen production in a gliding arc plasma reactor and achieved 38.6% of the highest H_2 yield during the experimentation [140]. Table 2.4 discusses other gliding arc plasma reactors and operating parameters for higher hydrogen yield. The hydrogen yield in the gliding arc plasma reactor depends on the O/C ratio, power, and feed flow rate. The O/C ratio between 0.4 and 0.7 at a power input of 30-32W is considered favourable for maximum hydrogen production, while in the case of methanol, the power input can reach as high as 120 W for effective results.

4.3.3. Microwave Plasma Reactor

A microwave (MW) plasma reactor is another plasma technique for hydrogen production that works between 300 MHz and 10 GHz frequency range. It utilizes electromagnetic radiation to excite electrons to higher energy levels, and these excited electrons break the hydrogen bonds to form •H radicals, which later combine to form H_2 molecules [141,142]. The discharge initiation happens when gas flows through a quartz tube and intersects with a rectangular waveguide. The plasma absorbs wave energy, and MWs spread through quartz tubes.

Czylkowski et al. used a microwave plasma reactor and determined the effects of spraying ethanol micro-droplets into Nitrogen (N_2) MW plasma flame at atmospheric pressure [141]. Direct spraying saved energy requirements for vaporizing ethanol. The results show hydrogen concentration and production rate of 28% and 1043 L/h at 3.7 L/h ethanol flow rate and 5 kW microwave power. *Wang et al.* investigated the liquid-phase methane reforming for hydrogen production in an MW plasma reactor [156]. The highest H_2 yield of 74% was achieved by 94.3% methane conversion and 900W power.

Sun et al. described a significant hydrogen production process from ethanol using a microwave discharge plasma reactor [143]. H_2 and CO are produced in the reactor, while other gases like CH_4, C_2H_2, and CO_2 are also in smaller quantities. The highest hydrogen concentration and energy yields obtained are 58.1% and 48.32 g/kWh at 1500 W with 70% ethanol concentration in the solution. Thus, a feasible on-board hydrogen production showed good potential with less energy demand.

Czylkowski et al. examined the ethanol conversion in a similar MW plasma reactor at atmospheric pressure by directly supplying ethanol from the induction vaporizer to the plasma flame [142]. The experiments showed that microwave power enhanced hydrogen production rate and volume concentration, while the increased ethanol mass flow rate gave higher hydrogen production efficiency.

Ogungbesan et al. investigated the methane dissociation at atmospheric pressure with a quartz tube to generate an MW plasma torch at 2 kW and 2.45 GHz [157]. The temperature caused by the microwave plasma torch is as high as $5000 \pm 250°C$, which is suitable for methane decomposition into hydrogen.

Chehade et al. designed an MW plasma reactor using a commercially available 2.45 GHz microwave oven for water plasmolysis [65]. The steam at 107°C enters the reactor, having a tungsten electrode with a flow rate of 2 bbl/s, and the effects of pure and ceriated tungsten electrodes are examined. The ceriated tungsten sustained a higher H_2 rate, and the H_2 production rate ranges between 1.65 and 4.7 L/h, respectively, while the highest hydrogen energy yield achieved is 13.3 g/kWh. Therefore, the fabricated microwave reactor generates hydrogen through water plasmolysis, making hydrogen production more affordable.

More MW plasma reactors with process parameters to achieve high H_2 yield are depicted in Table 2.4. The MW plasma reactors are based on electromagnetic waves; thus, the frequency of the electromagnetic waves, input power, and feed flow rate plays a significant role in the hydrogen production rate.

4.3.4. Pulsed Plasma Reactor

Pulsed discharge is chemically active and produces high current density, generating reactive ions, electrons, and radicals, which break the hydrogen bonds [15,158]. Corona discharge and spark discharge are two pulsed electrode plasma forms that depend on the variation in peak voltage. The low voltage generates corona discharge, which appears as many streamers, while high voltage results in spark discharge, which appears as a flash between electrodes.

Morgon and *ElSabbagh* observed that the methane flow rate of 100 standard cubic centimetres per minute (SCCM) is more effective in CH_4 conversion than a 200 SCCM flow rate, while the CH_4 conversion raises with applied voltage in both cases [15]. However, the H_2 selectivity at low voltage has similar results (as CH_4 conversion), and the opposite results were obtained at a voltage higher than 17 V. The reactor showed 92% CH_4 conversion and 44.6% H_2 selectivity at specific input conditions. Thus, the methane flow rate and applied voltage directly influence the reactor's CH_4 conversion and H_2 selectivity. Meanwhile, a valuable by-product (graphite oxide) is produced within the reactor by methane decomposition, which can be collected and purified for different applications in electronics, optics, chemistry, energy storage, and biology.

Xin et al. operated a pulsed discharge reactor with a needle-balls-like electrode configuration, generating hydrogen at a 66 L/h flow rate and a 141.3 g-(H_2)/kWh hydrogen energy yield at 30 kV [158]. During the discharge shock waves, the jumping of electrode balls increases the discharge randomness and strength, giving a higher energy yield. The study also includes pulsed discharge through constant rate comparison and found that formaldehyde (CH_2O) addition may significantly raise hydrogen flow rate.

Moshrefi and *Rashidi* investigated the methane conversion into hydrogen in a rotating plasma electrode reactor at almost ambient temperature and found no CO_X radicals generation in the reactor [12]. The method showed about 60% methane conversion and 1.46 mol/kJ energy efficiency without any expensive catalyst, thus making the process more energy efficient than a fixed electrode reactor.

Kheirollahivash et al. developed a screw-type electrode and recorded the reactor performance parameters to determine the impacts of arc extension and electrode traveling at different angular velocities [13]. The maximum CH_4 conversion, hydrogen production rate, and H_2 energy yield obtained with the double-helix electrode are 47%, 7.96 L/h, and 36.8 g/kWh, respectively. At the same time, it showed a 2.1 g/h carbon decomposition rate, where carbon has a graphite-like structure.

2.6.   Application in PEM Fuel Cell

Once the H_2 was produced, its utilization in power generation becomes very important. Various fuel cell technologies are available in the market, among all the proton exchange membrane (PEM) fuel cell is chosen in this study. A PEM fuel cell comprises an anode (negative), a cathode (positive), and an electrolyte. The fuel (hydrogen) is supplied to the anode and air to the cathode. It converts the chemical energy into electricity in a chemical reaction with oxygen (or any oxidizing substance). Consider fuel cells like batteries drain over time; fuel cells don't, and neither requires recharging as batteries do. As long as fuel is supplied, it will keep producing electricity and heat. The findings of work on PEM fuel cell are presented in Table 2.5.

Kumar and *Subramanian* determined the effects of various parameters on the performance of a PEM fuel cell [159]. Oxygen-enriched air (up to 45%) showed a 9% and 33% improvement in voltage efficiency and power output due to more oxygen reduction reactions. Whereas beyond 45% oxygen enrichment, the performance declined due to increased stack temperature. In contrast, a 50°C optimal temperature performed better between 40°C and 60°C. However, the hydrogen pressure showed the most minor significance in the PEM fuel cell performance.

Tang et al. discussed the temperature sensitivity of a PEM fuel cell to improve the durability and performance of the fuel cell stack [160]. Results showed that increasing the temperature speeds up the electrochemical reaction rate; thus, a significant rise in fuel cell performance was observed. In contrast, the higher temperatures have inverse impacts on the water content that reduces the cell's power output. Therefore, an optimal temperature must be mentioned to retain hydration in normal fuel cell operations.

Wang et al. simulated the cathode channel's water removal and heat transfer rate. It was observed that the inlet section has three evolution stages, whereas the middle and outlet section has only two evolution stages [161]. The growth, coalescence, and generation stages of water droplets occur in the inlet section of the cell. In contrast, the middle and outlet stages involve growth and water film formation to the upper channel surface.

Table 2.5. Studies on the proton exchange membrane (PEM) fuel cell

S. No.	Author's Name	Relevant Findings
1.	*Kumar* and *Subramanian* (2023) [159]	• O_2-enriched air improved 9% voltage efficiency and 33% power output. • Rise in stack temperature declined the cell performance declined beyond 45% O_2 enrichment. • 50℃ optimal temperature gave a better performance.
2.	*Eslami et al.* (2023) [162]	• A 1-2% improvement in stack performance for relative humidity (from 50% to 100%) and stoichiometry of the cathode (from 1.02 to 1.60) • Hydration of membranes and enhanced water and fuel management improved the cell performance.
3.	*Yang et al.* (2022) [163]	• At lower current density (say 200 mA/cm^2), membrane dehydration and uneven water distribution were observed. • Fuel cell performance is enhanced above 600 mA/cm^2 current density • The best cell performance was achieved at 45℃ and 2.2 m/s air velocity.
4.	*Dhimish et al.* (2021) [164]	• Maximum cell efficiency of 58% was measured at high hydrogen pressures. • When voltage is dropped between 75V and 95V, the membrane temperature reaches above 75℃. • The cell efficiency reduced in the range of 33-37%.
5.	*Al-Anazi et al.* (2021) [165]	• A significant variation was observed in PEM fuel cell performance during the winter and summer environment. • About 12% lesser efficiency was calculated in the winter as compared to the summer. • Humidification during the peak summer interval showed a 40% output enhancement.
6.	*Carcadea et al.* (2020) [166]	• GDL thickness results in the liquid water transport and gas flow rate in the fuel cell flow channel and catalyst layer. • A rise in GDL (cathode) porosity from 0.4 to 0.78 enhanced cell performance. • A slight variation in GDL thickness can contribute to significant variation in the cell performance.
7.	*Uzun et al.* (2020) [167]	• A rise of up to 10% in fuel cell performance was achieved with the TSC at below 25℃ ambient temperature. • A 60% rise in the thermal efficiency based on solar radiations was noticed.
8.	*Omran et al.* (2021) [168]	• Model shows a linear reliance between hydrogen feeding and the stack current. • Peak overall system efficiency of 47.5% was achieved at half the rated power of the fuel cell. • About 4.6% discrepancy was obtained between model and experimental values of the power output.
9.	*Ratlamwala et al.* (2012) [169]	• An increase of 40% in cell efficiency with the rise in the temperature. • A decline of 38% in cell efficiency was noticed with the surge in current density and membrane thickness. • To obtain the maximum power output parameter optimization is required.
10.	*Tang et al.* (2023) [160]	• Increasing the temperature speeds up the electrochemical reaction rate. • Higher temperatures have inverse impacts on the water content that reduces the power output of the cell.

Eslami et al. studied the effects of various operating parameters on the PEM fuel cell performance. The parameters studied include relative humidity, temperature, pressure, and stoichiometry [162]. Results showed a 1-2% improvement in stack performance for both relative humidity (from 50% to 100%) and stoichiometry of the cathode (from 1.02 to 1.60). Hydration of membranes and enhanced water and fuel management are behind the performance improvement. Similarly, a 4-6% improvement was observed for the temperature (from 50°C to 80°C) and reactants outlet pressure (from 0.5 bar to 2.0 bar), respectively.

Meng et al. investigated the effects of hydrogen circulation rate and water management on PEM fuel cell performance [170]. When the hydrogen circulation rate was increased, the lower liquid water was noticed in the cathode and anode flow channels, reducing the cell performance due to the membrane and catalyst layer drying that raised ohmic resistance. In contrast, the lower hydrogen circulation rate results in the flooding at hydrogen and air inlet regions. Hence, the hydrogen circulation rate must be raised with increasing current.

Yang et al. investigated the impacts of water transport mechanisms and water distribution in an open-channel PEM fuel cell. Membrane dehydration and uneven water distribution were observed at lower current density (say 200 mA/ cm^2) [163]. In contrast, at above 600 mA/ cm^2 current density, the cell performance is enhanced due to increased cell temperature and air velocity that removes extra water from gas diffusion and the catalyst layer. The best cell performance was achieved at 45°C and 2.2 m/s air velocity.

Al-Anazi et al. investigated the performance of a PEM fuel cell in winter and summer conditions in Saudi Arabia using an Ansys model. A significant variation was observed in PEM fuel cell performance during the winter and summer environment [165]. About 12% lesser efficiency was calculated in the winter compared to the summer due to the hot and humid conditions resulting in fast reaction kinetics and membrane hydration. Furthermore, the humidification during the peak summer interval showed a 40% output enhancement.

Dhimish et al. studied the effects of temperature and operating voltage on the performance and degradation of a PEM fuel cell. Maximum cell efficiency of 58% was measured at high hydrogen pressures [164]. In contrast, the membrane temperature ranged between 55℃ and 95℃ at 100 V of operating voltage. Whereas, when voltage is dropped between 75V and 95V, the membrane temperature reaches above 75℃, reducing the cell efficiency in the range of 33-37%, respectively.

During dead-end mode operation, *Shateri* and *Torabi* examined the proton exchange membrane fuel cell performance with liquid water accumulation at the anode. A large volume of liquid water accumulation was observed at the cathode due to dead-end operation [171]. The accumulated water covers the catalyst, which increases charge transfer resistance. The liquid water accumulation reduces the cell performance; therefore, regular purging becomes very important in the fuel cell operation.

Chinannai et al. studied the effects of temperature and coolant flow rate on the performance and functioning of a PEM fuel cell stack [172]. Cell voltage degradation forces to raise the coolant flow rate. The temperature rise inside the stack does not always result in the voltage decline. However, the cause could be local current density distribution as well. The voltage drop is an indication of cell malfunctioning.

Tao et al. identified the impacts of the cold start on the performance of PEM fuel cells using an analytical model. The developed fuel cell model simulates the catalyst layer and cold-start failure due to ice formation [173]. It was observed that an uneven distribution of current density results in the ohmic resistance within the fuel cell. The results showed the cold-start correlation between the experimental and simulation results of the fuel cell.

Qu et al. examined the PEM fuel cell performance for high-temperature applications [174]. Stable mechanical properties and high proton conductivity are mandatory for the cell to work at high temperatures and non-humid conditions. Phosphoric acid-doped polybenzimidazoles (PBI) are helpful when operating at higher temperatures. It provides mechanical stability and high proton conductivity at dry and high-temperature conditions.

Kulikovsky developed a PEM fuel cell model to investigate the cell impedance at variable airflow velocities in the cathode channel [175]. The oxygen transport in the channel through higher air flow velocity showed lower resistivity. In contrast, a relatively equal airflow velocity and cell potential showed total resistivity compensation in the PEM fuel cell model.

Taner investigated the impacts of various operating parameters on the thermodynamic efficiency of a PEM fuel cell [176]. A drop in thermodynamic efficiency of the fuel cell was observed with increasing pressure and mass flow rate of H_2. The decline in thermodynamic efficiency lies in the energy loss within the energy system. The pressure and mass flow rate inversely affect the thermodynamic efficiency.

Houreh et al. investigated the effects of different configurations of the humidifiers at different PEM fuel cell operating conditions [177]. The counter-flow humidifier showed a superior heat and water transfer rate than parallel and cross-flow humidifiers. The cross-flow humidifier has a better heat transfer rate than the parallel-flow humidifier. The reverse goes for the water transfer rate (i.e., the parallel-flow humidifier has a better water transfer rate than the cross-flow). The wet side inlet temperature significantly affects the humidifiers' performance in the fuel cells.

Carcadea et al. studied the impact of the gas diffusion layer (GDL) on the PEM fuel cell performance [166]. The GDL Thickness has noteworthy effects on the cell performance because the GDL thickness results in the liquid water transport and gas flow rate in the fuel cell flow channel and catalyst layer. A rise in GDL (cathode) porosity from 0.4 to 0.78 enhanced cell performance due to reduced mass transport resistance. Therefore, a slight variation in GDL thickness can contribute to significant variation in the cell performance.

Strahl et al. studied the effects of temperature on the PEM fuel cell performance. The study revealed a positive impact with the temperature rise due to lowering the activation barriers [178]. The lower water content due to higher temperature also reduced the electrochemical active sites in the cathode catalyst layer. Hence, temperature control becomes an essential parameter for fuel cell performance.

Ratlamwala et al. designed a proton exchange membrane for a fuel cell system and analyzed its performance with the temperature and membrane thickness [169]. Results showed an increase of 40% in cell efficiency with the rise in the temperature. In contrast, a decline of 38% in cell efficiency was noticed with the surge in current density and membrane thickness. Therefore, to obtain the maximum power output, parameter optimization is required.

Chugh et al. evaluated the performance of the PEM fuel cell and identified the various influencing parameters in fuel cell operation. The rise in the temperature improved the fuel cell performance as the gas diffusivity and current density improved at elevated temperatures [179]. The higher operating pressure also enhanced the cell performance. Humidification has a low impact on cell performance, but the fully hydrated membrane still showed the best outputs from the cell stack.

Uzun et al. examined the performance of a PEM fuel cell when the air is pre-heated using solar energy. The transpired solar collector (TSC) is used in the study to pre-heat the air [167]. It was observed that a rise of up to 10% in fuel cell performance was achieved with the TSC during below 25°C ambient temperatures. At the same time, a 60% improvement was noticed in the thermal efficiency based on solar radiation. Hence, about 30-70% enhancement in the cell efficiency was detected with the solar air pre-heater for cathode inlet air.

Omran et al. developed a PEM fuel cell mathematical model in MATLAB Simulink software to enhance the overall system efficiency and output power [168]. A linear dependence was observed between hydrogen feeding and the stack current. The peak overall system efficiency of 47.5% was achieved at half the rated capacity of the fuel cell. About a 4.6% discrepancy was obtained between the model and experimental values of the power output.

Mubin et al. investigated the performance of a PEM fuel cell at varying temperatures and pressure. The fuel cell performed better at higher temperatures and gas pressure values [180]. The fuel cell malfunctioning could occur when the temperature and pressure reach beyond a particular limit. It becomes essential to identify the working temperature and gas pressure to obtain the best power output.

2.7. Summary from the Literature Review

The following conclusions were drawn from the literature after studying and reviewing the works of various researchers/ scientists:

❖ Steam reforming is an energy-intensive method for hydrogen production.

❖ Low H_2 yield and H_2 selectivity and high CO_2 emissions are other drawbacks of hydrogen production via steam reforming.

❖ On the other hand, electrolysis is unreliable and has small-scale applications.

❖ Electrolysis also has problems like membrane corrosion, shorter life, and expensive catalyst requirements.

❖ Gasification has economic vial infrastructure; however, the feedstock purification and low system efficiency restrict its usage.

❖ Gasification produces gas containing impurities and tar formation; therefore, an additional carbon capture and storage unit must be installed, increasing cost and energy requirement.

❖ Anaerobic fermentation (Biohydrogen) is a bacterium-based process; therefore, bacterium sensitivity must be examined regularly.

❖ Plasma reforming is highly efficient and cost-effective; however, low H_2 production rate and small-scale production applications are drawbacks.

❖ Plasma reforming is divided into four main categories with advantages and limitations.

❖ Dielectric barrier discharge requires costly catalysts, and the catalyst has a shorter life.

❖ Gliding arc plasma uses two bean-shaped electrodes where plasma glides from the lower end to the upper end of the electrode. Low-feed plasma interaction is a big concern.

❖ Microwave plasma produces comparatively higher H_2 yield; however, higher electricity requirement makes it low energy efficient.

❖ Pulsed plasma has a low H_2 production rate since the plasma production is not continuous.

2.8. Literature Gaps

The following literature gaps were observed during studying and reviewing works of various researchers/ scientists:

❖ Plasma reforming is highly efficient and cost-effective; however, low H_2 production rate and small-scale production applications are not properly investigated.

❖ Dielectric barrier discharge requires costly catalysts, and the catalyst has a shorter life; the work on catalyst life assessment is limited.

❖ Gliding arc plasma uses two bean-shaped electrodes where plasma glides from the lower end to the upper end of the electrode. Low-feed plasma interaction is little explored.

❖ Microwave plasma produces comparatively higher H_2 yield, but its energy efficiency is not investigated.

❖ Pulsed plasma has a low H_2 production rate since the plasma production is not continuous. The parameter optimization is roughly available.

❖ The simulation-based study is also missing for the parameter optimization to enhance the H_2 production.

Therefore, a continuous plasma generation unit must be developed after determining the literature gaps. The continuous plasma generation will improve the interaction between plasma and feed, thus enhancing the H_2 yield.

2.9. Objectives

The major objectives of the present study are:

1) To design and develop a Hydrogen Production system.
2) To optimize the performance parameters in Hydrogen production to increase the yield and purity of the Hydrogen.
3) To investigate a fuel cell using Hydrogen.
4) To optimize the process parameters using Simulation software.

CHAPTER 3

METHODOLOGY

The various phases of the research activity are as discussed below:

▸ **Phase 1:** Conducted an extensive literature survey and analysed the potential of various hydrogen production methods

▸ **Phase 2:** Design and fabrication of experimental setup for plasma reforming of alcohol-water mixture.

▸ **Phase 3:** Characterised feed and identified the potential for Hydrogen production method in plasma reformer.

▸ **Phase 4:** Determined the effects of operating parameters and optimized influencing parameters to enhance hydrogen production rate.

▸ **Phase 5:** Developed a simulation model for hydrogen production and optimised the parameters for hydrogen selectivity and feed conversion rate (methanol-water mixture).

▸ **Phase 6:** Purified and characterized produced gas for hydrogen purity produced during experimentation.

▸ **Phase 7:** Performed experimentation on proton exchange membrane (PEM) fuel cell and regulated the input parameters for low feed flow rate and variable gas pressures.

Phase 1: Conducted an extensive literature survey and analysed the potential of various hydrogen production methods.
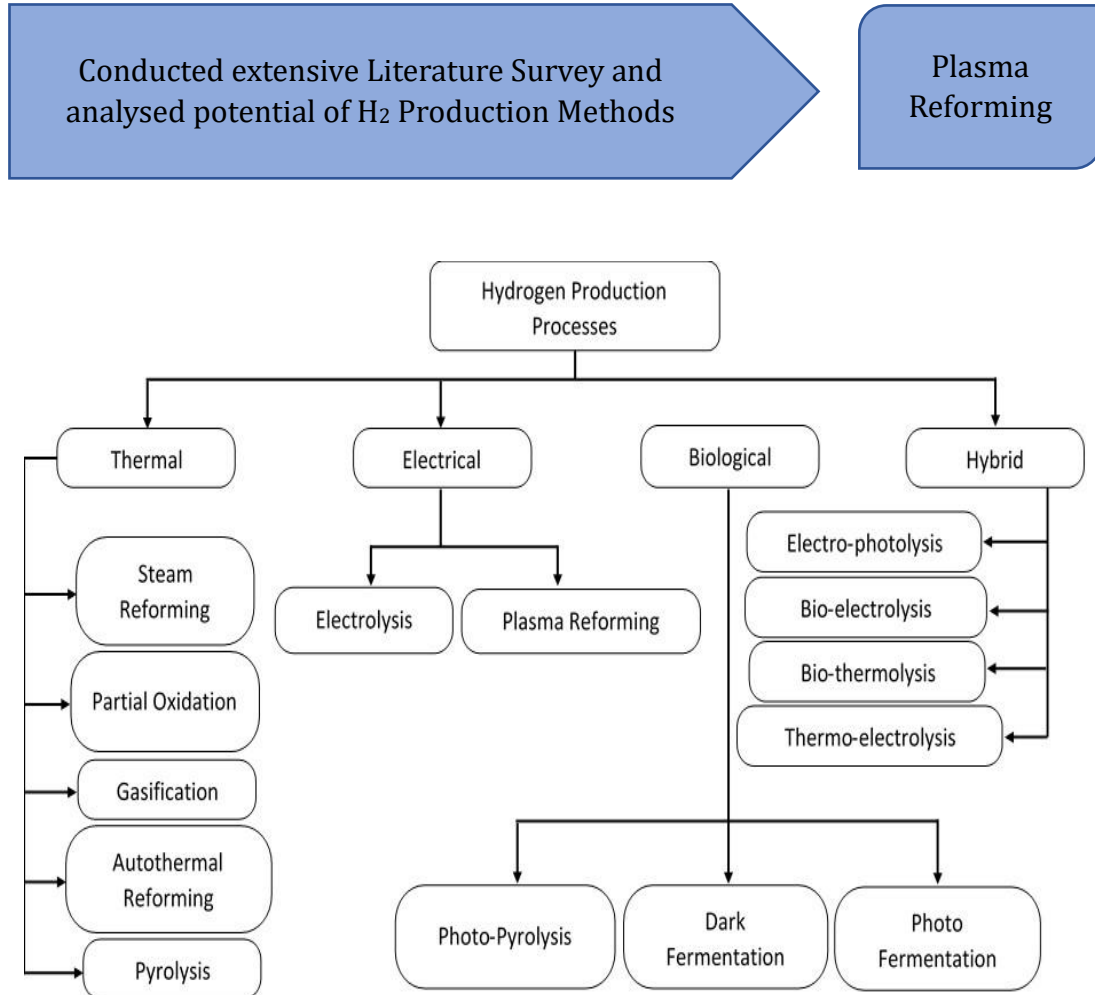
Figure 3.1. Various hydrogen production methods studied

An extensive literature review was performed to understand the various hydrogen production methods as stated in Figure 3.1. The working principles, raw materials and output gaseous mixture was studied thoroughly. The study revealed that among all hydrogen production methods, plasma reforming process was not much explored and there are still many loop holes that may be filled by extending the research towards this field. Therefore, the plasma reforming process was considered in the present study.

Phase 2: Design and fabrication of experimental setup for plasma reforming of alcohol-water mixture.
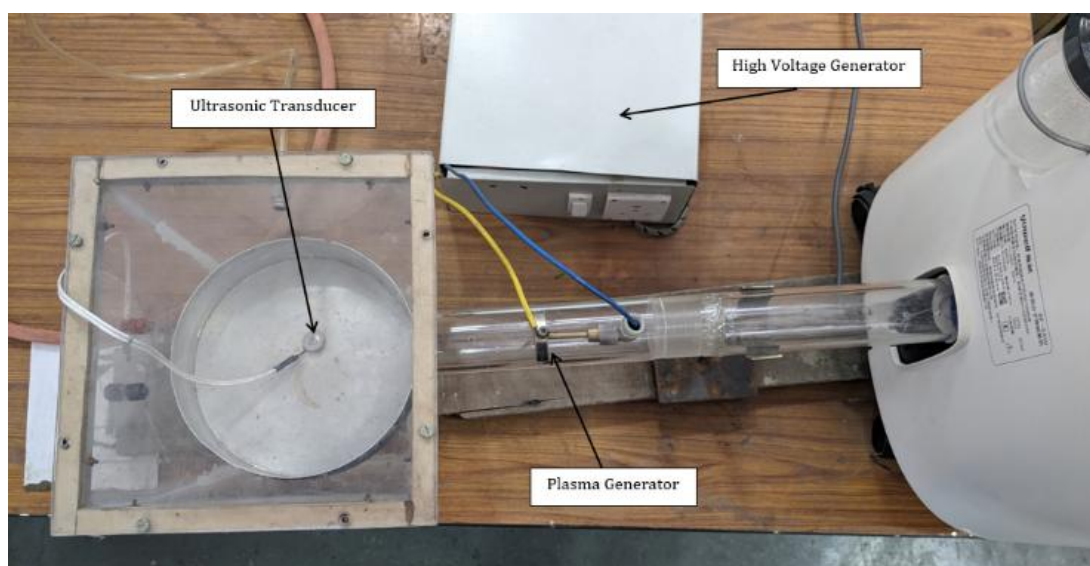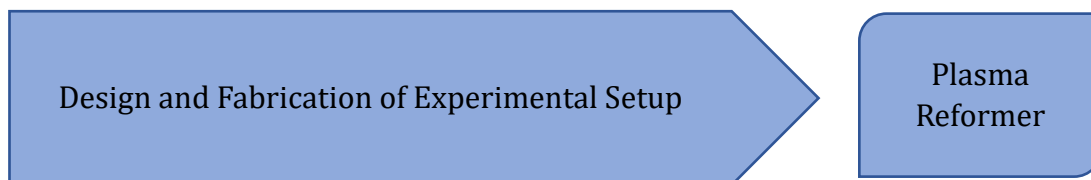
Figure 3.2. Plasma generator with atomizer

The research work required fabrication of a plasma reformer generator. The designing and fabrication process was performed within the laboratory and the plasma reformer fabricated is shown in Figure 3.2. A high voltage was generated using flyback transformer that has the potential of converting voltage at about 1 to 10 kV from an input of few volts. The two electrodes, one cylindrical road and another magnetic ring-type were used. The gapping between the two electrodes was maintained so that the plasma from one electrode may jump to another electrode. The magnetic ring-type electrode does not allow the jump from cylindrical electrode at single point, thus, a vortex at the reactor zone was created. Different atomizer having frequencies, 0.3 MHz, 1.7 MHz and 2.4 MHz were used to atomize water-alcohol mixture.

Phase 3: Characterised feed and identified the potential for Hydrogen production method in plasma reformer.
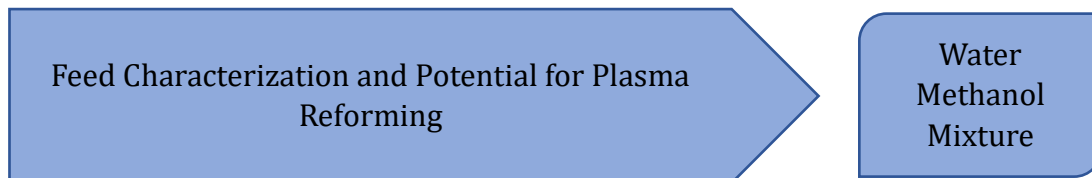
Figure 3.3. Raw material for plasma reformer

Table 3.1. Percentage content of raw material.

Sample No.	1	2	3	4	5	6	7	8
Water content (% vol.)	100	95	90	85	80	75	70	65
Methanol content (% vol.)	0	5	10	15	20	25	30	35

After through literature review, it was found that water-alcohol mixture has very high potential of generating hydrogen. The commercial grade methanol (ONGC/LPG/09/2015) and distilled water (de-ionized/ de-mineralized) were procured to prepare a water-methanol mixture at different methanol concentrations to be fed into the reactor. All the chemicals were high-grade and did not require any further processing to prepare samples for plasma reformer feed. The various samples tested in the plasma reactor are presented in Figure 3.3. The samples contained a water-methanol mixture in different compositions. The composition of various feeds is depicted in Table 3.1.

Phase 4: Determined the effects of operating parameters and optimized influencing parameters to enhance hydrogen production rate.

Experimentation: Effects of Parameter Determination and Optimization of Hydrogen Production Rate

DoE (RSM) & ANN-GA
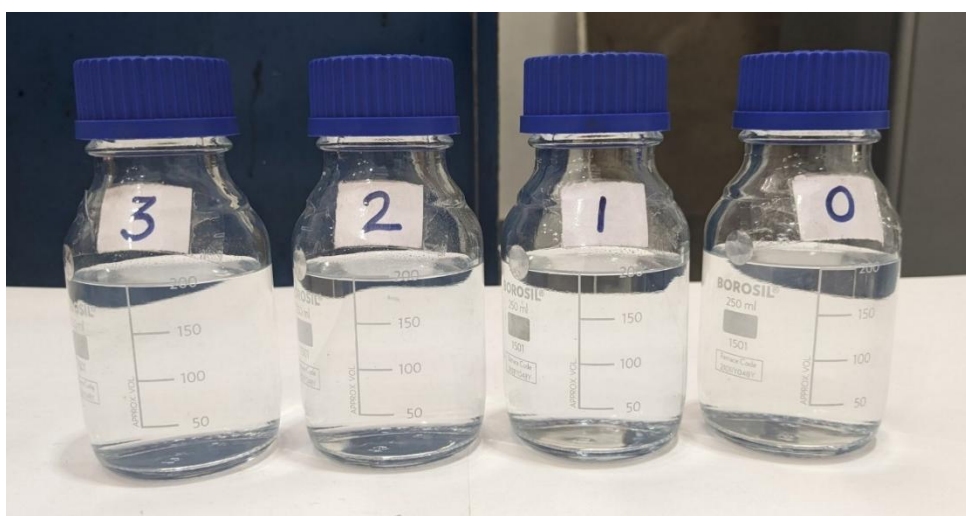
Figure3.4. Samples for parameter optimization

Table 3.2. Sample content for optimization

Sample No.	1	2	3	0
Water content (% vol.)	95	80	65	Optimized Value
Methanol content (% vol.)	5	20	35	

The process of water-methanol reforming was carried out in the plasma reformer. The plasma arc created in a high-temperature zone was used to break down the hydrogen bond of the feed, that splits water and methanol molecules into species like H, CO, and O ions. The process was then optimized using three different samples as shown in Figure 3.4. Whereas the content % by volume of water and methanol is depicted in Table 3.2. Here, 'Sample O' denotes the optimized values generated using RSM and ANN-GA model.

Phase 5: Developed a simulation model for hydrogen production and optimised the parameters for hydrogen selectivity and feed conversion rate (methanol-water mixture).

Developed Simulation Model and Optimized parameters for enhanced H₂ Production

Model Developed & RSM
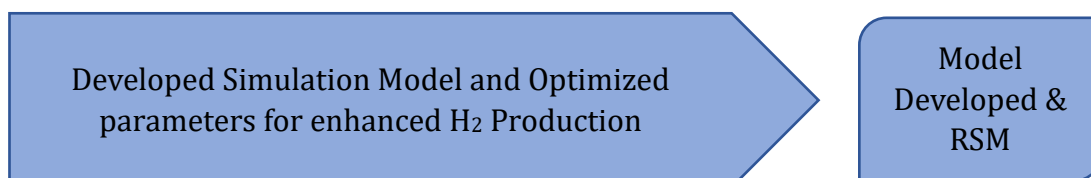
Figure 3.5. Simulation model for plasma reforming

A simulation model was developed, where an equilibrium reactor is used in the reforming process, and examined the effects of parameters like temperature, pressure, and Methanol-to-Water (M-to-W) molar ratio as shown in Figure 3.5. Hydrogen mole fraction and selectivity increase by roughly 18.5% and 10.5% when the reaction temperature increases from 100°C to 400°C. The effects of parameters in simulation model are investigated using RSM model where and DoE was generated and parameters were optimised for improved hydrogen selectivity and feed conversion rate.

Phase 6: Purified and characterized produced gas for hydrogen purity produced during experimentation.

Purification and Characterization of Purified Gas

Membrane Purification & GC-TCD

Figure 3.6. Tedler bags for sample collection

Figure 3.7. Gas chromatography for sample characterization

The gaseous mixture would contain compounds like H_2, CO_2, and CO. the samples from plasma reform and purification unit were collected in tedler bags (Figure 3.6), and tested using Agilent make GC-TCD for gas composition (Figure 3.7).

Phase 7: Performed experimentation on proton exchange membrane (PEM) fuel cell and regulated the input parameters for low feed flow rate and variable gas pressures.
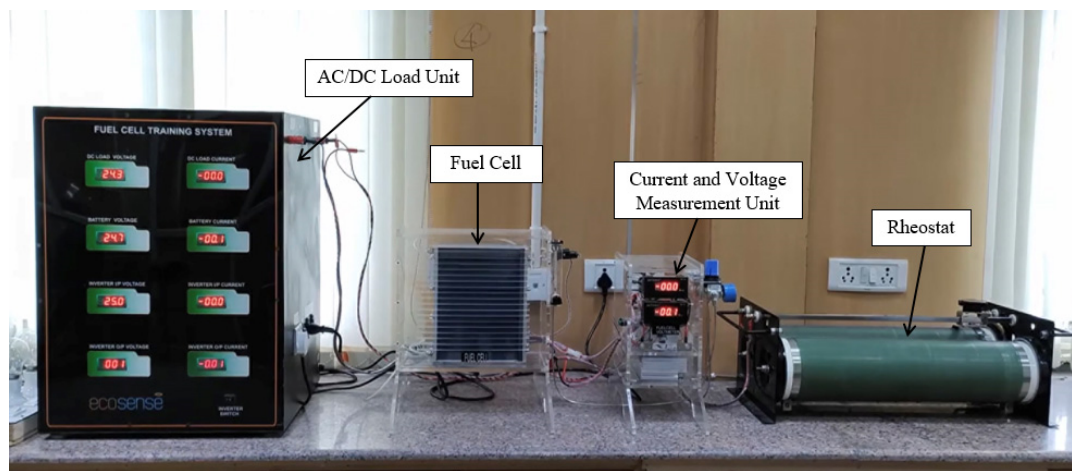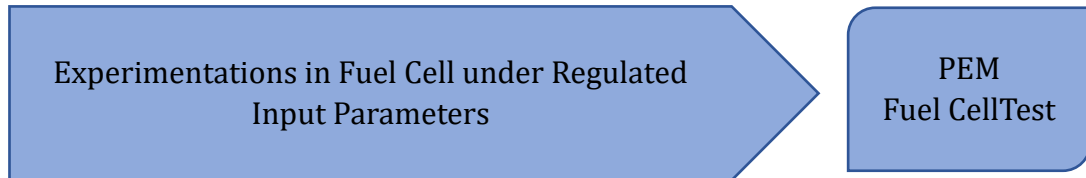
Figure 3.8. PEM fuel cell test setup

A proton exchange membrane (PEM) fuel cell containing 48 cells and a rated power of 1000 W was used as shown in Figure 3.8. The peak power was attained at about 28.8 V potential difference and 35 A current. The resistance was varied using a rheostat attached to the system and I-V characteristic, P-V characteristic and fuel stack efficiency were measured. The input parameters were regulated at lower hydrogen flow rate and gas pressure was varied to understand the performance of fuel cell at variable input parameters.

CHAPTER 4

HYDROGEN PRODUCTION AND OPTIMIZATION

4.1. Overview

Hydrogen energy is a non-polluting energy source. The commercial usage of hydrogen energy started long ago, but the production processes are still conventional [28,181]. About 97-98% of production was from steam reforming of natural gas, and 2-3% was from water electrolysis [11,18]. Water electrolysis is a cleaner hydrogen production process when combined with other renewable energy sources. In contrast, the hydrogen production rate for water electrolysis is very low. Hence, the industries were forced to consume hydrogen produced from conventional processes using non-renewable and polluting raw materials [182,183].

The over-exploitation of non-renewable energy sources has created many environmental problems. A group of countries sits annually for an annual environmental issues analysis and prepares a report on the actions taken and future roadmaps. This report was published as the 'CoP Sustainability Report'. The primary objective of the CoP is "To prevent global temperature surpassing 2°C by the end of the century, and progress towards this target is reviewed each year at the event." The CoP-26 was held in Glasgow, Scotland, United Kingdom [184]. The 197 parties in the event prioritized using low-carbon alternatives of energy sources. In addition, the CoP-27 held in Sharm El-Sheikh, Egypt, focused on carbon neutrality in energy sources [185]. Meanwhile, the recently held CoP-28 in Dubai, United Arab Emirates, debated whether fossil fuel phase-down or complete phase-out [186]. Hence, alternative energy sources were required to be produced from renewable and environmentally friendly raw materials such as biomass-based sources.

There are many such contenders for raw materials of alternative energy like biomass, biogas, biodiesel, and alcohol. In alcohols, the methanol has the highest hydrogen content, about 12.5% w/w of hydrogen. Methanol is considered carbon-neutral and can be produced from renewable sources by processes such as fermentation [21]. *Wu et al.* used methanol for the production of hydrogen in a steam reforming (SR) process [187]. The best result was obtained at 3600 mL/g.h gas hourly space velocity (GHSV) was 98% methanol conversion, whereas 6000 mL/g.h GHSV showed a 100.8 mL/min reformate flow rate. In contrast, *Ranjekar* and *Yadav* analyzed the reaction mechanism and reaction pathways involved in the methanol-reforming process [188]. *Bepari et al.* discussed the catalytic effects of carbon catalysts in methanol-reforming. The result showed 46% methanol conversion at 300°C while 40% methanol conversion at 250°C and gave more than 90% hydrogen selectivity with good stability for 42 hours [189]. Hence, methanol is a good raw material for hydrogen production; however, the most widely used method of hydrogen production is steam reforming.

Pinzari used nanocrystalline TiO_2 to produce hydrogen in a methanol reformer for enhanced methanol conversion. The testing was performed between 200°C and 400°C at 50.0 h^{-1} GHSV [190]. It was observed that TiO_2 nanocrystalline improved the methanol conversion and hydrogen production. *Jin et al.* performed methanol reforming using $NiTiO_3$ nano-catalyst and obtained a significant rise in hydrogen production [191]. The higher methanol conversion (> 95%) and about 90% hydrogen selectivity were achieved at 550-600°C. The study also showed that methanol decomposition was dominated at low temperatures, whereas higher temperatures showed dominance in the methanol-water decomposition. *Mironova et al.* studied methanol steam reforming using a metal-carbon catalyst for hydrogen production and found good stability for continuous operation for more than 30 hours [192]. *Hafeez et al.* conducted modelling of a methanol-reforming micro-reactor for hydrogen production. The computational fluid dynamics analysis showed higher methanol conversion while rising temperature, steam-to-methanol ratio, and residence time [193]. Hence, these parameters are significant for enhanced hydrogen production through methanol-reforming.

In contrast, *Budhraja et al.* generated a methanol-reforming model and observed 95% methanol conversion at 400°C. Meanwhile, the methanol-to-water ratio enhanced methanol conversion [194]. The reaction temperature significantly affected hydrogen production and showed a 10.5% rise in hydrogen selectivity from 100°C to 400°C [195]. *Chen et al.* simulated an integrated methanol-reformer and used heat from a proton exchange membrane fuel cell [196]. The study conducted a systematic investigation to understand the effects of various parameters. The steam-methanol ratio and reformer temperature significantly influenced the hydrogen production. *Zhao et al.* used a hybrid methanol reformer assisted with solar energy. The system utilized solar heat and heat from proton exchange membrane fuel cells for methanol conversion [197]. Thus, the study showed the importance of temperature in the methanol-reforming process. *Wang* and *Wang* performed methanol-reforming for hydrogen production in a micro-reactor reaction chamber. An increase of 2.6% and 5.46% in hydrogen production rate and methanol conversion was attained at 270°C and 0.95 h^{-1} space velocity [198].

4.2. Materials and Method

The raw materials and the production process used were discussed, and the purification method, mathematical calculations, and analysis implemented were also proposed in this section.

4.2.1. Materials

The commercial grade methanol (ONGC/LPG/09/2015) and distilled water (de-ionized/ de-mineralized) were procured to prepare a water-methanol mixture at different methanol concentrations to be fed into the reactor. All the chemicals were high-grade and did not require any further processing to prepare samples for plasma reformer feed. The various samples tested in the plasma reactor are presented in Figure 4.1.

Figure 4.1. Water-methanol mixtures feed into the plasma reformer

The samples contained a water-methanol mixture in different compositions. The composition of various feeds is depicted in Table 4.1.

Table 4.1. Composition of water-methanol feed

Sample No.	Water Content (%age)	Methanol Concentration (%age)
1	100	0
2	95	5
3	90	10
4	85	15
5	80	20
6	75	25
7	70	30
8	65	35

4.2.2. Feed Atomization

The water-methanol mixture cannot be fed directly to the plasma reformer/ reactor; therefore, the feed atomization was carried out. Three different ultrasonic transducers (or atomizers) with frequencies of 0.3 MHz, 1.7 MHz, and 2.4 MHz were installed for feed atomization. The average droplet size for 0.3 MHz, 1.7 MHz and 2.4 MHz are 200 nm, 130 nm and 50 nm, respectively [199]. The ultrasonic transducers and their circuit are shown in Figure 4.2. The working principle of the ultrasonic transducer depends on the sound frequency at the ultrasonic level generated by the metal diaphragm connected with the piezo-ceramic element. The ultrasonic sound waves vibrate the metal diaphragm to convert liquid feed into minute droplets with a

diameter within a few nanometres (nm) range. The atomized feed was then fed into the plasma reformer for further processing.
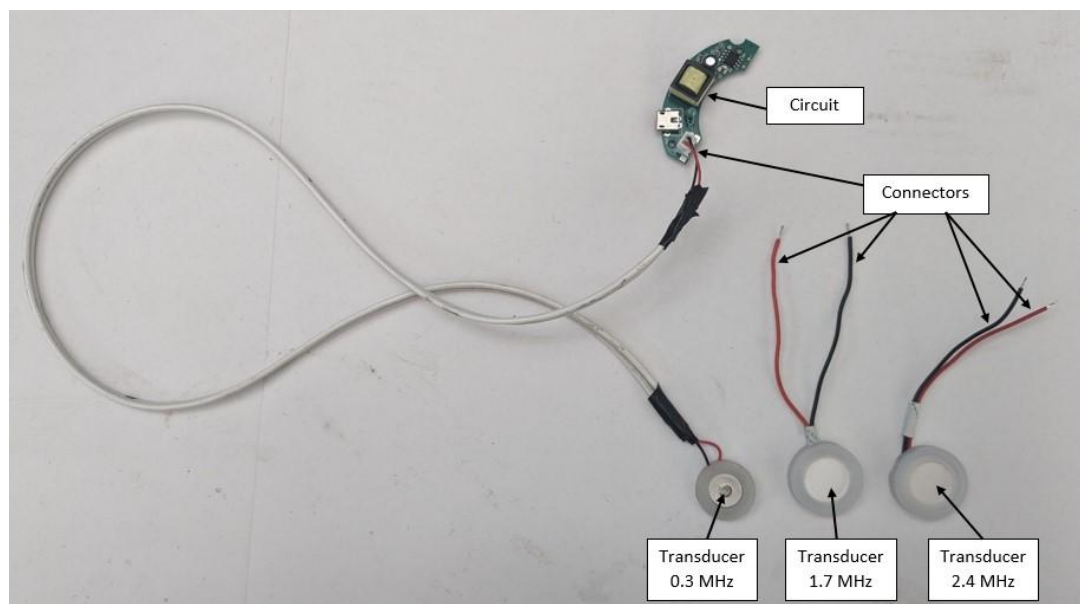
Figure 4.2. Various ultrasonic transducers with circuit

4.2.3. Plasma Reforming Process

The process of water-methanol reforming was carried out in the plasma reformer designed and developed within the laboratory (shown in Figure 4.3). The plasma reformer consists of two electrodes (one cylindrical copper-based alloy and another neodymium-based ring-type magnet) placed in a cylindrical tube of inner diameter 20 mm. A high-voltage generator was designed with a flyback transformer that generated a potential difference between $1.0\,kV$ and $10\,kV$ at the output terminals. The atomized feed was fed into the reformer and passed through the two electrodes. The plasma arc jumps from the Cu electrode to the magnet electrode when the distance between the two electrodes ranges from 7 mm to 13 mm. The plasma arc created a high-temperature zone that breaks down the hydrogen bond of the feed. Hence, water and methanol molecules split into species like H, CO, and O ions. These ions recombine to form compounds like H_2, CO_2, and CO. The H_2 molecules were separated and stored in hydrogen storage bags, and tedler bags of 1 L were used to collect samples to test the product's purity.
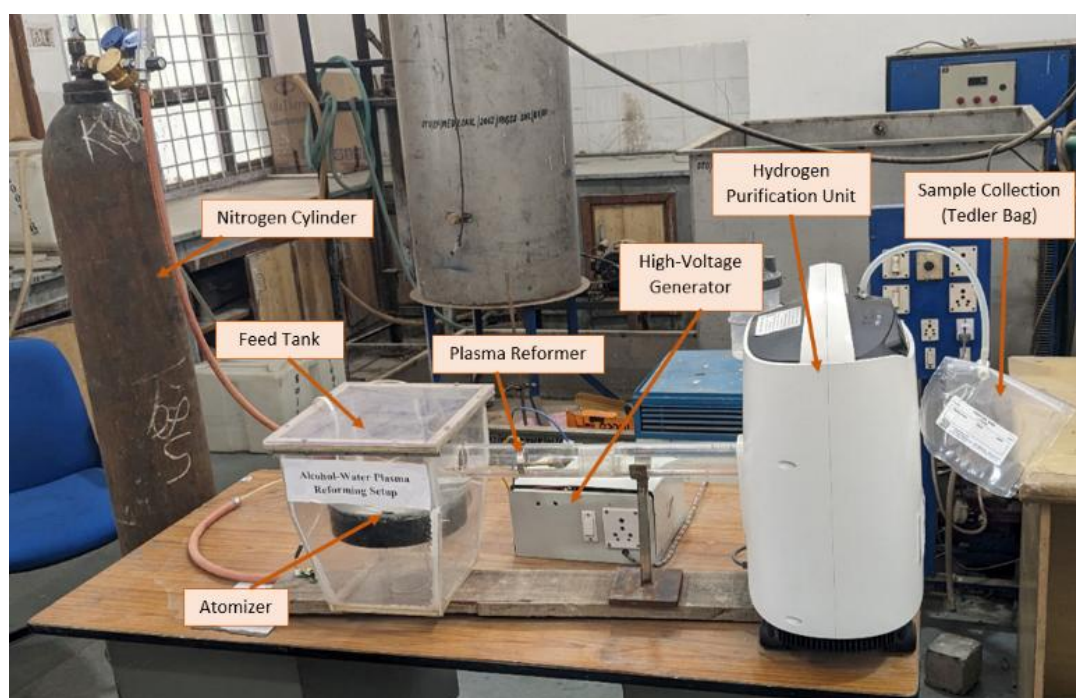
Figure 4.3. Experimental setup for plasma reforming

4.2.4. Hydrogen Purification

The hydrogen purification becomes very necessary to obtain pure hydrogen for applications such as fuel for fuel cell and other industrial applications. The gaseous mixture coming out the plasma reformer consists of H_2, N_2, CO, CO_2 etc. the hydrogen purification was performed by passing pressurised gaseous mixture through zeolite sieve. The void diameter of zeolite sieve was slightly more than the kinematic diameter of hydrogen molecules; thus, the hydrogen molecules pass through the sieve whereas other gaseous molecules being larger than the void diameter got stuck. Once the first sieve got chocked from larger gaseous molecules, the other sieve began working and a small amount of hydrogen gas after purification passes through first sieve in the reverse direction. In this process, the chocked voids get unblocked and become ready for operation after the second sieve got chocked. Therefore, an automatic ON/OFF switching of zeolite sieve perform a continuous hydrogen purification. The purified hydrogen was taken for sample testing in tedler bags for qualitative analysis using a gas chromatography.

4.2.5. Hydrogen Production Rate

The amount of hydrogen gas produced during the plasma reforming process was measured in hydrogen production rate, R_{H_2} (mol/day) using Equation (4.1),

$$R_{H_2} = \frac{W_{H_2}}{T} \tag{4.1}$$

Where W_{H_2} represents the amount of hydrogen produced in mol, and T represents the total time in hours.

4.2.6. Response Surface Methodology

The experimental variables in the hydrogen production process were optimized using the response surface methodology (RSM). As depicted in Table 4.2, the central composite design (CCD) generated a 20-run design of experiments (DoE) with three input variables at three levels. The RSM model generated empirical relationships between input and output variables to investigate the impacts of the various parameters at different levels. The various input variables involved in generating DoE for CCD were feed flow rate (FFR), methanol concentration (MeOH), and input voltage (Voltage).

Table 4.2. Operating parameters for the RSM model

Parameter	Unit	Levels		
		-1	0	1
P-Feed Flow Rate	LPM	0.5	2.5	4.5
Q-Methanol concentration	%	5	20	35
R-Voltage	kV	4	6	8

A CCD design consisting of 6-central, 6-axial, and 8-factorial points was used to generate a quadratic Equation (4.2) that represented Y as the response variable (Hydrogen production rate); P, Q, and R as input variables (depicted in Table 4.2); β as intercept; β_1, β_2 and β_3 as first-order coefficients; β_4, β_5 and β_6 as interactive

coefficients; β_7, β_8 and β_9 as a second-order coefficient and β_{10} as associated error, respectively.

$$Y = \beta_0 + \beta_1(P) + \beta_2(Q) + \beta_3(R) + \beta_4(PQ) + \beta_5(QR) + \beta_6(RQ) + \beta_7(P^2) + \beta_8(Q^2) + \beta_9(R^2) + \beta_{10} \qquad (4.2)$$

In the earlier study, *Budhraja et al.* used RSM-CCD to optimize hydrogen production from a water-methanol mixture via a reforming process [195]. The optimized hydrogen selectivity of 84.81% was achieved against the maximum simulated hydrogen selectivity of 82.76%. Similarly, in another study, *Budhraja et al.* optimized biohydrogen production using an anaerobic digester [200,201]. The optimized hydrogen yield of 25.27% was found against the maximum yield of 24.6%. In another study, *Budhraja et al.* optimized the biodiesel yield using the RSM model and observed a 92% optimized yield against 89% of the maximum experimental biodiesel yield [202].

4.3. Results and Discussions

This section describes the results obtained during experimentation and analyses the results through discussions. The effects of various process parameters, namely input voltage, methanol concentration, and feed flow rate, were studied. The three ultrasonic transducers with ultrasonic frequencies of 0.3 MHz, 1.7 MHz, and 2.4 MHz were used to atomize the water-methanol mixture, and the effects with different parameters were observed. The results obtained were discussed separately for each parameter, taking the other two parameters constant. The regression analysis and the interactive effects of the various parameters were also studied. The optimized results were obtained and compared with the experimental results obtained.

4.3.1. Effect of Parameters

a) Input Voltage

The input voltage is a significant parameter of plasma generation. A minimum and maximum input voltage is necessary for an electron to jump from one electrode to another in the air. The lower voltage will not produce enough energy for

an electron jump. Meanwhile, the higher voltage will make a continuous electron jump from a single closest point between two electrodes. Hence, a specific voltage range will produce a plasma vortex due to the magnetic effect.
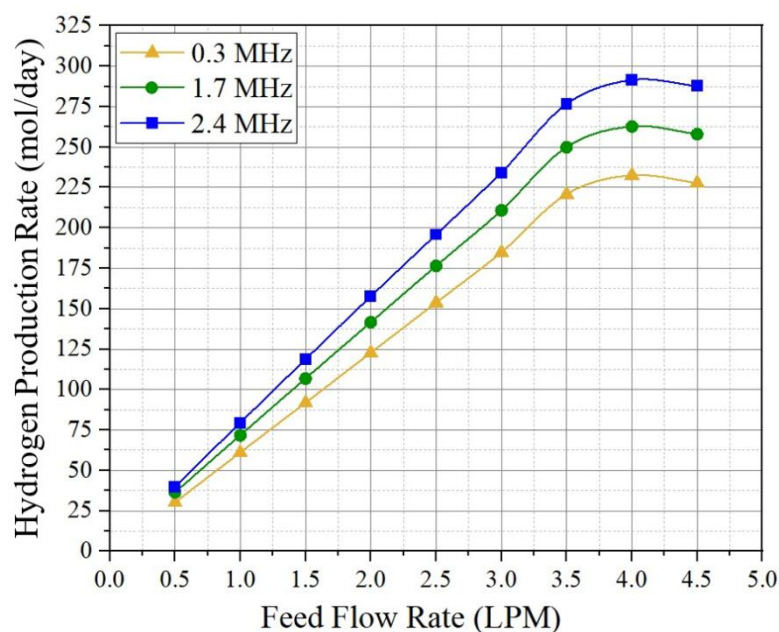
Figure 4.4. Hydrogen production rate with respect to input voltage

Figure 4.4 shows the influence of the input voltage from 4.0 kV to 8.0 kV on the hydrogen production rate (mol/day). The input voltage range was maintained between 4.0 kV and 8.0 kV because the electrons jump was not observed below 4.0 kV; hence, there was no plasma generation. In contrast, above 8.0 kV made a continuous electron jump from a single point, and no plasma arc vortex was generated. Therefore, the input voltage range was maintained between 4.0 and 8.0 kV. A water-methanol mixture with a 35% MeOH and FFR of 4.0 LPM was maintained.

The behaviour of three different curves for 0.3 MHz, 1.7 MHz, and 2.4 MHz ultrasonic transducer was represented in Figure 4.4. The H_2 production rate was observed between 215 mol/day and 306 mol/day. The highest HPR was achieved with a 2.4 MHz ultrasonic transducer followed by 1.7 MHz and 0.3 MHz transducers. The hydrogen production rate increased with the increase of input voltage and reached the peak value at about 7.5 kV. Beyond 7.5 kV, the hydrogen production rate showed a slight decline. The higher input voltage generated enough energy to ionize the

atomized water-methanol mixture. The ionization led to the breakdown of hydrogen bonds and, thus, generated hydrogen ions that combined to form hydrogen molecules. About a 14% rise in hydrogen production rate was observed when input voltage was increased from 4.0 kV to 7.5 kV for a 2.4 MHz ultrasonic transducer.

b)   Methanol Concentration

The methanol concentration in the mixture affects the hydrogen yield (or hydrogen production rate) during the plasma reforming process. The higher hydrogen content in the methanol, as opposed to water molecules, produces more hydrogen when the reforming process occurs. The methanol concentration range was maintained between 0% and 35% during the experimentation. The lower limit (0%) represents 100% water and no methanol content, whereas 35% means 65% water and 35% methanol content by volume. Beyond 35% methanol concentration, it was observed that the atomized mixture caught fire and started burning within the plasma reactor. Therefore, the methanol concentration was maintained below 35%.
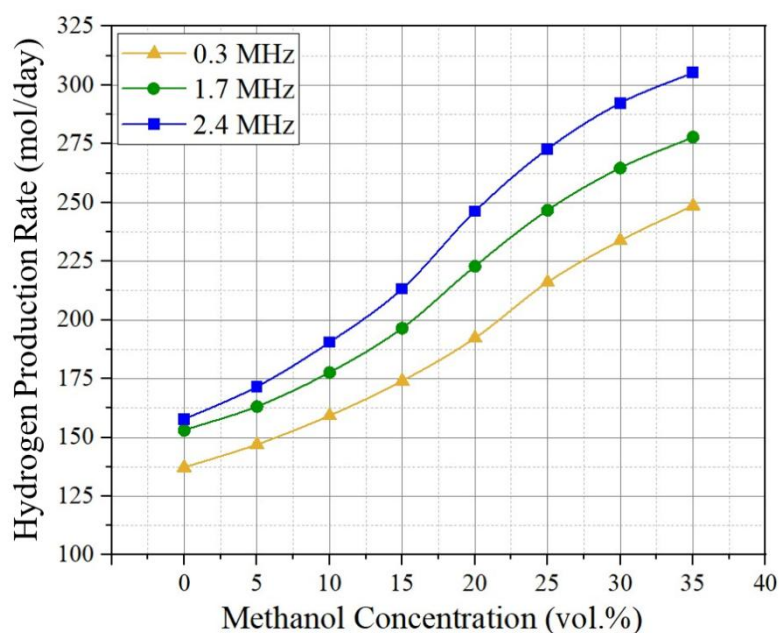
Figure 4.5. Hydrogen production rate with respect to methanol concentration

Figure 4.5 depicts the influence of methanol concentration on hydrogen production rate. The methanol concentration was maintained between 0% and 35%, and the input voltage and feed flow rate were retained at 3.5 kV and 4.0 LPM,

respectively. The various curves represented the ultrasonic transducers of 0.3 MHz, 1.7 MHz, and 2.4 MHz frequencies. Figure 4.5 showed that the highest hydrogen production rate was attained with a 2.4 MHz ultrasonic transducer followed by 1.7 MHz and 0.3 MHz transducers. The higher ultrasonic frequency tends to atomize liquid mixture molecules at finer droplets. The smaller the molecular droplets, the more smoothly molecular bond breakage occurs. The results showed a 90% rise in hydrogen production rate from 0% to 35% methanol concentration. A similar trend was observed for all ultrasonic transducers. Therefore, the higher methanol concentration in the water-methanol mixture gave a higher hydrogen production rate, and the highest hydrogen production rate of 306 mol/day was achieved for 35% methanol concentration using a 2.4 MHz ultrasonic transducer at 3.5 kV input voltage and 4.0 LPM feed flow rate.

c)   Feed Flow Rate

The feed flow rate is the amount of raw material (of feed) fed to the reactor at a given interval of time. The feed flow rate directly impacts the production rate because the more feed available, the more the product will generate. Here, the feed flow rate considered was between 0.5 LPM and 4.5 LPM. The experiments were also performed beyond 4.5 LPM, but the hydrogen production rate declined significantly. The other parameters, like input voltage and methanol concentration, were maintained at 3.5 kV and 35%.
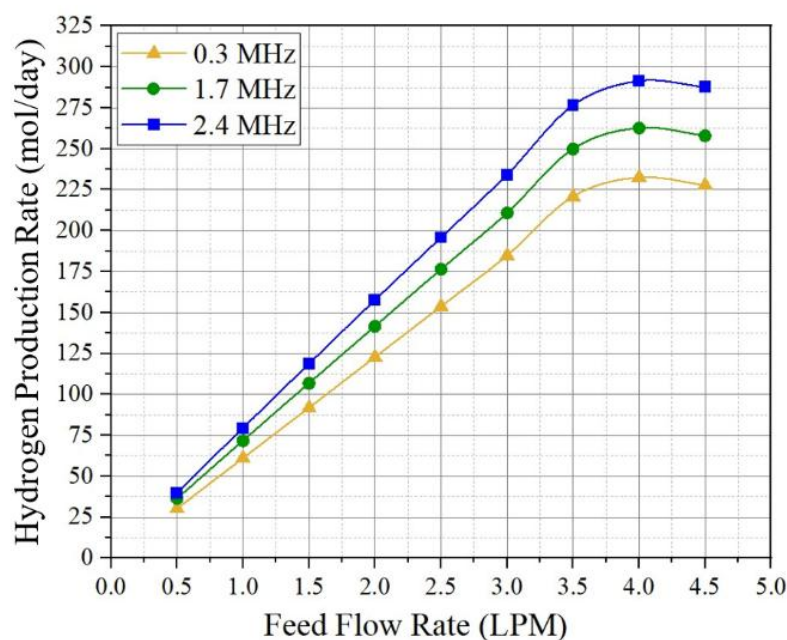
Figure 4.6. Hydrogen production rate with respect to feed flow rate

The influence of feed flow rate on hydrogen production rate for different ultrasonic frequency transducers was represented in Figure 4.6. The ultrasonic frequencies generated were 0.3 MHz, 1.7 MHz, and 2.4 MHz for feed atomization. The results showed a sudden rise from about 40 mol/h to 272 mol/h when the feed flow rate was increased from 0.5 LPM to 3.0 LPM for a 2.4 MHz ultrasonic transducer. It raised about 6.5 times the initial value, whereas the peak (288 mol/day) of hydrogen production rate was achieved at 3.5 LPM, and the rise was about 13%. The hydrogen production rate declined with a further rise in the feed flow rate. Similar trends were observed for 0.3 MHz and 1.7 MHz ultrasonic transducers.

Meanwhile, the highest H_2 production rate was obtained using a 2.4 MHz ultrasonic transducer. The higher feed availability in the reactor reduced the tendency of feed ionization, and much of the feed passed without contacting the plasma arc zone; therefore, fewer water-methanol molecules broke down to form radicals. In contrast, the lower feed flow rate reduced feed availability for reforming. Hence, the feed flow rate between 3.0 LPM and 4.0 LPM was considered significant for a higher H_2 production rate at 3.5 kV input voltage and 35% methanol concentration.

Beyond 4 LPM flow rate the hydrogen production rate start decreasing; however, the declining curve was smoother. The reason behind this behaviour was raw material flooding. Higher feed flow rate effects the plasma generation. At some instances, it was observed that the plasma vortex was not developed and the electron jump was occurring at a single point. It restricted the interaction between plasma and atomized feed, as a result, the hydrogen production rate started reducing.

d)   Optimal Parameters

Optimization aims to generate the best possible output from different combinations of input parameters. The output could be maximizing, minimizing, targeting, or maintaining a range of values, and the inputs are adjusted so that the response was satisfied. Table 4.3 shows that percentage errors for hydrogen production rate using RSM.

Table 4.3. Optimal parameters for HPR using RSM

Transducer Frequency (MHz)	Parameters			Hydrogen Production rate (mol/day)		%age error
	Feed Flow Rate (LPM)	Methanol concentration (%)	Voltage (kV)	Predicted	Experimental	
0.3	4.5	35	7.86	229.2	218.4	4.7
1.7	4.5	35	7.50	264.9	247.7	6.5
2.4	4.5	35	7.54	285.8	269.2	5.8

4.3.2. Hydrogen Purification and Qualitative Analysis

The purity of a compound becomes an essential criterion for its application. Similarly, H_2 applications like fuel cells for power generation demand H_2 gas input with a purity level of about 99.9% in proton exchange fuel cells. Hence, much research has been conducted to separate H_2 from a mixture of H_2-rich gases. Here, a H_2 purification unit that works on the principle of oxygen concentration was used; the composition of a gaseous mixture containing gases like H_2, carbon dioxide, nitrogen, and oxygen was determined using Agilent make gas chromatography (GC) having thermal conductivity detector (TCD). The chromatogram showing gas composition before purification is represented in Figure 4.7.
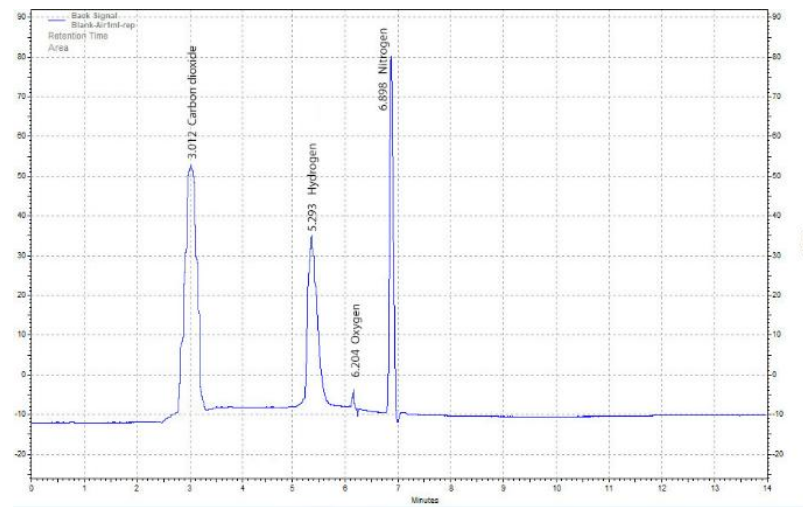
Figure 4.7. Composition of the gaseous mixture

The oxygen concentrator-type hydrogen purification unit has a compressor that compresses the gaseous mixture from the plasma reformer. The compressed gaseous mixture was then passed through a zeolite sieve membrane with a void diameter just above the kinematic diameter of H_2. Thus, the hydrogen molecules passed from the zeolite sieve membrane, leaving carbon dioxide, nitrogen, and other gases with bigger molecular diameters than sieve voids. However, in the process, the oxygen molecules also pass through the sieve because of their smaller molecular diameter than sieve voids. Therefore, the raw material chamber was kept oxygen-free by air tightening and injecting nitrogen gas from a nitrogen gas cylinder, allowing the nitrogen gas to flow for about 5 minutes before starting the plasma reformer.
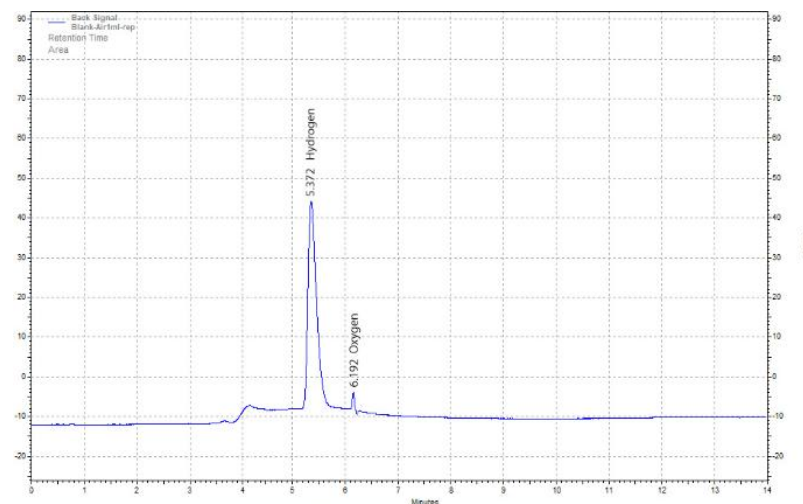
Figure 4.8. Gas composition of purified gas

The gas composition was also measured after the gaseous mixture passed through the hydrogen purification unit. The samples were collected in tedler bags of 1 L capacity and analyzed again in the GC-TCD. The chromatogram showing qualitative analysis was conducted in Figure 4.8. The results showed that the uncleaned gaseous mixture had about 32.2% hydrogen content. In contrast, the hydrogen content observed was 99% when passed through the hydrogen purification unit. In contrast, a small fraction of about 1% of oxygen was also present after purification. It was due to methanol-reforming, which contains oxygen content. The oxygen molecules may be captured using oxygen absorbers, and hydrogen gas of purity of more than 99% may be obtained.

4.4. Response Surface Methodology

4.4.1. Empirical Design & Regression Analysis

The three process parameters involved in the optimization process are feed flow rate (FFR), methanol concentration (MeOH), and input voltage (Voltage). Table 4.2 shows that a DoE was generated in CCD for three factors at three levels. A 20-run design matrix for hydrogen production rate (HPR) was developed using three different ultrasonic frequency transducers (0.3 MHz, 1.7 MHz and 2.4 MHz). The residual (or percentage error) was computed using actual and predicted values received through analysis and depicted in Table 4.4.

Experimental randomizations reduced the response variations. The predicted values were produced through a response model for each ultrasonic frequency transducer {Equation (4.3), Equation (4.4) and Equation (4.5)} with a 95% confidence level. Here, the terms FFR, MeOH, and Voltage were linear; $(FFR)^2$, $(MeOH)^2$, and $(Voltage)^2$ were quadratic terms; and (FFR x MeOH), (MeOH x Voltage) and (Voltage x FFR) were interactive terms for hydrogen production rate at relative frequencies.

Table 4.4. Matrix design of 20-runs (Experimental)

Run	Parameters			Hydrogen Production Rate (mol/day)								
				0.3 MHz			1.7 MHz			2.4 MHz		
	FFR (LPM)	MeOH (%)	Voltage (kV)	Actual Value	Predicted Value	Residual	Actual Value	Predicted Value	Residual	Actual Value	Predicted Value	Residual
1	0.5	35	4	26.7	23.6	3.10	34.2	32.6	1.61	39.1	41.0	-1.93
2	2.5	35	6	147.2	153.9	-6.67	166.8	174.4	-7.58	196.3	193.5	2.83
3	2.5	20	6	132.3	131.4	0.94	148.1	149.4	-1.31	169.8	172.2	-2.38
4	2.5	20	6	132.3	131.4	0.94	148.1	149.4	-1.31	169.8	172.2	-2.38
5	4.5	35	8	231.1	230.2	0.92	267.0	266.0	0.96	282.2	286.5	-4.28
6	0.5	5	4	15.0	15.2	-0.18	21.8	23.7	-1.94	31.7	29.2	2.50
7	2.5	5	6	109.3	105.6	3.75	145.6	134.1	11.52	164.6	160.3	4.31
8	2.5	20	6	132.3	131.4	0.94	148.1	149.4	-1.31	169.8	172.2	-2.38
9	2.5	20	6	132.3	131.4	0.94	148.1	149.4	-1.31	169.8	172.2	-2.38
10	0.5	35	8	28.7	29.6	-0.92	35.1	33.6	1.50	40.2	40.0	0.23
11	2.5	20	8	140.7	135.5	5.23	155.3	150.7	4.64	181.3	172.5	8.85
12	0.5	20	6	22.6	21.7	0.87	27.3	24.0	3.34	35.7	31.5	4.15
13	2.5	20	4	119.5	127.6	-8.15	145.3	146.0	-0.70	166.2	167.9	-1.71
14	2.5	20	6	132.3	131.4	0.94	148.1	149.4	-1.31	169.8	172.2	-2.38
15	4.5	5	8	139.6	142.0	-2.36	191.7	194.3	-2.59	232.1	231.9	0.15
16	0.5	5	8	9.9	12.7	-2.85	16.4	20.9	-4.50	21.9	26.8	-4.94
17	2.5	20	6	132.5	131.4	1.14	148.1	149.4	-1.31	169.8	172.2	-2.38
18	4.5	20	6	176.8	180.6	-3.79	221.9	221.3	0.60	254.1	251.1	2.99
19	4.5	35	4	215.7	212.1	3.59	257.4	253.9	3.52	278.2	275.0	3.16
20	4.5	5	4	134.0	132.4	1.66	183.5	186.0	-2.48	219.8	221.8	-2.01

$$HPR\ (0.3\ MHz) = -10.661 + 61.049\ FFR - 0.006\ MeOH - 1.950\ Voltage +$$
$$0.595\ FFR * MeOH + 0.753\ FFR * Voltage + 0.070\ MeOH * Voltage -$$
$$7.549\ FFR^2 - 0.007\ MeOH^2 + 0.051\ Voltage^2 \tag{4.3}$$

$$HPR\ (1.7\ MHz) = -11.837 + 68.784\ FFR - 0.937\ MeOH + 2.013\ Voltage +$$
$$0.492\ FFR * MeOH + 0.697\ FFR * Voltage + 0.032\ MeOH * Voltage -$$
$$6.694\ FFR^2 + 0.021\ MeOH^2 - 0.269\ Voltage^2 \tag{4.4}$$

$$HPR\ (2.4\ MHz) = -21.500 + 81.859\ FFR - 0.658\ MeOH + 4.952\ Voltage +$$
$$0.345\ FFR * MeOH + 0.781\ FFR * Voltage + 0.011\ MeOH * Voltage -$$
$$7.711\ FFR^2 + 0.021\ MeOH^2 - 0.499\ Voltage^2 \hspace{2cm} (4.5)$$

The F-values and p-values of the parameters were calculated from analysis of variance (ANOVA) tests. The proportion between the mean square errors is defined as the F-value. A higher F-value determined the significance of a parameter. Similarly, the variation between the group means describes the p-value. The relevance of a parameter was described by the p-value <0.001, respectively. Here, the ANOVA tables were developed for each ultrasonic frequency (Table 4.5, Table 4.6 and Table 4.7), and each parameter's significance was determined for the hydrogen production rate. Table 4.5, Table 4.6 and Table 4.7 concluded that the feed flow rate and the methanol concentration were the most significant parameters through F-values and p-values calculations for each ultrasonic frequency transducer.

Table 4.5. ANOVA table of 0.3 MHz ultrasonic frequency for HPR

Source	Sum of Squares	df	Mean Square	F-value	p-value	
Model	76566.51	9	8507.39	397.76	< 0.0001	significant
A-Feed Flow Rate	63091.25	1	63091.25	2949.84	< 0.0001	
B-Methanol concentration	5837.06	1	5837.06	272.91	< 0.0001	
C-Voltage	152.88	1	152.88	7.15	0.0233	
AB	2545.41	1	2545.41	119.01	< 0.0001	
AC	72.60	1	72.60	3.39	0.0952	
BC	35.70	1	35.70	1.67	0.2254	
A²	2507.36	1	2507.36	117.23	< 0.0001	
B²	7.45	1	7.45	0.3481	0.5683	
C²	0.1151	1	0.1151	0.0054	0.9430	
Residual	213.88	10	21.39			
Lack of Fit	213.85	5	42.77	6415.40	< 0.0001	significant
Pure Error	0.0333	5	0.0067			
Cor Total	76780.39	19				

Table 4.6. ANOVA table of 1.7 MHz ultrasonic frequency for HPR

Source	Sum of Squares	df	Mean Square	F-value	p-value	
Model	1.064E+05	9	11817.72	408.97	< 0.0001	significant
A-Feed Flow Rate	97357.69	1	97357.69	3369.18	< 0.0001	
B-Methanol concentration	4060.23	1	4060.23	140.51	< 0.0001	
C-Voltage	54.29	1	54.29	1.88	0.2005	
AB	1743.45	1	1743.45	60.33	< 0.0001	
AC	62.16	1	62.16	2.15	0.1732	
BC	7.41	1	7.41	0.2565	0.6235	
A²	1971.81	1	1971.81	68.24	< 0.0001	
B²	63.96	1	63.96	2.21	0.1677	
C²	3.19	1	3.19	0.1104	0.7465	
Residual	288.97	10	28.90			
Lack of Fit	288.97	5	57.79			
Pure Error	0.0000	5	0.0000			
Cor Total	1.066E+05	19				

Table 4.7. ANOVA table of 2.4 MHz ultrasonic frequency for HPR

Source	Sum of Squares	df	Mean Square	F-value	p-value	
Model	1.286E+05	9	14287.37	608.92	< 0.0001	significant
A-Feed Flow Rate	1.205E+05	1	1.205E+05	5136.32	< 0.0001	
B-Methanol concentration	2752.28	1	2752.28	117.30	< 0.0001	
C-Voltage	51.53	1	51.53	2.20	0.1692	
AB	856.98	1	856.98	36.52	0.0001	
AC	78.13	1	78.13	3.33	0.0980	
BC	0.8450	1	0.8450	0.0360	0.8533	
A²	2616.47	1	2616.47	111.51	< 0.0001	
B²	60.87	1	60.87	2.59	0.1383	
C²	10.95	1	10.95	0.4667	0.5100	
Residual	234.64	10	23.46			
Lack of Fit	234.64	5	46.93			
Pure Error	0.0000	5	0.0000			
Cor Total	1.288E+05	19				

Table 4.8. Regression table for hydrogen production rate

Transducer Frequency	0.3 MHz	1.7 MHz	2.4 MHz
R^2	0.9972	0.9973	0.9982
Adjusted R^2	0.9947	0.9949	0.9965
Predicted R^2	0.9791	0.9797	0.9835
Adeq Precision	66.4889	64.4920	75.8035
Std. Dev.	4.62	5.38	4.84
Mean	115.54	137.89	158.11
C.V. %	4.00	3.90	3.06

The coefficient of regression (R^2) values of each ultrasonic frequency transducer were also calculated for the hydrogen production rate. It determined the model's adequacy and showed the competence of the outcomes with the statistically predicted values. The values closer to unity showed better predictions for the model. Through Table 4.8, it was concluded that the R^2 values of the outputs from each ultrasonic frequency transducer were closer to 1 (unity). This showed a good correlation developed among the experimental and predicted values for hydrogen production rate.

4.4.2.   Interactive Effects of Parameter

The analysis of the interactive effects of the parameters generated a relationship between two parameters taken together to the response value. The relationship was developed using model equations for each response value. A 3D surface contour graph was developed with two parameters, and a response value described the interactive effects of the parameters considered during the analysis.
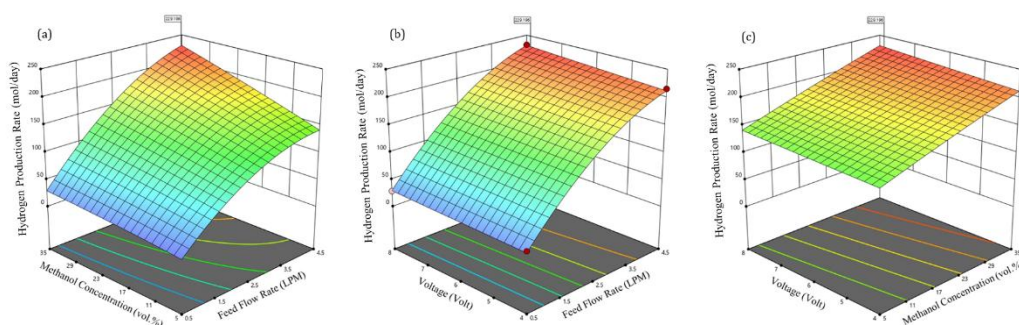
Figure 4.9. 3D Surface contour curve of hydrogen production rate for 0.3 MHz transducer frequency (a) MeOH vs FFR; (b) Voltage vs FFR; and (c) Voltage vs MeOH
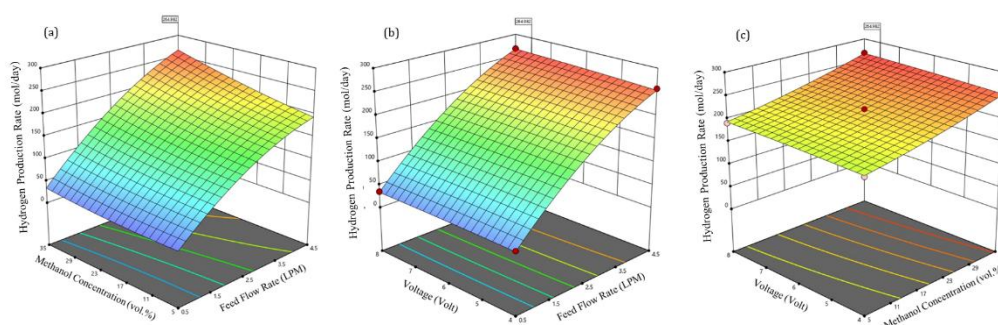
Figure 4.10. 3D Surface contour curve of hydrogen production rate for 1.7 MHz transducer frequency (a) MeOH vs FFR; (b) Voltage vs FFR; and (c) Voltage vs MeOH
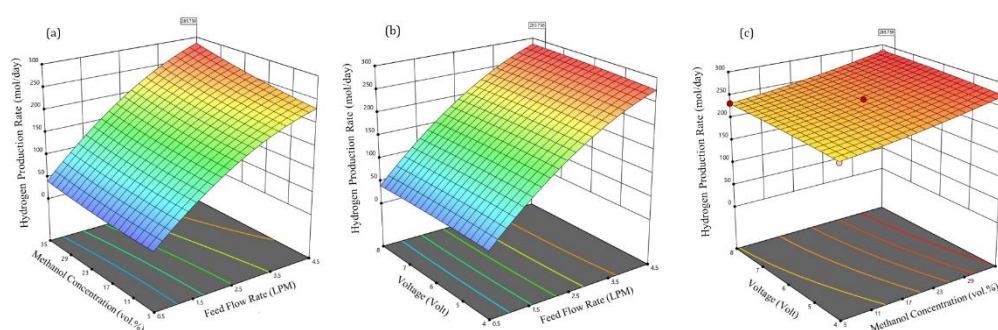
Figure 4.11. 3D Surface contour curve of hydrogen production rate for 2.4 MHz transducer frequency (a) MeOH vs FFR; (b) Voltage vs FFR; and (c) Voltage vs MeOH

The interactive effects of different parameters with a 0.3 MHz ultrasonic frequency transducer for HPR are shown in Figure 4.9. In Figure 4.9 (a), the FFR and MeOH were taken together, while in Figure 4.9 (b), the MeOH and Voltage and in Figure 4.9 (c), the Voltage and FFR were taken together. The results showed that the FFR of 4.5 LPM and MeOH of 35% vol. generated the highest HPR. Figure 4.9 (b) showed the highest HPR at 4.5 LPM and all input voltages. Similarly, Figure 4.9 (c) showed peak HPR at higher MeOH at all voltage ranges. Here, the peak HPR was 229.2 mol/day achieved with optimized parameters.

The interactive effects of different parameters on HPR using a 1.7 MHz ultrasonic frequency transducer are shown in Figure 4.10. Figure 4.10 (a) generated interaction between FFR and MeOH; Figure 4.10 (b) generated interaction between MeOH and Voltage; and Figure 4.10 (c) generated interaction between Voltage and FFR. The improvement in the HPR from the 0.3 MHz ultrasonic frequency transducer was seen, and the peak was attained at 265.0 mol/day. Figure 4.10 (a) showed a peak

value of HPR at FFR of 4.5 LPM and MeOH of 35% vol., whereas Figure 4.10 (b) showed the highest value at 4.5 LPM and all voltage ranges. Similarly, the peak value in Figure 4.10 (c) was at higher methanol concentrations and all voltage ranges.

The interactive effects of different parameters with a 2.4 MHz ultrasonic frequency transducer for HPR were presented in Figure 4.11. In Figure 4.11 (a), the FFR and MeOH were taken together, while in Figure 4.11 (b), the MeOH and Voltage were brought together, whereas in Figure 4.11 (c), the Voltage and FFR were taken together. The interactions of parameters showed the maximum HPR of 285.8 mol/day. Figure 4.11 (a) showed a peak value at 4.5 LPM and 35 % vol. methanol concentration. Figure 4.11 (b) showed maximum HPR at 4.5 LPM and all voltage ranges. Similarly, Figure 4.11 (c) showed the peak value of HPR for all voltage ranges and at 35% vol. methanol concentration. The discussion showed that the higher ultrasonic frequency contributed to a higher hydrogen production rate. Also, the higher methanol concentrations and feed flow rates contributed to enhanced hydrogen production rate, which showed that hydrogen generation was mainly due to methanol conversion.

4.5. Artificial Neural Network (ANN)

Another tool used to optimize process parameters was the artificial neural network-genetic algorithm (ANN-GA) model. An ANN-GA model is a computational model that performs data interpretation and predictions based on the human brain and natural evolution. The correlation coefficient (R) for the hydrogen production rate was computed. The model's R values reached unity, showing a reliable regression model (see Figure 4.12). The optimized value of HPR achieved was 267.0 mol/day at 4.5 LPM feed flow rate, 33.8% vol. methanol concentration, and 7.4 kV input voltage.
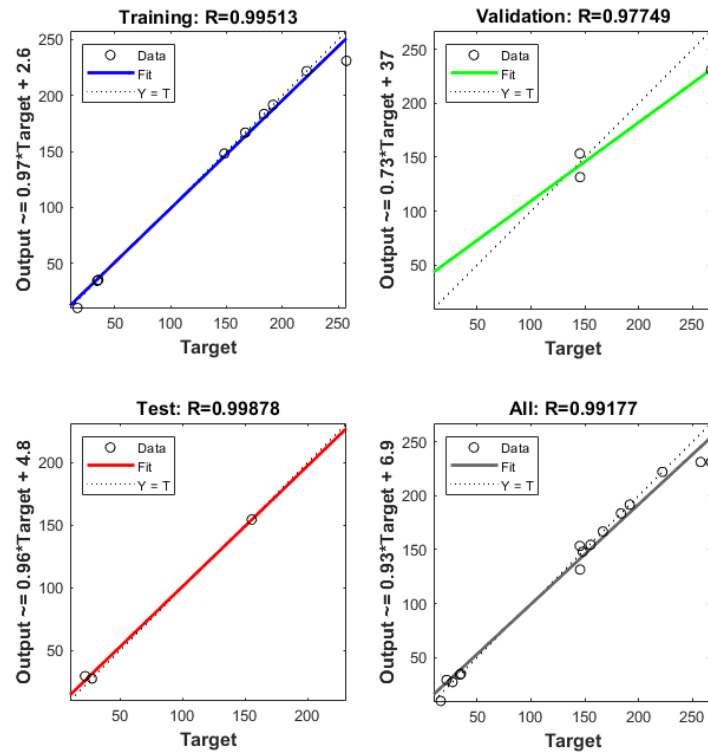
Figure 4.12. Coefficient of correlation (R) for hydrogen production rate

4.6. Optimal Values (Comparative Results)

This section discussed the comparative results obtained from RSM, ANN-GA, and experimental data. The optimal values of the parameters obtained from the RSM and ANN-GA model were used to perform experiments, and the results from the experimental data were computed for percentage error. The percentage errors for RSM values were observed to lie between 4% and 7%, whereas the percentage error for the ANN-GA model was about 2.5%. It showed that the ANN-GA model is superior in optimization to the RSM model.

4.7. System Efficiency

The system efficiency is a very critical parameter to determine the performance of a system. The system efficiency is defined as the ratio of output energy to the input energy. The input energy in the system is as follows,

Plasma reformer energy input = 26 Watts

Atomizer energy input = 4 Watts

Hydrogen purification energy input = 60 Watts

Total energy input = (26 + 4 + 60) = 90 Watts

Maximum hydrogen production = 306.2 mol/day

Energy density of hydrogen = 0.010 MJ/L at 1 bar and 20°C

Total energy production from hydrogen = 0.010 x (306.2/22.4) = 0.1367 MJ/L

Energy output in watts = 0.1367 x 277.78 = 38 Watts

Hence, the system efficiency = (38/90) x 100 = 42.2

$$\eta_{system} = 42.2\%$$

Therefore, the system efficiency was found to be 42.2%.

4.8. Summary

The experimental analysis of hydrogen production using plasma reforming of water-methanol mixture was performed. The study was conducted on the influence of three operating parameters: input voltage, methanol concentration, and feed flow rate at different ultrasonic transducer frequencies, i.e., 0.3 MHz, 1.7 MHz, and 2.4 MHz, respectively. The various operating parameters were varied to understand their interactive influence on hydrogen production rate. The data was optimized using response surface methodology and an artificial neural network-genetic algorithm. The following outcomes were observed:

- The atomization of the water-methanol mixture at 2.4 MHz ultrasonic frequency showed maximum hydrogen production rate, followed by 1.7 MHz and 0.3 MHz transducers.
- The hydrogen production rate rose by about 14%, with the input voltage rise from 4 kV to 7.5 kV.

- The maximum percentage rise of about 25% was observed at 1.7 MHz ultrasonic frequency.

- The higher methanol concentration showed a higher HPR and reached 306.2 mol/h hydrogen production rate using a 2.4 MHz ultrasonic transducer.

- The higher feed flow rate also positively influenced the hydrogen production rate and peaked at 3.5 LPM. Beyond 3.5 LPM, the HPR declined.

- All three ultrasonic transducers observed a similar trend for methanol concentration and feed flow rate, where 2.4 MHz showed the highest hydrogen production rate, followed by 1.7 MHz and 0.3 MHz, respectively.

- The hydrogen purity was observed at about 99% after using the hydrogen purification unit.

- Higher ultrasonic frequency has positive impacts on hydrogen production rate.

- The F-values and p-values of the methanol concentration and feed flow rate showed they were significant parameters in the plasma reforming process.

- The R^2 value from RSM showed good competence of the outcome with the statistically predicted values.

- The higher methanol concentration enhanced the hydrogen production rate.

- The ANN-GA model also showed correlation coefficient values close to unity; thus, the model was reliable.

- The experimental tests on the optimized values of RSM and ANN-GA models showed 4-7% and about 2.5% percentage errors, demonstrating the ANN-GA model's superiority over RSM.

- Plasma reforming with H_2 purification unit has the system efficiency of 42.2%.

Therefore, the experimental analysis of plasma reforming of a water-methanol mixture showed the potential of generating a gaseous mixture rich in hydrogen gas. Then, the hydrogen from the gaseous mixture can be extracted from different applications. Also, the hydrogen production was successfully optimized for enhanced production rate. The results obtained were reliable. Further work may be performed to up-scale the plasma reactor for commercialization, and other process parameters may also be considered for optimization.

CHAPTER 5

SIMULATION & OPTIMIZATION OF HYDROGEN PRODUCTION

5.1. Overview

In the last few years, the energy demand has increased at a very rapid pace. However, the Ukraine-Russia conflict worsened the scenario for many nations, especially Europe, and such situations may arise in the near future. Therefore, every country has been looking for domestic and sustainable energy sources that produce no or very few emissions to curb pollution from fossil fuels [203,204]. This way, the aim of sustainable fuel will also be fulfilled. Hydrogen energy is one such source that has the potential to replace most of the current fossil energy sources [205].

Hydrogen is the lightest element in the periodic table, and hydrogen compounds are available everywhere. However, hydrogen extraction from its compounds is challenging and requires enormous energy. Only a few technologies have been developed and commercialized for hydrogen production. *Chen et al.* performed ethanol steam reforming for hydrogen production and achieved a theoretical 73% hydrogen yield [206]. The authors used a Ni/Al_2O_3 catalyst to trigger the ethanol steam-reforming reaction. Similarly, *Dang et al.* used a Pd-promoted Ni-Ca-Al-O bifunctional catalyst and obtained 90% hydrogen yield from iso-octane steam reforming [207]. *Abbandanak et al.* combined $Cu-Zn-CeO_2-ZrO_2/MCM-41$ catalyst and $(Li-Na-K)NO_3.MgO$ absorbent for methanol steam reforming and obtained 99.8% hydrogen yield [208]. In contrast, *Qingli et al.* produced hydrogen from glycerol at a glycerol conversion percentage of 94.71%, respectively [209]. Therefore, different feedstock has the potential to produce hydrogen; however, methanol and water are very commonly used feedstock.

Methanol and water are notable and well-known sources of hydrogen production in various technologies. Methanol and water have more than 10% hydrogen content, and hydrogen extraction requires comparatively less energy than other sources. *Awasthi et al.* achieved a hydrogen production rate of 49 mol. H_2 per hour from methanol at 130°C [183]. Similarly, *Shen et al.* produced hydrogen from methanol at near room temperature through methanol dehydrogenation [210]. In contrast, *Khouya* used polymer electrolyte membrane electrolysis to produce hydrogen from water [211]. The author obtained significant results and an overall efficiency of 20%. *Palhares et al.* generated hydrogen at a rate of 2 litres per unit time in a solar-assisted alkaline water electrolyzer [97]. Any process before commercialization requires the simulation of various components. It helps in reducing the cost and achieving the targeted output results.

Modelling and simulation of various components of a chemical plant help determine the impacts of the different process parameters and cost considerations. *Ishaq* and *Dincer* designed a biomass and solar energy-based model for hydrogen production, where the overall system efficiency achieved is 29.9%, while the exergy efficiency is 31.5%, respectively [62]. *Bassyouni et al.* simulated a downdraft gasifier. The authors used date palm waste to produce syngas that contain a hydrogen content of 56.27%, while the other gases are carbon monoxide, carbon dioxide, and methane [63]. *Sanchez et al.* developed a model for an alkaline electrolysis system. The system simulation shows a maximum overall efficiency of 58% at 5 bar and 80°C of optimum conditions [64]. In contrast, *Chehade et al.* simulated and optimized natural gas steam-reforming plants for hydrogen production [212]. The results show 77.5% less energy consumption while optimizing the process parameters. Hence, optimizing process parameters helped reduce the energy requirement and improve hydrogen yield. Parameter optimization helps determine the main influencing parameters and achieve optimal results. *Liu et al.* used a mixed design to optimize hydrogen yield. The authors used a mixture of agricultural waste and obtained an optimized hydrogen yield of 21.0 mL/g [66]. In contrast, *Liu et al.* optimized process parameters in biohydrogen plants and achieved a 30.0 mL/g higher hydrogen yield at optimal conditions [67].

Bi et al. performed the parameter optimization analysis of a hydrogen liquefaction process. The authors observed a 22.06% drop in specific energy consumption and a 33.58% rise in the coefficient of performance [68]. Similarly, *Cao et al.* optimized reaction parameters in response surface methodology (RSM) and observed the interactive effects of parameters on ethanol reforming [69]. The results show ethanol-to-water molar ratio as the most influencing parameter, while the discharge power and total flow rate are comparatively lesser influencing parameters. Methanol has very close properties to ethanol in the alcohol group; therefore, similar parameters may be considered for the methanol–water-reforming process. Meanwhile, studying the various research articles on alcohol–water-reforming observed that reaction temperature, feed molar ratio, reactor pressure, and reactor type affect the hydrogen production rate.

5.2. Simulation Methodology

5.2.1. Simulation modelling

The simulation model is developed in Aspen Hysys for a methanol-reforming plant (see Figure 5.1), which uses mathematical models to simulate chemical processes in chemical plants and refineries. The high purity of methanol and water at a 1.0 molar ratio is considered for simulation because, in simulation and from published works, it is observed that the best methanol-to-water ratio lies between 0.5 and 1.5; therefore, the middle value is chosen. For determining the effect of the molar ratio, the molar ratio varied from 0.3 to 4 methanol-to-water ratios. The methanol and water are mixed in a mixer unit, and the mixture is then passed to a heat exchanger (part of the reformer) to adjust the temperature from 100°C to 400°C. Reactor pressure is another parameter considered for the simulation process, and its range is maintained between 1 atm. and 7 atm. similar parameter ranges (temperature from 50°C to 500°C and pressure from 1 atm. to 5 atm.) were also considered for glycerol steam reforming [58].
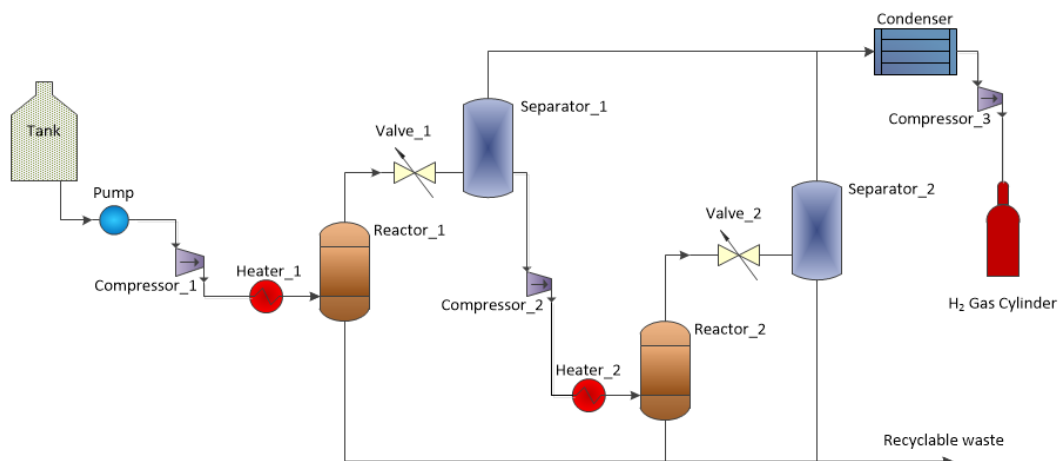
Figure 5.1. Schematic diagram of methanol-water reforming plant.

The parameter ranges are taken from previously published work [206]. Table 5.1 describes the various parameters and their range in the simulation process.

Table 5.1. Simulating parameters and their values

Parameter	Unit	Values
Temperature	°C	100, 150, 200, 250, 300, 350, 400
Reactor pressure	atm.	1, 2, 3, 4, 5, 6, 7
Methanol-to-Water (M-to-W) molar ratio	---	0.3, 0.4, 0.5, 0.6, 0.7, 0.8, 0.9, 1.0, 1.1, 1.2, 1.3, 1.4, 1.5, 1.6, 2.0, 2.5, 3.0, 3.5, 4.0

5.2.2. Reactor Type

Aspen Hysys is used in the analysis process modelling and integrating design tools. It performs the steady-state and flexible modelling of the distillation column [213]. It also provides easy-to-use, quick, and effective models for defined processes [214]. The comprehensive library includes a distillation column, process reactors, heat transfer components, controllers, and logical operations. The various components used are described in Figure 5.1. The catalyst considered in the study is nickel-supported alumina (Ni/Al_2O_3), which was used by researchers for the reforming [82]. The surface area, pore volume, and average pore size of the Ni/Al_2O_3 catalysts are in the range of 111-218 m^2/g, 0.129-0.205 cm^3/g, and 3.2-6.0 nm [215].

Basic reactions involved in methanol-reforming are represented in Equation (5.1) where methanol decomposes by steam into CO_2 and H_2 molecules, Equation (5.2) where direct decomposition of methanol results in CO and H_2 molecules, and Equation (5.3) is the water gas shift reaction; here, water molecule decomposes by CO into CO_2 and H_2, respectively.

$$CH_3OH + H_2O \leftrightarrow CO_2 + 3H_2 \tag{5.1}$$

$$CH_3OH \leftrightarrow CO + 2H_2 \tag{5.2}$$

$$CO + H_2O \leftrightarrow CO_2 + H_2 \tag{5.3}$$
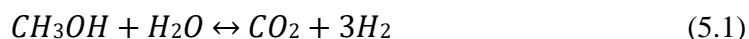
Considering the above reactions, the reactor type considered for the simulation process is an equilibrium reactor. It is used for equilibrium reactor sets that reach chemical and physical equilibrium. Here, the sensitivity of the operation is defined by the input parameters. The design parameters Reactor_1 are represented in Table 5.2, and similar parameters are considered for Reactor_2, respectively.

The following assumptions are made while performing the process analysis.

1) The whole system works in steady-state and steady-flow conditions.

2) Methanol used is 99.99% pure.

3) Methanol and water are fed at constant temperature and pressure.

4) Free carbon formation is not considered in the simulation.

5) Fluid flow is turbulent.

6) Streams are adiabatic in nature.

7) The flow rate is constant.

8) In the system, gases behave like ideal gases.

9) Methanol-water mixture remains constant throughout the simulation.

10) Hydrogen coming out is at a constant temperature (40°C).

Table 5.2. Design parameters of the reactor

Reactor Parameters	Units	Values
Diameter	meter	0.7620
Total Length	meter	3.048
L/D Ratio	-	4
Material Type	-	SS316
Mass Density	kg/m³	8027
Chemical Eng. Index	-	252.5
Maximum Allowable Vapour Velocity	m/s	1.25

5.2.3. Thermodynamic Model
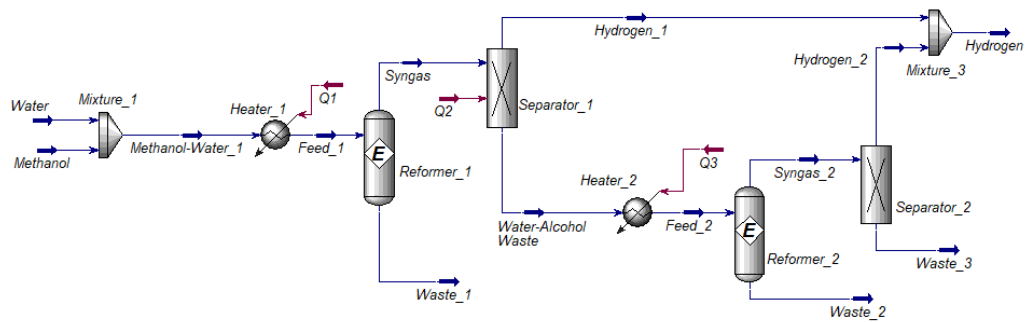
Figure 5.2. Simulation model for methanol-water reforming.

Simulation and modelling depend upon the thermodynamic fluid package selected. Different fluid packages are available in the Aspen Hysys simulator, such as Peng-Robinson, Soave Redlich Kwong, NRTL, PRSV, etc [63]. In the current study, the Peng-Robinson fluid package is selected, and the simulation diagram is shown in Figure 5.2. The mathematical equation developed in the Peng-Robinson model is presented in Equation (5.4),

$$P \ = \ \frac{RT}{(c + V_m) - b} \ - \ \frac{a}{(V_m + c)\,(V_m + c + b) + b\,(V_m + c - b)} \tag{5.4}$$

Where P is the gas pressure, R is the gas constant, T is the temperature, V_m is the molar volume, and a, d, and c are constants.

5.2.4. Response Surface Methodology

Mathematical models and statistical optimization are performed in RSM [216]. In an experimental design, RSM generates empirical models to determine the correlation between the input variables and output responses. It validates and optimizes the parameters comparatively faster than the Taguchi method. The analysis is performed in several runs to determine the best possible outcome. This study uses RSM's central composite design (CCD) to investigate the influence of the reaction temperature, reactor pressure, and methanol-to-water molar ratios on hydrogen selectivity and feed conversion percentage. The CCD performs consecutive runs and determines the suitability of data for lack of fit. The design performs 20 runs with RT, RP, and M-to-W molar ratio at three levels from -α to +α, as shown in Table 5.3.

Table 5.3. Operating parameters for the RSM model

Parameter	Unit	Levels		
		-α	0	+α
Reaction temperature	°C	200	300	400
Reactor pressure	atm.	1	3	5
Methanol-to-Water molar ratio	-	0.5	1	1.5

The design consists of 6-central points, 6-axial points, and 8-factorial points and uses the quadratic Equation (5.5) for analysis.

$$Y = \alpha_0 + \alpha_1(A) + \alpha_2(B) + \alpha_3(C) + \alpha_4(AB) + \alpha_5(BC) + \alpha_6(CA) + \alpha_7(A^2) + \alpha_8(B^2) + \alpha_9(C^2) + \alpha_{10} \tag{5.5}$$

Where Y is the response variable; A, B, and C are process parameters; α_0 is intercept; α_1, α_2, and α_3 are linear coefficients; α_4, α_5, and α_6 are interaction coefficients; α_7, α_8, and α_9 are second-order coefficients; and α_{10} is associated error. Parameter normalization is required in the regression analysis since various parameters are available at different values or ranges.

5.2.5. Hydrogen Selectivity and Feed Conversion Percentage

The mole fraction of hydrogen {Equation (5.6)} and methanol {Equation (5.7)} were used to determine the system's hydrogen selectivity and methanol conversion percentage. Here, x_{H_2} and x_{MeOH} are the mole fraction of hydrogen and methanol, W_{H_2} is the hydrogen production rate in mol/h, W_{MeOH} is the methanol flow rate in mol/h, and W_{total} Wtotal is the total feed flow rate in mol/h.

$$x_{H_2} = \frac{W_{H_2}}{W_{total}} \tag{5.6}$$

$$x_{MeOH} = \frac{W_{MeOH}}{W_{total}} \tag{5.7}$$

The methanol conversion percentage and hydrogen selectivity are calculated via Equation (5.8) and Equation (5.9).

$$Conversion\ percentage_{(MeOH)} = \frac{W_{MeOH_{in}} - W_{MeOH_{out}}}{W_{MeOH_{in}}} \times 100 \tag{5.8}$$

$$Selectivity_{H_2}(\%age) = \frac{W_{H_2}}{3(W_{MeOH_{in}} - W_{MeOH_{out}})} \times 100 \tag{5.9}$$

where $W_{MeOH_{in}}$ and $W_{MeOH_{out}}$ are methanol feed rates into the reactor in mol/h and unreacted methanol flow rate out of the system in mol/h.

5.3. Results and Discussions

5.3.1. Process Modelling and Validation

The developed Aspen Hysys model is validated against the four different experimental setups under similar conditions, and the feedstock selected is methanol. The aim is to verify the replication of the developed model at different process parameters and conditions. Following are the case studies:

- **Case 1:** *Lee* and *Kim* used a tubular quartz reactor with annular-shaped electrodes for methanol conversion into hydrogen through electric discharge, in which CuO/ZnO/Al$_2$O$_3$ was used as a catalyst [18]. Results showed about 57.6% methanol conversion at about 220°C. Likewise, the Aspen Hysys model simulation achieved a closer 59.3% methanol conversion result at 220°C. This shows a variation of 2.95% compared to the experimental results.

- **Case 2:** *Wang* and *Wang* performed catalytic methanol-reforming, where $CuO/ZnO/Al_2O_3$ catalyst was filled in the micro-reactor designed for hydrogen production [198]. An 87.1% methanol conversion was obtained at about 270°C inlet temperature. However, the Aspen Hysys model with similar experimental conditions and parameters achieved a methanol conversion of 89%. It shows a 2.18% deviation from the experimental results.

- **Case 3:** *Kim et al.* performed methanol-reforming in a prototype reactor filled with $CuO/ZnO/Al_2O_3$ catalyst [217]. Methanol conversion was calculated at different temperatures, and the highest (96%) methanol conversion was obtained at 290°C. When similar experimental conditions are created in the Aspen Hysys model, the methanol conversion shows a 1.25% reduction from the experimental results. In contrast, the highest methanol conversion obtained was 94.8% in simulation as against 96% in experimental results at 290°C.

- **Case 4:** *Liu et al.* used $1Pt/3In_2O_3/CeO_2$ catalyst for H_2 production from methanol in a process called methanol steam reforming [218]. Experimentally, a very high methanol conversion of 98.7% was achieved at 325°C. When the experimental conditions are put into the Aspen Hysys model, a similar methanol conversion of 98.2% is obtained, which is just 0.51% lower than the experimental results.

Therefore, it concludes that the Aspen Hysys model has minimal variations (below 5%) from the experimental results, as observed in Cases 1, 2, 3, and 4. Hence, the developed model is applicable for methanol reforming and determining the effects of various process parameters in the methanol conversion and hydrogen production process with percentage differences (as shown in Table 5.4).

Table 5.4. Case study-based validation from earlier published data for methanol feedstock

	Operating Temperature	Catalyst Type	Experimental Methanol Conversion	Simulated Methanol Conversion	Difference (%)
Case 1	220°C	$CuO/ZnO/Al_2O_3$	57.6%	59.3%	+2.95
Case 2	270°C	$CuO/ZnO/Al_2O_3$	87.1%	89.0%	+2.18
Case 3	290°C	$CuO/ZnO/Al_2O_3$	96.0%	94.8%	-1.25
Case 4	325°C	$1Pt/3In_2O_3/CeO_2$	98.7%	98.2%	-0.51

5.3.2. Effects of Process Parameters

a)   Reaction Temperature

Figure 5.3 depicts the variation of components' mole fraction versus temperature curves, while Figure 5.4 describes the methanol and water conversion rate into hydrogen at elevated temperatures. The methanol-reforming is performed at atmospheric pressure and a methanol-to-water ratio of 1.0, respectively.
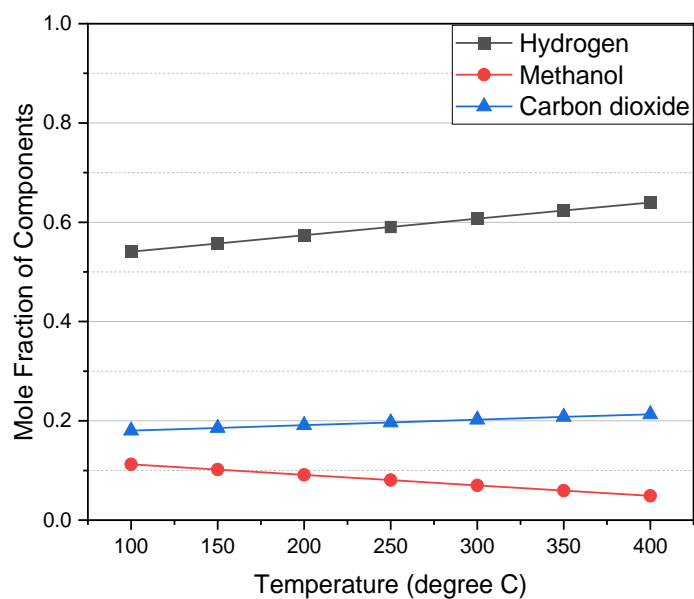
Figure 5.3. Mole fraction of components at elevated temperature
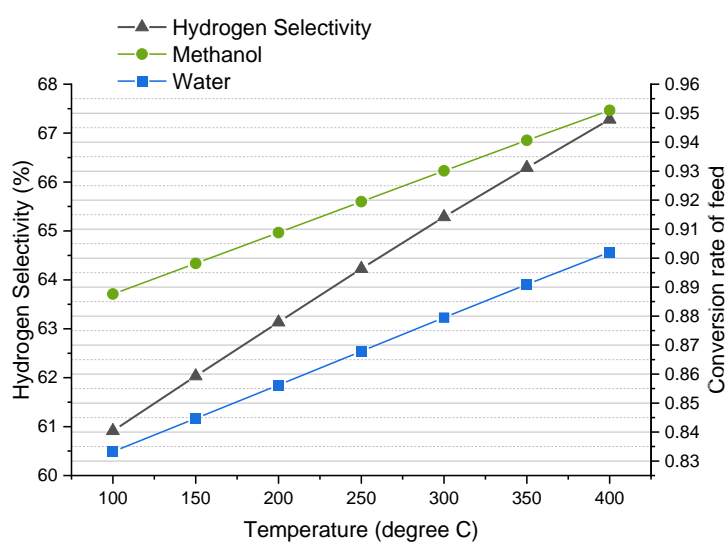
Figure 5.4. Hydrogen selectivity and feed conversion rate curves at elevated temperatures

A significant rise in hydrogen mole fraction is observed with the increase in reaction temperature from 100°C to 400°C (as shown in Figure 5.3). In contrast, the methanol mole fraction reduces uniformly. The water mole fraction curve is almost flat. This is due to the higher methanol conversion rate than water, as represented in Figure 5.4. It also shows a sharp increase in hydrogen selectivity with the rise in the reaction temperature. At 400°C, the hydrogen selectivity and mole fraction obtained are 67.28% and 0.64, respectively. A similar surge in hydrogen mole fraction and the feed conversion rate was observed in the findings of *Zaccara et al.* and *Pashchenko*, where the higher temperature gives a higher hydrogen mole fraction [219,220].

b)   Reactor Pressure

The reactor pressure plays a crucial role in the reaction pathway. The impact of reactor pressure on the mole fraction of various components is presented in Figure 5.5. At the same time, the variation in hydrogen selectivity, methanol, and water conversion rate is shown in Figure 5.6. The methanol-reforming is performed at 400°C, and a methanol-to-water ratio of 1.2 is chosen for simulation.
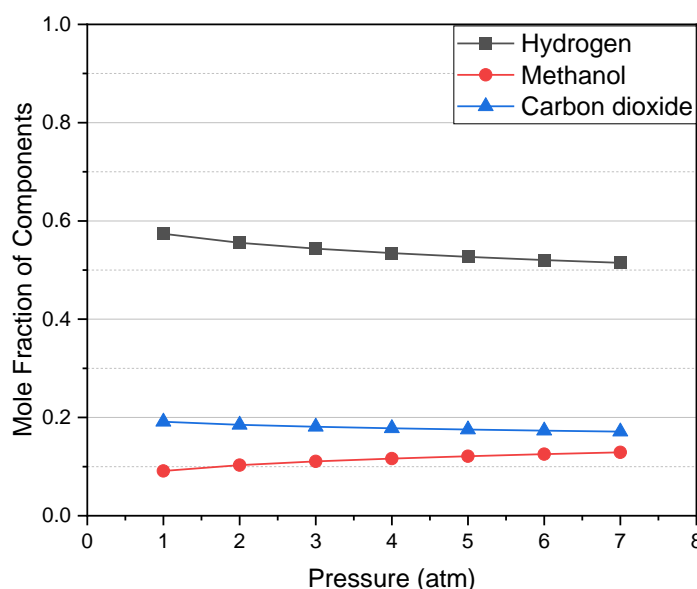
Figure 5.5. Mole fraction of components curves versus reactor pressure
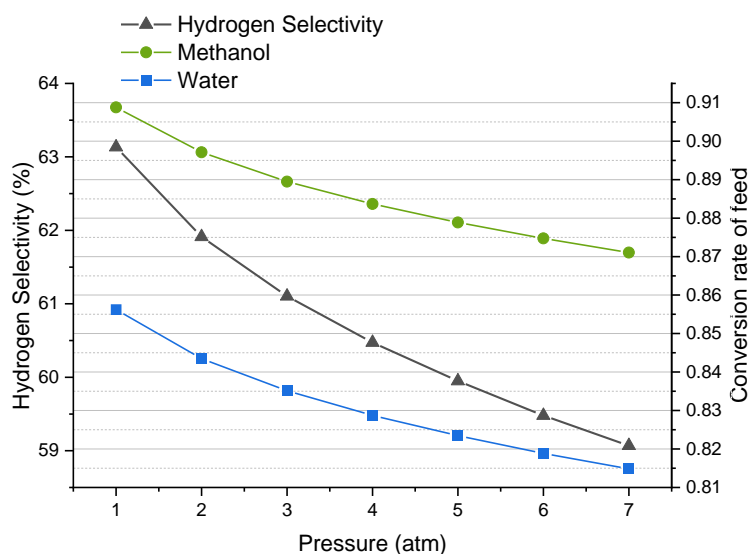
Figure 5.6. Hydrogen selectivity and feed conversion rate curves versus reactor pressure

The curves in Figure 5.5 show a drastic reduction in hydrogen and water mole fractions, whereas the methanol mole fraction rises when the reactor pressure goes from 1 atm. to 7 atm. The variation indicates that methanol contributes more than water to produce hydrogen. Similarly, in Figure 5.6, a decline is observed in hydrogen selectivity from 63.13% to 59.07% when reactor pressure is raised from 1 atm. to 7 atm. This decline can also be observed in methanol and water conversion rates, as both curves show a fall with a pressure rise. Similar results were followed by *Hakandai et al.*, where a higher reactor pressure sharply reduces the hydrogen mole fraction in the syngas [221].

c)   Alcohol-to-Water Molar Ratio

The molar ratio is another factor that is very important in increasing the concentrations of desired products. An optimum molar ratio generates the best results desirable in a reaction. In contrast, a higher or lower product concentration can shift the reaction pathway, thus, reducing the concentration of the desired product. Figure 5.7 and Figure 5.8 present the influence of the molar ratio (methanol-to-water ratio, from 0.3 to 4.0) on the mole fraction of products, hydrogen selectivity, and feed conversion rates. The reactor pressure and temperature maintained for the simulation process are 1 atm. and 400°C, respectively.
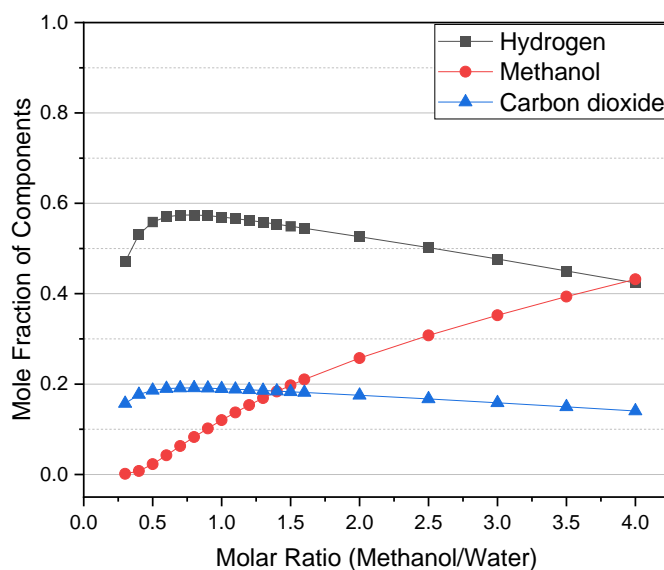
Figure 5.7. Mole fraction of components versus methanol-to-water molar ratio
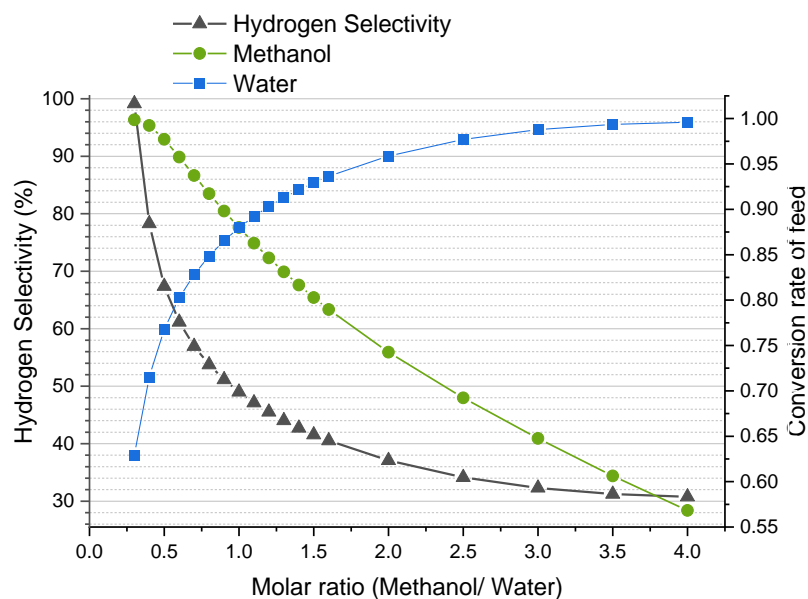
Figure 5.8. Hydrogen selectivity and feed conversion rate curves versus methanol-to-water molar ratio

From Figure 5.7 and Figure 5.8, it was observed that a methanol-to-water (M-to-W) molar ratio between 0.5 and 1.5 favours H_2 production at a much higher rate. The hydrogen mole fraction initially increases from 0.47 (at 0.3 M-to-W) to 0.574 (at 0.9 M-to-W) and then reduces to 0.42 at 4.0 M-to-W molar ratio. The methanol conversion rate showed a sharp decline, and a relative reduction was observed in H_2

selectivity. The water conversion rate rises in this case because the water concentration reduces with the increase in the M-to-W molar ratio. The behaviour of reduction in H_2 production due to molar ratio was also observed by *Unlu* and *Hilmioglu*, where a higher molar ratio significantly reduced H_2 production [58].

5.3.3. Parameter Optimization

a)   Empirical Design & Regression Analysis

During the simulation process, three process parameters, namely, reaction temperature (RT), reactor pressure (RP), and methanol-to-water (M-to-W) molar ratio, are considered for optimized hydrogen production. A CCD is employed with three factors at three levels, as depicted in Table 5.3. A 20-run design matrix is generated with all parameters and their levels with two responses, that is, hydrogen selectivity and feed conversion percentage, that was successfully performed. The results obtained from the analysis, simulation model, and matrix design (predicted values) are represented in Table 5.5.

Table 5.5. Matrix design of 20-runs

Run	Parameters			Hydrogen Selectivity (%)			Feed Conversion (%)		
	RT (°C)	RP (atm.)	M-to-W molar ratio	Actual Value	Predicted Value	Residual	Actual Value	Predicted Value	Residual
1	200	1	0.5	73.97	73.60	0.3675	81.95	81.56	0.0039
2	200	1	1.5	83.63	84.21	-0.5889	81.64	81.09	0.0055
3	200	3	1.0	80.55	80.09	0.4531	85.91	87.82	-0.0191
4	200	5	0.5	74.97	75.23	-0.2536	81.88	81.45	0.0043
5	200	5	1.5	86.10	86.08	0.0220	81.38	80.84	0.0055
6	400	1	0.5	80.07	80.21	-0.1398	83.18	83.73	-0.0055
7	400	1	1.5	85.49	85.35	0.1358	93.43	93.86	-0.0043
8	400	3	1.0	82.88	82.86	0.0181	97.26	95.34	0.0192
9	400	5	0.5	80.09	79.62	0.4711	83.17	83.72	-0.0055
10	400	5	1.5	84.51	84.99	-0.4852	93.32	93.71	-0.0039
11	300	1	1.0	79.51	79.29	0.2254	91.55	91.51	0.0004
12	300	5	1.0	80.17	79.92	0.2458	91.34	91.38	-0.0003
13	300	3	0.5	76.07	76.51	-0.4452	82.78	82.49	0.0028
14	300	3	1.5	85.43	84.51	0.9163	86.98	87.25	-0.0028
15	300	3	1.0	80.06	80.22	-0.1570	91.45	91.45	-0.0000
16	300	3	1.0	80.06	80.22	-0.1570	91.45	91.45	-0.0000
17	300	3	1.0	80.06	80.22	-0.1570	91.45	91.45	-0.0000
18	300	3	1.0	80.06	80.22	-0.1570	91.45	91.45	-0.0000
19	300	3	1.0	80.06	80.22	-0.1570	91.45	91.45	-0.0000
20	300	3	1.0	80.06	80.22	-0.1570	91.45	91.45	-0.0000

The randomization in the experimental runs helps reduce the possibility of response variations. Thus, a response model {Equation (5.10) and Equation (5.11)} is formed with a 95% confidence level to generate the predicted values in the design matrix that represents RT, RP, and M-to-W as linear terms; RT^2, RP^2, and $(M\text{-to-W})^2$ as quadratic terms; and RT x RP, RP x M-to-W, and M-to-W x RT as interactive terms whereas Y_1 as hydrogen selectivity and Y_2 as feed conversion percentage.

$$Y_1 = +68.222 - 0.026(RT) + 1.85(RP) + 13.665(M-to-W) - 0.003(RT * RP) - 0.027(RT * M-to-W) + 0.059(M-to-W * RT) + 0.00013(RT)^2 - 0.153(RP)^2 + 1.184(M-to-W)^2 \tag{5.10}$$

$$Y_2 = +0.663 - 0.00024(RT) - 0.00024(RP) + 0.416(M-to-W) + 1.283e^{-06}(RT * RP) + 0.00053(RT * M-to-W) - 0.00036(M-to-W * RT) + 1.305e^{-07}(RT)^2 - 0.00002(RP)^2 - 0.263(M-to-W)^2 \tag{5.11}$$

Analysis of variance (ANOVA) tests the model significance by calculating the F-values and p-values of the parameters' regression coefficient. F-value is defined as the ratio between the mean squares between values to the mean squares error. The higher F-value indicates the significance of the variable. In contrast, the p-value determines the difference between the group's means to be statistically significant. The p-values of <0.0001 signify the relevance of the response values. Here, ANOVA tables (Table 5.6 and Table 5.7) are generated for hydrogen selectivity and feed conversion percentage to test the significance of the process parameters. In Table 5.6 and Table 5.7, the F-values of 89.17 and 55.21 and the p-values of <0.0001 signify the relevance of both hydrogen selectivity and feed conversion percentage models. In contrast, the RT and M-to-W molar ratios have p-values <0.0001 in both models, rendering them significant parameters in the models.

Table 5.6. ANOVA table for hydrogen selectivity.

Source	Sum of Squares	df	Mean Square	F-value	p-value	
Model	204.21	9	22.69	89.17	< 0.0001	significant
A-Reaction Temperature	19.12	1	19.12	75.13	< 0.0001	
B-Reactor Pressure	1.00	1	1.00	3.95	0.0750	
C-Methanol-to-Water molar ratio	159.82	1	159.82	628.08	< 0.0001	
AB	2.47	1	2.47	9.70	0.0110	
AC	14.99	1	14.99	58.90	< 0.0001	
BC	0.0274	1	0.0274	0.1078	0.7495	
A²	4.38	1	4.38	17.20	0.0020	
B²	1.03	1	1.03	4.04	0.0722	
C²	0.2408	1	0.2408	0.9462	0.3536	
Residual	2.54	10	0.2545			
Lack of Fit	2.54	5	0.5089			
Pure Error	0.0000	5	0.0000			
Cor Total	206.76	19				

Table 5.7. ANOVA table for feed conversion percentage.

Source	Sum of Squares	df	Mean Square	F-value	p-value	
Model	0.0466	9	0.0052	55.21	< 0.0001	significant
A-Reaction Temperature	0.0141	1	0.0141	150.76	< 0.0001	
B-Reactor Pressure	4.273E-06	1	4.273E-06	0.0456	0.8353	
C-Methanol-to-Water molar ratio	0.0057	1	0.0057	60.36	< 0.0001	
AB	5.266E-07	1	5.266E-07	0.0056	0.9418	
AC	0.0056	1	0.0056	59.96	< 0.0001	
BC	1.016E-06	1	1.016E-06	0.0108	0.9192	
A²	4.680E-06	1	4.680E-06	0.0499	0.8277	
B²	1.744E-08	1	1.744E-08	0.0002	0.9894	
C²	0.0119	1	0.0119	126.93	< 0.0001	
Residual	0.0009	10	0.0001			
Lack of Fit	0.0009	5	0.0002			
Pure Error	0.0000	5	0.0000			
Cor Total	0.0475	19				

The adequacy of the models is also determined using R^2 values from Table 5.8 and Table 5.9. R^2 measures how well the outcomes are predicted by the statistical model. The model makes better predictions if the R^2 is closer or equal to 1 (unity). Table 5.8 shows an R^2 value of 0.9877 for hydrogen selectivity, whereas Table 5.9 shows an R^2 value of 0.9803 for feed conversion percentage. Since, in both the models (model generated for hydrogen selectivity and model generated for feed conversion percentage), the R^2 values approach close to unity, this states that a better correlation is generated between the experimental (simulated) and predicted values.

Table 5.8. Regression table for hydrogen selectivity.

R²	0.9877	Std. Dev.	0.5044
Adjusted R²	0.9766	Mean	80.69
Predicted R²	0.8560	C.V. %	0.6252
Adeq Precision	34.9823		

Table 5.9. Regression table for feed conversion percentage.

R²	0.9803	Std. Dev.	0.0097
Adjusted R²	0.9625	Mean	0.8822
Predicted R²	0.8468	C.V. %	1.10
Adeq Precision	21.1839		
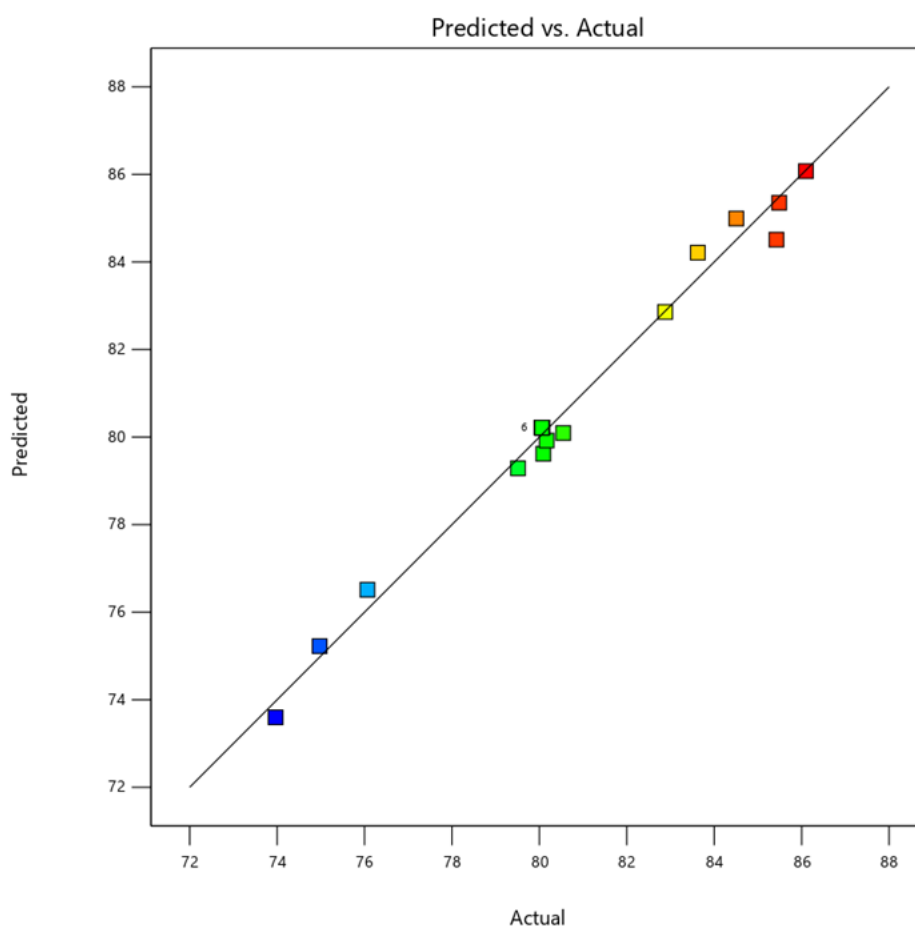
Figure 5.9. Predicted versus actual graph for hydrogen selectivity.
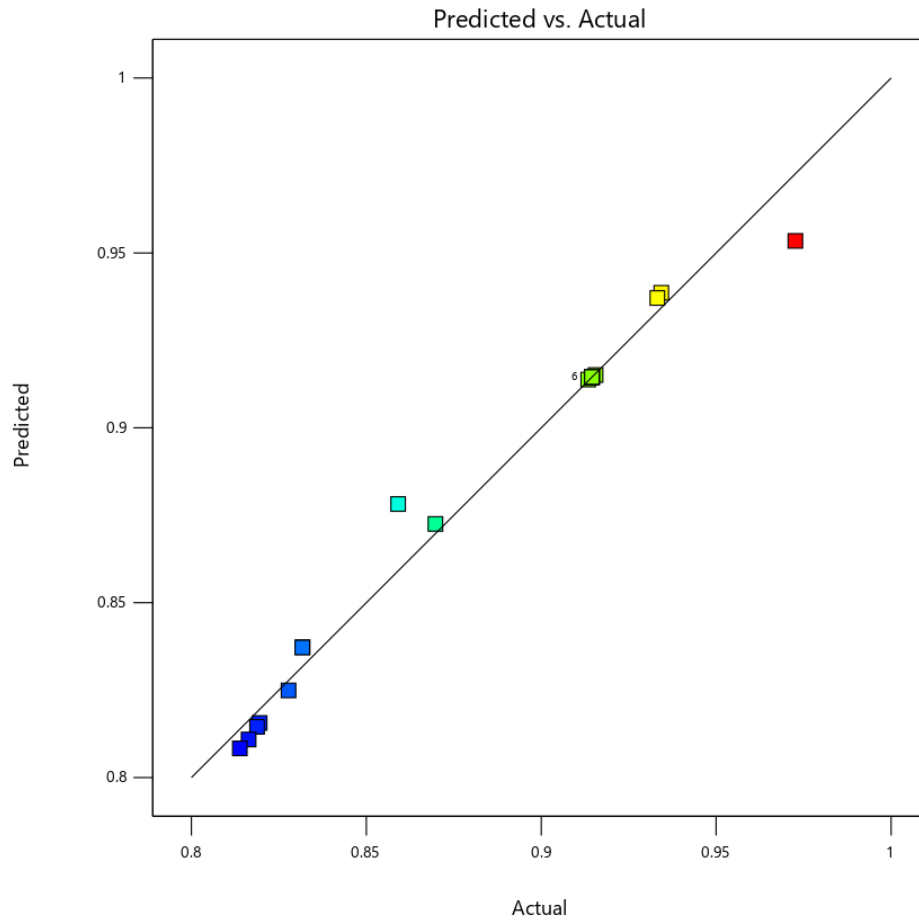
Figure 5.10. Predicted versus actual graph for feed conversion percentage.

The lack of fit for both models is determined using Figure 5.9 for HS and Figure 5.10 for FCP. The inclined solid line represents the perfect fit line, while scattered square points describe the predicted values. The points in both graphs are closer to the adequate association between the projected model and simulated values, validating the adequacy of the model.

b)   Interactive Effects of Parameters

The model equations generated during regression analysis are helpful in determining the interactive effects of various parameters (or inputs) on the response (or output). A 3D surface contour plot is generated with two parameters simultaneously on two axes, while the third axis represents the response. Similarly, the different surface contour plots are developed with both the responses (HS and FCP).

The interactive effects between RT and RP on responses (a) hydrogen selectivity and (b) feed conversion percentage are described in Figure 5.11. It was observed that the RP has the minimum effect in raising HS and FCP as described by flatter curves on the RP axis. In contrast, the RT is crucial in increasing FCP, while HS also increases beyond 350°C. However, the range of HS remains between 74% and 86%, whereas the FCP reaches above 97% at 390°C from about 81% at 200°C reaction temperature. Similar results were obtained by *Zhang et al.*, where a temperature rise enhances hydrogen selectivity and methanol conversion rate [28].
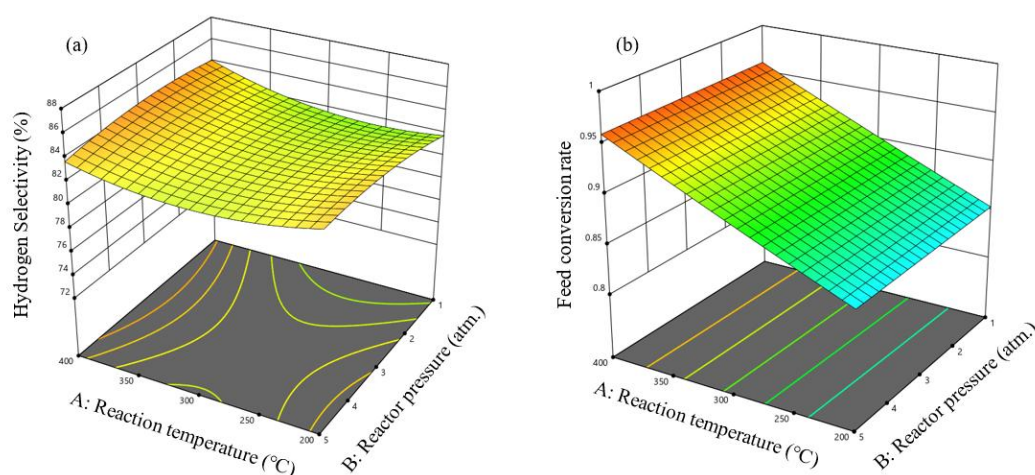
Figure 5.11. RT versus RP surface contour curves for a) HS and b) FCP.
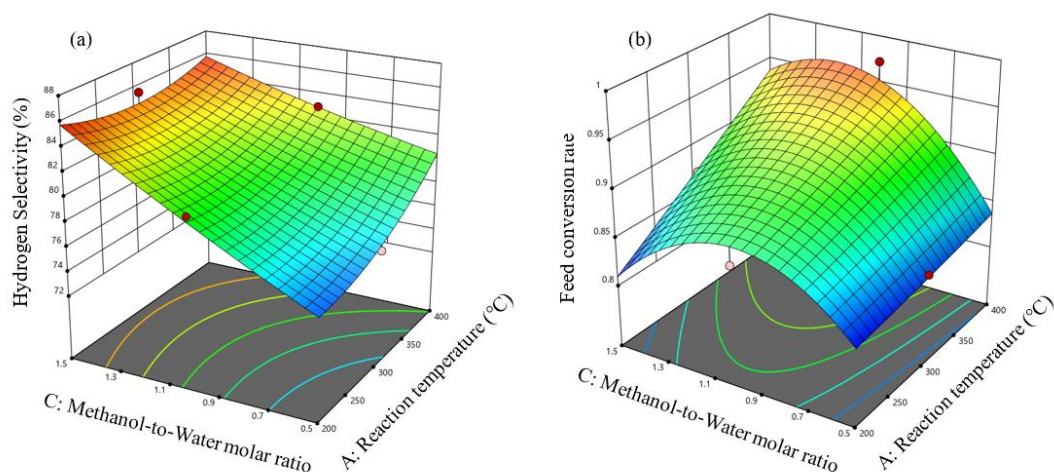
Figure 5.12. M-to-W molar ratio versus RT surface contour curves for a) HS and b) FCP.

In Figure 5.12, the interaction of RT and M-to-W on a) hydrogen selectivity and b) feed conversion percentage is represented in surface contour plots. Here, the values of both M-to-W and RT influence hydrogen production. A higher M-to-W molar ratio favours the hydrogen selectivity, and RT raise also shows positive effects; however, the maximum HS of 86% is achieved at 200°C and 1.5 M-to-W molar ratio. In contrast, the FCP increases with the increase in RT, but the maximum value of 97.3% is achieved between 0.9 and 1.35 M-to-W molar ratio. Beyond the 1.35 M-to-W molar ratio, the FCP reduction is observed. The reason is the excess methanol concentration that fails to decompose into hydrogen molecules and other smaller compounds. *Cao et al.* found similar results where a higher ethanol molar ratio in feed resulted in higher hydrogen conversion [69]. Similarly, *Giwa* and *Giwa* observed higher hydrogen production at higher reaction temperatures [222].

Figure 5.13 shows the surface contour plot showing the interactive effect of M-to-W molar ratio and RP on a) hydrogen selectivity and b) feed conversion percentage. As already discussed, the rise in the M-to-W molar ratio positively affects both HS and FCP. Therefore, similar results are obtained for HS, whereas the FCP is maximum between 0.9 and 1.35 M-to-W molar ratio. Also, the trends of RP are identical to the previous discussion since RP has significantly less influence in HS and FCP. In contrast, a slight rise is observed near about 2.5 atm. of reactor pressure.
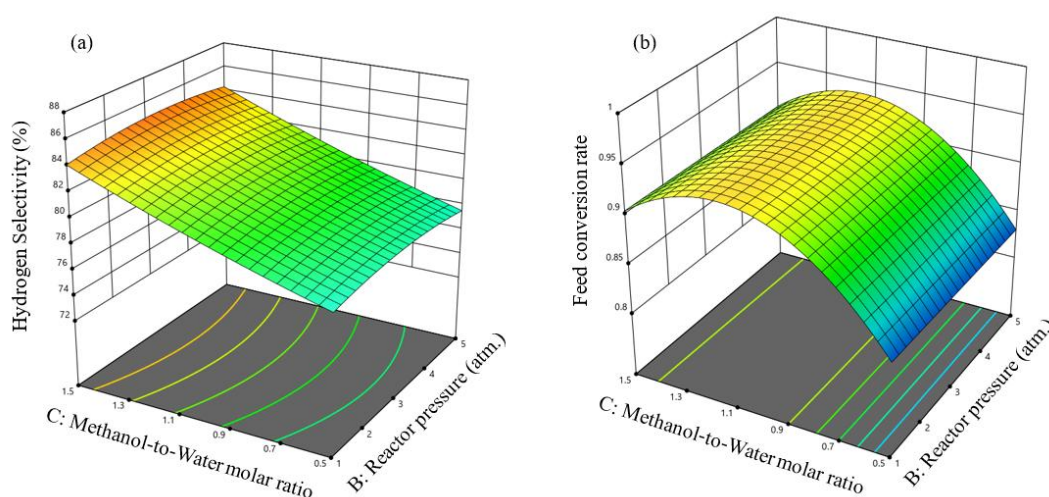
Figure 5.13. M-to-W molar ratio versus RP surface contour curves for a) HS and b) FCP

c)   Optimal Parameters

Optimization aims to define the best possible inputs that will satisfy the targets. The desirability describes the closeness of optimal values to the highest and lowest values of the inputs. Here, the input variables like RT, RP, and M-to-W molar ratio are optimized to achieve the targets, that is, the highest hydrogen selectivity and feed conversion percentage. A ramp function graph of desirability is generated in Figure 5.14, while a bar graph showing desirability for the responses is presented in Figure 5.15.
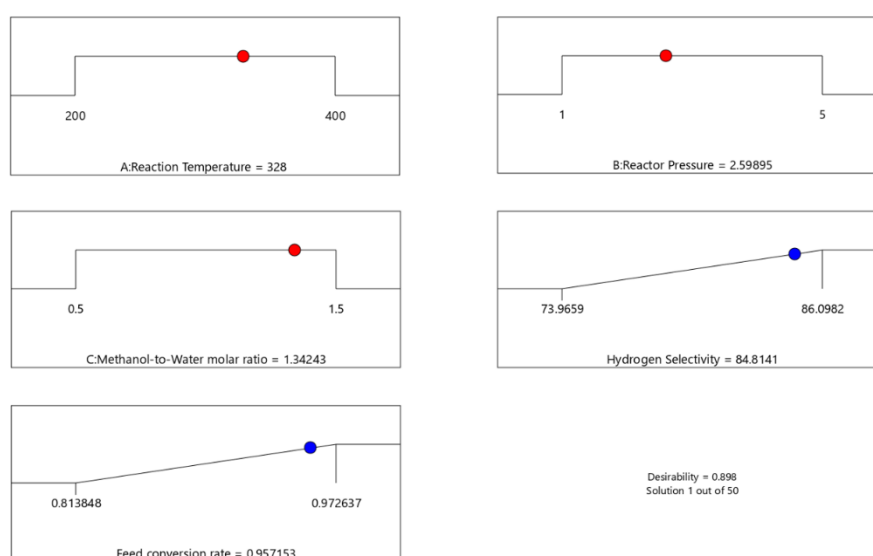
Figure 5.14. Ramp desirability function graph for HS and FCP.
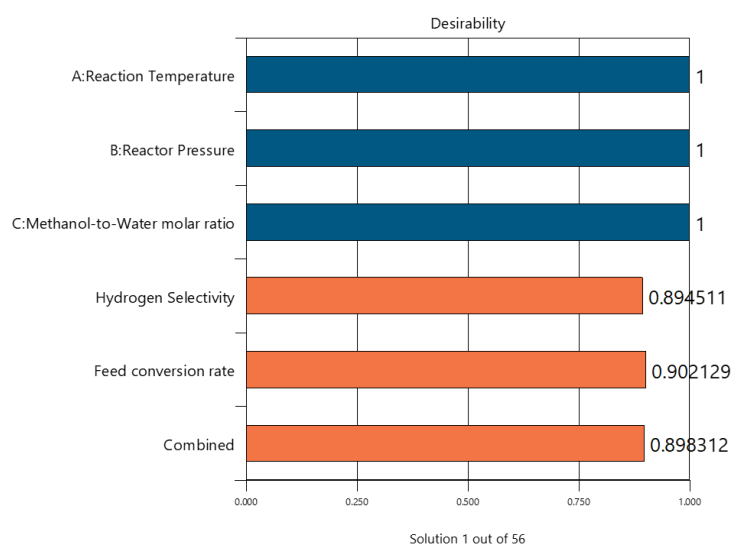
Figure 5.15. Desirability bar graph for process parameters, HS, FC, and combined HS-FCP.

The best results obtained through the ramp function graph include RT 328°C, RP 2.6 atm., and M-to-W molar ratio of 1.34 at a desirability value of 0.898. However, the optimized hydrogen selectivity and feed conversion percentage obtained at optimal values are 84.81% and 95.71%, respectively. In contrast, the bar graph represents the total desirability function of both the responses and ranges between 0 and 1, where 1 is considered satisfactory.

Table 5.10. Stream table for optimal parameters of RSM model (RT 328°C, RP 2.6 atm. and M-to-W ratio 1.34).

	Unit	Feed	H_2	CO_2	Unreacted Feed
Molecular Weight	---	26.08	2.016	44.01	29.80
Vapor Fraction	---	1	1	1	0.4186
Temperature	°C	328	40	135.7	70
Pressure	atm.	1	1	1	1
Mole Flow	kg-mole/h	120	161.2	49.47	21.06
Mass Flow	kg/h	3130	324.9	2177	627.5
Volume Flow	m^3/h	3.699	4.651	2.638	0.7806
Molar Enthalpy	kJ/kg-mole	-200400	426.6	-389400	-175000
Mass Enthalpy	kJ/kg	-7685	211.6	-8848	-5873
Enthalpy Flow	kJ/h	-24050000	68750	-19260000	-3685000
Molar Entropy	kJ/kg-mole-°C	188.3	124.4	185.0	156.3
Mass Entropy	kJ/kg-°C	7.218	61.71	4.204	5.313
Molar Density	kg-mole/m^3	0.0473	0.0389	0.0299	0.0359
Mass Density	kg/m^3	1.233	0.0784	1.314	1.069

Table 5.11. Composition table for optimal parameters of RSM model.

Components	Feed	Syngas	Unreacted Feed
Methanol	0.5750	0.1243	0.6241
Carbon monoxide	0.0000	0.0301	0.3033
Hydrogen	0.0000	0.4885	0.0000
Water	0.4250	0.0229	0.0762
Carbon dioxide	0.0000	0.3342	0.0000

The stream table describes the thermodynamic properties of a stream going in and out of the system, taking the complete simulation as a system; the stream table is presented in Table 5.10. The thermodynamic properties of feed input, hydrogen and carbon dioxide output, and unreacted feed are measured. In contrast, the composition of feed, syngas, and unreacted feed is depicted in Table 5.11. The optimal conditions from the RSM model (RT 328°C, RP 2.6 atm., and M-to-W ratio 1.34) are used to generate the stream and the component composition table. An HS and FCP obtained from the optimal conditions when run on the simulation model are 82.67% and 92.51%. It shows 2.5% and 3.34% errors for HS and FCP, which are within acceptable limits.

5.3.4. Comparative Results

Hydrogen purity is essential for its applications. A comparison with earlier published work gives an insight into the improvements in the results of the present work. However, few simulation and modelling articles based on methanol-water reforming using the Aspen Hysys simulator are available. Hence, the experimental outcomes are considered for comparison in Table 5.12. It was observed that optimization helped in enhancing hydrogen selectivity and feed conversion percentage significantly. Therefore, the study provides a good understanding of influencing parameters and their optimization in methanol-water reformer reactors.

Table 5.12. Comparative table for HS and FCP (from methanol feedstock)

Model/ Reactor	Temperature (°C)	H_2 selectivity (%)	Feed conversion (%)	Reference
Simulation Model	328	82.67	92.51	This work[*]
RSM Model	328	84.81	95.71	This work[*]
DBD plasma reactor	-	51.5	65.5	[69]
Fixed bed microreactor	350	99	72	[28]
Packed bed	300	91	58	[223]
Fixed bed	280	70.9	35	[224]
U-Shaped microreactor	200	72	68	[225]
Fixed bed	275	65	85	[226]

5.4. Summary

A methanol-water reforming reactor simulation model is developed for hydrogen generation using the Aspen Hysys simulator, and the Peng–Robinson thermodynamic model, suitable for the reforming process, is used in the model. A design of experiment (DoE) is generated to optimize parameters for hydrogen selectivity and feed conversion percentage. The data from the simulation results are used to create DoE, and optimal values of influencing parameters are determined. The parameters considered in the simulation and optimization process include reaction temperature (200°C to 400°C), reactor pressure (1-5 atm.), and methanol-to-water molar ratio (0.5-1.5), while the target values (or response variables) are hydrogen selectivity (HS) and feed conversion percentage (FCP). The following findings are reported in the study:

- A drastic increase in hydrogen mole fraction from 0.54 to 0.64 is observed with a temperature rise from 100°C to 400°C, showing an 18.5% rise in hydrogen mole fraction.

- Similarly, a sharp rise in hydrogen selectivity is obtained with the temperature rise. At the same time, the methanol conversion rate is more than the water conversion rate, which shows more influence of methanol than water in hydrogen production.

- The hydrogen selectivity curve also showed the importance of the M-to-W molar ratio. The higher molar ratio results in a lower methanol conversion rate and, thus, a reduction in hydrogen selectivity is observed.

- The simulation shows the HS values in the 74% and 86% range, while the FCP values range from 81.4% to 97.3%.

- R^2 values of HS and FCP are 0.9877 and 0.9803, which show a better correspondence between the simulated and predicted values.

- The M-to-W molar ratio is the most significant parameter for hydrogen production, and the range from 0.9 to 1.35 shows the highest hydrogen production potential.

- Reactor pressure has the least significance and only a slight increase in HS is observed near about 2.5 atm. reactor pressure.

- Reaction temperature shows intermediate significance, while it was observed that the higher temperature has more potential to generate hydrogen.

- An optimized HS and FCP of 84.81% and 95.71% were obtained at 328°C RT, 2.6 atm. RP, and 1.34 M-to-W molar ratio.

- The optimal parameters were run in the simulation model, and errors of 2.5% and 3.34% for HS and FCP were obtained, which are within acceptable limits.

Therefore, the response (or target) values are successfully optimized for methanol-water reforming in the simulation model. The optimal values of parameters may be used to generate maximum H_2 selectivity in the commercialized plants.

CHAPTER 6

PERFORMANCE OF PEM FUEL CELL

6.1. Overview

Burning fossil fuels was the root cause of air pollution that degraded the environment and human health. According to a few studies, the average age of the urban population in developing countries has reduced by up to 10 years in the last few decades due to severe air pollution that adversely affected living cells. To minimize pollution generated from fossil fuels, new and reliable alternative energy sources are being practiced [227]. Hydrogen energy is one such alternative that fulfills the present energy requirement and generates no harmful emissions after burning. The fuel cells were employed to generate electricity from hydrogen and oxygen reactions in a controlled system. Many fuel cells are available, while the proton exchange membrane (PEM) fuel cell is widely employed for electricity production and comes in different power capacities [228].

The PEM fuel cell comprises two graphite electrodes coated with platinum (Pt) catalyst, a catalyst layer, a gas diffusion layer, and terminal plates assembled with channel plates for hydrogen and oxygen flow [229]. The pure hydrogen (about 99.995% pure) enters the anode side, and O_2 (from the air or separate oxygen cylinder) enters the cathode side. The oxidation of hydrogen occurs at the anode that splits it into hydrogen ions and electrons [9]. In contrast, the reduction reaction occurs at the cathode. The O_2 reacts with hydrogen ions to form H_2O molecules [176]. An external path (or circuit) was connected for electron transfer generated during hydrogen oxidation. *Kulikovsky* developed a PEM fuel cell model to investigate the cell impedance at variable airflow velocities in the cathode channel [175]. The oxygen transport in the channel through higher air flow velocity showed lower resistivity. In contrast, a relatively equal airflow velocity and cell potential showed total resistivity compensation in the fuel cell model.

Water produced humidified the membrane and improved the electron transfer, enhancing the cell efficiency. In contrast, the over-flooding of the catalyst layer (CL) would result in pores blockage that hinders the electron movement, reducing the cell efficiency. *Al-Anazi et al.* investigated the performance of a PEM fuel cell in winter and summer conditions in Saudi Arabia using an Ansys model. A significant variation was observed in cell performance during winter and summer environments. About 12% lesser efficiency was calculated in the winter compared to the summer due to the hot and humid conditions resulting in fast reaction kinetics and membrane hydration [165]. Furthermore, the humidification during the peak summer interval showed a 40% output enhancement. *Houreh et al.* investigated the effects of different humidifier configurations at different PEM fuel cell operating conditions. The counter-flow humidifier showed a superior heat and water transfer rate than other humidifiers [177]. In contrast, the cross-flow humidifier has a better heat transfer rate than the parallel-flow humidifier. In contrast, the reverse goes for the water transfer rate (i.e., the parallel-flow humidifier has a better water transfer rate than the cross-flow humidifier). However, the wet side inlet temperature significantly influenced the humidifiers' performance.

During dead-end mode operation, *Shateri* and *Torabi* examined the proton exchange membrane fuel cell performance with liquid water accumulation at the anode [171]. A large volume of liquid water accumulated at the cathode due to the dead-end operation. The accumulated moisture covers the catalyst, increasing charge transfer resistance. Thus, the liquid water accumulation reduces the cell performance; therefore, regular purging becomes significant in the cell operation. In contrast, *Tang et al.* discussed the temperature sensitivity of a PEM fuel cell to improve the durability and performance of the fuel cell stack. Results showed that rising the temperature paces up the electrochemical reaction rate; thus, a significant rise in the performance was observed [160]. In contrast, the higher temperatures have inverse impacts on the water content that dropped the cell's power output. Therefore, an optimal temperature must be mentioned to retain hydration in normal fuel cell operations.

The whole process was influenced by various operating parameters like hydrogen flow rate, hydrogen pressure, moisture content, etc. Thus, the fuel cell study at varying parameters became essential. *Kumar* and *Subramanian* determined the effects of various parameters on the performance of a PEM fuel cell. Oxygen-enriched air (up to 45%) showed a 9% and 33% improvement in voltage efficiency and power output due to more oxygen reduction reactions [159]. Whereas beyond 45% oxygen enrichment, the performance declined due to increased stack temperature. In contrast, a 50°C optimal temperature performed better between 40°C and 60°C. However, the hydrogen pressure showed the most minor significance in the cell performance. *Eslami et al.* studied the effects of various operating parameters on the PEM fuel cell performance. The parameters studied include relative humidity, temperature, pressure, and stoichiometry [162]. Results showed a 1-2% improvement in stack performance for both relative humidity (from 50% to 100%) and stoichiometry of the cathode (from 1.02 to 1.60). Hydration of membranes and enhanced water and fuel management are behind the performance improvement. Similarly, a 4-6% improvement was observed for the temperature (from 50°C to 80°C) and reactants outlet pressure (between 0.5 and 2.0 bar), respectively.

Mubin et al. investigated the performance of a PEM fuel cell at varying temperatures and pressure. The cell performed better at higher temperatures and gas pressure [180]. In contrast, the problem of fuel cell malfunctioning could occur when the temperature and pressure reach beyond a particular limit. In the current work, a 1 kW PEM fuel cell was tested for its performance at varying hydrogen flow rates and gas pressure. A hydrogen production and purification unit was introduced to supply hydrogen to the PEM fuel cell at a 99.995% purity level. The unit had a lower hydrogen flow rate than the rated value. Hence, the experiment also determined the net effect on fuel cell power and efficiency at a lower hydrogen flow rate. In contrast, the range of gas pressure was considered a little higher to find the effects of low hydrogen flow rate at higher gas pressures. It will help reduce hydrogen wastage during fuel cell operation for longer-term electricity production.

6.2. Materials and Method

A fuel cell is an electrochemical device that converts chemical energy into electrical energy. It comprises components such as two electrodes (cathode and anode), terminal plates, gas diffusion layer (GDL), MEA consisting of solid polymer electrolyte, porous anode and cathode with Pt catalyst, current collectors, and supporters. Hydrogen and oxygen pass through the hydrogen flow channel and oxygen flow channel. The chemical reactions occur at the catalyst surface, and the hydrogen molecule splits into hydrogen ions and free electrons. The MEA lets hydrogen ions pass over it. The electrons require an external circuit to react on the positive cell side. Therefore, a voltage was generated across the two terminals that may be used to run electrical appliances after AC/DC conversion. Figure 6.1 represents the PEM fuel cell along with different components.
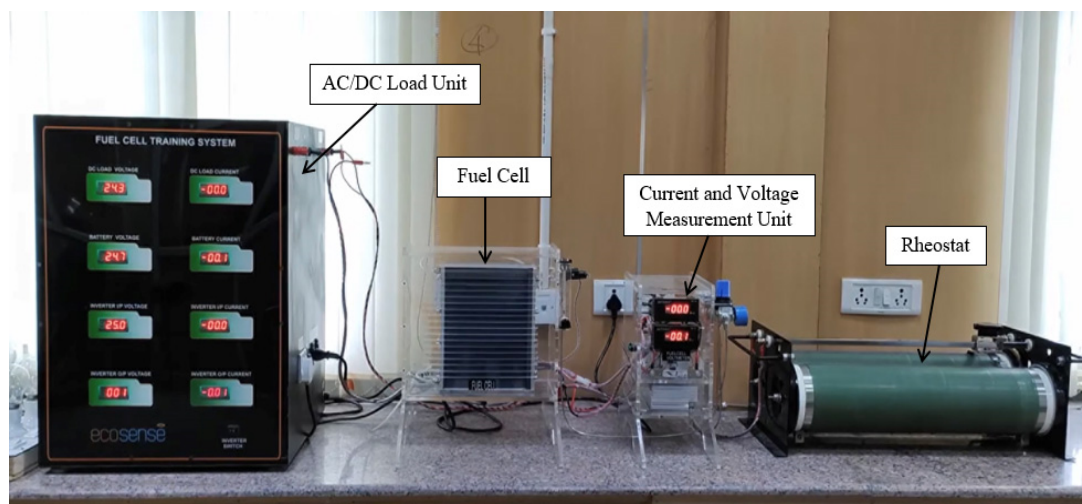
Figure 6.1. PEM fuel cell

6.2.1. Experimental setup

A proton exchange membrane (PEM) fuel cell containing 48 cells and a rated power of 1000 W was used. The peak power was attained at about 28.8 V potential difference and 35 A current. It was a self-humidified and air-cooled (integrated cooling fan) system. The controller weight was about 400 g, while the stack weight (with fan and casing) was about 4000 g. The stack efficiency was measured at about 40% at a 28.8 V potential difference. The cell was fitted with an auto-shutdown

controller at a voltage below 24 V, current 42 A, and stack temperature above 65°C for safety purposes. The fuel cell generated maximum power output at 13 LPM hydrogen flow rate (HFR). Other specifications are represented in Table 6.1.

Table 6.1. Specifications of PEM fuel cell

Parameter	Unit	Range
Fuel cell Type	---	Proton Exchange Membrane (PEM)
Number of cells	---	48
Rated power	Watt	1000
Peak Performance	---	28.8 V @ 35 A
H_2 Supply valve voltage	Volt	12
Purging valve voltage	Volt	12
Blower voltage	Volt	12
Input gases	---	Hydrogen and Oxygen (from air)
External temperature range	Degree Celsius	5 to 30
Gas pressure range (at Peak)	Bar	0.45 to 0.55
Hydrogen purity (dry)	Percentage	99.995
Humidification method	---	Self-humidified
Cooling	---	Air-cooled
Stack weight (with fan & casing)	Gram	4000 (±100)
Controller weight	Gram	400 (±30)
Fuel cell dimensions	Centimetres	23.3 x 26.8 x 12.3
Flow rate (at max. output)	Litre per minute	13
Start-up time	Second	≤ 30
Stack efficiency	Percentage	40
Shut down voltage (low)	Volt	24
Shut down current (high)	Ampere	42
Shut down temperature (high)	Degree Celsius	65

The hydrogen purity requirement for fuel cells was more than 99.995% level. Oxygen gas was taken from the atmosphere (air), and hydrogen supply had two options (either from a Grade-I hydrogen cylinder supplied by 'Sigma Gases and Services' or a hydrogen-producing and purifying unit developed within the laboratory). The HFR was measured using a 'FLOWSTAR' make (Model: FSA 100) rotameter while the hydrogen pressure was regulated using a 'JEL' make (Model: AR2000-02) pressure regulator. The voltage and current were measured at different operating parameters varying resistance through 'STEAD' make rheostat. Figure 6.2 depicts the experimental setup of the fuel cell.
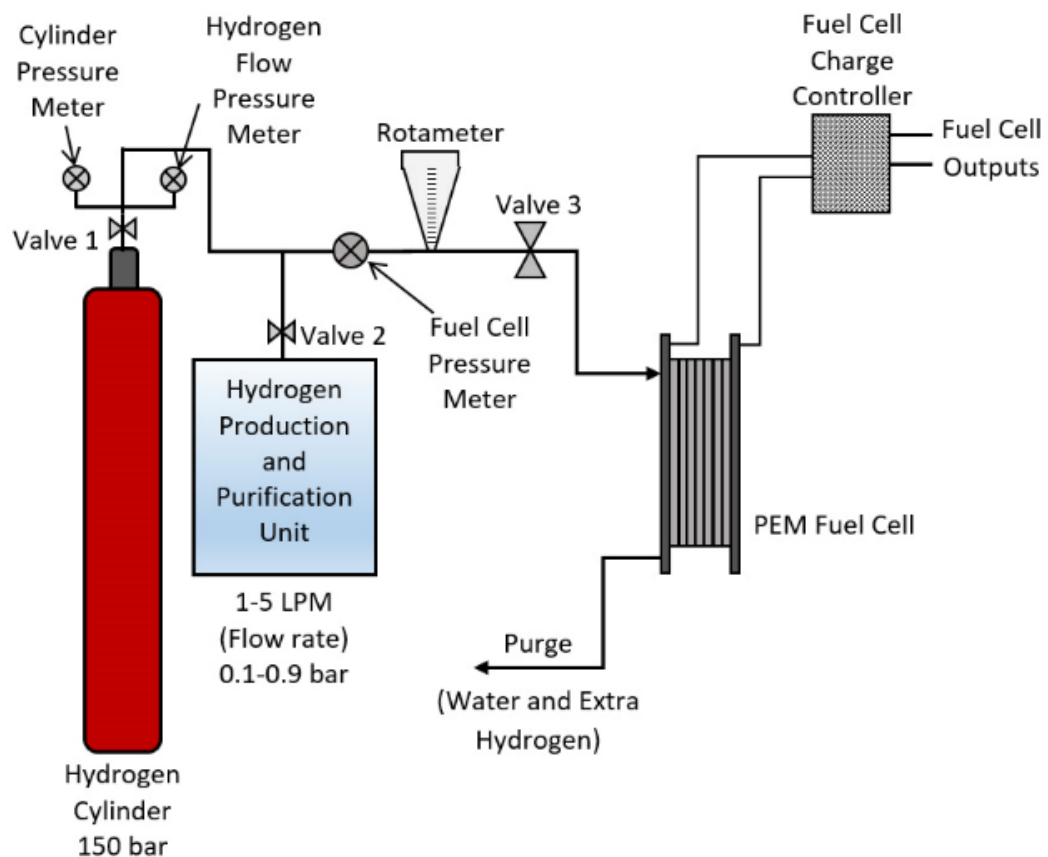

Figure 6.2. Diagram of PEM fuel cell connected with hydrogen production and purification unit

6.2.2.   Procedure

A fuel cell is an electrochemical device that generates electricity till it receives the fuel. Hence, the continuous fuel supply must be ensured throughout the experimentation. Initially, the hydrogen cylinder valve (Valve 1) was opened, and any leakage was tested using a hydrogen leak detection device. Once no hydrogen leakage was detected, the hydrogen pressure was adjusted at about 1.5 bar pressure. Another pressure regulator was attached before the fuel cell, which finally regulates the gas pressure entering the fuel cell. Here, the pressure is maintained between 0.1 and 1.0 bar, depending on the requirement. Before connecting the external hydrogen gas supply, the fuel cell stabilized after running for 10 minutes through hydrogen from the cylinder. Once the readings from the fuel cell were under acceptable limits, the Valve 1 may be closed and hydrogen production and purification unit may be started with opening Valve 2. The hydrogen gas coming out from the hydrogen production and purification unis may be used for the experimentation at varying hydrogen gas pressure and hydrogen flow rate (HFR).

A hydrogen flow meter was attached to ensure the HFR was at acceptable limits; however, the maximum hydrogen flow rate from the hydrogen production and purification unit was 5 LPM. Therefore, the experiments were conducted between 1 LPM and 5 LPM range. Similarly, the gas pressure range was maintained between 0.4 and 0.9 bar, as depicted in Table 6.2. The hydrogen pressure range was chosen as the fuel cell had 0.4 bar, the lowest operating pressure, and the hydrogen production and purification unit generated a maximum hydrogen pressure of 0.9 bar, respectively.

Table 6.2. Operating parameters for PEM fuel cell performance

Parameters	Units	Experimental values	Rated peak values
Hydrogen flow rate	Litre per minute (LPM)	1, 2, 3, 4, 5	13
Gas pressure	bar	0.4, 0.5, 0.6, 0.7, 0.8, 0.9	0.45

After adjusting the required gas pressure and HFR, the H_2 entered the fuel cell through the anode, and the oxygen was taken from the atmosphere (air) and entered through the cathode. There were separate air channels for hydrogen and oxygen within the fuel cell stack that transported hydrogen to the anode catalyst layer and oxygen to the cathode catalyst layer. At the anode, the H_2 gas splits into hydrogen ions and free electrons as Equation (6.1),

$$H_2 \rightarrow 2H^+ + 2e^- \tag{6.1}$$

The hydrogen ions cross the separating polymer membrane while the electrons stay at the anode side. Whereas at the cathode, the hydrogen ions reacted with oxygen molecules, and water was generated as Equation (6.2),

$$2H^+ + 2e^- + \frac{1}{2}O_2 \rightarrow H_2O \tag{6.2}$$
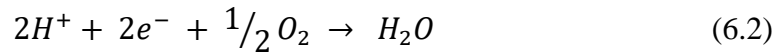
Therefore, the overall reaction became as Equation (6.3),

$$H_2 + \frac{1}{2}O_2 \rightarrow H_2O \tag{6.3}$$

The external circuit was connected to the positive and negative terminals of the fuel cell output. The electrons travel through the external circuit, creating a potential difference across both terminals. The potential difference induced was calculated using Equation (6.4), where 'E' denoted the output voltage, 'E_o' denoted the standard voltage, 'R' denoted Universal gas constant, 'T' denoted temperature, 'n' denoted the number of moles, 'f' denoted Faraday's constant, 'p' denoted pressure and subscripts 'H_2O, H_2, O_2' denoted water, hydrogen, and oxygen, respectively,

$$E = E_o - \frac{RT}{nf} \ln\left[\frac{p_{H_2O}}{p_{H_2}\sqrt{p_{O_2}}}\right] \tag{6.4}$$

Moisture produced in the fuel cell humidified the membrane and improved the electron transfer, enhancing cell efficiency. The over-flooding of the catalyst layer (CL) would result in pores blockage that hinders the electron movement, reducing the cell efficiency. Hence, a purging valve was installed to ensure the regular escape of extra H_2 and water from the fuel cell stack. The output from the fuel cell was connected to AC/DC loads to determine the cell performance at variable operating parameters.

After the experimentation, the fuel cell was again run on hydrogen from a hydrogen cylinder for 10 minutes. A reference reading was also taken at rated input parameters to compare the output with the experimental results.

6.2.3. Mathematical relations

The operating parameters for the fuel cell performance were analyzed using various empirical relationships in the open literature. The potential difference generated at the two terminals of the fuel cell was measured to determine the electrical work (W_E) in watts, as given in Equation (6.5),

$$W_E = E \times Q \tag{6.5}$$

Where 'E' represents the potential difference in volt and 'Q' represents the charge in coulomb. Here, the electrons carried the charge (Q), where the change (Q) is measured using Equation (6.6),

$$Q = n \times F \tag{6.6}$$

Where 'n' denotes the number of moles of electrons and 'F' denotes the Faraday's constant in coulomb per mole. Gibbs free energy of an electrochemical reaction gives the reversible voltage for the process. Using the values of n and F, the Gibbs free energy was calculated as Equation (6.7),

$$\Delta G = -nFE_O \tag{6.7}$$

The overall reaction was given by Equation (6.8),

$$H_2 + {}^1\!/_2\, O_2 \rightleftharpoons H_2O \tag{6.8}$$

As per standard conditions, the liquid water molecules had -237 kJ/mol of Gibbs free energy (ΔG). Hence, rearranging Equation (6.7) and from Equation (6.8), the reversible voltage (E_O) was given by Equation (6.9),

$$E_O = -\frac{\Delta G_O}{nF} \tag{6.9}$$

Where 'ΔG' represented the Gibbs free energy at standard conditions.

The fuel cell efficiency (η) was the ratio of useful work extracted from the system to the total amount of energy supplied to the system, as Equation (6.10),

$$\eta \;=\; \frac{useful\ work}{amount\ of\ total\ energy} \tag{6.10}$$

When the work extracted was from a chemical reaction, the amount of total energy becomes the change of enthalpy (ΔH), as Equation (6.11),

$$\Delta H \;=\; H_P - H_R \tag{6.11}$$

Where H_P and H_R denoted the enthalpies of the products and reactants. Hence, the fuel cell efficiency (η) after rearrangement was given as Equation (6.12),

$$\eta \;=\; \frac{useful\ work}{change\ of\ enthalpy} \tag{6.12}$$

6.3. Results and discussion

The results and discussions section analyzed the results obtained through various experiments. The input process parameters were varied, and the results were obtained at each input. The input parameters involved were hydrogen flow rate (HFR) and gas pressure to determine the PEM fuel cell performance. In contrast, the output results were the output current and voltage used to determine output power and fuel cell stack efficiency through various mathematical relationships. Thus, the cell performance was determined by varying hydrogen flow rate and gas pressure.

6.3.1. Effects of hydrogen flow rate (HFR)

The HFR is an essential parameter in determining cell performance. A fuel cell generates electricity till it receives the fuel (or hydrogen). The HFR described the amount of fuel available for the chemical reaction in the fuel cell. Here, the impacts of HFR on the output current and voltage were evaluated, and then the variation in output power against voltage at different hydrogen flow rates was studied. For reference, the output at 13 LPM (rated value) hydrogen flow rate that generated the maximum rated output was also measured. It will help compare the variation caused in the output when the fuel cell performs at lower hydrogen flow rates.
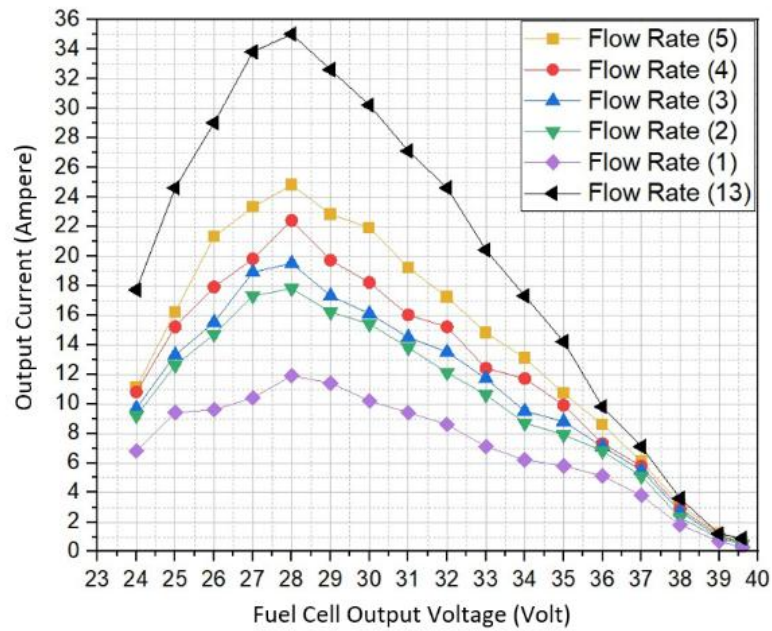
Figure 6.3. I-V characteristic at the variable hydrogen flow rates

Figure 6.3 presents the variation of the output current (in Ampere) for variable voltage (in Voltages). The HFR from the hydrogen production and purification unit was observed to be between 1 LPM and 5 LPM. The gas pressure was maintained at 0.45 (rated value) per the manufacturer's specifications. The rise in the output current was observed as the voltage increased from 24 V and attained the peak value at about 28 V. After 28 V, the output current again declined. A similar trend was observed for each HFR.

In contrast, when the HFR was increased from 1 LPM to 5 LPM, the output curves had more inclination and approached the rated maximum output at 13 LPM (maximum rated hydrogen flow rate). Hence, a reduction of about 29% in output current was observed for 5 LPM against 13 LPM. At the same time, the input (hydrogen flow rate) showed a significant reduction of about 61% from 13 LPM to 5 LPM. Similar differences were also observed at other hydrogen flow rates.
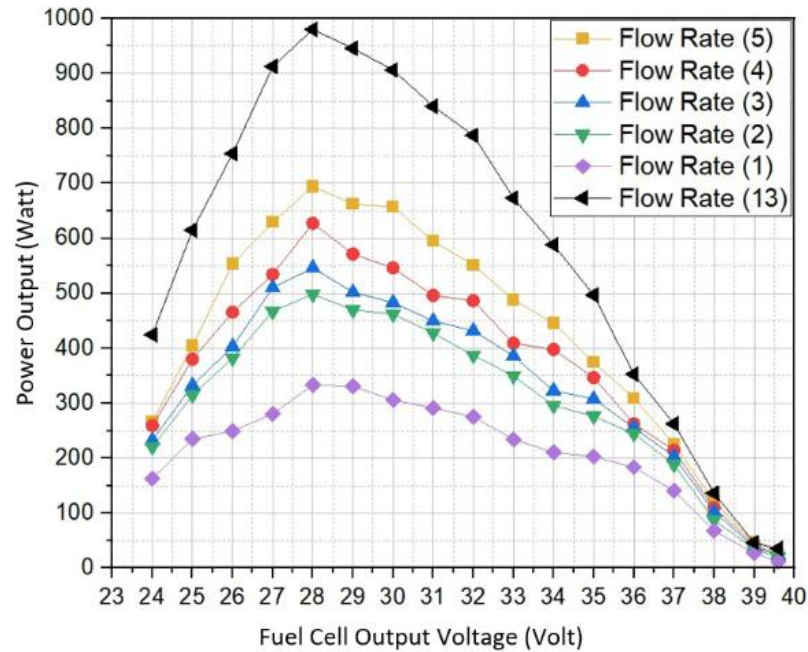
Figure 6.4. P-V characteristic at the variable hydrogen flow rates

Figure 6.4 illustrates the correlation between the output power (in watts) and voltage (in volts). Similar to Figure 6.3, the HFR varied between 1 LPM and 5 LPM, while the gas pressure was maintained at 0.45 bar per the specifications. With the reduction of about 60-61% hydrogen flow rate, about 29% reduction was observed in output power at peak value. It indicated that a slight compromise in output power would save a significant amount of hydrogen. It will reduce the hydrogen wastage during purging. The peak output power was 980 W at 13 LPM, whereas the peak output power at 1 LPM, 2 LPM, 3 LPM, 4 LPM, and 5 LPM were 333 W, 498.8 W, 546 W, 627 W, and 694.4 W, respectively.

6.3.2.   Effects of hydrogen pressure

Another essential operating parameter observed during experimentation was gas pressure. The fuel cell required an optimized input gas pressure to function at its peak or rated potential. The fuel pressurization affects the moisture management within the fuel cell. The moisture improves the cell output, but flooding of electrodes results in a sudden drop in output. The gas pressure significantly influences the diffusivity of the gas diffusion layer. Therefore, the gas flow channels were designed

to smoothen hydrogen and oxygen flow to the catalytic electrode plates. Here, the reference gas pressure of 0.45 bar was taken as mentioned by the manufacturer. The testing was performed by varying the gas pressure generated by the hydrogen production and purification unit to understand the range of gas pressure required to run a fuel cell while enhancing the output with the least wastage of hydrogen fuel.
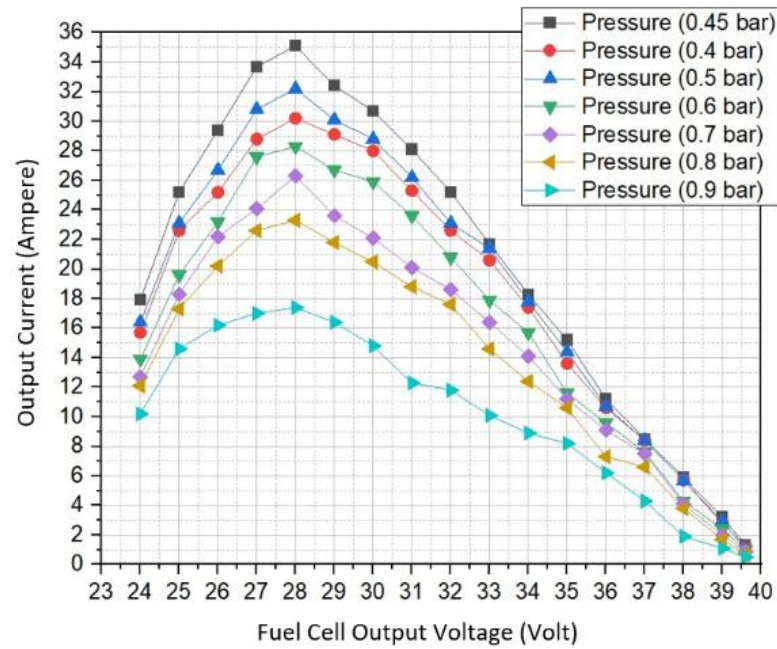
Figure 6.5. I-V characteristics at different gas pressures

Figure 6.5 shows the output current variation (in Ampere) for the voltage (in Voltage). The gas pressure range was maintained between 0.4 bar and 0.9 bar. The lower limit (0.4 bar) was the minimum gas pressure required to run the fuel cell, whereas the upper limit (0.9 bar) was the maximum gas pressure attained by the hydrogen production and purification unit. The results showed that the higher gas pressure beyond 0.5 bar reduced the output current. The maximum current output was achieved at the rated gas pressure of 0.45 bar, whereas an 8% and 14% decline was observed for 0.5 bar and 0.4 bar gas pressures against the rated gas pressure value. In contrast, the further rise in the gas pressure reduced the output current of the cell. A 10% addition or reduction in the gas pressure from the rated value slightly reduced fuel cell output. Beyond that, the reduction showed a significant drop in output.

Figure 6.6 illustrates the correlation between output power (in watts) and voltage (in volts). The gas pressure was changed from 0.4 bar to 0.9 bar, and the variation in the output power was recorded. The reference gas pressure of 0.45 bar was considered for comparison. A 100% rise in gas pressure from 0.45 bar to 0.9 bar was observed to have a 50% reduction (from 982.8 W to 487.2 W) in the output power, which is a very significant variation. The output power for 0.4 bar, 0.5 bar, 0.6 bar, 0.7 bar, and 0.8 bar was 845.6 W, 901.6 W, 792.4 W, 736.4 W, and 652.4 W at 28 V.
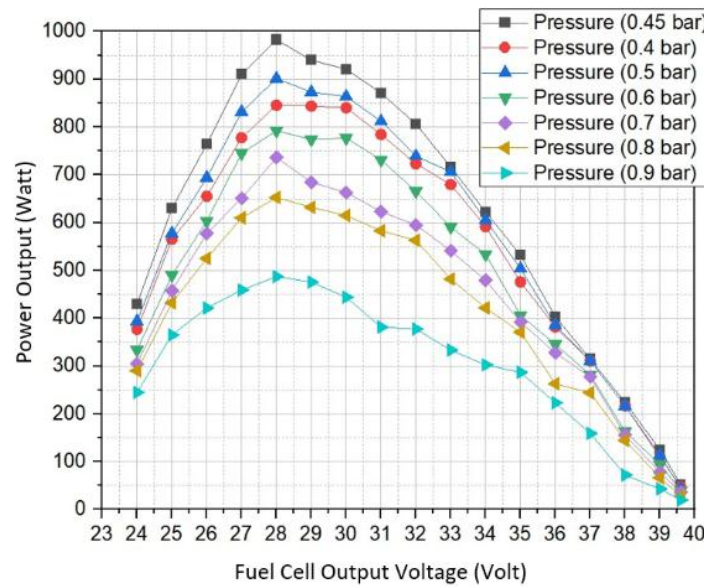
Figure 6.6. P-V characteristics at different gas pressures

6.3.3.   Variation in Fuel Cell Stack Efficiency

The fuel cell efficiency is the ratio of useful electrical energy generated to the amount of H_2 input in terms of energy. Hence, the efficiency can be enhanced by improving the output or reducing the input for the same input/output. The generalized efficiency equation was represented in Equation 6.10, whereas the efficiency in the form of fuel enthalpy was represented in Equation 6.12. The fuel cell stack efficiency depends on various parameters, including the type of fuel cell, operating parameters, moisture, temperature, etc. In the current work, the cell efficiency was determined by varying the two operating parameters (HFR and gas pressure). The lower HFR was considered depending on the H_2 production and purification unit. In contrast, gas pressures as high as 0.9 bar were tested to compensate for the loss due to the low HFR.

Figure 6.7. Variation of fuel cell stack efficiency at variable hydrogen flow rate

Figure 6.7 explains the deviation in fuel cell stack efficiency (in percentage) for the voltage (in volts) at variable HFR. The HFR ranged between 1 LPM and 5 LPM as generated by the hydrogen production and purification unit; however, a 13 LPM of HFR was also considered for reference at the peak output per manufacturer specifications. The results showed a rise in the fue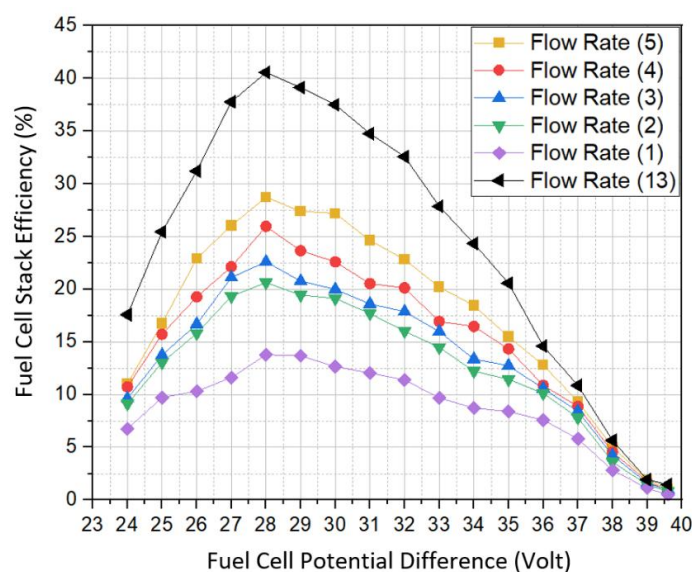l cell stack efficiency with a surge in the fuel cell potential difference, which reached the maximum at about 28 V. Beyond 28 V, the efficiency declined and reached a minimum (nearly zero) at about 39.5 V. In contrast, the higher fuel cell stack efficiency was observed at higher HFR. The HFR had a crucial role in determining the dominance of oxygen partial pressure over hydrogen. The higher HFR represented more H_2 molecule intake, resulting in better chemical reactions within the fuel cell. More H_2 molecules increased H_2 wastage and produced more water that cause electrode flooding if not removed.

Figure 6.8 shows the relationship between fuel cell stack efficiency (in percentage) and fuel cell potential difference (in volts) at various gas pressures. The gas pressure was changed from 0.4 bar to 0.9 bar, and 0.45 bar was taken as the reference (or rated) gas pressure per the manufacturer's specifications. The results showed a 10% decline from the rated gas pressure (0.45 bar) and a 15% reduction in the fuel cell stack efficiency at 5 LPM. In contrast, a 10% addition in the rated gas pressure had a 10% reduction in the cell efficiency at 5 LPM.
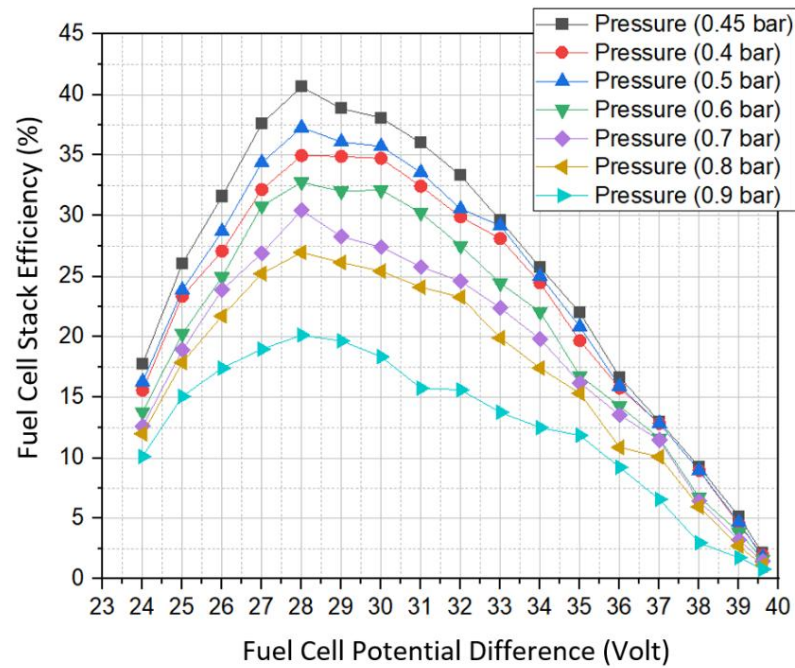
Figure 6.8. Variation of fuel cell stack efficiency at different pressures

6.4. Summary

The performance of a 1 kW capacity PEM fuel cell was studied. The operating parameters, such as hydrogen flow rate (HFR) and gas pressure, were considered to investigate the output from the fuel cell. A hydrogen production and purification unit was connected, and the tests were conducted from higher to lower hydrogen flow rate and gas pressure limits. In contrast, the readings at the rated peak operating parameters were also measured for reference. During experimentation, the hydrogen flow rate ranged between 1 LPM and 5 LPM, whereas 13 LPM was the rated peak hydrogen flow rate. Similarly, the gas pressures were between 0.4 bar and 0.9 bar with a raise of 0.1 bar, whereas 0.45 bar was the rated gas pressure per manufacturer specifications. The following findings were observed:

- The rated peak values of the operating parameters gave the maximum output during experimentation.
- The hydrogen flow rate of 5 LPM showed a 29% decline in output, whereas the hydrogen flow rate reduction was about 61%. Thus, reducing the hydrogen

flow rate would save a considerable amount of hydrogen with comparatively less effect on the output.

- The gas pressure showed an 8% and 14% decline for 10% increased and decreased input gas pressure. Whereas beyond 0.5 bar gas pressure, the output drop was significant.

- The fuel cell stack efficiency declined at a lower HFR because of the fewer H_2 molecules for chemical reactions.

- Similarly, the fuel cell stack efficiency declined by 10% and 15%, with a 10% addition and 10% reduction in rated gas pressure.

Therefore, the lower hydrogen flow rate and higher gas pressure negatively impacted the fuel cell output. However, the drop in the output is comparatively less than the reduction in input. The study will help augment the cell performance and lessen the hydrogen wastage due to extra hydrogen molecules at a higher hydrogen flow rate.

CHAPTER 7

CONCLUSIONS AND FUTURE SCOPE

7.1. Conclusions

The following are the findings from the current research work:

Experimental findings:

- The influencing parameters in plasma reactors are feed flow rate, reactor temperature, and feed molar ratio.

- The atomization of the water-methanol mixture at 2.4 MHz ultrasonic frequency showed maximum hydrogen production rate, followed by 1.7 MHz and 0.3 MHz transducers.

- The hydrogen production rate rose by about 14%, with the input voltage rise from 4 kV to 7.5 kV.

- The maximum percentage rise of about 25% was observed at 1.7 MHz ultrasonic frequency.

- The higher methanol concentration showed a higher hydrogen production rate and reached 306.2 mol/day hydrogen production rate using a 2.4 MHz ultrasonic transducer.

- The higher feed flow rate also positively influenced the hydrogen production rate and peaked at 3.5 LPM. Beyond 3.5 LPM, the HPR declined.

- All three ultrasonic transducers observed a similar trend for methanol concentration and feed flow rate, where 2.4 MHz showed the highest hydrogen production rate, followed by 1.7 MHz and 0.3 MHz, respectively.

- The hydrogen purity was observed at about 99% after using the hydrogen purification unit.

- The plasma reforming with hydrogen purification unit has the system efficiency of 42.2%.

Simulation findings:

- A sharp rise in H_2 selectivity was obtained with the temperature rise. At the same time, the methanol conversion rate is more than the water conversion rate, which shows more influence of methanol than water in hydrogen production.

- A rise in reactor pressure adversely affects hydrogen concentration, represented by lower H_2 mole fraction and selectivity at higher pressures.

- The higher molar ratio resulted in a lower methanol conversion rate and, thus, a reduction in hydrogen selectivity was observed.

- The simulation showed the HS values in the 74% and 86% range, while the FCP values range from 81.4% to 97.3%.

- R^2 values of HS and FCP are 0.9877 and 0.9803, which showed a better correspondence between the simulated and predicted values.

- M-to-W molar ratio is the most significant parameter for hydrogen production, and the range from 0.9 to 1.35 shows the highest H_2 production potential.

- Reaction temperature showed intermediate significance, while it was observed that the higher temperature has more potential to generate hydrogen.

- An optimized HS and FCP of 84.81% and 95.71% were obtained at 328 °C RT, 2.6 atm. RP, and 1.34 M-to-W molar ratio.

PEM Fuel Cell Performance:

- The reduction in hydrogen flow rate would save a considerable amount of hydrogen with comparatively less effect on the output.

- The gas pressure showed an 8% and 14% decline for 10% increased and decreased input gas pressure. Whereas beyond 0.5 bar gas pressure, the output drop was significant.

- The fuel cell stack efficiency also declined at a lower HFR because of the lower number of H_2 molecules that exist for chemical reactions.

- Similarly, the fuel cell stack efficiency declined by 10% and 15% with a 10% addition and 10% reduction in rated gas pressure.

7.2. Future scope

- Other parameters that can also be considered for simulation are reactor length and diameter, type of feed, and higher feed flow rate.
- A better optimization tool may be applied to find better optimal results.
- A bigger Plasma reformer may be designed for high-capacity Hydrogen Production.
- Higher ultrasonic frequency waves may be used for finer atomization of feed.
- Higher alcohols, methane gas, and other feedstocks may be used to generate hydrogen.
- The hydrogen generated in the experiment is about 99% purity level; therefore, it may be considered for fuel in fuel cells after further purification to >99.9% purity for power generation and other industrial applications.
- LCA analysis of Plasma Reforming for Hydrogen Production may be performed using software like SimaPro, OpenLCA to assess the environmental impacts.

<u>REFERENCES</u>

[1]   Dodds PE, Staffell I, Hawkes AD, Li F, Grünewald P, McDowall W, et al. Hydrogen and fuel cell technologies for heating: A review. Int J Hydrogen Energy 2015;40:2065–83. https://doi.org/10.1016/j.ijhydene.2014.11.059.

[2]   Tartakovsky L, Sheintuch M. Fuel reforming in internal combustion engines. Prog Energy Combust Sci 2018;67:88–114. https://doi.org/10.1016/j.pecs.2018.02.003.

[3]   Dincer I, Acar C. Review and evaluation of hydrogen production methods for better sustainability. Int J Hydrogen Energy 2014;40:11094–111. https://doi.org/10.1016/j.ijhydene.2014.12.035.

[4]   Gao Y, Jiang J, Meng Y, Yan F, Aihemaiti A. A review of recent developments in hydrogen production via biogas dry reforming. Energy Convers Manag 2018;171:133–55. https://doi.org/10.1016/j.enconman.2018.05.083.

[5]   Kalinci Y, Hepbasli A, Dincer I. Biomass-based hydrogen production: A review and analysis. Int J Hydrogen Energy 2009;34:8799–817. https://doi.org/10.1016/j.ijhydene.2009.08.078.

[6]   Chen F, Huang X, Cheng DG, Zhan X. Hydrogen production from alcohols and ethers via cold plasma: A review. Int J Hydrogen Energy 2014;39:9036–46. https://doi.org/10.1016/j.ijhydene.2014.03.194.

[7]   Kim S, Chen J, Cheng T, Gindulyte A, He J, He S, et al. PubChem 2019 update: improved access to chemical data. Nucleic Acids Res 2019;47:D1102–9. https://doi.org/10.1093/nar/gky1033.

[8]   A. Lanz, J. Heffel, C. Messer and C of the D. Hydrogen fuel cell engines and related technologies, College of the Desert, Energy Technology Training Center,; 2001, p. 1–25.

[9]   Blumenthal G. Kuhn and the Chemical Revolution: a re-assessment. Found Chem 2013;15:93–101. https://doi.org/10.1007/s10698-011-9129-6.

[10]   Nikolaidis P, Poullikkas A. A comparative overview of hydrogen production processes. Renewable and Sustainable Energy Reviews 2017;67:597–611. https://doi.org/10.1016/j.rser.2016.09.044.

[11]   Budhraja N, Pal A, Mishra RS. Plasma reforming for hydrogen production: Pathways, reactors and storage. Int J Hydrogen Energy 2023;48:2467–82. https://doi.org/10.1016/j.ijhydene.2022.10.143.

[12] Moshrefi MM, Rashidi F. Hydrogen Production from Methane Decomposition in Cold Plasma Reactor with Rotating Electrodes. Plasma Chemistry and Plasma Processing 2018;38:503–15. https://doi.org/10.1007/s11090-018-9875-5.

[13] Kheirollahivash M, Rashidi F, Moshrefi MM. Hydrogen Production from Methane Decomposition Using a Mobile and Elongating Arc Plasma Reactor. Plasma Chemistry and Plasma Processing 2019;39:445–59. https://doi.org/10.1007/s11090-018-9950-y.

[14] Janev RK, Reiter D. Collision processes of CHy and CHy+ hydrocarbons with plasma electrons and protons. Phys Plasmas 2002;9:4071. https://doi.org/10.1063/1.1500735.

[15] Morgan NN, ElSabbagh M. Hydrogen Production from Methane Through Pulsed DC Plasma. Plasma Chemistry and Plasma Processing 2017;37:1375–92. https://doi.org/10.1007/s11090-017-9829-3.

[16] Hrabovsky M, Hlina M, Kopecky V, Maslani A, Krenek P, Serov A, et al. Steam Plasma Methane Reforming for Hydrogen Production. Plasma Chemistry and Plasma Processing 2018;38:743–58. https://doi.org/10.1007/s11090-018-9891-5.

[17] Li P, Chen L, Xia S, Kong R, Ge Y. Total entropy generation rate minimization configuration of a membrane reactor of methanol synthesis via carbon dioxide hydrogenation. Sci China Technol Sci 2022;65:657–78. https://doi.org/10.1007/s11431-021-1935-4.

[18] Lee DH, Kim T. Plasma-catalyst hybrid methanol-steam reforming for hydrogen production. Int J Hydrogen Energy 2013;38:6039–43. https://doi.org/10.1016/j.ijhydene.2012.12.132.

[19] Wang W, Zhu C, Cao Y. DFT study on pathways of steam reforming of ethanol under cold plasma conditions for hydrogen generation. Int J Hydrogen Energy 2010;35:1951–6. https://doi.org/10.1016/j.ijhydene.2009.12.170.

[20] O-Thong S, Prasertsan P, Birkeland NK. Evaluation of methods for preparing hydrogen-producing seed inocula under thermophilic condition by process performance and microbial community analysis. Bioresour Technol 2009;100:909–18. https://doi.org/10.1016/j.biortech.2008.07.036.

[21] Budhraja N, Pal A, Kumar A. Investigations on Ethanol as the Raw Material for Hydrogen Production, Storage, and Applications. In: Kumar A, Pal A, Kachhwaha SS, Jain PK, editors., Singapore: Springer Singapore; 2021, p. 317–26. https://doi.org/10.1007/978-981-15-9678-0_28.

[22] Xin Y, Sun B, Zhu X, Yan Z, Zhao X, Sun X, et al. Characteristics and pathways of hydrogen produced by pulsed discharge in ethanol-water mixtures. Int J Hydrogen Energy 2020;45:1588–96. https://doi.org/10.1016/j.ijhydene.2019.11.101.

[23] Rivkin C, Burgess R, Buttner W, Rivkin C, Burgess R, Buttner W. Hydrogen Technologies Safety Guide. National Renewable Energy Laboratory, USA: 2015.

[24] Chang ACC, Lee KY. Biogas reforming by the honeycomb reactor for hydrogen production. Int J Hydrogen Energy 2016;41:4358–65. https://doi.org/10.1016/j.ijhydene.2015.09.018.

[25] Yoo J, Park S, Song JH, Yoo S, Song IK. Hydrogen production by steam reforming of natural gas over butyric acid-assisted nickel/alumina catalyst. Int J Hydrogen Energy 2017;42:28377–85. https://doi.org/10.1016/j.ijhydene.2017.09.148.

[26] Han SJ, Song JH, Yoo J, Park S, Kang KH, Song IK. Sorption-enhanced hydrogen production by steam reforming of ethanol over mesoporous Co/CaO–Al2O3 xerogel catalysts: Effect of Ca/Al molar ratio. Int J Hydrogen Energy 2017;42:5886–98. https://doi.org/10.1016/j.ijhydene.2016.12.075.

[27] Lu J, Li X, He S, Han C, Wan G, Lei Y, et al. Hydrogen production via methanol steam reforming over Ni-based catalysts: Influences of Lanthanum (La) addition and supports. Int J Hydrogen Energy 2017;42:3647–57. https://doi.org/10.1016/j.ijhydene.2016.08.165.

[28] Zhang R, Huang C, Zong L, Lu K, Wang X, Cai J. Hydrogen Production from Methanol Steam Reforming over TiO2 and CeO2 Pillared Clay Supported Au Catalysts. Applied Sciences 2018;8:176. https://doi.org/10.3390/app8020176.

[29] Casanovas A, Galvis A, Llorca J. Catalytic steam reforming of olive mill wastewater for hydrogen production. Int J Hydrogen Energy 2015;40:7539–45. https://doi.org/10.1016/j.ijhydene.2014.11.083.

[30] Rabbani M, Dincer I. Energetic and exergetic assessments of glycerol steam reforming in a combined power plant for hydrogen production. Int J Hydrogen Energy 2014;40:11125–32. https://doi.org/10.1016/j.ijhydene.2015.04.012.

[31] Yilmaz F, Ozturk M, Selbas R. Design and thermodynamic analysis of coal-gasification assisted multigeneration system with hydrogen production and liquefaction. Energy Convers Manag 2019;186:229–40. https://doi.org/10.1016/j.enconman.2019.02.053.

[32] Seyitoglu SS, Dincer I, Kilicarslan A. Energy and exergy analyses of hydrogen production by coal gasification. Int J Hydrogen Energy 2017;42:2592–600. https://doi.org/10.1016/j.ijhydene.2016.08.228.

[33]   Yuksel YE, Ozturk M, Dincer I. Energy and exergy analyses of an integrated system using waste material gasification for hydrogen production and liquefaction. Energy Convers Manag 2019;185:718–29. https://doi.org/10.1016/j.enconman.2019.02.033.

[34]   Hasan A, Dincer I. Comparative assessment of various gasification fuels with waste tires for hydrogen production. Int J Hydrogen Energy 2019;44:18818–26. https://doi.org/10.1016/j.ijhydene.2018.11.150.

[35]   Kang K, Azargohar R, Dalai AK, Wang H. Hydrogen production from lignin, cellulose and waste biomass via supercritical water gasification: Catalyst activity and process optimization study. Energy Convers Manag 2016;117:528–37. https://doi.org/10.1016/j.enconman.2016.03.008.

[36]   Doranehgard MH, Samadyar H, Mesbah M, Haratipour P, Samiezade S. High-purity hydrogen production with in situ CO2 capture based on biomass gasification. Fuel 2017;202:29–35. https://doi.org/10.1016/j.fuel.2017.04.014.

[37]   Kuo JH, Lin CL, Chang TJ, Weng WC, Liu JY. Impact of using calcium oxide as a bed material on hydrogen production in two-stage fluidized bed gasification. Int J Hydrogen Energy 2016;41:17283–9. https://doi.org/10.1016/j.ijhydene.2016.07.144.

[38]   Wu MH, Lin CL, Chiu CM. Influences of temperature arrangement on hydrogen production during two-stage gasification process. Int J Hydrogen Energy 2019:5212–9. https://doi.org/10.1016/j.ijhydene.2018.08.037.

[39]   Yan M, Su H, Hantoko D, Kanchanatip E, Shahul Hamid FB, Zhang S, et al. Experimental study on the energy conversion of food waste via supercritical water gasification: Improvement of hydrogen production. Int J Hydrogen Energy 2019;44:4664–73. https://doi.org/10.1016/j.ijhydene.2018.12.193.

[40]   Deniz I, Vardar-Sukan F, Yüksel M, Saglam M, Ballice L, Yesil-Celiktas O. Hydrogen production from marine biomass by hydrothermal gasification. Energy Convers Manag 2015;96:124–30. https://doi.org/10.1016/j.enconman.2015.02.048.

[41]   Chakik F ezzahra, Kaddami M, Mikou M. Effect of operating parameters on hydrogen production by electrolysis of water. Int J Hydrogen Energy 2017;42:25550–7. https://doi.org/10.1016/j.ijhydene.2017.07.015.

[42]   Yu JW, Jung G bin, Su YJ, Yeh CC, Kan MY, Lee CY, et al. Proton exchange membrane water electrolysis system-membrane electrode assembly with additive. Int J Hydrogen Energy 2019;44:15721–6. https://doi.org/10.1016/j.ijhydene.2018.11.192.

[43]   Villagra A, Millet P. An analysis of PEM water electrolysis cells operating at elevated current densities. Int J Hydrogen Energy 2019;44:9708–17. https://doi.org/10.1016/j.ijhydene.2018.11.179.

[44]   Bidin N, Azni SR, Abu Bakar MA, Johari AR, Abdul Munap DHF, Salebi MF, et al. The effect of sunlight in hydrogen production from water electrolysis. Int J Hydrogen Energy 2017;42:133–42. https://doi.org/10.1016/j.ijhydene.2016.11.203.

[45]   Belleville P, Guillet F, Pons A, Deseure J, Merlin G, Druart F, et al. Low voltage water electrolysis: Decoupling hydrogen production using bioelectrochemical system. Int J Hydrogen Energy 2018;43:14867–75. https://doi.org/10.1016/j.ijhydene.2018.06.080.

[46]   Dukić A. Autonomous hydrogen production system. Int J Hydrogen Energy 2015;40:7465–74. https://doi.org/10.1016/j.ijhydene.2015.02.003.

[47]   Guban D, Muritala IK, Roeb M, Sattler C. Assessment of sustainable high temperature hydrogen production technologies. Int J Hydrogen Energy 2019. https://doi.org/10.1016/j.ijhydene.2019.08.145.

[48]   Bareiß K, de la Rua C, Möckl M, Hamacher T. Life cycle assessment of hydrogen from proton exchange membrane water electrolysis in future energy systems. Appl Energy 2019;237:862–72. https://doi.org/10.1016/j.apenergy.2019.01.001.

[49]   Yokoyama H, Waki M, Ogino A, Ohmori H, Tanaka Y. Hydrogen fermentation properties of undiluted cow dung. J Biosci Bioeng 2007;104:82–5. https://doi.org/10.1263/jbb.104.82.

[50]   Yokoyama H, Waki M, Moriya N, Yasuda T, Tanaka Y, Haga K. Effect of fermentation temperature on hydrogen production from cow waste slurry by using anaerobic microflora within the slurry. Appl Microbiol Biotechnol 2007;74:474–83. https://doi.org/10.1007/s00253-006-0647-4.

[51]   Budhraja N, Pal A, Mishra RS. Various treatment methods for enhanced bio-hydrogen production. Mater Today Proc 2023. https://doi.org/10.1016/j.matpr.2023.03.198.

[52]   Pang Y, Hammer T, Müller D, Karl J. Investigation on the influence of non-thermal plasma on reaction degree of wood gasification in a drop tube reactor. Fuel 2019;253:95–105. https://doi.org/10.1016/j.fuel.2019.04.165.

[53]   Bulychev NA, Kazaryan MA, Averyushkin AS, Chernov AA, Gusev AL. Hydrogen production by low-temperature plasma decomposition of liquids. Int J Hydrogen Energy 2017;42:20934–8. https://doi.org/10.1016/j.ijhydene.2016.09.226.

[54] Huang DY, Jang JH, Tsai WR, Wu WY. Improvement in hydrogen production with plasma reformer system. Energy Procedia 2016;88:505–9. https://doi.org/10.1016/j.egypro.2016.06.070.

[55] Shiraishi R, Nomura S, Mukasa S, Nakano R, Kamatoko R. Effect of catalytic electrode and plate for methanol decomposition by in-liquid plasma. Int J Hydrogen Energy 2018;43:4305–10. https://doi.org/10.1016/j.ijhydene.2018.01.060.

[56] Lian H-Y, Li X-S, Liu J-L, Zhu X, Zhu A-M. Oxidative pyrolysis reforming of methanol in warm plasma for an on-board hydrogen production. Int J Hydrogen Energy 2017;42:13617–24. https://doi.org/10.1016/j.ijhydene.2016.10.166.

[57] Yue M, Lambert H, Pahon E, Roche R, Jemei S, Hissel D. Hydrogen energy systems: A critical review of technologies, applications, trends and challenges. Renewable and Sustainable Energy Reviews 2021;146. https://doi.org/10.1016/j.rser.2021.111180.

[58] Unlu D, Hilmioglu ND. Application of aspen plus to renewable hydrogen production from glycerol by steam reforming. Int J Hydrogen Energy 2020;45:3509–15. https://doi.org/10.1016/j.ijhydene.2019.02.106.

[59] Mohammadidoust A, Omidvar MR. Simulation and modeling of hydrogen production and power from wheat straw biomass at supercritical condition through Aspen Plus and ANN approaches. Biomass Convers Biorefin 2020. https://doi.org/10.1007/s13399-020-00933-5.

[60] Tavares R, Monteiro E, Tabet F, Rouboa A. Numerical investigation of optimum operating conditions for syngas and hydrogen production from biomass gasification using Aspen Plus. Renew Energy 2020;146:1309–14. https://doi.org/10.1016/j.renene.2019.07.051.

[61] Ye G, Xie D, Qiao W, Grace JR, Lim CJ. Modeling of fluidized bed membrane reactors for hydrogen production from steam methane reforming with Aspen Plus. Int J Hydrogen Energy 2009;34:4755–62. https://doi.org/10.1016/j.ijhydene.2009.03.047.

[62] Ishaq H, Dincer I. Design and performance evaluation of a new biomass and solar based combined system with thermochemical hydrogen production. Energy Convers Manag 2019;196:395–409. https://doi.org/10.1016/j.enconman.2019.05.100.

[63] Bassyouni M, Ul Hasan SW, Abdel-Aziz MH, Abdel-Hamid SMS, Naveed S, Hussain A, et al. Date palm waste gasification in downdraft gasifier and simulation using ASPEN HYSYS. Energy Convers Manag 2014;88:693–9. https://doi.org/10.1016/j.enconman.2014.08.061.

[64] Sánchez M, Amores E, Abad D, Rodríguez L, Clemente-Jul C. Aspen Plus model of an alkaline electrolysis system for hydrogen production. Int J Hydrogen Energy 2020;45:3916–29. https://doi.org/10.1016/j.ijhydene.2019.12.027.

[65] Chehade G, Lytle S, Ishaq H, Dincer I. Hydrogen production by microwave based plasma dissociation of water. Fuel 2020;264:116831. https://doi.org/10.1016/j.fuel.2019.116831.

[66] Liu S, Wang CY, Yin LL, Li WZ, Wang ZJ, Luo LN. Optimization of hydrogen production from agricultural wastes using mixture design. International Journal of Agricultural and Biological Engineering 2017;10:246–54. https://doi.org/10.3965/j.ijabe.20171003.2688.

[67] Liu S, Li W, Zheng G, Yang H, Li L. Optimization of Cattle Manure and Food Waste Co-Digestion for Biohydrogen Production in a Mesophilic Semi-Continuous Process. Energies (Basel) 2020;13:3848. https://doi.org/10.3390/en13153848.

[68] Bi Y, Yin L, He T, Ju Y. Optimization and analysis of a novel hydrogen liquefaction process for circulating hydrogen refrigeration. Int J Hydrogen Energy 2022;47:348–64. https://doi.org/10.1016/j.ijhydene.2021.10.012.

[69] Cao G, Xiao Y, Huang WM, Chen CH, Baltrusaitis J. DBD plasma-assisted ethanol steam reforming for green H2 production: Process optimization through response surface methodology (RSM). Int J Hydrogen Energy 2022. https://doi.org/10.1016/j.ijhydene.2022.09.237.

[70] Gao N, Liu S, Han Y, Xing C, Li A. Steam reforming of biomass tar for hydrogen production over NiO/ceramic foam catalyst. Int J Hydrogen Energy 2015;40:7983–90. https://doi.org/10.1016/j.ijhydene.2015.04.050.

[71] Xie H, Yu Q, Wei M, Duan W, Yao X, Qin Q, et al. Hydrogen production from steam reforming of simulated bio-oil over Ce-Ni/Co catalyst with in continuous CO2 capture. Int J Hydrogen Energy 2015;40:1420–8. https://doi.org/10.1016/j.ijhydene.2014.11.137.

[72] Pu Y-C, Li S-R, Yan S, Huang X, Wang D, Ye Y-Y, et al. An improved Cu/ZnO catalyst promoted by Sc2O3 for hydrogen production from methanol reforming. Fuel 2019;241:607–15. https://doi.org/10.1016/j.fuel.2018.12.067.

[73] Ji H, Lee J, Choi E, Seo I. Hydrogen production from steam reforming using an indirect heating method. Int J Hydrogen Energy 2018;43:3655–63. https://doi.org/10.1016/j.ijhydene.2017.12.137.

[74] Zheng B, Sun P, Meng J, Liu Y, Wang G, Tang S, et al. Effects of fin structure size on methane-steam reforming for hydrogen production in a reactor heated by waste heat. Int J Hydrogen Energy 2019. https://doi.org/10.1016/j.ijhydene.2019.10.143.

[75] Kim CH, Han JY, Kim S, Lee B, Lim H, Lee KY, et al. Hydrogen production by steam methane reforming in a membrane reactor equipped with a Pd composite membrane deposited on a porous stainless steel. Int J Hydrogen Energy 2018;43:7684–92. https://doi.org/10.1016/j.ijhydene.2017.11.176.

[76] Yang J Il, Kim TW, Chan Park J, Lim TH, Jung H, Chun DH. Development of a stand-alone steam methane reformer for on-site hydrogen production. Int J Hydrogen Energy 2016;41:8176–83. https://doi.org/10.1016/j.ijhydene.2015.10.154.

[77] Hou T, Zhang S, Chen Y, Wang D, Cai W. Hydrogen production from ethanol reforming: Catalysts and reaction mechanism. Renewable and Sustainable Energy Reviews 2015;44:132–48. https://doi.org/10.1016/j.rser.2014.12.023.

[78] Song C, Liu Q, Ji N, Kansha Y, Tsutsumi A. Optimization of steam methane reforming coupled with pressure swing adsorption hydrogen production process by heat integration. Appl Energy 2015;154:392–401. https://doi.org/10.1016/j.apenergy.2015.05.038.

[79] Wang F, Wang G. Performance and cold spot effect of methanol steam reforming for hydrogen production in micro-reactor. Int J Hydrogen Energy 2016;41:16835–41. https://doi.org/10.1016/j.ijhydene.2016.07.083.

[80] Zhang R, Huang C, Zong L, Lu K, Wang X, Cai J. Hydrogen Production from Methanol Steam Reforming over TiO2 and CeO2 Pillared Clay Supported Au Catalysts. Applied Sciences 2018;8:176. https://doi.org/10.3390/app8020176.

[81] González-Gil R, Herrera C, Larrubia MÁ, Kowalik P, Pieta IS, Alemany LJ. Hydrogen production by steam reforming of DME over Ni-based catalysts modified with vanadium. Int J Hydrogen Energy 2016;41:19781–8. https://doi.org/10.1016/j.ijhydene.2016.05.074.

[82] Chen CC, Tseng HH, Lin YL, Chen WH. Hydrogen production and carbon dioxide enrichment from ethanol steam reforming followed by water gas shift reaction. J Clean Prod 2017;162:1430–41. https://doi.org/10.1016/j.jclepro.2017.06.149.

[83] Sepehri S, Rezaei M, Wang Y, Younesi A, Arandiyan H. The evaluation of autothermal methane reforming for hydrogen production over Ni/CeO2 catalysts. Int J Hydrogen Energy 2018:22340–6. https://doi.org/10.1016/j.ijhydene.2018.10.016.

[84] Zhang S, Wang X, Xu X, Li P. Hydrogen production via catalytic autothermal reforming of desulfurized Jet-A fuel. Int J Hydrogen Energy 2017;42:1932–41. https://doi.org/10.1016/j.ijhydene.2016.11.004.

[85] Chen J, Wang M, Wang S, Li X. Hydrogen production via steam reforming of acetic acid over biochar-supported nickel catalysts. Int J Hydrogen Energy 2018;43:18160–8. https://doi.org/10.1016/j.ijhydene.2018.08.048.

[86] Macedo MS, Soria MA, Madeira LM. Glycerol steam reforming for hydrogen production: Traditional versus membrane reactor. Int J Hydrogen Energy 2019;44:24719–32. https://doi.org/10.1016/j.ijhydene.2019.07.046.

[87] Xie H, Li R, Wang Z, Yao X, Yu Q. Hydrogen production of bio-oil steam reforming combining heat recovery of blast furnace slag: Thermodynamic analysis. Int J Hydrogen Energy 2019;44:25514–23. https://doi.org/10.1016/j.ijhydene.2019.08.014.

[88] Pushkareva IV, Pushkarev AS, Grigoriev SA, Modisha P, Bessarabov DG. Comparative study of anion exchange membranes for low-cost water electrolysis. Int J Hydrogen Energy 2019. https://doi.org/10.1016/j.ijhydene.2019.11.011.

[89] Dobó Z, Palotás ÁB. Impact of the current fluctuation on the efficiency of Alkaline Water Electrolysis. Int J Hydrogen Energy 2017;42:5649–56. https://doi.org/10.1016/j.ijhydene.2016.11.142.

[90] Manolova M, Schoeberl C, Freudenberger R, Ellwein C, Kerres J, Stypka S, et al. Development and testing of an anion exchange membrane electrolyser. Int J Hydrogen Energy 2015;40:11362–9. https://doi.org/10.1016/j.ijhydene.2015.04.149.

[91] Kim JH, Lee JN, Yoo CY, Lee KB, Lee WM. Low-cost and energy-efficient asymmetric nickel electrode for alkaline water electrolysis. Int J Hydrogen Energy 2015;40:10720–5. https://doi.org/10.1016/j.ijhydene.2015.07.025.

[92] Lamy C. From hydrogen production by water electrolysis to its utilization in a PEM fuel cell or in a SO fuel cell: Some considerations on the energy efficiencies. Int J Hydrogen Energy 2016;41:15415–25. https://doi.org/10.1016/j.ijhydene.2016.04.173.

[93] AlZahrani AA, Dincer I. Modeling and performance optimization of a solid oxide electrolysis system for hydrogen production. Appl Energy 2018;225:471–85. https://doi.org/10.1016/j.apenergy.2018.04.124.

[94] Ehteshami SMM, Vignesh S, Rasheed RKA, Chan SH. Numerical investigations on ethanol electrolysis for production of pure hydrogen from renewable sources. Appl Energy 2016;170:388–93. https://doi.org/10.1016/j.apenergy.2016.03.001.

[95] Cardoso DSP, Amaral L, Santos DMF, Šljukić B, Sequeira CAC, Macciò D, et al. Enhancement of hydrogen evolution in alkaline water electrolysis by using nickel-rare earth alloys. Int J Hydrogen Energy 2015;40:4295–302. https://doi.org/10.1016/j.ijhydene.2015.01.174.

[96] Huang PH, Kuo JK, Wu ZD. Applying small wind turbines and a photovoltaic system to facilitate electrolysis hydrogen production. Int J Hydrogen Energy 2016;41:8514–24. https://doi.org/10.1016/j.ijhydene.2016.02.051.

[97] de Fátima Palhares DDA, Vieira LGM, Damasceno JJR. Hydrogen production by a low-cost electrolyzer developed through the combination of alkaline water electrolysis and solar energy use. Int J Hydrogen Energy 2018;43:4265–75. https://doi.org/10.1016/j.ijhydene.2018.01.051.

[98] Rabady RI, Kenaan B. Power spectral shaping for hydrogen production from silicon based hybrid thermo-photovoltaic water electrolysis. Energy 2017;133:1–8. https://doi.org/10.1016/j.energy.2017.05.100.

[99] Rahim AHA, Tijani AS, Fadhlullah M, Hanapi S, Sainan KI. Optimization of Direct Coupling Solar PV Panel and Advanced Alkaline Electrolyzer System. vol. 79. Elsevier B.V.; 2015. https://doi.org/10.1016/j.egypro.2015.11.464.

[100] Kovač A, Marciuš D, Budin L. Solar hydrogen production via alkaline water electrolysis. Int J Hydrogen Energy 2019;44:9841–8. https://doi.org/10.1016/j.ijhydene.2018.11.007.

[101] Tebibel H, Khellaf A, Menia S, Nouicer I. Design, modelling and optimal power and hydrogen management strategy of an off grid PV system for hydrogen production using methanol electrolysis. Int J Hydrogen Energy 2017;42:14950–67. https://doi.org/10.1016/j.ijhydene.2017.05.010.

[102] Tebibel H. Off grid PV system for hydrogen production using PEM methanol electrolysis and an optimal management strategy. Int J Hydrogen Energy 2017;42:19432–45. https://doi.org/10.1016/j.ijhydene.2017.05.205.

[103] Tebibel H, Medjebour R. Comparative performance analysis of a grid connected PV system for hydrogen production using PEM water, methanol and hybrid sulfur electrolysis. Int J Hydrogen Energy 2018;43:3482–98. https://doi.org/10.1016/j.ijhydene.2017.12.084.

[104] Toklu E, Coskun Avci A, Kaygusuz K, Gur M. A research on hydrogen production from industrial waste heat by thermal water splitting. Int J Hydrogen Energy 2016;41:10071–9. https://doi.org/10.1016/j.ijhydene.2015.12.131.

[105] Hu L, Lindbergh G, Lagergren C. Operating the nickel electrode with hydrogen-lean gases in the molten carbonate electrolysis cell (MCEC). Int J Hydrogen Energy 2016;41:18692–8. https://doi.org/10.1016/j.ijhydene.2016.06.037.

[106] Vincent I, Kruger A, Bessarabov D. Development of efficient membrane electrode assembly for low cost hydrogen production by anion exchange membrane electrolysis. Int J Hydrogen Energy 2017;42:10752–61. https://doi.org/10.1016/j.ijhydene.2017.03.069.

[107] Abuşoğlu A, Demir S, Özahi E. Energy and economic analyses of models developed for sustainable hydrogen production from biogas-based electricity and sewage sludge. Int J Hydrogen Energy 2016;41:13426–35. https://doi.org/10.1016/j.ijhydene.2016.05.105.

[108] Mostafavi E, Mahinpey N, Rahman M, Sedghkerdar MH, Gupta R. High-purity hydrogen production from ash-free coal by catalytic steam gasification integrated with dry-sorption CO2 capture. Fuel 2016;178:272–82. https://doi.org/10.1016/j.fuel.2016.03.026.

[109] Tian T, Li Q, He R, Tan Z, Zhang Y. Effects of biochemical composition on hydrogen production by biomass gasification. Int J Hydrogen Energy 2017;42:19723–32. https://doi.org/10.1016/j.ijhydene.2017.06.174.

[110] Chen J, Xu W, Zhang F, Zuo H, E J, Wei K, et al. Thermodynamic and environmental analysis of integrated supercritical water gasification of coal for power and hydrogen production. Energy Convers Manag 2019;198:111927. https://doi.org/10.1016/j.enconman.2019.111927.

[111] Ibrahimoglu B, Yilmazoglu MZ. Numerical modeling of a downdraft plasma coal gasifier with plasma reactions. Int J Hydrogen Energy 2020;45:3532–48. https://doi.org/10.1016/j.ijhydene.2018.12.198.

[112] Favas J, Monteiro E, Rouboa A. Hydrogen production using plasma gasification with steam injection. Int J Hydrogen Energy 2017;42:10997–1005. https://doi.org/10.1016/j.ijhydene.2017.03.109.

[113] Verma A, Kumar A. Life cycle assessment of hydrogen production from underground coal gasification. Appl Energy 2015;147:556–68. https://doi.org/10.1016/j.apenergy.2015.03.009.

[114] Pallozzi V, Di Carlo A, Bocci E, Villarini M, Foscolo PU, Carlini M. Performance evaluation at different process parameters of an innovative prototype of biomass gasification system aimed to hydrogen production. Energy Convers Manag 2016;130:34–43. https://doi.org/10.1016/j.enconman.2016.10.039.

[115] Salkuyeh YK, Saville BA, MacLean HL. Techno-economic analysis and life cycle assessment of hydrogen production from different biomass gasification processes. Int J Hydrogen Energy 2018;43:9514–28. https://doi.org/10.1016/j.ijhydene.2018.04.024.

[116] Li B, Yang H, Wei L, Shao J, Wang X, Chen H. Hydrogen production from agricultural biomass wastes gasification in a fluidized bed with calcium oxide enhancing. Int J Hydrogen Energy 2017;42:4832–9. https://doi.org/10.1016/j.ijhydene.2017.01.138.

[117] Shayan E, Zare V, Mirzaee I. Hydrogen production from biomass gasification; a theoretical comparison of using different gasification agents. Energy Convers Manag 2018;159:30–41. https://doi.org/10.1016/j.enconman.2017.12.096.

[118] Kocer A, Yaka IF, Gungor A. Evaluation of greenhouse residues gasification performance in hydrogen production. Int J Hydrogen Energy 2017;42:23244–9. https://doi.org/10.1016/j.ijhydene.2017.05.110.

[119] Chutichai B, Patcharavorachot Y, Assabumrungrat S, Arpornwichanop A. Parametric analysis of a circulating fluidized bed biomass gasifier for hydrogen production. Energy 2015;82:406–13. https://doi.org/10.1016/j.energy.2015.01.051.

[120] Cao W, Guo L, Yan X, Zhang D, Yao X. Assessment of sugarcane bagasse gasification in supercritical water for hydrogen production. Int J Hydrogen Energy 2018;43:13711–9. https://doi.org/10.1016/j.ijhydene.2017.12.013.

[121] Jin H, Guo L, Guo J, Ge Z, Cao C, Lu Y. Study on gasification kinetics of hydrogen production from lignite in supercritical water. Int J Hydrogen Energy 2015;40:7523–9. https://doi.org/10.1016/j.ijhydene.2014.12.095.

[122] Sivasangar S, Zainal Z, Salmiaton A, Taufiq-Yap YH. Supercritical water gasification of empty fruit bunches from oil palm for hydrogen production. Fuel 2015;143:563–9. https://doi.org/10.1016/j.fuel.2014.11.073.

[123] Liao B, Guo LJ. Concentrating Solar Thermochemical Hydrogen Production by Biomass Gasification in Supercritical Water. Energy Procedia 2015;69:444–50. https://doi.org/10.1016/j.egypro.2015.03.051.

[124] Blom PWE, Basson GW. Non-catalytic plasma-arc reforming of natural gas with carbon dioxide as the oxidizing agent for the production of synthesis gas or hydrogen. Int J Hydrogen Energy 2013;38:5684–92. https://doi.org/10.1016/j.ijhydene.2013.03.042.

[125] Punčochář M, Ruj B, Chatterjee PK. Development of process for disposal of plastic waste using plasma pyrolysis technology and option for energy recovery. Procedia Eng 2012;42:420–30. https://doi.org/10.1016/j.proeng.2012.07.433.

[126] Putra AEE, Amaliyah N, Nomura S, Rahim I. Plasma generation for hydrogen production from banana waste. Biomass Convers Biorefin 2020:3–8. https://doi.org/10.1007/s13399-020-00765-3.

[127] Ulejczyk B, Nogal Ł, Młotek M, Krawczyk K. Hydrogen production from ethanol using dielectric barrier discharge. Energy 2019;174:261–8. https://doi.org/10.1016/j.energy.2019.02.180.

[128] Hayakawa Y, Miura T, Shizuya K, Wakazono S, Tokunaga K, Kambara S. Hydrogen production system combined with a catalytic reactor and a plasma membrane reactor from ammonia. Int J Hydrogen Energy 2019;44:9987–93. https://doi.org/10.1016/j.ijhydene.2018.12.141.

[129] Hayakawa Y, Kambara S, Miura T. Hydrogen production from ammonia by the plasma membrane reactor. Int J Hydrogen Energy 2020;45:32082–8. https://doi.org/10.1016/j.ijhydene.2020.08.178.

[130] Song L, Kong Y, Li X. Hydrogen production from partial oxidation of methane over dielectric barrier discharge plasma and NiO/Γ-Al2O3 catalyst. Int J Hydrogen Energy 2017;42:19869–76. https://doi.org/10.1016/j.ijhydene.2017.06.008.

[131] El-Shafie M, Kambara S, Hayakawa Y, Miura T. "Preliminary results of hydrogen production from water vapor decomposition using DBD plasma in a PMCR reactor." Int J Hydrogen Energy 2019;44:20239–48. https://doi.org/10.1016/j.ijhydene.2019.05.199.

[132] Zhang X, Wenren Y, Chen J, Zhang L, Jin Y, Liu Z, et al. Partial oxidation of n-pentane to syngas and oxygenates in a dielectric barrier discharge reactor. Fuel 2022;307. https://doi.org/10.1016/j.fuel.2021.121814.

[133] Shareei M, Taghvaei H, Azimi A, Shahbazi A, Mirzaei M. Catalytic DBD plasma reactor for low temperature partial oxidation of methane: Maximization of synthesis gas and minimization of CO2. Int J Hydrogen Energy 2019;44:31873–83. https://doi.org/10.1016/j.ijhydene.2019.10.120.

[134] Kim SC, Chun YN. Development of a gliding arc plasma reactor for CO 2 destruction. Environmental Technology (United Kingdom) 2014;35:2940–6. https://doi.org/10.1080/09593330.2014.925979.

[135] Wang B, Peng Y, Yao S. Oxidative reforming of n-heptane in gliding arc plasma reformer for hydrogen production. Int J Hydrogen Energy 2019;44:22831–40. https://doi.org/10.1016/j.ijhydene.2019.07.042.

[136] Baowei W, Shize L, Yeping P, Chengyu W. Gliding arc plasma reforming of toluene for on-board hydrogen production. Int J Hydrogen Energy 2020;45:6138–47. https://doi.org/10.1016/j.ijhydene.2019.12.184.

[137] Lian HY, Liu JL, Li XS, Zhu AM. Disclosure of water roles in gliding arc plasma reforming of methanol for hydrogen production. Plasma Processes and Polymers 2020;17. https://doi.org/10.1002/ppap.202000069.

[138] Song L, Liang T, Liu C, Li X. Experimental investigation of hydrogen production by CH4–CO2 reforming using rotating gliding arc discharge plasma. Int J Hydrogen Energy 2019;44:29450–9. https://doi.org/10.1016/j.ijhydene.2019.05.245.

[139] Wang B, Liu S, Peng Y, Wang C, Zou J. Heptane dry reforming and coupling with partial oxidation in gliding arc discharge plasma for H2 production. Fuel Processing Technology 2021;221:106943. https://doi.org/10.1016/j.fuproc.2021.106943.

[140] Liu S, Wang B, Cheng Y, Wang C, Zou J. Ethanol partial oxidative reforming in gliding arc discharge plasma: A better understanding by a kinetic model study. Fuel 2022;328. https://doi.org/10.1016/j.fuel.2022.125309.

[141] Czylkowski D, Hrycak B, Jasiński M, Dors M, Mizeraczyk J. Hydrogen production by direct injection of ethanol microdroplets into nitrogen microwave plasma flame. Int J Hydrogen Energy 2018;3:21196–208. https://doi.org/10.1016/j.ijhydene.2018.09.143.

[142] Czylkowski D, Hrycak B, Jasiński M, Dors M, Mizeraczyk J. Hydrogen production by conversion of ethanol injected into a microwave plasma. European Physical Journal D 2017;71. https://doi.org/10.1140/epjd/e2017-80566-x.

[143] Sun B, Zhao X, Xin Y, Zhu X. Large capacity hydrogen production by microwave discharge plasma in liquid fuels ethanol. Int J Hydrogen Energy 2017;42:24047–54. https://doi.org/10.1016/j.ijhydene.2017.08.052.

[144] Hrycak B, Czylkowski D, Jasiński M, Dors M, Mizeraczyk J. Hydrogen Production via Synthetic Biogas Reforming in Atmospheric-Pressure Microwave (915 MHz) Plasma at High Gas-Flow Output. Plasma Chemistry and Plasma Processing 2019;39:695–711. https://doi.org/10.1007/s11090-019-09962-z.

[145] Zhu T, Sun B, Zhu X, Wang L, Xin Y, Liu J. Mechanism analysis of hydrogen production by microwave discharge in ethanol liquid. J Anal Appl Pyrolysis 2021;156:105111. https://doi.org/10.1016/j.jaap.2021.105111.

[146] Zhu T, Liu J, Xin Y, Zhu X, Sun B. Hydrogen production by microwave discharge in liquid: Study on the characteristics effect of suspended electrode. J Anal Appl Pyrolysis 2022;164:105529. https://doi.org/10.1016/j.jaap.2022.105529.

[147] Akande O, Lee B. Plasma steam methane reforming (PSMR) using a microwave torch for commercial-scale distributed hydrogen production. Int J Hydrogen Energy 2022;47:2874–84. https://doi.org/10.1016/j.ijhydene.2021.10.258.

[148] Lee H, Park YK. Hydrogen production from a solution plasma process of bio-oil. Int J Hydrogen Energy 2020;45:20210–5. https://doi.org/10.1016/j.ijhydene.2019.11.185.

[149] Xin Y, Sun B, Zhu X, Yan Z, Sun X. Hydrogen-rich syngas production by liquid phase pulsed electrodeless discharge. Energy 2021;214:118902. https://doi.org/10.1016/j.energy.2020.118902.

[150] Ghanbari M, Binazadeh M, Zafarnak S, Taghvaei H, Rahimpour MR. Hydrogen production via catalytic pulsed plasma conversion of methane: Effect of Ni–K2O/Al2O3 loading, applied voltage, and argon flow rate. Int J Hydrogen Energy 2020;45:13899–910. https://doi.org/10.1016/j.ijhydene.2020.03.099.

[151] Chung KH, Jeong S, Kim BJ, An KH, Park YK, Jung SC. Enhancement of photocatalytic hydrogen production by liquid phase plasma irradiation on metal-loaded TiO2/carbon nanofiber photocatalysts. Int J Hydrogen Energy 2018;43:11422–9. https://doi.org/10.1016/j.ijhydene.2018.03.190.

[152] King B, Patel D, Zhu Chen J, Drapanauskaite D, Handler R, Nozaki T, et al. Comprehensive process and environmental impact analysis of integrated DBD plasma steam methane reforming. Fuel 2021;304. https://doi.org/10.1016/j.fuel.2021.121328.

[153] Piavis W, Turn S. An experimental investigation of reverse vortex flow plasma reforming of methane. Int J Hydrogen Energy 2012;37:17078–92. https://doi.org/10.1016/j.ijhydene.2012.08.126.

[154] Baowei W, Shize L, Yeping P, Chengyu W. Gliding arc plasma reforming of toluene for on-board hydrogen production. Int J Hydrogen Energy 2020;45:6138–47. https://doi.org/10.1016/j.ijhydene.2019.12.184.

[155] Ma Y, Harding JD, Tu X. Catalyst-free low temperature conversion of n-dodecane for co-generation of COx-free hydrogen and C2 hydrocarbons using a gliding arc plasma. Int J Hydrogen Energy 2019;44:26158–68. https://doi.org/10.1016/j.ijhydene.2019.08.067.

[156] Wang Q, Wang J, Zhu T, Zhu X, Sun B. Characteristics of methane wet reforming driven by microwave plasma in liquid phase for hydrogen production. Int J Hydrogen Energy 2021;46:34105–15. https://doi.org/10.1016/j.ijhydene.2021.08.006.

[157] Ogungbesan B, Kumar R, Su L, Sassi M. Experimental validation of local thermal equilibrium in a MW plasma torch for hydrogen production. Int J Hydrogen Energy 2013;38:15210–8. https://doi.org/10.1016/j.ijhydene.2013.09.099.

[158] Xin Y, Sun B, Liu J, Wang Q, Zhu X, Yan Z. Effects of electrode configurations, solution pH, TiO2 addition on hydrogen production by in-liquid discharge plasma. Renew Energy 2021;171:728–34. https://doi.org/10.1016/j.renene.2021.02.150.

[159] Kumar R, Subramanian KA. Enhancement of efficiency and power output of hydrogen fuelled proton exchange membrane (PEM) fuel cell using oxygen enriched air. Int J Hydrogen Energy 2023;48:6067–75. https://doi.org/10.1016/j.ijhydene.2022.11.141.

[160] Tang X, Zhang Y, Xu S. Temperature sensitivity characteristics of PEM fuel cell and output performance improvement based on optimal active temperature control. Int J Heat Mass Transf 2023;206:123966. https://doi.org/10.1016/j.ijheatmasstransfer.2023.123966.

[161] Wang M, Ding Y, Hu J, Xu L, Yang X. Numerical simulation of water and heat transport in the cathode channel of a PEM fuel cell. Int J Hydrogen Energy 2022;47:11007–27. https://doi.org/10.1016/j.ijhydene.2022.01.143.

[162] Eslami N, Ranjbar AA, Rahimi-Esbo M, Rahgoshay SM. Experimental Analysis of Large Active Area Polymer Electrolyte Membrane Fuel Cell Stack for Determining Optimal Operating Conditions. Arab J Sci Eng 2023;48:11873–98. https://doi.org/10.1007/s13369-023-07603-4.

[163] Yang Y, Jia H, Liu Z, Bai N, Zhang X, Cao T, et al. Overall and local effects of operating parameters on water management and performance of open-cathode PEM fuel cells. Appl Energy 2022;315:118978. https://doi.org/10.1016/j.apenergy.2022.118978.

[164] Dhimish M, Vieira RG, Badran G. Investigating the stability and degradation of hydrogen PEM fuel cell. Int J Hydrogen Energy 2021;46:37017–28. https://doi.org/10.1016/j.ijhydene.2021.08.183.

[165] Al-Anazi A, Wilberforce T, Khatib FN, Vichare P, Olabi AG. Performance evaluation of an air breathing polymer electrolyte membrane (PEM) fuel cell in harsh environments – A case study under Saudi Arabia's ambient condition. Int J Hydrogen Energy 2021;46:23463–79. https://doi.org/10.1016/j.ijhydene.2020.10.258.

[166] Carcadea E, Varlam M, Ismail M, Ingham DB, Marinoiu A, Raceanu M, et al. PEM fuel cell performance improvement through numerical optimization of the parameters of the porous layers. Int J Hydrogen Energy 2020;45:7968–80. https://doi.org/10.1016/j.ijhydene.2019.08.219.

[167] Uzun A, Bokor B, Eryener D. PEM fuel cell performance with solar air preheating. Int J Hydrogen Energy 2020;45:34654–65. https://doi.org/10.1016/j.ijhydene.2020.01.129.

[168] Omran A, Lucchesi A, Smith D, Alaswad A, Amiri A, Wilberforce T, et al. Mathematical model of a proton-exchange membrane (PEM) fuel cell. International Journal of Thermofluids 2021;11. https://doi.org/10.1016/j.ijft.2021.100110.

[169] Ratlamwala TAH, El-Sinawi AH, Gadalla MA, Aidan A. Performance analysis of a new designed PEM fuel cell. Int J Energy Res 2012;36:1121–32. https://doi.org/10.1002/er.1877.

[170] Meng X, Ren H, Yang X, Tao T, Shao Z. Experimental study of key operating parameters effects on the characteristics of proton exchange membrane fuel cell with anode recirculation. Energy Convers Manag 2022;256:115394. https://doi.org/10.1016/j.enconman.2022.115394.

[171] Shateri M, Torabi F. Influence of liquid water accumulation on the impedance of a PEM fuel cell operating in dead end mode: Physical modeling and experimental validation. Electrochim Acta 2023;443:141940. https://doi.org/10.1016/j.electacta.2023.141940.

[172] Chinannai MF, Lee J, Ju H. Study of the characteristics of temperature rise and coolant flow rate control during malfunction of PEM fuel cells. Int J Hydrogen Energy 2021;46:11160–75. https://doi.org/10.1016/j.ijhydene.2020.04.221.

[173] Tao J, Wei X, Ming P, Wang X, Jiang S, Dai H. Order reduction, simplification and parameters identification for cold start model of PEM fuel cell. Energy Convers Manag 2022;274. https://doi.org/10.1016/j.enconman.2022.116465.

[174] Qu E, Hao X, Xiao M, Han D, Huang S, Huang Z, et al. Proton exchange membranes for high temperature proton exchange membrane fuel cells: Challenges and perspectives. J Power Sources 2022;533:231386. https://doi.org/10.1016/j.jpowsour.2022.231386.

[175] Kulikovsky A. Performance of a PEM fuel cell with oscillating air flow velocity: A modeling study based on cell impedance. ETransportation 2021;7:100104. https://doi.org/10.1016/j.etran.2021.100104.

[176] Taner T. The novel and innovative design with using H2 fuel of PEM fuel cell: Efficiency of thermodynamic analyze. Fuel 2021;302:121109. https://doi.org/10.1016/j.fuel.2021.121109.

[177] Baharlou Houreh N, Ghaedamini M, Shokouhmand H, Afshari E, Ahmaditaba AH. Experimental study on performance of membrane humidifiers with different configurations and operating conditions for PEM fuel cells. Int J Hydrogen Energy 2020;45:4841–59. https://doi.org/10.1016/j.ijhydene.2019.12.017.

[178] Strahl S, Husar A, Puleston P, Riera J. Performance improvement by temperature control of an open-cathode PEM fuel cell system. Fuel Cells, vol. 14, John Wiley and Sons Ltd; 2014, p. 466–78. https://doi.org/10.1002/fuce.201300211.

[179] Chugh S, Meenakshi S, Sonkar K, Sharma A, Kapur GS, Ramakumar SSV. Performance evaluation of PEM fuel cell stack on hydrogen produced in the oil refinery. Int J Hydrogen Energy 2020;45:5491–500. https://doi.org/10.1016/j.ijhydene.2019.06.160.

[180] Mubin ANA, Bahrom MH, Azri M, Ibrahim Z, Rahim NA, Raihan SRS. Analysis performance of proton exchange membrane fuel cell (PEMFC). IOP Conf Ser Mater Sci Eng 2017;210:012052. https://doi.org/10.1088/1757-899X/210/1/012052.

[181] Zhao J, Shi R, Li Z, Zhou C, Zhang T. How to make use of methanol in green catalytic hydrogen production? Nano Select 2020;1:12–29. https://doi.org/10.1002/nano.202000010.

[182] Shen Q, Cai Z, Chen G, Zhang X, Li S, Yang G. Optimization of the sol gel synthesis process parameters by orthogonal experiment of novel spinel oxide catalyst CuFe1.2Al0.8O4 with improved performance for methanol steam reforming. J Solgel Sci Technol 2023;107:490–502. https://doi.org/10.1007/s10971-023-06136-4.

[183] Awasthi MK, Rai RK, Behrens S, Singh SK. Low-temperature hydrogen production from methanol over a ruthenium catalyst in water. Catal Sci Technol 2021;11:136–42. https://doi.org/10.1039/D0CY01470B.

[184] COP26 SUSTAINABILITY REPORT. https://unfccc.int/sites/default/files/resource/COP26-Sustainability-Report_Final.pdf (accessed November 12, 2023)

[185] COP27 OFFICIAL SUSTAINABILITY REPORT. https://unfccc.int/sites/default/files/resource/cop27_sustainability_report.pdf (accessed December 11, 2023).

[186] COP28 SUSTAINABILITY REPORT. https://researchbriefings.files.parliament.uk/documents/CBP-9884/CBP-9884.pdf (accessed February 9, 2024).

[187] Wu Q, Wang Y, Zhou H, Qiu X, Mei D. Measurement of reaction temperature distribution inside of methanol steam reforming microreactor using infrared thermography. Appl Therm Eng 2024;238:121909. https://doi.org/10.1016/j.applthermaleng.2023.121909.

[188] Ranjekar AM, Yadav GD. Steam Reforming of Methanol for Hydrogen Production: A Critical Analysis of Catalysis, Processes, and Scope. Ind Eng Chem Res 2021;60:89–113. https://doi.org/10.1021/acs.iecr.0c05041.

[189] Bepari S, Khan M, Li X, Mohammad N, Kuila D. Effect of Ce and Zn on Cu-Based Mesoporous Carbon Catalyst for Methanol Steam Reforming. Top Catal 2023;66:375–92. https://doi.org/10.1007/s11244-022-01772-6.

[190] Pinzari F. The effect of nanocrystalline TiO2 on structure and catalytic activity of CuO–ZnO in combined methanol reforming. Reaction Kinetics, Mechanisms and Catalysis 2023;136:367–79. https://doi.org/10.1007/s11144-023-02357-4.

[191] Jin Q, Meng X, Wu P, Li Y, Xu M, Zhou R, et al. Methanol steam reforming for hydrogen production over NiTiO $_3$ nanocatalyst with hierarchical porous structure. RSC Adv 2023;13:16342–51. https://doi.org/10.1039/D3RA02891G.

[192] Mironova EY, Payen-Lytkina AA, Ermilova MM, Orekhova N V., Zhilyaeva NA, Efimov MN, et al. Methanol Steam Reforming on Metal–Carbon Catalysts Having Different Carbon Supports. Inorganic Materials 2023;59:729–35. https://doi.org/10.1134/S0020168523070117.

[193] Hafeez S, Aristodemou E, Manos G, Al-Salem SM, Constantinou A. Modelling of packed bed and coated wall microreactors for methanol steam reforming for hydrogen production. RSC Adv 2020;10:41680–92. https://doi.org/10.1039/d0ra06834a.

[194] Budhraja N, Pal A, Mishra RS. Modeling and analysis for enhanced hydrogen production in process simulation of methanol reforming. Energy Sources, Part A: Recovery, Utilization, and Environmental Effects 2023;45:11553–65. https://doi.org/10.1080/15567036.2023.2262414.

[195] Budhraja N, Pal A, Mishra RS. Optimizing Methanol Reforming Parameters for Enhanced Hydrogen Selectivity in an Aspen Hysys Simulator using Response Surface Methodology. Energy Technology 2023;11. https://doi.org/10.1002/ente.202300203.

[196] Chen Z, Yin B, Wei Z, Dong F. Coupling of high-temperature proton exchange membrane fuel cells with methanol steam reforming: Modeling and simulation for an integrated coupled for power generation system. Energy Convers Manag 2024;301:118044. https://doi.org/10.1016/j.enconman.2023.118044.

[197] Zhao K, Kong H, Tan S, Yang X-G, Zheng H, Yang T, et al. Analysis of a hybrid system combining solar-assisted methanol reforming and fuel cell power generation. Energy Convers Manag 2023;297:117664. https://doi.org/10.1016/j.enconman.2023.117664.

[198] Wang F, Wang G. Performance and cold spot effect of methanol steam reforming for hydrogen production in micro-reactor. Int J Hydrogen Energy 2016;41:16835–41. https://doi.org/10.1016/j.ijhydene.2016.07.083.

[199] Kudo T, Sekiguchi K, Sankoda K, Namiki N, Nii S. Effect of ultrasonic frequency on size distributions of nanosized mist generated by ultrasonic atomization. Ultrason Sonochem 2017;37:16–22. https://doi.org/10.1016/j.ultsonch.2016.12.019.

[200] Budhraja N, Pal A, Mishra RS. Simulation and Optimization of Biohydrogen Production from Biomass Feed via Anaerobic Digestion. Chem Eng Technol 2024;47:706–15. https://doi.org/10.1002/ceat.202300395.

[201] Budhraja N. Simulation and optimization for biohydrogen production potential of various organic waste via anaerobic digestion. Fuel 2024;360:130563. https://doi.org/10.1016/j.fuel.2023.130563.

[202] Budhraja N, Pal A, Mishra RS. Parameter optimization for enhanced biodiesel yield from Linum usitatissimum oil through solar energy assistance. Biomass Convers Biorefin 2022. https://doi.org/10.1007/s13399-022-03649-w.

[203] Yin L, Ju Y. Process optimization and analysis of a novel hydrogen liquefaction cycle. International Journal of Refrigeration 2020;110:219–30. https://doi.org/10.1016/j.ijrefrig.2019.11.004.

[204] Phan TS, Pham Minh D, Espitalier F, Nzihou A, Grouset D. Hydrogen production from biogas: Process optimization using ASPEN Plus®. Int J Hydrogen Energy 2022. https://doi.org/10.1016/j.ijhydene.2022.01.100.

[205] Motazedi K, Salkuyeh YK, Laurenzi IJ, MacLean HL, Bergerson JA. Economic and environmental competitiveness of high temperature electrolysis for hydrogen production. Int J Hydrogen Energy 2021;46:21274–88. https://doi.org/10.1016/j.ijhydene.2021.03.226.

[206] Chen LN, Hou KP, Liu YS, Qi ZY, Zheng Q, Lu YH, et al. Efficient Hydrogen Production from Methanol Using a Single-Site Pt1/CeO2 Catalyst. J Am Chem Soc 2019;141:17995–9. https://doi.org/10.1021/jacs.9b09431.

[207] Dang C, Li H, Yang G, Cao Y, Wang H, Peng F, et al. High-purity hydrogen production by sorption-enhanced steam reforming of iso -octane over a Pd-promoted Ni-Ca-Al-O bi-functional catalyst. Fuel 2021;293:120430. https://doi.org/10.1016/j.fuel.2021.120430.

[208] Hosseini Abbandanak M, Taghizadeh M, Fallah N. High-purity hydrogen production by sorption-enhanced methanol steam reforming over a combination of Cu–Zn–CeO2–ZrO2/MCM-41 catalyst and (Li–Na–K) NO3·MgO adsorbent. Int J Hydrogen Energy 2021;46:7099–112. https://doi.org/10.1016/j.ijhydene.2020.11.250.

[209] Qingli X, Zhengdong Z, Kai H, Shanzhi X. Ni supported on MgO modified attapulgite as catalysts for hydrogen production from glycerol steam reforming. Int J Hydrogen Energy 2021;46:27380–93. https://doi.org/10.1016/j.ijhydene.2021.06.028.

[210] Shen Y, Zhan Y, Li S, Ning F, Du Y, Huang Y, et al. Hydrogen generation from methanol at near-room temperature. Chem Sci 2017;8:7498–504. https://doi.org/10.1039/c7sc01778b.

[211] Khouya A. Hydrogen production costs of a polymer electrolyte membrane electrolysis powered by a renewable hybrid system. Int J Hydrogen Energy 2021;46:14005–23. https://doi.org/10.1016/j.ijhydene.2021.01.213.

[212] El Hajj Chehade AM, Daher EA, Assaf JC, Riachi B, Hamd W. Simulation and optimization of hydrogen production by steam reforming of natural gas for refining and petrochemical demands in Lebanon. Int J Hydrogen Energy 2020;45:33235–47. https://doi.org/10.1016/j.ijhydene.2020.09.077.

[213] Dai M. In situ mathematically simulation for CO2 internal corrosion in wet natural gas gathering pipelines system by HYSYS. Eng Fail Anal 2021;122. https://doi.org/10.1016/j.engfailanal.2021.105265.

[214] Azad AK, Rasul MG, Khan MMK, Mondal SK, Islam R. Modeling and Simulation of Heat and Mass Flow by ASPEN HYSYS for Petroleum Refining Process in Field Application. Thermofluid Modeling for Energy Efficiency Applications, Elsevier Inc.; 2016, p. 227–57. https://doi.org/10.1016/B978-0-12-802397-6.00010-5.

[215] Zhao A, Ying W, Zhang H, Ma H, Fang D. Ni-Al 2O 3 catalysts prepared by solution combustion method for syngas methanation. Catal Commun 2012;17:34–8. https://doi.org/10.1016/j.catcom.2011.10.010.

[216] Kombe EY, Lang'at N, Njogu P, Malessa R, Weber CT, Njoka F, et al. Process modeling and evaluation of optimal operating conditions for production of hydrogen-rich syngas from air gasification of rice husks using aspen plus and response surface methodology. Bioresour Technol 2022;361. https://doi.org/10.1016/j.biortech.2022.127734.

[217] Kim DH, Kim JH, Jang YS, Kim JC. Hydrogen production by oxidative steam reforming of methanol over anodic aluminum oxide-supported Cu-Zn catalyst. Int J Hydrogen Energy 2019;44:9873–82. https://doi.org/10.1016/j.ijhydene.2018.11.009.

[218] Liu X, Men Y, Wang J, He R, Wang Y. Remarkable support effect on the reactivity of Pt/In2O3/MOx catalysts for methanol steam reforming. J Power Sources 2017;364:341–50. https://doi.org/10.1016/j.jpowsour.2017.08.043.

[219] Zaccara A, Petrucciani A, Matino I, Branca TA, Dettori S, Iannino V, et al. Renewable hydrogen production processes for the off-gas valorization in integrated steelworks through hydrogen intensified methane and methanol syntheses. Metals (Basel) 2020;10:1–24. https://doi.org/10.3390/met10111535.

[220] Pashchenko D. Thermochemical waste-heat recuperation as on-board hydrogen production technology. Int J Hydrogen Energy 2021;46:28961–8. https://doi.org/10.1016/j.ijhydene.2020.11.108.

[221] Hakandai C, Sidik Pramono H, Aziz M. Conversion of municipal solid waste to hydrogen and its storage to methanol. Sustainable Energy Technologies and Assessments 2022;51. https://doi.org/10.1016/j.seta.2022.101968.

[222] Giwa SO, Giwa A, Giwa O. Application of Aspen Plus to Hydrogen Production from Alcohols by Steam Reforming: Effects of Reactor Temperature. International Journal of Engineering Research & Technology 2013;2:648–57.

[223] Kulprathipanja A, Falconer JL. Partial oxidation of methanol for hydrogen production using ITO/Al 2O3 nanoparticle catalysts. Appl Catal A Gen 2004;261:77–86. https://doi.org/10.1016/j.apcata.2003.10.034.

[224] Araiza DG, Gómez-Cortés A, Díaz G. Partial oxidation of methanol over copper supported on nanoshaped ceria for hydrogen production. Catal Today 2017;282:185–94. https://doi.org/10.1016/j.cattod.2016.06.055.

[225] Ou TC, Chang FW, Roselin LS. Production of hydrogen via partial oxidation of methanol over bimetallic Au-Cu/TiO2 catalysts. J Mol Catal A Chem 2008;293:8–16. https://doi.org/10.1016/j.molcata.2008.06.017.

[226] Chang FW, Ou TC, Roselin LS, Chen WS, Lai SC, Wu HM. Production of hydrogen by partial oxidation of methanol over bimetallic Au-Cu/TiO2-Fe2O3 catalysts. J Mol Catal A Chem 2009;313:55–64. https://doi.org/10.1016/j.molcata.2009.08.002.

[227] Karimi MB, Mohammadi F, Hooshyari K. Recent approaches to improve Nafion performance for fuel cell applications: A review. Int J Hydrogen Energy 2019;44:28919–38. https://doi.org/10.1016/j.ijhydene.2019.09.096.

[228] Manso AP, Marzo FF, Barranco J, Garikano X, Garmendia Mujika M. Influence of geometric parameters of the flow fields on the performance of a PEM fuel cell. A review. Int J Hydrogen Energy 2012;37:15256–87. https://doi.org/10.1016/j.ijhydene.2012.07.076.

[229] Escobar-Yonoff R, Maestre-Cambronel D, Charry S, Rincón-Montenegro A, Portnoy I. Performance assessment and economic perspectives of integrated PEM fuel cell and PEM electrolyzer for electric power generation. Heliyon 2021;7:e06506. https://doi.org/10.1016/j.heliyon.2021.e06506.

LIST OF PUBLICATIONS

1) *N. Budhraja*, A. Pal, R. S. Mishra*. Plasma reforming for hydrogen production: Pathways, reactors and storage. **International Journal of Hydrogen Energy** (Elsevier); 2023. (**SCIE, IF- 8.1**).

2) *N. Budhraja*, A. Pal, R. S. Mishra*. Parameter optimization for enhanced biodiesel yield from Linum usitatissimum oil through solar energy assistance. **Biomass Conversion and Biorefinery** (Springer); 2022. (**SCIE, IF- 3.5**).

3) *N. Budhraja*, A. Pal, R. S. Mishra.* Optimizing Methanol Reforming Parameters for Enhanced Hydrogen Selectivity in an Aspen Hysys Simulator using Response Surface Methodology. **Energy Technology** (Wiley); 2023. (**SCIE, IF- 3.6**).

4) *N. Budhraja*.* Simulation and optimization for biohydrogen production potential of various organic waste via anaerobic digestion. **Fuel** (Elsevier); 2024. (**SCIE, IF- 6.7**).

5) *N. Budhraja*, A. Pal, R. S. Mishra*. Modeling and analysis for enhanced hydrogen production in process simulation of methanol reforming. **Energy Sources, Part A: Recovery, Utilization, and Environmental Effects** (Taylor & Francis); 2023. (**SCIE, IF- 2.9**).

6) *N. Budhraja*, A. Pal, R. S. Mishra*. Simulation and Optimization for BioHydrogen Production from Biomass Feed via Anaerobic Digestion. **Chemical Engineering & Technology** (Wiley); 2024. (**SCIE, IF- 1.8**).

7) *N. Budhraja*, A. Pal, R. S. Mishra*. Experimental Analysis of Hydrogen Production from Atomized Water-Methanol Mixture through High-Voltage Plasma Reforming. *Under-Review.*

8) *N. Budhraja*, A. Pal, R. S. Mishra*. Vortex Flow Plasma Reforming for Hydrogen Production from Atomized Water-Methanol Mixture and Parameter Optimization using RSM and ANN-GA. *Under-Review.*

9) *N. Budhraja*, A. Pal, R. S. Mishra*. Experimental Analysis of Hydrogen Generated through Plasma Reforming in a PEM Fuel Cell. *Under-Review.*

10) *N. Budhraja*, A. Pal, R. S. Mishra*. Various treatment methods for enhanced bio-hydrogen production. **Materials Today: Proceedings** (Elsevier); 2023. (**Scopus**).

11) *N. Budhraja*, R. S. Mishra*. Optimized biodiesel yield in a hydrodynamic cavitation reactor using response surface methodology. **Advances in Energy Research** (Techno Press); 2022. (**ESCI, WoS**).

12) *S. Lalhriatpuia, N. Budhraja*, K. Pal*. Optimization of Liquid Metal Nanocomposites and Biogas Addition Rate Using ANN-GA. **Journal of Polymer & Composites** (STM Journals); 2023. (**ESCI, WoS**).

Papers presented in Conferences

1) *"Investigations on Ethanol as the Raw Material for Hydrogen Production, Storage and Applications"* 2nd International Conference on Recent Advances in Mechanical Engineering (**RAME-2020**), September 18-19, Delhi Technological University, Delhi, India.

2) *"Comparative Analysis of the Engine Emissions from CI Engine using Diesel-Biodiesel-Ethanol Blends"* 2nd International Conference on Recent Advances in Mechanical Engineering (**RAME-2020**), September 18-19, Delhi Technological University, Delhi, India.

3) "*Effect of orifice plates in transesterification of fried oil using hydrodynamic cavitation reactor and engine performance with biogas*" International Conference on Energy and Environment (**ICEE-2021**), April 09-10, Jyothi Engineering College, Cheruthuruthy, Thrissur, Kerala, India.

4) *"Various Treatment Methods for Enhanced Bio-Hydrogen Production"* 3rd International Conference on Recent Advances in Materials, Manufacturing and Thermal Engineering (**RAMMTE-2022**), July 8-9, Delhi Technological University, Delhi, India.

5) *"Optimized Biodiesel Yield in a Hydrodynamic Cavitation Reactor using Response Surface Methodology"* 3rd International Conference on Recent Advances in Materials, Manufacturing and Thermal Engineering (**RAMMTE-2022**), July 8-9, Delhi Technological University, Delhi, India.

Book Chapters

1. **Chapter: Investigations on Ethanol as the Raw Material for Hydrogen Production, Storage, and Applications.** Recent Advances in Mechanical Engineering. ISBN 978-981-15-9677-3. pp 317–326.

2. **Chapter: Comparative Analysis of the Engine Emissions from CI Engine Using Diesel–Biodiesel–Ethanol Blends.** Recent Advances in Mechanical Engineering. ISBN 978-981-15-9677-3. pp 363–370.

Patent

1. **Plasma Reformer with Atomizer for Hydrogen Production**, Journal No. 47/2024, Dated 22/11/2024, page no. 109951. ***Published.***

Curriculum Vitae/ Brief Profile

I am *Neeraj Budhraja*, a young and dynamic researcher working in the field of energy and IC engines. I completed my graduation (B. Tech.) in Mechanical and Automotive engineering in 2015 and post-graduation (M. Tech.) in Renewable Energy Technology in 2018 from Delhi Technological University, Delhi. Recently, I completed my PhD thesis on Hydrogen Production and Utilization in Fuel Cells. My key interest areas are Hydrogen energy, Biofuels like biogas and biodiesel, IC engines, and Environmental pollution reduction. I have 6 SCIE research papers in reputed peer-review international journals, 2 ESCI and 1 SCOPUS research article along with 2 Book chapters in LNME (Springer). I have also qualified UGC NET 2017 in Environmental Studies and GATE 2014, 2016, 2019, 2021, 2024 in Mechanical Engineering. I have actively participated and being in the organizing committee of many workshops, seminars, and faculty development programs. I have working knowledge of the softwares like Design Expert, Minitab, Aspen Plus & Hysys, OpenLAC and SimaPro.

Review Article

Plasma reforming for hydrogen production: Pathways, reactors and storage

Neeraj Budhraja[*], Amit Pal, R.S. Mishra

Department of Mechanical Engineering, Delhi Technological University, Delhi, 110042, India

HIGHLIGHTS

- Hydrogen production via the methane reforming pathway is discussed.
- Ethanol decomposes into intermediate species that further splits into •H radical
- Various plasma reforming reactors for H_2 production are discussed.
- Influencing parameters in plasma reforming are identified.
- Various process parameters affecting H_2 production are reviewed.

ARTICLE INFO

ABSTRACT

Hydrogen is an energy carrier with a very high energy density (>119 MJ/kg). Pure hydrogen is barely available; thus, it requires extraction from its compounds. Steam reforming and water electrolysis are commercially viable technologies for hydrogen production from water, alcohols, methane, and other hydrocarbons; however, both processes are energy-intensive. Current study aims at understanding the methane and ethanol-water mixture pathway to generate hydrogen molecules. The various intermediate species (like CH_X, CH_2O, CH_3CHO) are generated before decomposing methane/ethanol into hydrogen radicals, which later combine to form hydrogen molecules. The study further discusses the various operating parameters involved in plasma reforming reactors. All the reactors work on the same principle, generating plasma to excite electrons for collision. The dielectric barrier discharge reactor can be operated with or without a catalyst; however, feed flow rate and discharge power are the most influencing parameters. In a pulsed plasma reactor, feed flow rate, electrode velocity, and gap are the main factors that can raise methane conversion (40—60%). While the gliding arc plasma reactor can generate up to 50% hydrogen yield at optimized values of oxygen/carbon ratio and residence time, the hydrogen yield in the microwave plasma reactor is affected by flow rate and feed concentration. Therefore, all the reactors have the potential to generate hydrogen at lower energy demand.

© 2022 Hydrogen Energy Publications LLC. Published by Elsevier Ltd. All rights reserved.

ORIGINAL ARTICLE

Parameter optimization for enhanced biodiesel yield from *Linum usitatissimum* oil through solar energy assistance

Neeraj Budhraja[1] · Amit Pal[1] · R. S. Mishra[1]

Abstract

Biodiesel is a biofuel produced from vegetable oils and animal fats. The study describes the solar-assisted biodiesel production from linseed oil and the parameter optimization using Taguchi's L_{27} orthogonal approach and response surface methodology (RSM). A solar paraboloid dish of collector area 6.1 m^2 and concentration ratio approx. 200 is used for the transesterification process. Yearly and daily solar radiation data shows that May–June has more extended solar radiation availability during the daytime and are favorable months for experimentation. Results show that Taguchi's approach gives a maximum biodiesel yield of 89.14%, while the RSM model offers a slightly higher 91.9% yield. However, the RSM analysis predicted 91.1% (maximum biodiesel yield) at molar ratio (MR) 8.92:1, reaction time (RT) 108.97 min, and catalyst concentration (CC) 0.61 wt%, respectively. ANOVA analysis found that the MR has the highest percentage contribution of 75.67%, followed by CC (15.9%) and RT (5.69%). Biodiesel composition is determined using gas chromatography and FTIR analysis, and the various other fuel properties are measured as per ASTM testing methods. The study successfully confirms the use of solar heating for the transesterification process.

Keywords Biodiesel · Linseed Oil · Taguchi's method · Solar paraboloid dish · Response surface methodology

Abbreviations

ANOVA	Analysis of variance
ASTM	American Society for Testing and Materials
CC	Catalyst concentration
CCD	Central composite design
CV	Calorific value
FAME	Fatty acid methyl ester
FID	Flame ionization detector
FFA	Free fatty acid
FTIR	Fourier transform infrared
GC	Gas chromatography
KOH	Potassium hydroxide
LSME	Linseed methyl ester
IC	Internal combustion
MR	Molar ratio
min	Minutes
RT	Reaction time
RSM	Response surface methodology
S/N	Signal-to-noise
UV	Ultraviolet
wt%	Weight percentage

✉ Neeraj Budhraja
neeraj_budhraja@yahoo.com

1   Department of Mechanical Engineering, Delhi Technological University, New Delhi- 110042, India

1 Introduction

Energy is essential for every nation to develop infrastructure, industries, transportation, and other basic needs. The energy is mainly extracted from fossil fuels like crude oil and coal. The extensive crude oil usage has become a significant economic problem for countries with lower crude oil reserves [1, 2], leading to higher demand for crude oil internationally. This situation has resulted in higher crude oil prices, thus creating an imbalance in the World's economy; however, it showed no impact on the demand side, which is breaking records year by year. The crude oil burning also adds toxic gases to the air leading to increased annual death rates due to air pollution. These are some reasons behind restricting and minimizing crude oil usage [3, 4]. Therefore, other compatible alternatives for crude oil have been explored for many years; and biodiesel is one such alternative [4–6].

Biodiesel is an alkyl ester produced by the reaction between vegetable oil and alcohol in the presence of a catalyst [7]. Biodiesel has a vast history; however, the higher

Optimizing Methanol Reforming Parameters for Enhanced Hydrogen Selectivity in an Aspen Hysys Simulator using Response Surface Methodology

Neeraj Budhraja, Amit Pal, and Radhey Shyam Mishra*

Hydrogen is the prominent fuel for a nation's industrial and infrastructural development. Hydrogen fuel fulfills the energy requirement and reduces environmental pollution concerns. Hence, every country is looking for efficient and greener hydrogen production technologies. Herein, a simulation model of a methanol-water (as feed) reformer is developed, and the effects of reaction temperature (RT), reactor pressure (RP), and methanol-to-water (*M*-to-W) ratio are investigated. In contrast, the optimal conditions for hydrogen selectivity (HS) and feed conversion percentage (FCP) are determined using response surface methodology. Results show a significant effect of the *M*-to-W molar ratio in the range of 0.9 and 1.35, whereas higher RT has a good affinity for higher HS and FCP. The regression analysis shows R_2 values of 0.9877 and 0.9803 for HC and FCP, which are close to unity. Hence, both experimental (and simulated) and predicted values have better correspondence with each other. In contrast, the optimal HS and FCP of 84.81% and 95.71% are observed at 328 °C RT, 2.6 atm. RP, and 1.34 M-to-W molar ratio, respectively. Therefore, the present simulation and optimization provide results that may help to enhance the hydrogen production percentage in commercialized plants.

1. Introduction

In the last few years, the energy demand has increased at a very rapid pace. However, the Ukraine-Russia conflict worsened the scenario for many nations, especially Europe, and such situations may arise in the near future. Therefore, every country has been looking for domestic and sustainable energy sources that produce no or very few emissions to curb pollution from fossil fuels.[1,2] This way, the aim of sustainable fuel will also be fulfilled. Hydrogen energy is one such source that has the potential to replace most of the current fossil energy sources.[3]

Hydrogen is the lightest element in the periodic table, and hydrogen compounds are available everywhere. However, hydrogen extraction from its compounds is challenging and requires

enormous energy. Only a few technologies have been developed and commercialized for hydrogen production. Chen et al.[4] performed ethanol steam reforming for hydrogen production and achieved a theoretical 73% hydrogen yield. The authors used Ni/Al_2O_3 catalyst to trigger the ethanol steam-reforming reaction. Similarly, Dang et al.[5] used a Pd-promoted Ni–Ca–Al–O bifunctional catalyst and obtained 90% hydrogen yield from iso-octane steam reforming. Abbandanak et al.[6] combined $Cu–Zn–CeO_2–ZrO_2/MCM$-41 catalyst and (Li–Na–K) $NO_3.MgO$ absorbent for methanol steam reforming and obtained 99.8% hydrogen yield. In contrast, Qingli et al.[7] produced hydrogen from glycerol at a glycerol conversion percentage of 94.71%, respectively. Therefore, different feedstocks have the potential to produce hydrogen; however, methanol and water are very commonly used feedstock.

Methanol and water are notable and well-known sources of hydrogen production in various technologies. Methanol and water have more than 10% hydrogen content, and hydrogen extraction requires comparatively less energy than other sources. Awasthi et al.[8] achieved a hydrogen production rate of 49 mol. H_2 per hour from methanol at 130 °C. Similarly, Shen et al.[9] produced hydrogen from methanol at near room temperature through methanol dehydrogenation. In contrast, Khouya[10] used polymer electrolyte membrane electrolysis to produce hydrogen from water. The author obtained significant results and an overall efficiency of 20%. Palhares et al.[11] generated hydrogen at a rate of 2 liters per unit time in a solar-assisted alkaline water electrolyzer. Any process before commercialization requires the simulation of various components. It helps in reducing the cost and achieving the targeted output results.

Modeling and simulation of various components of a chemical plant help determine the impacts of the different process parameters and cost considerations .[12] Ishaq and Dincer[13] designed a biomass and solar energy-based model for hydrogen production, where the overall system efficiency achieved is 29.9%, while the exergy efficiency is 31.5%, respectively. Bassyouni et al.[14] simulated a downdraft gasifier. The authors used date palm waste to produce syngas that contains a hydrogen content of 56.27%, while the other gases are carbon monoxide, carbon dioxide, and methane. Sanchez et al.[15] developed a model for an alkaline

N. Budhraja, A. Pal, R. S. Mishra
Department of Mechanical Engineering
Delhi Technological University
Delhi 110042, India
E-mail: neeraj_budhraja@yahoo.com

ⓘ The ORCID identification number(s) for the author(s) of this article can be found under https://doi.org/10.1002/ente.202300203.
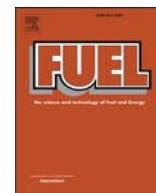
Full Length Article

Simulation and optimization for biohydrogen production potential of various organic waste via anaerobic digestion

Neeraj Budhraja

Department of Mechanical Engineering, Delhi Technological University, Delhi 110042, India

ARTICLE INFO	ABSTRACT
	A simulation model was developed for biohydrogen production from organic feeds such as cow dung (CD), banana stem (BS), and waste paper pulps (WPP). Data from the model was used to generate a design of experiment (DoE) that analysed the data and optimizes the input parameters for optimized biohydrogen yield. Three input parameters taken for optimization were pretreatment temperature (PTT), hydraulic retention time (HRT), and feed-to-water (F/W) ratio. Results showed the optimal sequence of influencing parameters is PTT > HRT > F/W ratio. The optimal value of PTT was 75 °C for all feeds. In contrast, the HRT and F/W ratios were 13.1 days and 0.5 ratio for CD, 16.6 days and 1.5 ratio for BS, and 11.7 days and 1.4 ratio for WPP. At the same time, the optimal biohydrogen yield was 24.59 % (CD), 25.27 % (BS), and 24.21 % (WPP). Therefore, the current simulation and optimization had convincing results in optimizing commercial plants' biohydrogen production.

1. Introduction

Waste disposal has become a tragic problem in developed and developing nations. As the number and volume of urban cities have been increasing rapidly, waste generation is setting new records every day. Scientists and environmentalists have shown that waste is valuable when appropriately utilized [1]. However, the proper utilization has many challenges. The inorganic waste can be reused, recycled, or recovered for secondary products. The lack of awareness made the process very difficult. Similarly, organic waste can generate various biofuels, whether biogas, bioethanol, or biohydrogen [2]. Hydrogen is an energy source that has exceptional properties of the highest energy density by weight and no harmful emissions with burning [3]. Therefore, biohydrogen can solve many problems like waste disposal, energy demand, and cleaner and sustainable development.

All these biofuels were generated through an anaerobic fermentation process, where anaerobic microbes digest organic feeds and break down higher hydrocarbon compounds into smaller hydrocarbons like methane, ethanol, etc. it has been found that several organic feeds were suitable for producing biofuels [4]. However, each feed has different chemical constituents; thus, the quantity and quality of biofuels may vary. *Liu et al.* assessed the crop straw's potential to produce hydrogen in China [5]. The authors found an approximate 4.54 x 10^8 tonne available crop residue within China that could produce 1.31 x 10^{11} m^3 biohydrogen and reduce about 2.42 x 10^8 tonne $CO_{2\text{-eq}}$ greenhouse gas

emissions annually. *Foglia et al.* showed the potential of various waste organic feeds to produce biohydrogen at a feasible energy demand [6]. Similarly, *Xing et al.* studied the feasibility of dairy manure such as cow dung for biohydrogen production. The result showed a decent yield of 38.6 % hydrogen content with acid pretreatment to maintain feed at about 5.0 pH [7].

The environment inside the digester is a very crucial parameter for the survival of anaerobic microbes [8,9]. A slight environmental change will kill the microbes, and the whole plant will stop producing desirable biofuel. The anaerobic microbes include hydrogen-producing and hydrogen-consuming (or methanogenic) microbes. Depending upon the desirable end products, favorable conditions are created for microbe culture. *Bansal et al.* investigated the effects of pretreatment temperatures between 50°C and 100°C for biohydrogen production. The authors found that a linear rise in biohydrogen production was observed from 21 % biohydrogen yield at 50°C to 48 % biohydrogen yield at 80°C, which is about a 130 % rise (from biohydrogen yield at 50°C) [10]. Similarly, *Kotsopoulos et al.* noted a hydrogen yield of 3.65 cm^3/g-volatile solid when the pig slurry is treated under 70°C temperature in a Continuous Stirred Tank Reactor (CSTR) [11].

The substantial organic waste requires large size anaerobic digesters for their disposal. Due to the size and capital cost of construction, the plant design becomes essential before the installation process [12,13]. Few tools/software/simulators are available to create plant working models. With the help of these models, the simulation is performed to

E-mail address: neeraj_budhraja@yahoo.com.

Taylor & Francis
Taylor & Francis Group

Check for updates

Modeling and analysis for enhanced hydrogen production in process simulation of methanol reforming

Neeraj Budhraja (iD), Amit Pal (iD), and R. S. Mishra (iD)

Department of Mechanical Engineering, Delhi Technological University, Delhi, India

ABSTRACT

Hydrogen has emerged as the most suitable fuel for a nation's greener and sustainable development. In contrast, the feedstock and hydrogen production methods remain a concern for environmental pollution. This study uses methanol as the feedstock for hydrogen production via a low-temperature methanol-reforming process. A simulation model was developed in Aspen Hysys, where an equilibrium reactor is used in the reforming process, and examined the effects of parameters like temperature, pressure, and Methanol-to-Water (M-to-W) molar ratio. Hydrogen mole fraction and selectivity increase by roughly 18.5% and 10.5% when the reaction temperature increases from 100°C to 400°C. At the same time, the methanol conversion rate reaches 95% at 400°C. Reactor pressure shows inverse effects where pressure rises from 1 atm. to 7 atm. that reduces hydrogen mole fraction and selectivity by about 10% and 6%, and a similar reduction of 5% is noticed in the methanol conversion rate. M-to-W molar ratio plays a crucial role in the reaction pathway and the M-to-W ratio between 0.5 and 1.5 at 400°C and 1 atm. reactor pressure showed the highest hydrogen mole fraction (>0.57) and a maximum methanol conversion rate (>90%). Therefore, the present simulation model successfully determines the impacts of various parameters to help design a commercial plant for large-scale hydrogen production via the reforming process.

Introduction

The global energy demand is rising with the development of the human race. After technological advancement and environmental concerns, new and renewable energy sources have been developed (Qureshi et al. 2022). But each renewable energy source has its disadvantages- solar energy is dynamic in nature and available during sunshine hours, wind energy is recommended for seashore areas where sufficient wind speed is available, hydropower affects flora and fauna of the region, and biomass energy requires large land masses for cultivation and storage. The transportation of energy to the place of utilization during demand time is also a big challenge for most renewable energy sources (Garcia et al. 2021). Therefore, a lot of work has been performed in the last few years to develop an energy source that can overcome these drawbacks without causing damage to the environment. And Hydrogen is one such alternative.

Hydrogen is an energy carrier that can store energy and be transported to any place and time when demanded (Budhraja, Pal, and Mishra 2023b). In contrast, greener hydrogen production is still a challenge to meet the demand of industries. Therefore, the need is met using conventional methods and fossil fuels to generate hydrogen, contributing to about 98% of the total hydrogen production worldwide (Ranjekar and Yadav 2021). Fossil fuels like coal, oil, and natural gas, and conventional methods like steam reforming, partial oxidation, and auto-thermal reforming directly or indirectly add

Research Article

Neeraj Budhraja*

Amit Pal

Radhey Shyam Mishra

Simulation and Optimization of Biohydrogen Production from Biomass Feed via Anaerobic Digestion

Biomass energy is a renewable energy source that is carbon-neutral, versatile, and can never go extinct. In the current study, a simulation model of an anaerobic digester with parameters such as pretreatment temperature (PTT), hydraulic retention time (HRT), and feed-to-water (F/W) ratio was developed and a design of experiment was created. The results showed that the higher hemicellulose content in sugarcane bagasse (SB) gave a decent H_2 yield (13–23 %). The significance sequence was PTT > F/W > HRT. The optimal values were HRT of 15–16 d; F/W of 1.5 (SB), 1.26 [rice straw (RS)], and 0.5 [sawdust (SD)]; and PTT of 63.3 (SB), 68.8 (RS), and 75 °C (SD). The optimal H_2 yield was 19.80 (SB), 20.94 (RS), and 21.41 % (SD). Therefore, the present simulation and optimization showed concrete results to raise H_2 yield.

1 Introduction

India, as an agrarian country, faces a very big problem of agricultural waste disposal. Every year, farmers are forced to burn the waste generated from their crops. This reduces soil fertility and produces air pollution that leads to respiratory diseases and even lung cancer. To tackle this problem, scientists and researchers have come up with the idea of converting agricultural waste to energy, and this is termed biomass energy [1].

Nowadays, biomass energy is a hot topic for scientists and researchers. The abundant availability and carbon-neutral nature are the main advantages of biomass energy. Other advantages include waste disposal, an add-on to farmers' income, versatility, and never going extinct [2]. Hence, energy from biomass will reduce pressure on fossil fuels-based energy. Several techniques have been developed to get maximum benefits from biomass. Among them, a few popular techniques are direct combustion to generate heat, pyrolysis for degradation into single-carbon molecules and generating producer gas, conversion to biodiesel as an alternative to conventional diesel, and anaerobic fermentation to produce biogas and bioethanol [3].

Bloch et al. discussed the various biohydrogen production methods and reactor designs, and found anaerobic digestion to be a harmless and greatly beneficial biohydrogen-producing method [4]. *Escherichia coli* is very useful in biohydrogen production. Poladyan et al. used brewery waste and *E. coli* to generate biohydrogen via anaerobic fermentation, and achieved a hydrogen yield of about 0.75 mmol-H_2/L with a Pt redox electrode [5]. Similarly, Mirzoyan et al. utilized mixed carbon sources consisting of glucose, glycerol, and formic acid in an

E. coli batch fermentation. The results showed the highest hydrogen yield of 8.8 mmol-H_2/L at about pH 7.5. Therefore, a decent biohydrogen potential was observed from different compositions of carbon sources in *E. coli* batch fermentation [6].

Biohydrogen is hydrogen produced from the biological activities of microbes (anaerobic bacteria). During the anaerobic fermentation process, both hydrogen-producing and hydrogen-consuming microbes are present. However, their activities mainly depend on the conditions available during the fermentation process [7]. The biohydrogen production process is similar to the biogas production process. The only difference lies in the feed pretreatment to mitigate the activity of hydrogen-consuming microbes, which further raises biohydrogen yield [8]. Kamaraj et al. studied various food and biomass wastes to generate biohydrogen and concluded that food wastes have excellent potential for biohydrogen production, while biomass with a few pretreatment methods can also generate a decent amount of biohydrogen [9]. The pretreatment methods include thermal pretreatment, physical pretreatment, chemical pretreatment, and biological pretreatment. All these pretreatments are performed before the feed is fed to the anaerobic digester

Neeraj Budhraja https://orcid.org/0000-0002-9349-4892 (neeraj_budhraja@yahoo.com), Prof. Amit Pal, Prof. Radhey Shyam Mishra
Delhi Technological University, Department of Mechanical Engineering, Delhi, 110033, India.